Halogen Bonding, Hydrogen Bonding and Lewis Acidic Receptors for Anion Recognition

Stuart Cornes

Wadham College, Oxford

A thesis submitted for the degree of Doctor of Philosophy

Inorganic Chemistry Laboratory

University of Oxford

Trinity Term 2016

Halogen Bonding, Hydrogen Bonding and Lewis Acidic Receptors for Anion Recognition

Stuart Cornes, Wadham College, University of Oxford

Abstract of thesis submitted for the degree of D. Phil., Trinity Term 2016

This thesis describes the preparation of acyclic, macrocyclic and interlocked receptors for the recognition of anions in competitive organic and aqueous solvent media.

Chapter One introduces the field of anion supramolecular chemistry, with a particular focus on the non-covalent interactions used for anion recognition and the synthesis of mechanically interlocked molecules.

Chapter Two discusses the preparation of halogen bonding and hydrogen bonding acyclic and interlocked pyridinium-based receptors. Investigations into their anion selectivity trends are undertaken using ^{1}H NMR titration experiments. The anion sensing properties of analogous hosts containing a fluorescent quinolinium motif are also described.

Chapter Three presents the synthesis of acyclic and macrocyclic receptors containing the dicationic 1,2-bis(pyridinium)ethane motif. Attempts towards the preparation of interlocked receptors containing the motif are also discussed.

Chapter Four focuses on a series of water-soluble receptors based around functionalised α-cyclodextrins. Isothermal titration calorimetry experiments are used to investigate differences in the thermodynamics of anion binding to halogen bonding and hydrogen bonding analogues.

Chapter Five details the preparation of a [2]rotaxane containing a Lewis acidic triarylborane motif. Investigations into its anion binding properties are conducted using multinuclear NMR and UV-visible spectroscopies.

Chapter Six provides the experimental details and characterisation data for the compounds discussed in Chapters Two to Five. Protocols for the titration experiments conducted are also described.

Full crystallographic data is provided in the Appendix.

Acknowledgements

This work has by no means been a solo effort and there are a number of people I wish to thank for their contributions.

Firstly, I am indebted to my supervisor, Professor Paul Beer, for giving me the opportunity to work on such interesting projects within his research group. The support, ideas, encouragement and mentorship he has provided over the last eight years have been invaluable and I look forward to collaborating with him in the near future. A special thanks also goes to my industrial supervisor, Dr. Mark Sambrook, along with my industrial sponsor, Dstl, for the funds used to conduct this research.

I have thoroughly enjoyed my time as a member of the Beer group and this is entirely due to the amazing group of people I have worked with, who I know will be lifelong friends. A huge thank you goes to Dr. Asha Brown for the crystallographic work she has done and the incredible amount of synthetic advice she has given me, as well as to Tim Barendt, Jason Lim, Sean Robinson, Alex Hess, Mike Chudzinski, Dr. Rich Knighton, Dr. Michal Řezanka and Dr. Remi Tirfoin for the countless helpful discussions we have had. Several of these people were also kind enough to assist in the proofreading of this work for which I am truly grateful. I must also thank, Dr. Jim Mercurio, Dr. Matthew Langton, Hena Bagha, Harry Klein and George Li for making S7 such a great place to work.

During my time as a DPhil I have been fortunate enough to supervise two Part 2 students, the exceptional Charlie Davies and the distinctly average David Blyghton. Their contributions to the work in Chapter Two are greatly appreciated.

Finally, I am eternally grateful for the unwavering support and encouragement I have received from Issy, my parents and the rest of my family. None of this would have been possible without them and this thesis is dedicated to them.

Stuart Cornes, 12th May, 2016.

Contents

Glossary of Abbreviations

δ	chemical shift
Δ	change, heat
λ	wavelength
μ	micro
Å	Angstrom
AcO^-	acetate anion
app.	apparent
aq.	Aqueous
Ar	aryl
ATP	adenosine triphosphate
Bn	benzyl
br.	broad
Bu	butyl
^tBu	tertiary butyl
^oC	degrees Celsius
cat.	catalytic
CD	cyclodextrin
Celite	diatomaceous silica
conc.	concentrated
COSY	homonuclear correlation spectroscopy
CuAAC	copper(I)-catalyzed azide–alkyne cycloaddition
d	deuterated
d	doublet
DB24c8	dibenzo-24-crown-8
DBU	1,8-diazabicycloundec-7-ene
dd	double doublet
DIBAL-H	diisobutylaluminium hydride
DIPEA	*N,N'*-diisopropylethylamine

DMF	*N*,*N'*-dimethylformamide
DMSO	dimethylsulfoxide
DNA	deoxyribonucleic acid
e.g.	*exempli gratia*
equiv./eq.	equivalent
ESI	electrospray ionisation
Et	ethyl
g	gram, gas
G	Gibbs free energy
Grubbs' II	Grubbs' second generation catalyst
H	enthalpy
HB	hydrogen bond
h	hour
HRMS	high resolution mass spectrometry
Hz	Hertz
ITC	Isothermal titration calorimetry
IUPAC	International Union of Pure and Applied Chemistry
J	joule
J	coupling constant
^{2}J	three bond coupling constant
^{3}J	three bond coupling constant
^{4}J	four bond coupling constant
K	Kelvin
K_a	association constant
K_{SV}	Stern-Volmer constant
L	litre
m	milli, multiplet
m	meta
M	moles per litre

mV	millivolts
Me	methyl
Mes	mesityl
MHz	megahertz
min	minute
MLCT	metal-to-ligand charge transfer
mol	mole
MS	mass spectrometry
Ms	mesyl
m/z	mass/charge ratio
n	nano
nm	nanometre
NMR	nuclear magnetic resonance
o	ortho
p	*para*
PBP	phosphate binding protein
PET	photo-induced electron transfer
Ph	phenyl
pH	$-\log_{10}[H^+]$
pK_a	$-\log_{10}K_a$
ppm	parts per million
Pr	propyl
Py	pyridine/pyridinium
q	quartet
quin.	quinoline/quinolinium
R	alkyl or aryl substituent
RCM	ring closing metathesis
R_f	Retention factor
ROESY	rotating-frame nuclear Overhauser effect correlation spectroscopy

rt	room temperature
s	singlet
S	entropy
sat.	saturated
SBP	sulfate binding protein
t	triplet
t, *tert*	*tertiary*
TBA	tetrabutylammonium cation
TBTA	tris[(1-benzyl-1,2,3-triazol-4-yl)methyl]amine
TFA	trifluoroacetic acid
TfO^-	triflate anion
THF	tetrahydrofuran
THP	tetrahydropyran
TLC	thin layer chromatography
TMS	trimethylsilyl
TOCSY	two-dimensional nuclear magnetic resonance spectroscopy
Ts	4-toluenesulfonyl
UV	ultraviolet
vdW	van der Waals
wt.	weight
X	halogen atom
XB	halogen bond

Chapter One

Introduction

1.1 Anion supramolecular chemistry

The origins of the field of anion supramolecular chemistry can be traced back to the seminal work of Park and Simmons in 1968, which demonstrated the ability of synthetic ammonium cage structures to complex halide anions.[1] Following this initial breakthrough, relatively few reports of anion host systems emerged for a number of years, with a much greater focus being paid to the recognition of cationic species. Indeed, pioneering studies by Pedersen,[2] Lehn[3] and Cram[4] into the coordination of alkali metal cations using crown ethers, cryptands and spherands respectively was acknowledged with the award of a Nobel Prize in 1987 (**Figure 1.1**). During his prize lecture, Lehn highlighted the then unestablished area of anion coordination chemistry, stating the importance of its future development due to the relevance of anions from both chemical and biological perspectives.

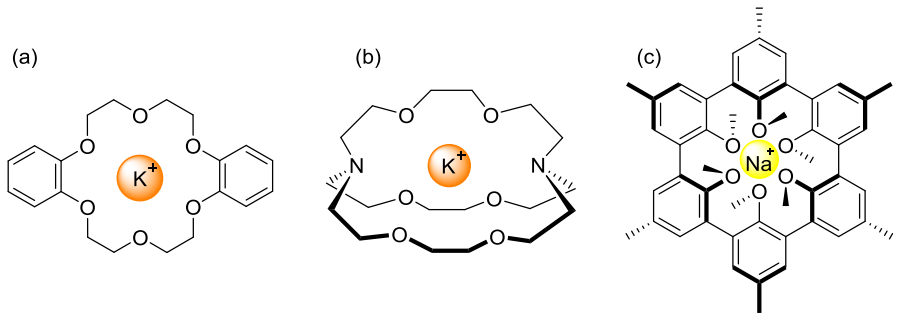

Figure 1.1: Receptors for metal cations: (a) Pedersen's dibenzo-18-crown-6,[2] (b) Lehn's [2.2.2]cryptand,[3] (c) Cram's spherand[4]

Today, anion supramolecular chemistry is a highly active field of research, which has extended far beyond the preparation of receptors, with anions now used in the templated synthesis of complex architectures, as well as for applications in areas such as catalysis and materials chemistry.[5]

Of relevance to the research theme of this thesis, this introductory chapter will discuss host systems that have been used for anion recognition in the solution phase, with a particular focus on the types of non-covalent interactions they exploit and the challenges faced in their

design. Attention will then turn to the templated synthesis and properties of interlocked structures.

1.1.1 The importance of anions

Interest in anionic species stems from the pivotal roles they play in a wide variety of fundamental biological processes. This is exemplified by the fact that many crucial biological molecules contain negatively-charged groups. These include the macromolecule DNA, which contains the genetic information required for all organisms to develop and reproduce, as well as the co-enzyme ATP, commonly referred to as the energy currency of life, both of which contain multiple anionic phosphate groups. Furthermore, around 70% of enzyme substrates and co-factors are negatively charged. The recognition and transport of these molecules is fundamental to all living things.[6]

A number of common illnesses in humans are related to the misregulation of anion transport, such as cystic fibrosis, which is a hereditary disease caused by the malfunction of the cystic fibrosis transmembrane conductance regulator (CFTR) chloride transport channel.[7] The introduction of certain anions into our bodies can also have detrimental implications towards our health: for example, a chronic over exposure to fluoride, a common additive to drinking water and toothpaste, can cause dental or skeletal fluorosis,[8] whilst other anions, such as cyanide, are known to act as lethal poisons, even when administered in small quantities.[9]

Several environmental issues have been caused by anthropogenic activities; phosphates and nitrates, present in fertilizers, have been identified as the primary cause of eutrophication in rivers, lakes and coastal water supplies.[10] Also worthy of note is the pertechnetate anion, a radioactive water pollutant, which is released as a by-product of the nuclear fuel industry.[11]

For the above reasons and many more, the design and construction of highly selective receptors, which are capable of sensing and/or extracting a desired anionic target, is of

paramount importance. For such systems to have the maximum level of applicability, it is highly desirable that they can function in aqueous media.

1.1.2 Challenges of anion recognition

The design of selective receptors for target anions is particularly challenging, owing to the intrinsic properties that they possess. Firstly, halide anions generally have larger ionic radii than their isoelectronic cations, which imparts them with a much lower charge density. Hence, receptors that utilise electrostatic interactions to bind these anions are less effective. Anions also adopt a wide range of geometries, including spherical (halides), linear (azide, hydroxide and cyanide) trigonal planar (nitrate and carbonates), tetrahedral (phosphates and sulfates) and octahedral (hexafluorophosphate) (**Figure 1.2**). This means that both the size and shape of the binding pocket of a potential host must be carefully considered.

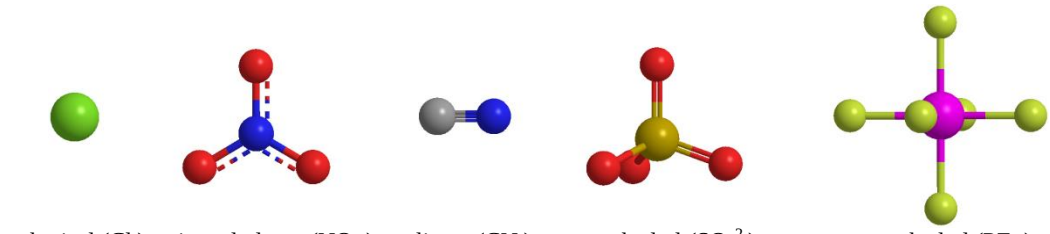

Figure 1.2: Examples of different anion geometries

In the solution phase, host-guest association strength is strongly influenced by the solvent media. This is most apparent in polar, protic solvents such as alcohols and water, where both receptor and anion can form strong hydrogen bonding interactions with the solvent molecules. This significantly weakens the interactions between them, making recognition in these solvents extremely challenging. The degree to which anions are solvated in aqueous media is outlined by the Hofmeister series (**Figure 1.3**).[12]

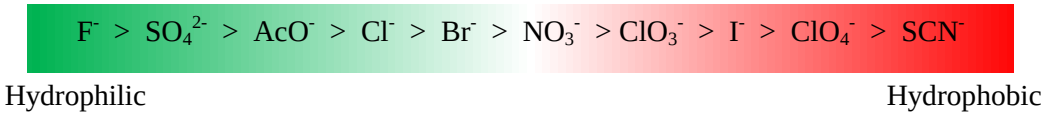

Figure 1.3: The Hofmeister series[12]

In less polar, non-protic solvent systems, solvation energies are generally much lower and binding strengths are typically much greater. The selectivity trends of receptors in these solvents generally mirror anion basicity, however in some cases, highly basic anions such as fluoride and acetate may deprotonate hosts that contain acidic hydrogen atoms.[5,13–16] Most commonly observed in chlorinated solvents, ion-pairing may occur when the interaction between an anion and its counter cation is strong enough to act as a competing interaction with association of the anion to a receptor.[17–19] This was found by Sessler and co-workers when they determined association constants between calix[4]pyrrole and chloride, added as its tetrabutylammonium (TBA) salt, in a variety of solvents (**Figure 1.4**).[19] The anomalously low value calculated in dichloromethane was attributed to strong ion-pairing between chloride and the TBA cation.

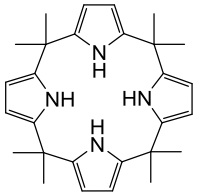

Solvent	K_a (M^{-1})
CD_3CN	2.5 x 10^5
CD_3NO_2	2.4 x 10^4
d_6-DMSO	2.2 x 10^3
CD_2Cl_2	4.3 x 10^2

Figure 1.4: Chloride association constants of calix[4]pyrrole in a range of solvents[19]

In aqueous media, the pH range over which an anionic species will exist must be considered, as many anions are able to undergo multiple protonation equilibria. Receptors containing positively charged, hydrogen bond donor groups, such as ammonium or pyridinium motifs, are also pH-sensitive. In many cases there exists a "pH window" in which both receptor and anion are in the required protonation state for binding to occur.

1.1.3 Non-covalent interactions

Supramolecular chemists have a range of non-covalent interactions at their disposal when designing an anion receptor. These include electrostatics, hydrogen bonding, halogen bonding, anion-π interactions, coordinate bond formation and solvophobic effects, all of which are discussed in further detail below (**Figure 1.5**).

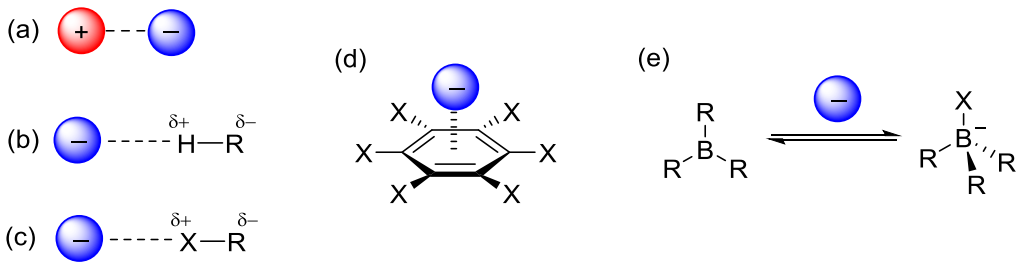

Figure 1.5: Anion binding interactions (a) ion-ion, (b) hydrogen bond, (c) halogen bond, (d) anion-π, (e) coordinate bond

Electrostatics

Owing to their inherent negative charge, anions undergo attractive Coulombic interactions with both positively-charged species (ion-ion interaction) and the positively-polarised regions of dipolar molecules (ion-dipole interaction). Ion-ion interactions are the strongest class of supramolecular interaction, making positively-charged groups a common feature of many anion receptors. However, their isotropic nature means that they are non-directional and hence, they are commonly used in concert with more directional interactions to enhance selectivity.

Hydrogen bonds

Hydrogen bonds are a specific category of ion-dipole or dipole-dipole interaction, involving the attractive force between a hydrogen atom attached to a more electronegative atom, such as nitrogen or oxygen, and an anion or dipole. The strength of such interactions can vary substantially (4-120 kJ mol^{-1})[20] depending on the nature of the species involved, as well as the geometry of the hydrogen bond. The strongest interactions are formed when bond angles are close to 180°. Hydrogen bonds are the most prevalent of the non-covalent interactions used for anion recognition in both synthetic and naturally occurring receptors (*vide infra*).

Halogen bonds

As recently defined by IUPAC "*A halogen bond occurs when there is evidence of a net attractive interaction between an electrophilic region associated with a halogen atom in a molecular entity and a nucleophilic region in another, or the same, molecular entity*".[21] The

electrophilic region, often referred to as a σ-hole, is generated when a halogen atom X is covalently linked to an electron withdrawing group R, and is positioned at the terminus of the R-X bond. This necessitates that interactions occur in an approximately co-linear orientation to the R-X axis, with usually only small deviations from this observed. The strength of halogen bonds are highly dependent on the electron withdrawing properties of the R-group as well as the type of halogen atom X, with the strongest interactions generally formed by donors containing the larger and more polarisable halogens, bromine and iodine. The nature of the halogen bond acceptor also strongly impacts the strength of the interaction.

Parallels have been drawn between halogen bonds and hydrogen bonds due to the similarity of their interaction energies and their stringent directionality.[22,23] However, whilst hydrogen bonds are electrostatic interactions,[24,25] the nature of halogen bonding interactions is a subject of current debate, with both theoretical and experimental studies suggesting that electrostatics, charge-transfer, polarisation and dispersion forces make varying degrees of contribution that are dependent upon the specific halogen bond donor and acceptor species involved.[26–31]

The use of halogen bonding interactions for anion recognition purposes is still very much in its infancy, however, they have been extensively used in crystal engineering[32–35] and in the preparation of functional materials (**Figure 1.6a**).[36–39] In the solution phase, the interaction has recently been used for applications in diverse fields such as catalysis (**Figure 1.6b**),[40–43] self-assembly[44–47] and medicinal chemistry (**Figure 1.6c**).[48,49]

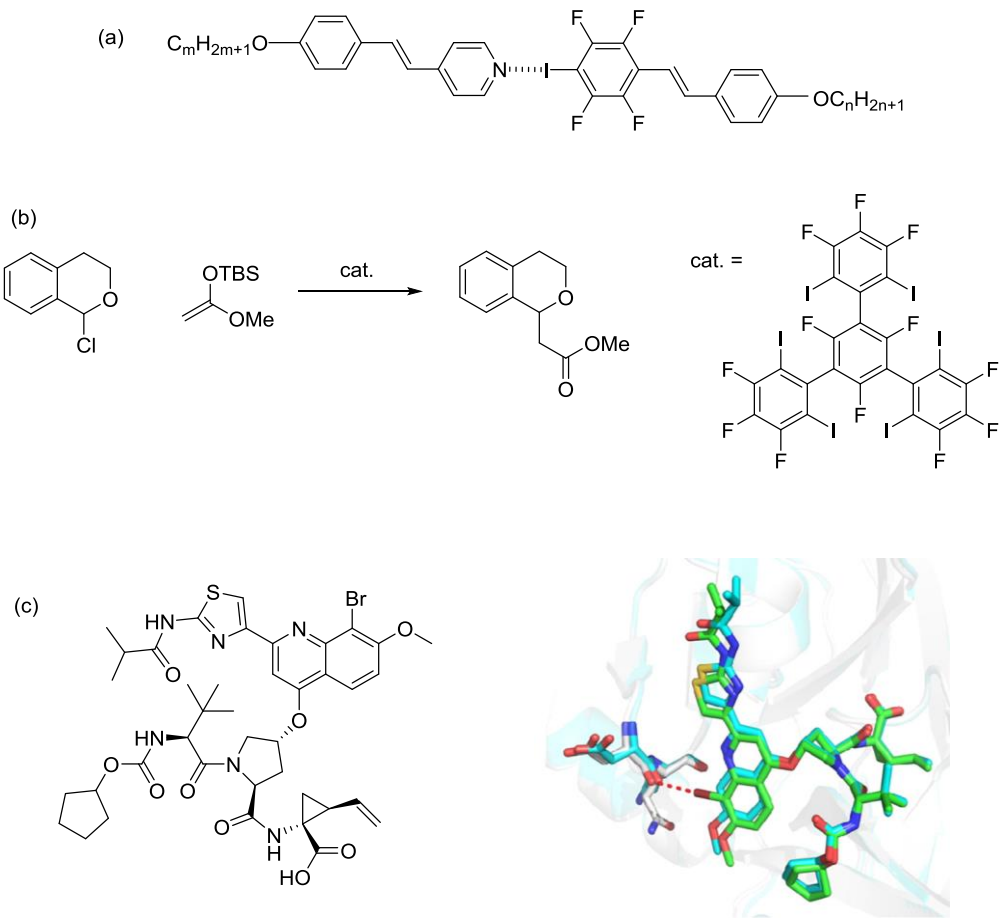

Figure 1.6: Applications of halogen bonding; (a) liquid crystal formation,[37] (b) halogen bonding catalyst,[43] (c) halogen bonding inhibitor of hepatitis C virus[48]

Anion-π interactions

Anion-π interactions occur when an anion interacts with the electron deficient π-surface of an aromatic molecule and arise through a combination of electrostatic and polarisation forces. Theoretical calculations suggest that the energies of such interactions fall in the range of 20-70 kJ mol^{-1}.[50] Evidence for their formation initially came from examination of solid-state X-ray structures,[51–53] however several recent examples of solution state anion-π interactions have also been observed.[54–57]

Coordinate bonds

Although not conventionally classified as supramolecular interactions, due to their highly covalent character, coordinate bonds are widely utilised in anion recognition chemistry. The inherent Lewis basicity of anions allows them to form strong interactions with either main

group or transition metal Lewis acidic centers such as boron,[58,59] tin,[60–64] mercury,[65,66] copper,[67–69] zinc[70,71] and silver.[72,73]

Solvophobic effects

The degree to which both anion and receptor are solvated can, in some cases, act as a driving force for their association. This is most frequently observed in aqueous environments when anions with low hydration energies bind within a poorly-solvated cavity of a host. This is commonly referred to as the hydrophobic effect and was classically believed to be caused by the favourable entropy gain associated with the release of highly-ordered water molecules from the receptor upon complexation of the anion. However, several cases of non-classical hydrophobic effects have emerged recently, where anion recognition is instead enthalpically driven.[74–77] This has been attributed to the release of high-energy water molecules from the receptor, which form fewer or weaker hydrogen bonding interactions when encapsulated than when in the bulk solution. Nau and co-workers have suggested that the disruption of the structure of the bulk solution caused by hydrophobic anions may also contribute to this effect, with the reformation of hydrogen bonds between water molecules upon anion complexation adding a further enthalpic driving force.[76]

1.1.4 Principles of anion receptor design

Several key design principles underpin the preparation of all effective supramolecular host systems. The most fundamental of these is complementarity: the idea that the size, shape and electronic properties of the binding pocket of a receptor should be matched to those of a target guest. This concept was introduced by Fischer as early as 1894, when he used a 'lock and key' analogy to describe the association of an enzyme with its substrate.[78] Although more recent theories suggest that this interaction is better described by an 'induced fit' model,[79] the idea is still of upmost importance in anion receptor design. This was demonstrated by Schmidtchen, who showed that the anion selectivity of tetracationic ammonium cage-like

receptors could be modified by changing the size of their internal cavities (**Figure 1.7**).[80,81] In aqueous media, the smaller receptor was found to bind bromide selectively, whilst the larger host bound *para*-nitrophenolate most strongly.

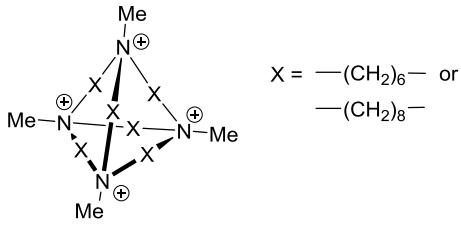

Figure 1.7: Schmidtchen's quaternary ammonium cage-like receptors[80]

The concept of complementarity can be further extended to that of preorganisation, a term first used by Cram in his work on alkali metal cation coordination. He stated that "*the more highly hosts and guests are organized for binding and low solvation prior to their complexation, the more stable will be their complexes*".[82,83] This implies that association strength will be greater if the binding groups of a receptor are fixed in the orientation they adopt upon complexation, prior to addition of the guest. This is demonstrated by a comparison of the acetate binding affinity of two isophthalamide receptors reported by Smith (**Figure 1.8**).[84] In the receptor incorporating boronic ester functionality, the amide hydrogen bond donors are held in a convergent conformation through interaction between the carbonyl oxygens and the two boron centres. The acetate association constant of this receptor is twenty times greater than that of the unfunctionalised analogue (K_a = 2100 and 110 M^{-1}, respectively in d_6-DMSO), in which the amide groups are not preorganised and can freely rotate.

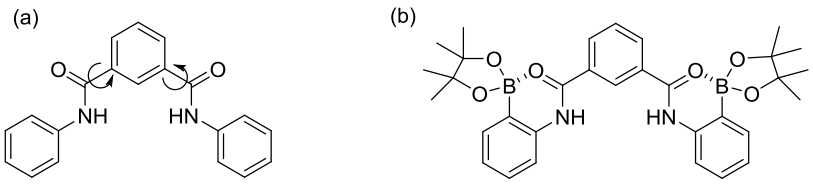

Figure 1.8: Isophthalamide receptors[84] (a) non-preorganised (b) preorganised

Other principles from the field of cation recognition chemistry have also been applied to that of anion recognition, such as the chelate and macrocyclic effects.[85,86] Both effects are thermodynamic in nature and have enthalpic and entropic contributions.[87]

1.1.5 Naturally occurring anion receptors

As with many fields of chemistry, the design of synthetic anion receptors takes inspiration from the natural world. The elucidation of the X-ray crystal structures of several naturally occurring protein-anion complexes over the last few decades has allowed the modes of binding and the type of interactions involved in these highly complex and elegant frameworks to be visualised. In most cases, a combination of non-covalent interactions are employed to afford a strong association and high degrees of selectivity. An example of such a natural receptor is the phosphate binding protein (PBP), which is responsible for the transport of phosphate into bacterial cells (**Figure 1.9a)**.[88] The protein is composed of two globular domains with a binding cavity between them, wherein a desolvated hydrogen phosphate anion binds, forming twelve hydrogen bonding interactions with a combination of charged and neutral peptide residues. The PBP binds hydrogen phosphate around five orders of magnitude more strongly than sulfate, owing to the negatively charged Asp156 residue within the binding cavity that forms an attractive hydrogen bond with the partially protonated hydrogen phosphate anion and a repulsive electrostatic interaction with the doubly-charged sulfate anion.

The sulfate binding protein (SBP) found in *Salmonella typhirium* has a similar function and structure to that of the PBP.[89] However, in this case, selective sulfate binding is mediated through seven hydrogen bonding interactions with exclusively neutral peptide residues (**Figure 1.9b**).

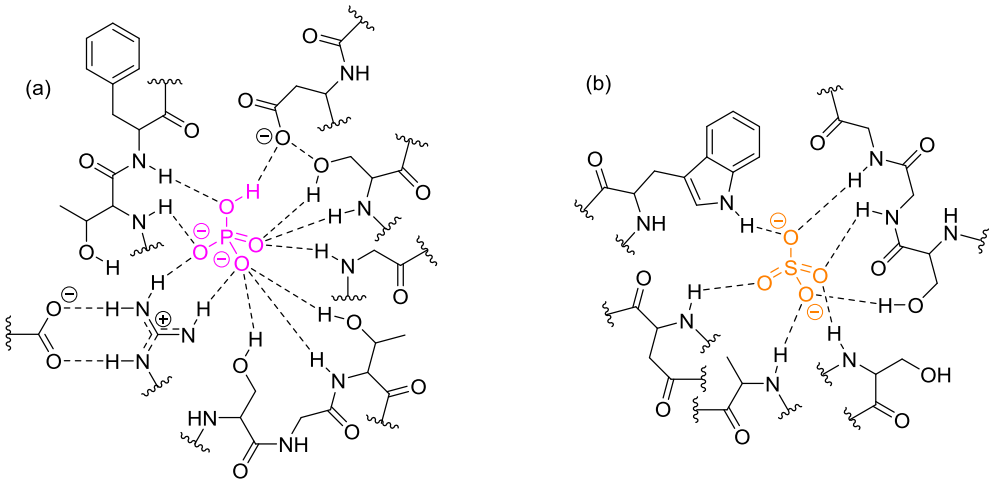

Figure 1.9: Anion binding pockets of (a) phosphate binding protein,[88] (b) sulfate binding protein.[89]

1.1.6 Synthetic hydrogen bonding anion receptors

As previously mentioned, hydrogen bonding is the most commonly employed non-covalent interaction in synthetic anion receptors. A wide range of both positively-charged and neutral hydrogen bond donor motifs have been utilised and are discussed below.

Polyammonium receptors

In the first example of anion recognition by a synthetic host, Park and Simmons demonstrated that a bicyclic structure containing protonated secondary ammonium groups at its bridgeheads, referred to as a katapinand, could coordinate halide anions using a combination of electrostatic and hydrogen bonding interactions in a 50% TFA solution (**Figure 1.10a**).[1] Since this initial report, a plethora of acyclic and macrocyclic ligands containing protonated polyamines have been prepared, which are capable of complexing anions in competitive aqueous solvent media due to their highly charged nature.[90]

In groundbreaking work by Lehn, the binding properties of a range of bis-tren azacryptands were investigated. By varying the length of the spacer between the tren units, the selectivity of the receptor could be tailored to anions of differing shapes and sizes. [91–93] For example, ethylene spacers gave a receptor with a small cavity which was shown to have remarkable selectivity for fluoride over chloride in aqueous solution at pH 6 (log K_a = 8.8 for fluoride

and 1.2 for chloride) (**Figure 1.10b**).[94] More recently, Bencini and co-workers prepared three receptors containing two 1,4,7-triazacyclononane macrocycles linked by different spacer units (**Figure 1.10c**).[95] Binding studies in water showed that selectivity preferences between mono-, di- and tri-phosphate were dependent on the distance between the positively-charged rings.

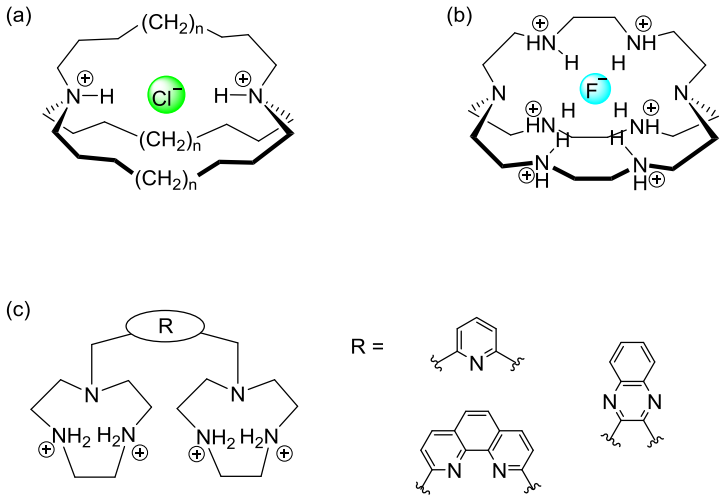

Figure 1.10: Ammonium receptors: (a) Park and Simmons' katapinand,[1] (b) Lehn's bis-tren azacryptand,[94] (c) Bencini's triazacyclononane-based receptor[95]

Guanidinium receptors

The guanidinium motif is another extensively used, positively-charged, hydrogen-bond donor motif. The parallel arrangement of two N-H donors imparts receptors with selectivity towards 'Y-shaped' anions such as carboxylates, whilst the relatively low acidity of the motif (pK_a ~ 13) allows these receptors to function over a much wider pH range, when compared with ammonium-based systems. An early report by Hamilton showed that a simple acyclic system containing two guanidinium groups linked by a xylene spacer could bind glutarate, a dicarboxylate, in a 3:1 DMSO/D_2O mixture (K_a ~ 500 M^{-1}) (**Figure 1.11a**).[96]

Incorporation of the guanidinium motif into a bicyclic framework has been used to prepare receptors with a greater level of preorgansation. Schmidtchen's chiral, preorganised bis-guanidinium macrocyclic host (**Figure 1.11b**) was shown to discriminate enantiomers of chiral dicarboxylates.[97] For example, isothermal titration calorimetry (ITC) studies in

acetonitrile, revealed the receptor bound (*S*,*S*)-tartarate 3.5 times more strongly than (*R*,*R*)-tartarate.

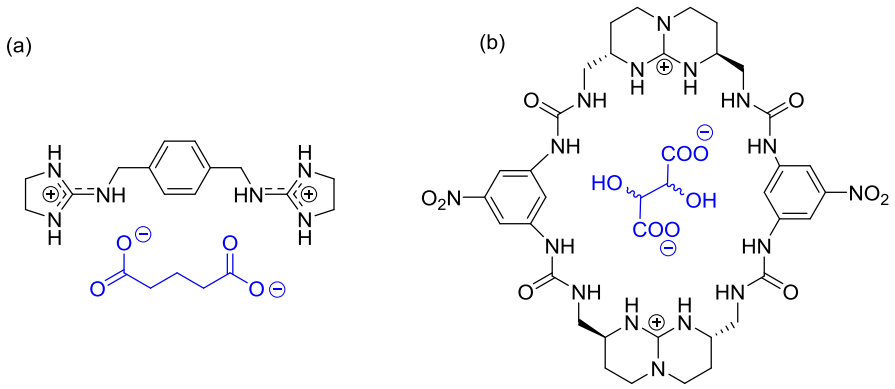

Figure 1.11: Guanidinium receptors: (a) Hamilton's acyclic receptor,[96] (b) Schmidtchen's chiral, macrocyclic dicarboxylate receptor[97]

Amide, urea and thiourea based receptors

Proteins, such as the PBP and the SBP, utilise the hydrogen bonding ability of amide groups present in their polypeptide backbones to facilitate the anion recognition process.[88,89] However, the charge neutrality of these groups means that they form relatively weak interactions with anions, and therefore, synthetic amide receptors usually only function effectively in polar aprotic solvents.

Many hosts containing amide groups have taken inspiration from Crabtree's seminal work on a series of relatively simple isophthalamide based receptors, which were shown to selectively bind chloride in CD_2Cl_2.[98] For example, Bowman-James and co-workers prepared two macrobicyclic receptors, containing six amide groups that converge on the central cavity (**Figure 1.12a**).[99,100] Binding studies conducted in d_6-DMSO revealed a selectivity preference for fluoride, over the other halides and a range of oxoanions.

Kubik and co-workers have pioneered work in the area of anion recognition in water using a range of neutral cyclic hexapeptide host systems that bind anions using a combination of the hydrophobic effect and hydrogen bonding interactions.[101,102] Recently they showed that a receptor containing two hexapeptide macrocycles (**Figure 1.12b**), connected by a flexible

linker, is capable of binding iodide and sulfate strongly in 95:5 D_2O/CD_3OD (log K_a = 3.70 and 3.96 respectively).[103]

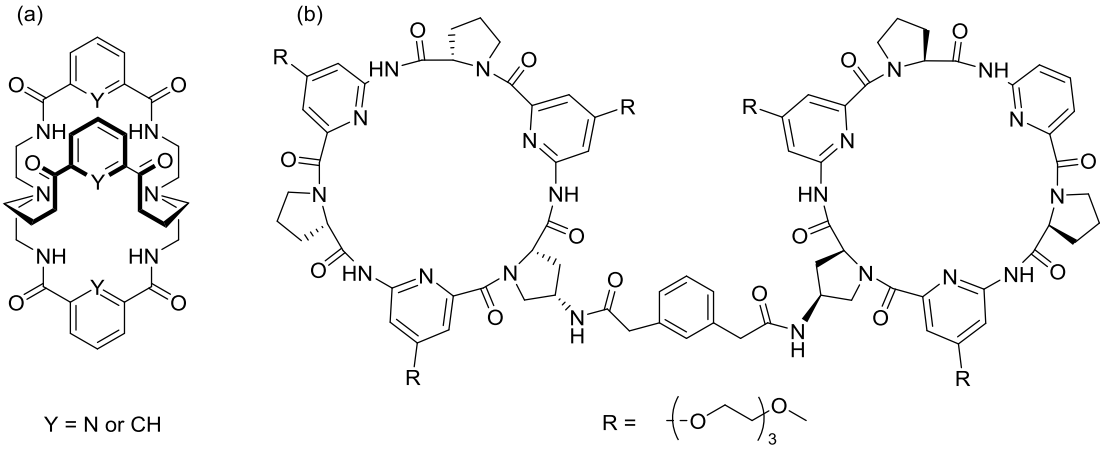

Figure 1.12: Amide receptors: (a) Bowman-James' cryptands,[99,100] (b) Kubik's bis-cyclopeptide receptor[103]

Ureas and thioureas are another class of neutral N-H hydrogen bond donors that have been used for anion recognition purposes.[104] Much like the guanidinium motif they donate two parallel hydrogen bonds, making them particularly useful in the recognition of oxoanions. This was demonstrated by Wu and co-workers who prepared a tripodal receptor containing six urea motifs, capable of donating a total of twelve hydrogen-bonds (**Figure 1.13**).[105] X-ray structural analysis showed the receptor to coordinatively saturate a sulfate anion, making it the first example of a single organic host molecule able to do this. ^{1}H NMR titrations in competitive 3:1 d_6-DMSO/D_2O solvent mixture estimate the association constant with sulfate to be greater than 10^4 M^{-1}.

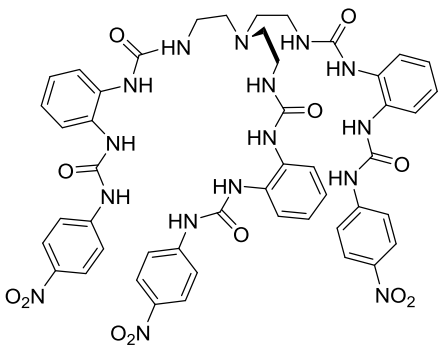

Figure 1.13: Wu's urea-based tripodal sulfate receptor[105]

Receptors containing heterocyclic donors

Many of the nitrogen-containing heterocyclic rings contain polarised hydrogen atoms allowing them to function as hydrogen bond donors. This is seen in the SBP, where the indole moiety of a tryptophan side-chain acts as an N-H donor.[89] Pyrroles are another class of neutral N-H hydrogen-bond donors that have been frequently incorporated into synthetic anion receptors over the last two decades.[106] Calix[4]pyrrole was the first example of a neutral synthetic pyrrole-based receptor, and many derivatives have since been reported.[107] For example, Sessler recently prepared a bipyrrole-strapped calix[4]pyrrole, which displayed enhanced anion recognition capabilities in comparison to the parent calix[4]pyrrole receptor, and was capable of extracting sulfate anions from aqueous media into chloroform (**Figure 1.14a**).[108]

Another example of a hydrogen bonding heterocycle is the 1,2,3-triazole motif, a neutral C-H donor. Recent advances in copper(I)-mediated 'click' chemistry[109] has led to its integration into anion receptor design.[110] Flood described a range of macrocyclic hosts containing four 1,2,3-triazole groups, referred to as triazolophanes.[111] These receptors typically displayed selectivity towards chloride and bromide anions ($K_a > 10^6$ M^{-1} in CH_2Cl_2), attributed to the fixed cavity size they possess. More recently the group has used computer-aided design in the synthesis of a more flexible receptor capable of binding a linear bifluoride anion with a similar strength to chloride in CH_2Cl_2 (**Figure 1.14b**).[112]

Methylation of the 1,2,3-triazole heterocycle produces the triazolium motif, in which the positive charge provides an electrostatic contribution to binding and also further polarises the C-H bond, increasing the strength of binding interactions. Molina and co-workers recently reported an acyclic receptor containing two 1,2,3-triazolium motifs (**Figure 1.14c**), which was found to selectively bind hydrogenpyrophosphate (K_a = 3000 M^{-1}) in 9:1 CD_3CN/CD_3OD. Theoretical calculations and experimental evidence suggest that one

triazolium motif forms a hydrogen bonding interaction with the anion, whilst the other forms an anion-π interaction.[113]

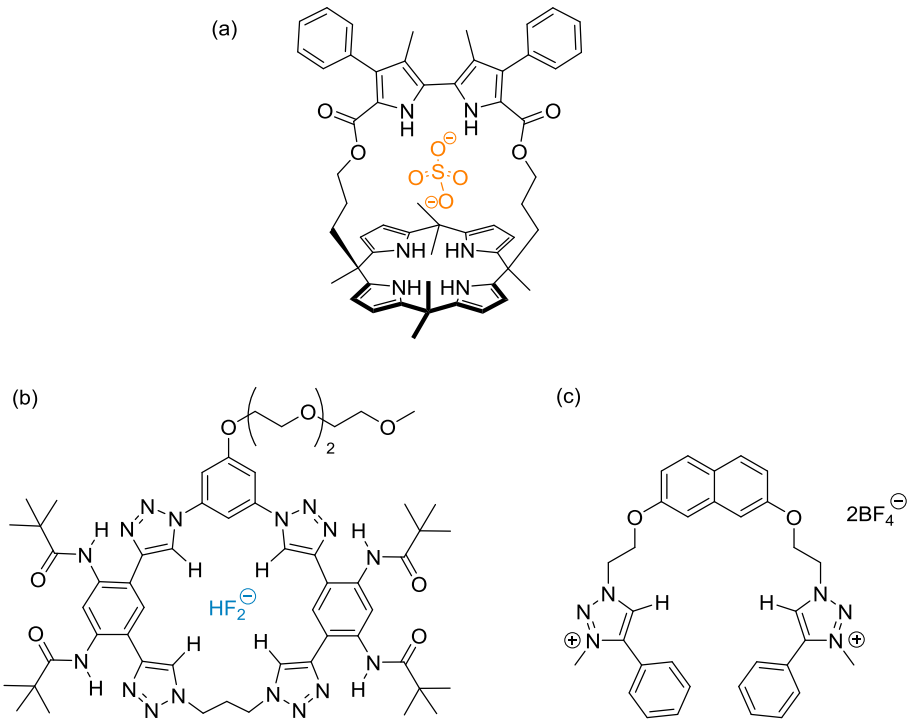

Figure 1.14: (a) Sessler's bipyrrole-strapped calix[4]pyrrole receptor[108], (b) Flood's computer designed triazolophane[112] and (c) Molina's acyclic triazolium receptor[113]

1,3-Substituted imidazolium cations are another class of positively-charged C-H hydrogen bond donors. The groups of Yoon and Kim reported a water-soluble tetraimidazolium receptor for the selective recognition of ATP over other nucleoside triphosphates, in 20 mM HEPES buffer solution (K_a = 1.03 x 10^4 M^{-1}).[114] The ATP complex is stabilised by a combination of hydrogen bonding and π-π donor-acceptor interactions (**Figure 1.15a**).

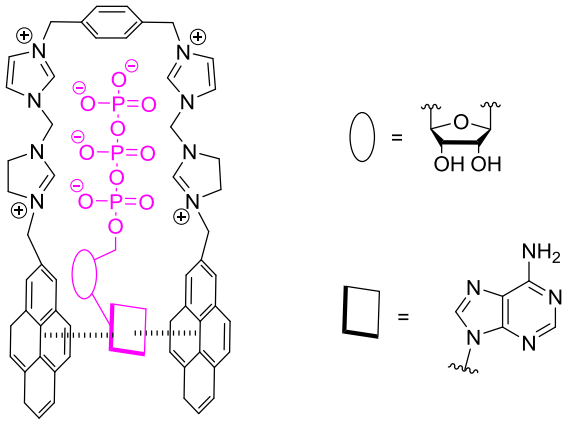

Figure 1.15: Yoon and Kims' tetraimidazolium ATP receptor[114]

1.1.7 Halogen bonding anion receptors

In comparison to the multitude of hydrogen bonding anion hosts reported to date, examples of halogen bonding receptors that recognise anions in the solution phase are limited.[115] The first example was a heteroditopic tripodal receptor designed for the recognition of sodium halide salts, by Resnati and Metrangolo (**Figure 1.16a**).[116] ^{1}H NMR titration experiments in $CDCl_3$ showed the association strength followed the order NaI > NaBr > NaCl. Furthermore, an X-ray crystal structure of the sodium iodide complex provided evidence for the formation of a halogen bonding interaction between the iodide anion and one of the three *para*-iodotetrafluorophenyl motifs attached to the arms.

Taylor also utilised the halogen bonding ability of iodoperfluoroarenes in a range of multivalent receptors,[117,118] including a tripodal host system which bound chloride selectively, in d_6-acetone, through three convergent halogen bonds (K_a = 19000 M^{-1}, **Figure 1.16b**).[117]

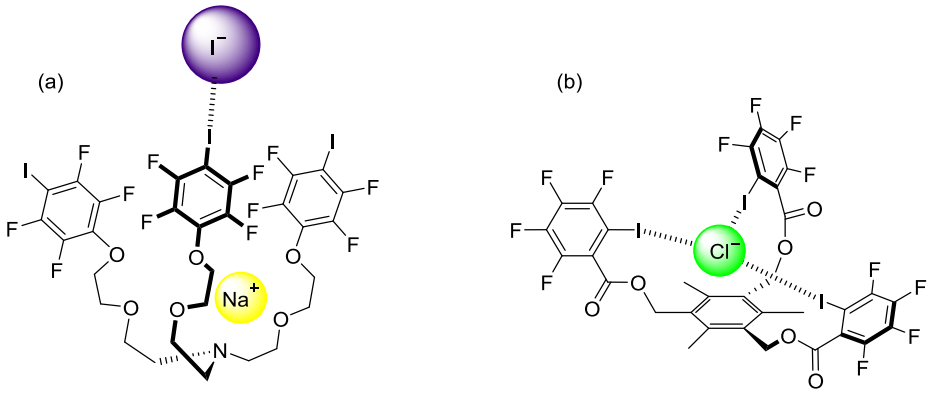

Figure 1.16: Halogen bonding receptors: (a) Resnati and Metrangolos' heteroditopic receptor,[116] (b) Taylor's tripodal receptor[117]

Halo-functionalised heterocycles have also been demonstrated to function as effective halogen bond donor motifs. In cases where hosts have incorporated positively-charged heterocycles, anion recognition in highly competitive solvent systems has been possible. For example, Beer and co-workers prepared macrocycles containing bromo- and iodo-functionalised imidazolium motifs (**Figure 1.17a**). Using fluorescence titration experiments in aqueous 9:1 CH_3OH/H_2O solvent mixture, selectivity for iodide and bromide was observed for the respective macrocycles.[119] More recently, Schubert and co-workers have conducted a systematic study into the anion binding properties of a series of bidentate receptors containing 5-halo-1,2,3-triazole and -triazolium motifs.[120] The strongest affinities were obtained with a bidentate receptor (**Figure 1.17b**), displaying the anion selectivity trend $SO_4^{2-} > H_2PO_4^- > AcO^- > Cl^- > Br^- > I^-$.

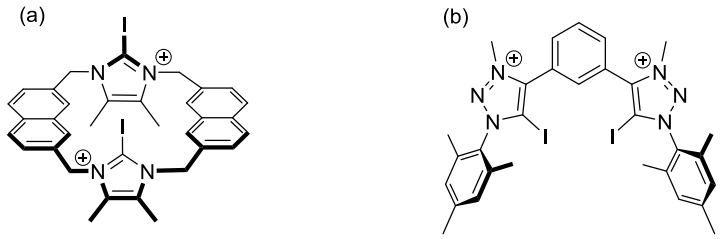

Figure 1.17: Halogen bonding receptors: (a) Beer's iodo-imidazolium macrocycle,[119] (b) Schubert's acyclic iodo-triazolium receptor[120]

1.1.8 Lewis acidic anion receptors

The first example of anion recognition by a Lewis acidic receptor came from Shriver and Biallas, who reported the ability of a bidentate boron derivative to coordinate a methoxide anion in a chelating fashion (**Figure 1.18a**).[121] Since this discovery, a wide range of receptors containing Lewis acidic main group elements have been reported.[6,58] For example, Newcomb and co-workers prepared tin-containing macrobicyclic structures.[60] As evidenced from ^{119}Sn NMR, the smallest host (**Figure 1.18b**) bound fluoride five orders of magnitude more strongly than chloride in $CDCl_3$.[61] More recently, Gabbaï described the ability of an antimony-based receptor to bind fluoride strongly in 7:3 THF/H_2O (K_a = 16100 M^{-1}) (**Figure 1.18c**).[122] The same group demonstrated a tricationic borane receptor to selectively bind cyanide in pure water.[123]

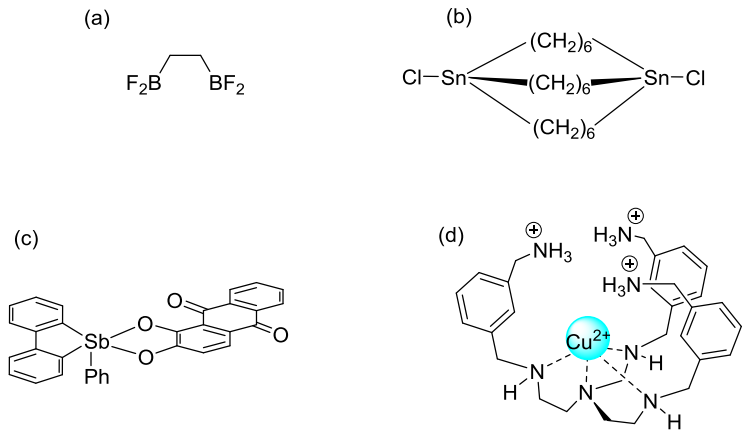

Figure 1.18: Lewis acidic anion receptors: (a) bidentate borane receptor,[121] (b) Newcomb's tin-containing macrobicycles,[61] (c) Gabbaï's antinomy-based fluoride receptor,[122] (d) Anslyn's Cu(II)-based tripodal receptor[68]

Numerous receptors that exploit the coordination of anions to transition metal centres have also been reported.[70,124–126] For example, Anslyn described a tripodal receptor containing a Cu(II) centre that selectively binds phosphate anions (**Figure 1.18d**).[68] The interaction of phosphate with the metal is augmented by hydrogen bonding interactions from ammonium groups attached to each arm of the tripod, resulting in strong association in 98:2 H_2O/CH_3OH at neutral pH ($K_a \sim 10^4$ M^{-1}).

1.1.9 Anion receptors exploiting the hydrophobic effect

Recently, a handful of receptors that utilse the hydrophobic effect as a driving force for anion coordination in water have emerged. Of particular interest are those that consist of a macrocyclic framework containing a hydrophobic core with negatively-charged solubilising groups, such as carboxylates, appended to the periphery.[75,127,128] For example, Sindelar and co-workers reported the preparation of a water-soluble analogue of the bambusuril macrocycle (**Figure 1.19**).[74] ^{1}H NMR studies in phosphate buffer solution showed that the anion selectivity trend of the receptor mirrored the hydration energies of the anions investigated, with perchlorate (ClO_4^-) bound most strongly (K_a = 5.5 x 10^7 M^{-1}) and fluoride bound the weakest (K_a = 110 M^{-1}). Moreover, using ITC measurements, anion coordination was found to be enthalpically driven.

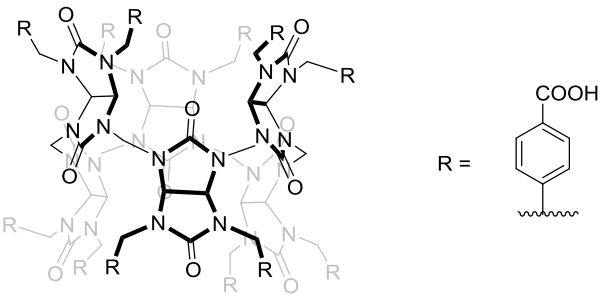

Figure 1.19: Sindelar's water-soluble bambusuril receptor[74]

1.2 Anion Sensing

The incorporation of a photo- or redox-active group in close proximity to an anion binding site produces an anion sensor with the capability of detecting a target analyte through an optical or electrochemical response.

Other approaches that utilise discrete molecular species to sense anions have also been demonstrated. Indicator displacement assays exploit the competitive binding between an indicator and an anion to a receptor. A substantial difference in the optical properties of the indicator in its bound and unbound state are required, and therefore strongly colored or

fluorescent dyes are often used. A third type of anion sensing involves the use of chemodosimeters: species which can undergo an irreversible reaction with an anion to generate an observable change. Examples of various types of anion sensors are given below.

1.2.1 Colorimetric anion sensors

Sensors which undergo a colour change upon exposure to a specific anion are highly attractive as they allow detection to occur with the 'naked-eye'. Several fluoride selective sensors that change colour when deprotonated by this highly basic anion have been reported.[129,130] For example, a coumarin-based system that changes from yellow to blue upon deprotonation of its hydrazone motif in MeCN, was described by Liu and co-workers (**Figure 1.20a**).[131] Chemodosimeters have been utilised for colorimetric sensing of cyanide. Martínez-Máñez and co-workers used a *para*-quinomethane derivative that selectively reacted with this anion in aqueous media (Borax buffer, pH 10.6), producing a pink to colorless colour change (**Figure 1.20b**).[132]

Ghosh and co-workers have used the displacement of a uranine dye (fluorescein) from a dicationic pyridinium hydrogen bonding receptor to detect hydrogen pyrophosphate in 4:1 CH_3CN/H_2O at pH 6.5 (**Figure 1.20c**).[133]

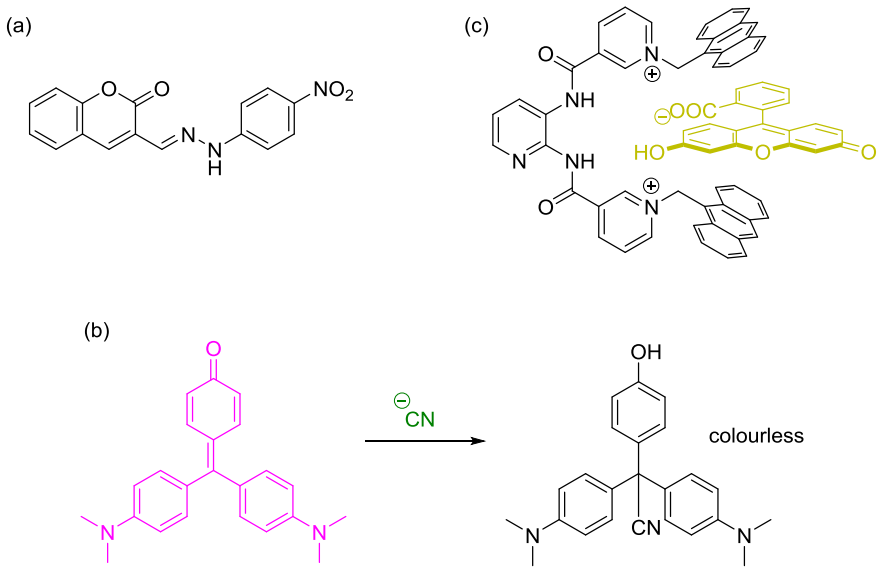

Figure 1.20: Colorimetric anion sensors: (a) Liu's fluoride sensor,[131] (b) Martínez-Máñez's chemodosimeter for cyanide,[132] (c) Ghosh's fluorescein-based displacement assay[133]

1.2.2 Luminescent anion sensors

Owing to the highly sensitive nature of luminescence spectroscopy, sensors which function through a modulation of their luminescent properties have proven useful in the detection of anions at very low concentrations. This has been demonstrated in a range of systems containing luminescent transition metal[70,125,134] or lanthanide[135] complexes. For example, Ye and co-workers have recently reported the ability of an imidazole-based bimetallic Ru(II)-complex to selectively detect micromolar quantities of cyanide in water at pH 7, *via* a decrease in its' MLCT emission intensity (**Figure 1.21a**).[136]

Organic fluorophores have also been used in the sensing of anions. Gunnlaugsson and co-workers used a naphthalamide-based receptor in the detection of fluoride and acetate anions in DMSO (**Figure 1.21b**).[137] Hydrogen bonding interactions between the anions and the thiourea motif resulted in quenching of the sensor's fluorescence *via* a photo-induced electron transfer (PET) mechanism.

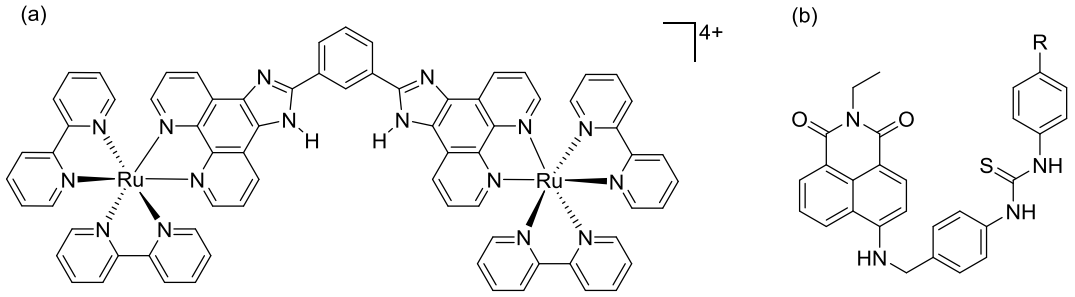

Figure 1.21: Luminescent anion sensors: (a) Ye's bimetallic Ru(II)-based cycnide sensor,[136] (b) Gunnlaugsson's naphthalamide-based sensor[137]

1.2.3 Electrochemical anion sensors

Anions can also be detected by receptors incorporating electrochemically-active groups, when binding results in a perturbation of the respective redox couple. The most commonly exploited redox-active functionality for this type of sensing is ferrocene.[5,138] On addition of anions, cathodic shifts of the ferrocene/ferrocenium redox couple is typically observed, where the proximal bound anion stabilizes the ferrocenium redox state. For example, Tucker and co-

workers have demonstrated the ability of a chiral ferrocene-appended urea receptor to electrochemically discriminate between enantiomers of chiral carboxylate anions in MeCN (**Figure 1.22a**).[139] Cyclic voltammetry experiments showed that (*S*)-*N*-benzenesulfonyl proline was bound 1.7 times more strongly than its (*R*)-enantiomer.

Becher and co-workers have used a calix[4]pyrrole-based receptor containing a redox-active tetrathiafulvalene motif to sense halide anions in MeCN (**Figure 1.22b**).[140] Addition of chloride or bromide, as their TBA salts, resulted in a 40 mV cathodic shift in the first oxidation potential of the tetrathiafulvalene unit.

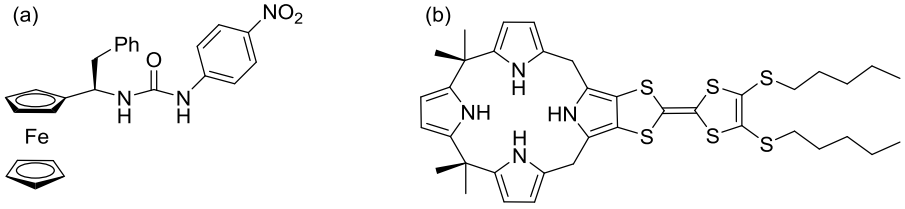

Figure 1.22: Electrochemical anion sensors: (a) Tucker's ferrocene-based sensor,[139] (b) Becher's tetrathiofulvalene-based receptor[140]

1.3 Mechanically Interlocked Molecules

A mechanically interlocked molecule consists of two or more molecules held together by mechanical rather than covalent bonds, with separation of the components requiring the cleavage of a chemical bond. The design and synthesis of such systems has captured the imagination of chemists for the last fifty years or so. This initially stemmed from the challenge associated with their preparation as well as their aesthetically pleasing nature. However, in recent years interest has turned towards their use for practical applications, such as the construction of molecular devices.[141] In the context of anion recognition, interlocked molecules have been demonstrated to function as highly selective receptors.[142,143] Their complex topologies generate three-dimensional binding pockets that are shielded from solvent, and they can therefore be considered as mimics of the anion binding proteins previously discussed (Section 1.1.5).

The most widely investigated forms of interlocked structures are [n]catenanes and [n]rotaxanes, where the [n] prefix refers to the number of molecular components within the structure. Catenanes are species composed of two or more interlocked macrocyclic molecules (**Figure 1.23a**), whilst rotaxanes consist of one or more linear molecules, referred to as axles, threaded through one or more macrocyclic molecules. Bulky stopper groups are attached to both ends of the axle components to prevent dethreading (**Figure 1.23b**). The term pseudorotaxane is used to refer to a system in which the threading components have no stopper groups attached allowing the interpenetrated assembly to form in a reversible fashion (**Figure 1.23c**).

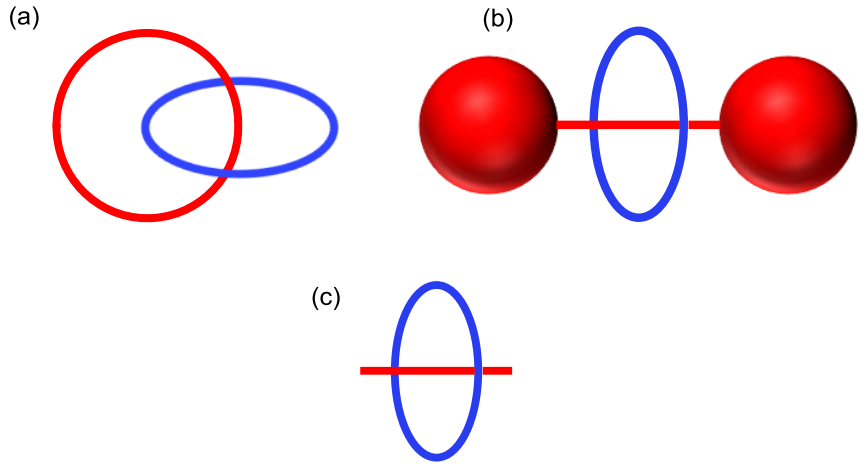

Figure 1.23: Cartoon representations of: (a) [2]catenane, (b) [2]rotaxane, (c) [2]pseudorotaxane

1.3.1 Synthesis of interlocked molecules

Several methods for preparing interlocked structures have been reported to date. For rotaxanes, one of the most commonly used is 'stoppering', which involves the attachment of bulky stopper groups to a preformed pseudorotaxane assembly (**Figure 1.24a**). Another frequently used synthetic strategy is 'clipping', whereby a macrocycle precursor molecule is closed around an axle (**Figure 1.24b**). Less common methods include 'slippage'[144] of a macrocycle over the stopper group of an axle at elevated temperature as well as 'swelling'[145] of a stopper or 'shrinkage'[146,147] of the macrocycle after a pseudorotaxane has been formed.

For catenanes, closure of an acyclic molecule around a macrocycle (**Figure 1.24c**) or double cyclisation methodologies may be employed (**Figure 1.24d**).

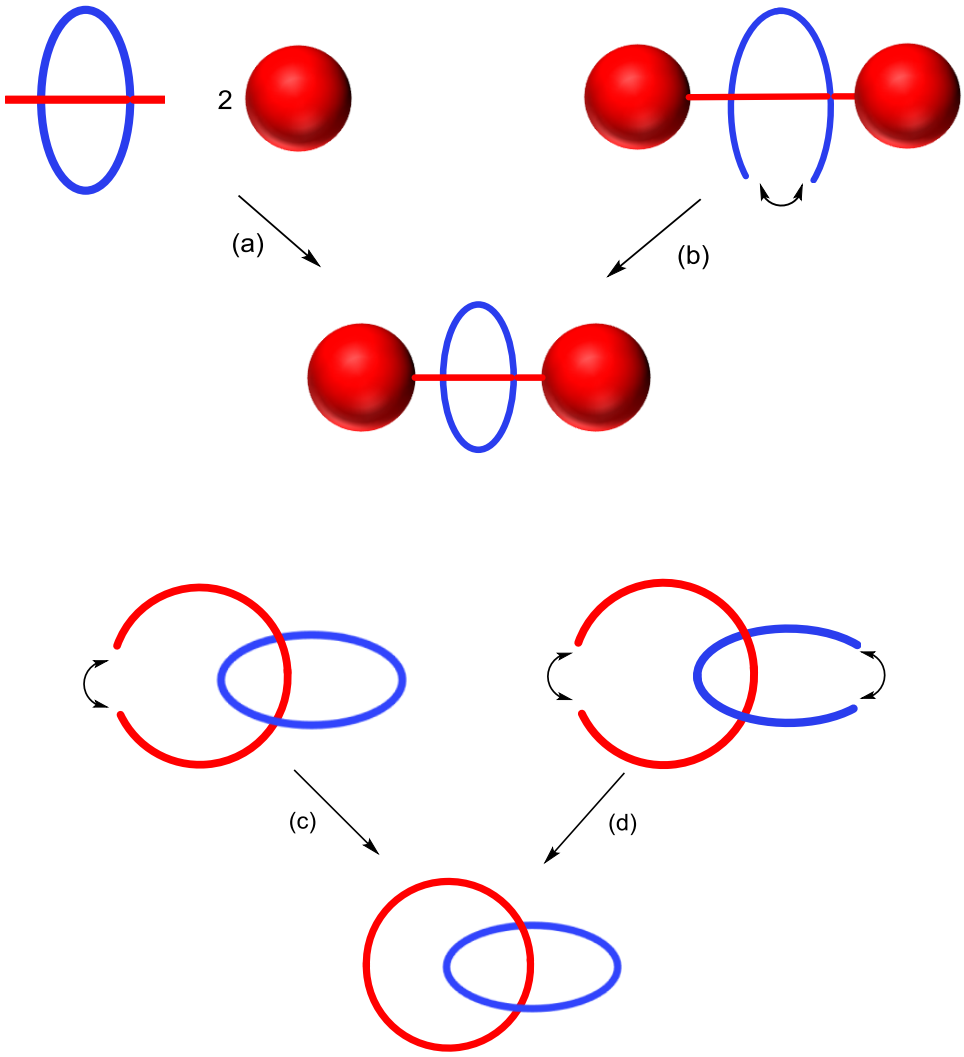

Figure 1.24: Methods of preparing interlocked structures: (a) stoppering and (b) clipping of a [2]rotaxane; (c) clipping and (d) double clipping for a [2]catenane

Another crucial aspect of the synthesis of interlocked structures is the driving force used to bring together their constituent parts. Initially, purely statistical methods were employed; however, these resulted in extremely poor yields.[148,149] For example, Wasserman obtained a less than 1% yield in the first reported synthesis of a [2]catenane (**Scheme 1.1**).[148]

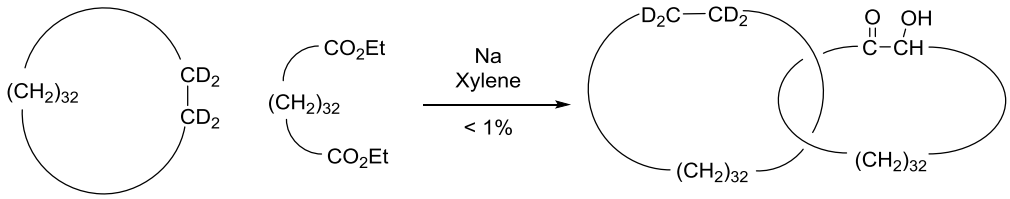

Scheme 1.1: Wasserman's statistical preparation of a [2]catenane[148]

The advent of template-directed synthesis marked an important turning point in this field, allowing for dramatic improvements in yields. The chemical template was first defined by Busch as a species that "*organises an assembly of atoms with respect to one or more geometric loci, in order to achieve a particular linking of atoms*".[150] A variety of templating strategies have been exploited in the synthesis of interlocked molecules, including the use of discrete species such as metal ions or anions, as well as direct interactions between the components of the structure through non-covalent forces such as hydrogen bonding, π-π stacking and the hydrophobic effect.[151,152]

1.3.2 Cation-templated synthesis of interlocked molecules

The first example of the templated synthesis of an interlocked molecule was reported by Sauvage in 1983, who used a Cu(I)-ion in the preparation of a [2]catenane.[153,154] The strategy exploited the tetrahedral coordination geometry preference of the metal, which allowed the formation of an orthogonal complex between a macrocycle and an acyclic molecule, both containing the 2,9-diphenyl-1,10-phenathroline motif. A subsequent Williamson ether macrocyclisation of the acyclic component afforded the interlocked catenane product in a 42% yield (**Scheme 1.2**).

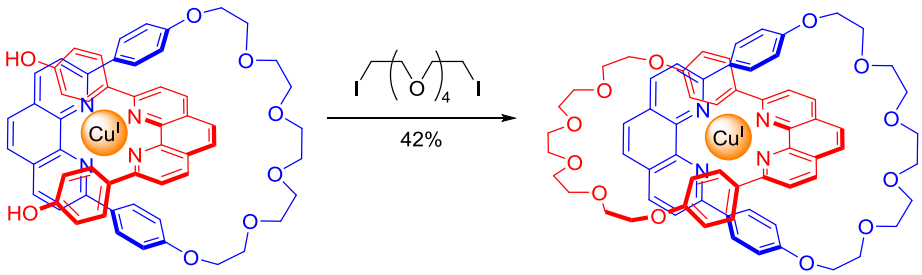

Scheme 1.2: Sauvage's Cu(I)-templated [2]catenane[154]

Since this initial discovery, there have been a multitude of examples of both rotaxanes and catenanes formed using transition metal templates that adopt a diverse range of coordination geometries, including octahedral,[155,156] linear,[157] square planar[158,159] and trigonal bipyramidal.[160] Increasingly complex structures have been prepared, such as Leigh's impressive triply interlocked 'Star of David' [2]catenane, templated by six octahedrally coordinated Fe(II)-ions (**Figure 1.25**).[161]

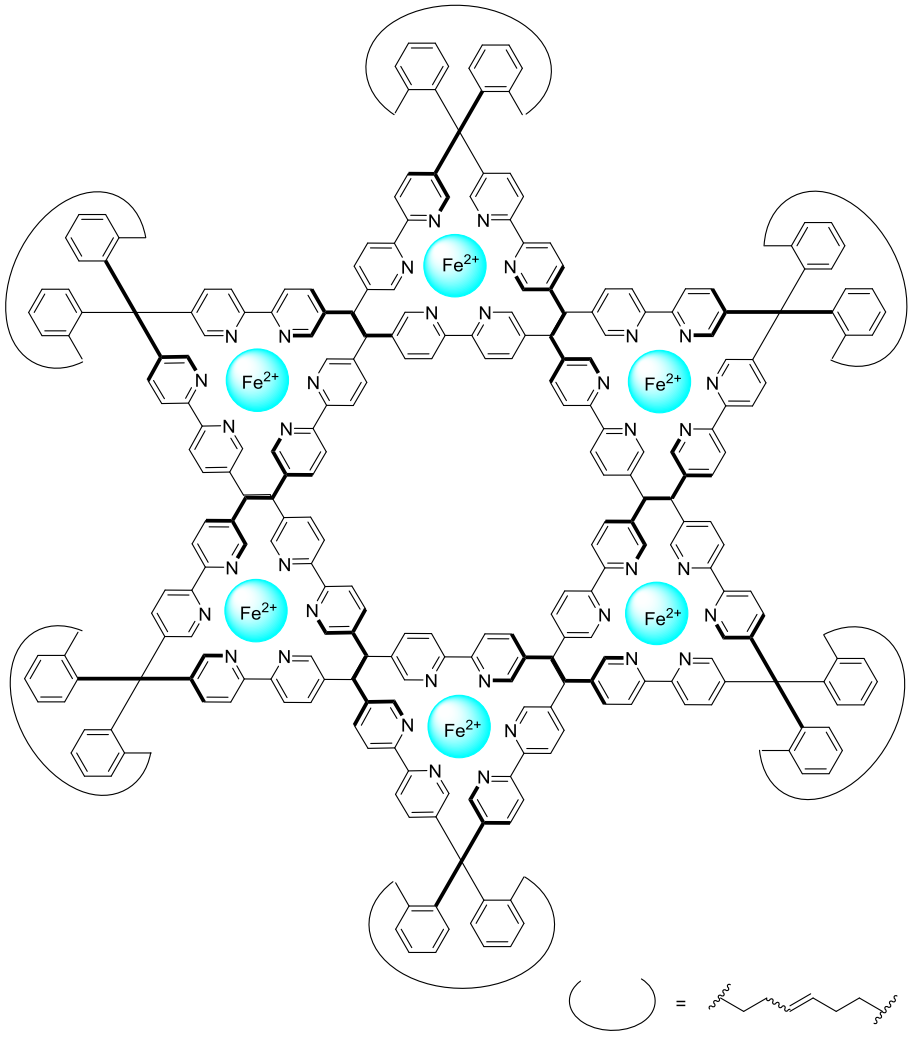

Figure 1.25: Leigh's 'Star of David' [2]catenane[161]

Lanthanide[162,163] and alkali metal cations[164,165] have also been used as templating species, although much less extensively. Chiu and co-workers recently prepared a [2]catenane using sodium cation templation: encapsulation of the metal ion by the ethylene glycol units of two diamine molecules leads to the formation of an orthogonal complex, and a subsequent double

cyclisation Schiff base condensation reaction, with a dialdehyde, gave the interlocked product (**Scheme 1.3**).[164] Importantly, the sodium salt used contained a weakly coordinating tetrakis(3,5-trifluoromethylphenyl)borate (TFPB) counter-anion to maximise the templating effect.

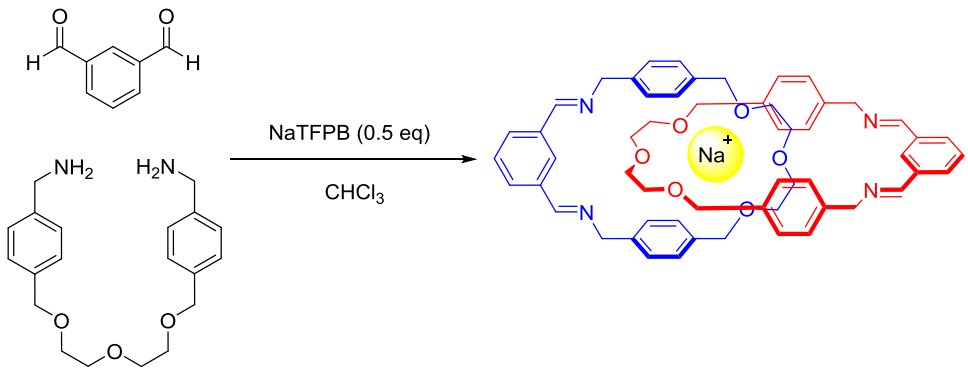

Scheme 1.3: Chiu's sodium cation templated [2]catenane[164]

The above examples describe the use of metals as passive templates, which play a purely organisational role. However in the last decade, the ability of transition metals to catalyse covalent bond formation has been used in conjunction with this templating ability to afford interlocked structures by a process referred to as 'active metal-templation'.[166] Many of the molecules prepared by this technique have utilised copper mediated reactions, such as azide-alkyne cycloadditions[167] or alkyne-alkyne couplings,[168] as they are high-yielding and require relatively mild conditions. Goldup and co-workers have prepared a series of [2]rotaxanes containing macrocycles of varying sizes by this method (**Scheme 1.4**). Coordination of a Cu(I)-ion to the bipyridyl unit of the macrocycles allows catalysis of a 'click' reaction between azide- and alkyne-appended stopper groups to occur within the cyclic cavity.[169] Due to the catalytic nature of the reaction a sub-stoichiometric quantity of the metal can be used.

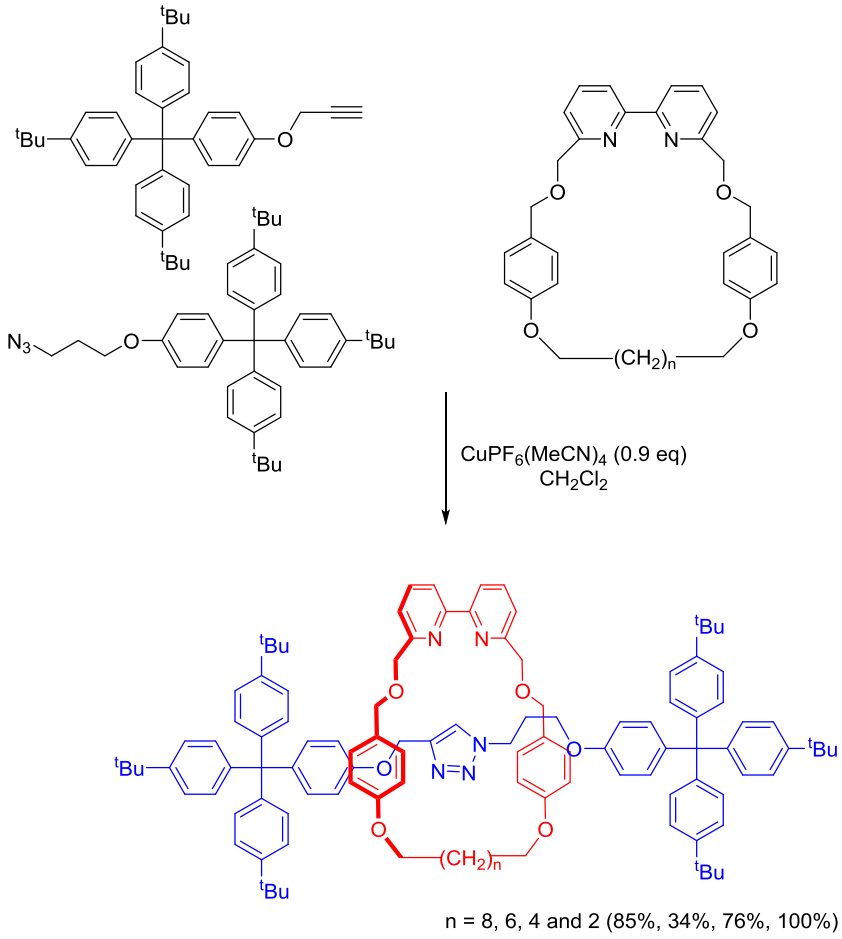

Scheme 1.4: Goldup's active-metal templated [2]rotaxanes[169]

Organic cation templates have also been widely exploited in the preparation of interlocked molecules. In particular, the ability of crown ether macrocycles to complex species such as secondary alkyl ammonium cations and 4,4'-bipyridinium derivatives has been commonly employed as a templating interaction.[170–172] For example, Schalley and co-workers prepared a hetero[3]rotaxane containing an axle component, with two secondary ammonium functionalities, interlocked with dibenzo-24-crown-8 and benzo-21-crown-7 macrocycles (**Scheme 1.5**).[173] The sequence specificity of the macrocycles within the structure is attributed to the ability of the larger 24-membered ring to pass over the central phenyl group of the axle-precursor; in contrast, the smaller benzo-21-crown-7 macrocycle cannot do this.

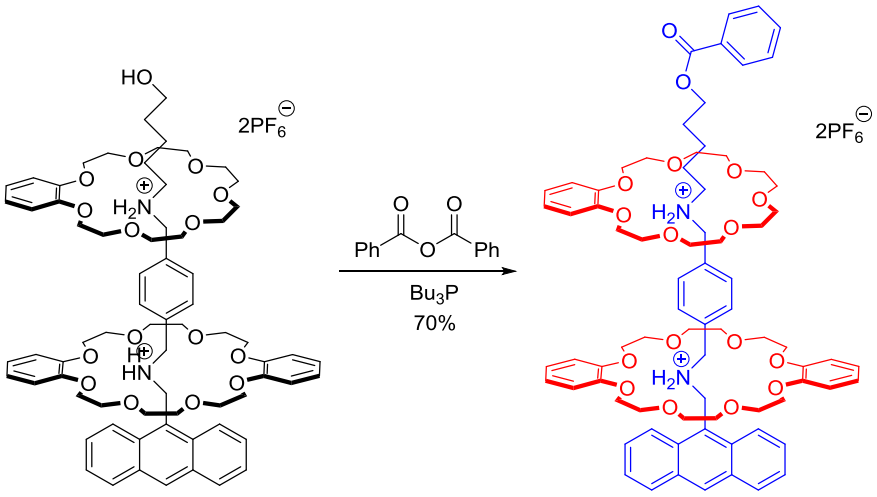

Scheme 1.5: Schalley's hetero[3]rotaxane[173]

Cucurbiturils are another class of macrocyclic molecules that form strong complexes with organic cations. In water, this association is mediated through a combination of the hydrophobic effect and favorable electrostatic and hydrogen bonding interactions with their negatively-polarised carbonyl portals.[174–176] Examples of interlocked structures containing six, seven and eight membered homologues of this macrocycle have been reported, such as Sindelar's [2]rotaxane which contains cucurbit[6]uril and a bis-pyridinium ethylene based axle (**Figure 1.26a**).[177]

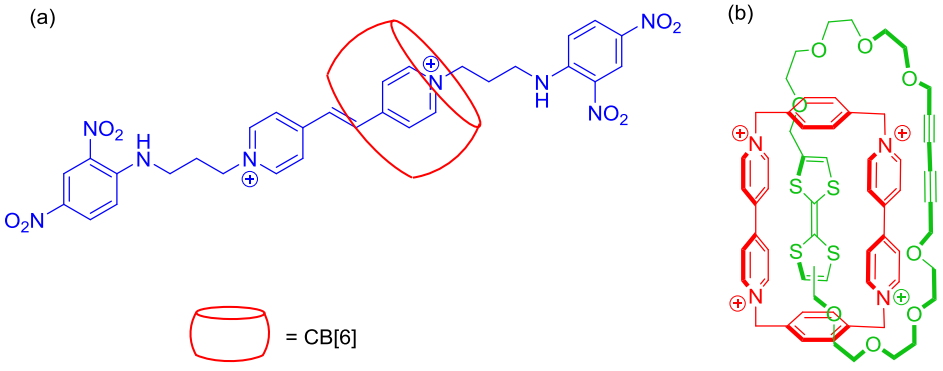

Figure 1.26: Interlocked structures incorporating organic cations: (a) Sindelar's CB[6]-containing [2]rotaxane,[177] (b) Stoddart's $CBPQT^{4+}$ containing [2]catenane[178]

Stoddart has pioneered the use of the cyclobis(paraquat-*p*-phenylene) ($CBPQT^{4+}$) macrocycle in the construction of a series of rotaxanes and catenanes.[179] The π-electron deficient nature of $CBPQT^{4+}$ allows it to form strong π-π donor–acceptor interactions with electron-rich aromatic

species, which can be exploited for templation, as demonstrated by the synthesis of a [2]catenane containing a single tetrathiafulvalene motif (**Figure 1.26b**).[178]

1.3.3 Neutral templated synthesis

The formation of neutral catenane species incorporating tetralactam macrocycles was independently reported by Vögtle and Hunter over twenty years ago (**Scheme 1.6**).[180,181] These serendipitous discoveries attributed the formation of the interlocked products to the ability of such macrocycles to form intermolecular carbonyl-isophthalamide hydrogen bonds.

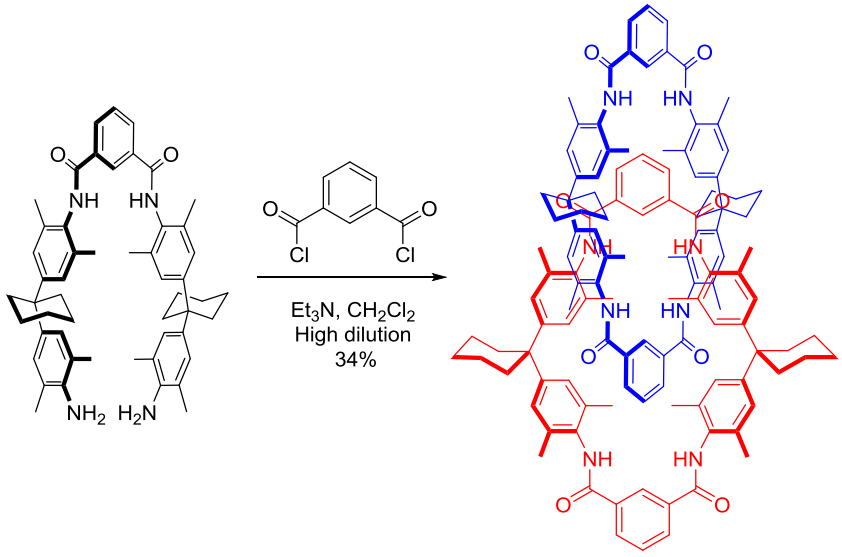

Scheme 1.6: Hunter's teralactam-based homo[2]catenane[181]

Subsequently, a series of rotaxanes containing derivatives of these macrocycles have been reported that are templated through hydrogen bonding interactions with zwitterionic axle components,[182–185] such as Leigh's nitrone-based system (**Figure 1.27a**).[183]

Cyclodextrin macrocycles have frequently been used in the preparation of interlocked molecules in aqueous media, due to their ability to form strong complexes with hydrophobic species.[151] For example, Takata and co-workers synthesised a [3]rotaxane *via* a stoppering methodology, which involved the initial formation of a [3]pseudorotaxane between two α-cyclodextrins and 1,12-diaminododecane (**Figure 1.27b**).[186]

Sanders and co-workers have utilised the π-π donor-acceptor interactions formed between neutral dioxynaphthalene and naphthalenediimide derivatives in the preparation of a [2]catenane using a dynamic combinatorial library approach.[187] The mixing of monomers, in water, afforded a product comprised of interlocked heterodimeric macrocycles, with the stacking groups arranged in the order: donor-acceptor-acceptor-donor (**Figure 1.27c**).

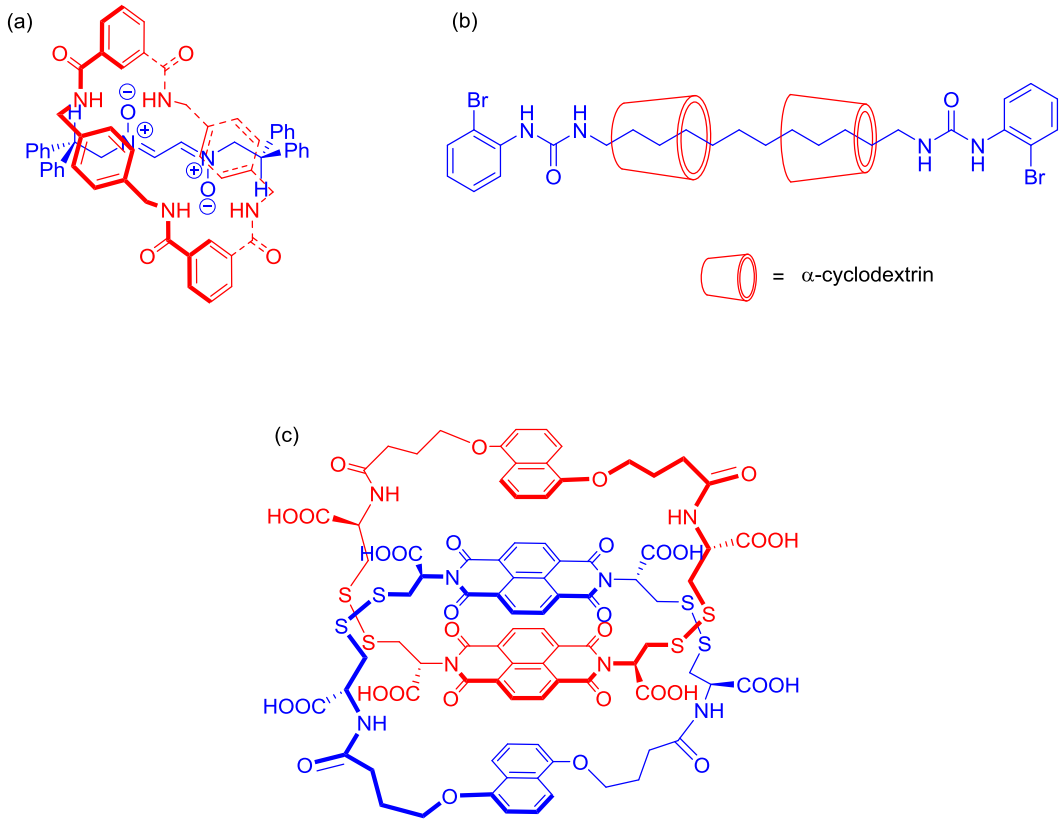

Figure 1.27: Interlocked structures prepared using neutral templating interactions: (a) Leigh's hydrogen-bond templated [2]rotaxane,[183] (b) Takata's α-cyclodextrin [3]rotaxane,[186] (c) Sanders' donor-acceptor templated [2]catenane[187]

1.3.4 Anion templated synthesis

Examples of interlocked structures templated by anionic species are relatively limited in comparison to the large number of structures prepared by the methods discussed above.[142,188] This can be ascribed to the poorly defined coordination geometries present in anion complexes, which makes it difficult to arrange the components of a target interlocked molecule in the desired orientation.[152]

The first interlocked molecule prepared by anion templation was reported as recently as 1999 by Vögtle, who exploited the hydrogen bonding interaction between a phenoxide anion and a tetralactam macrocycle in the synthesis of a [2]rotaxane. Reaction of the complexed anion with an alkyl bromide-appended stopper group afforded the interlocked product in an impressive yield of 95% (**Scheme 1.7**).[189]

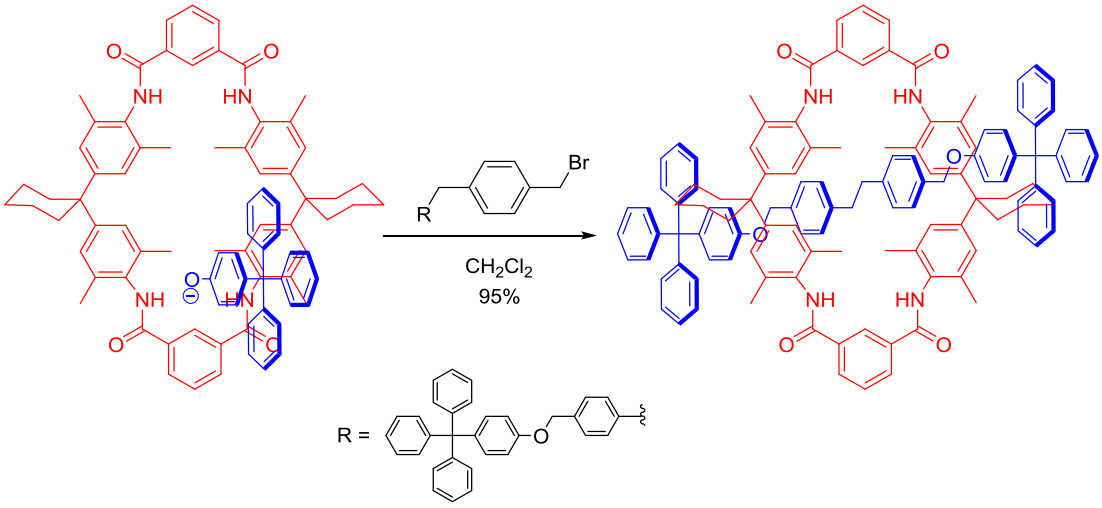

Scheme 1.7: Vögtle's phenoxide template [2]rotaxane[189]

Shortly after this, Beer and co-workers demonstrated the use of discrete anion templation in the preparation of a [2]rotaxane by a clipping method.[190] Taking inspiration from Sauvage's seminal work on Cu(I) templation,[153] their strategy involved the initial formation of an orthogonal complex between an isophthalamide macrocycle precursor and a pyridinium bis-amide axle, with both components forming hydrogen bonding interactions with a templating chloride anion. The stability of this assembly is further augmented by π-π aromatic donor-acceptor interactions between the pyridinium ring and the hydroquinone groups of the macrocycle precursor, as well as additional hydrogen bonding interactions between ethylene glycol units and the *N*-methyl pyridinium group. Subsequently, a ring closing metathesis reaction was used to give the interlocked product in a 47% yield (**Scheme 1.8**).

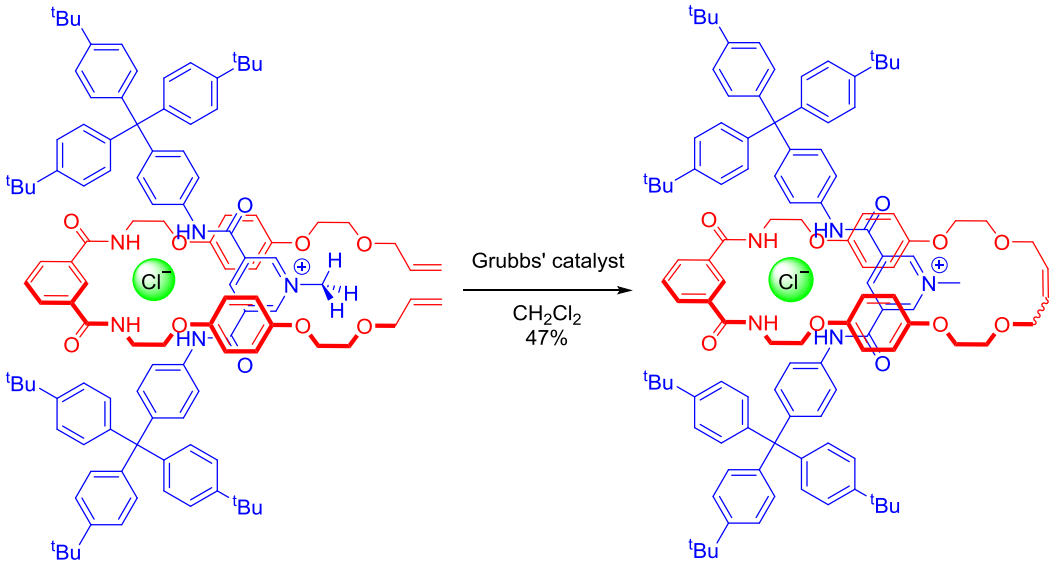

Scheme 1.8: Beer's seminal [2]rotaxane, prepared using discrete chloride templation[190]

Following this report, a variety of interlocked structures have been prepared that exploit a range of anion templates[191–195] as well as different hydrogen bond donor motifs, such as triazole,[196,197] triazolium[198–200] and imidazolium.[201] For example, Beer utilized the trigonal planar geometry of nitrate in the construction of a [2]rotaxane,[193] whilst Jeong and co-workers reported an indolocarbazole-based homo[2]catenane prepared by chloride templation (**Figure 1.28a**).[202]

The interaction between halogen bond donors and anions has recently been recognised as another templating interaction that can be used to prepare interlocked architectures.[115] The first example, reported by Beer in 2010, used bromide anion templation in the formation of a [2]rotaxane containing a 5-iodotriazolium axle component and an isophthalamide macrocycle (**Figure 1.28b**).[45]

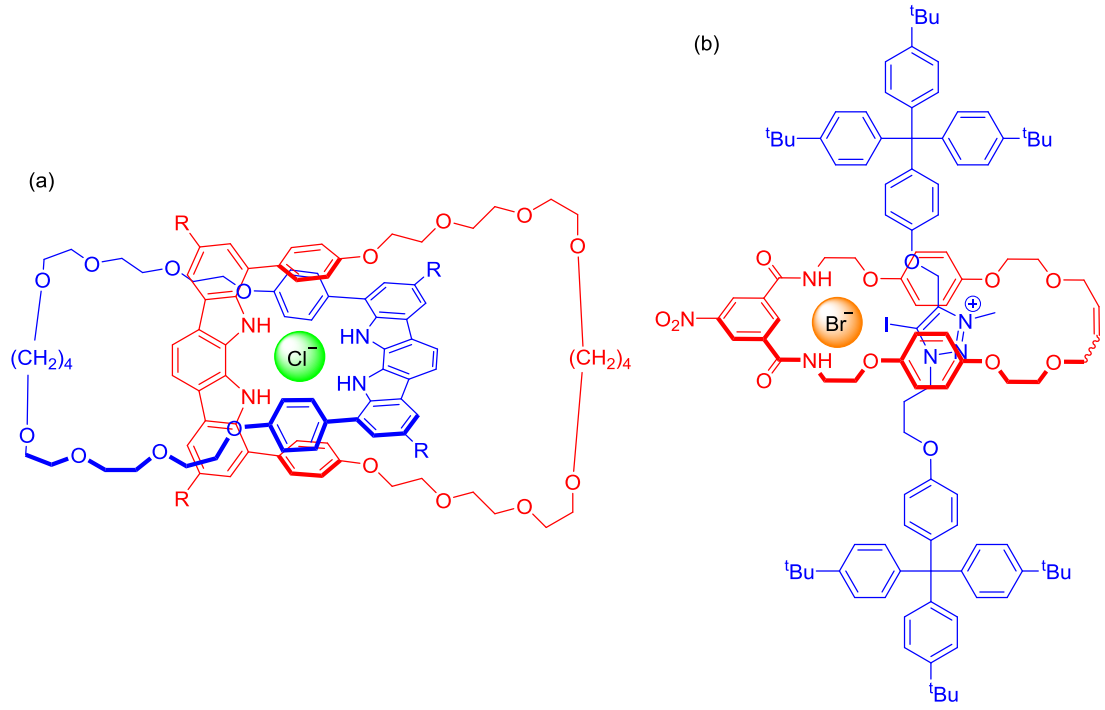

Figure 1.28: Interlocked structures prepared using discrete anion templation: (a) Jeong's chloride templated indolocarbazole [2]catenane,[202] (b) Beer's halogen bond templated [2]rotaxane[45]

1.3.5 Interlocked molecules as anion receptors and sensors

As previously mentioned, the topologically unique three-dimensional binding pockets present between the components of interlocked molecules allows them to function as host systems. In cases where a discrete anion template has been used during synthesis, its replacement with a non-coordinating anion leads to the formation of a receptor that typically shows selectivity towards the templating species. For example, Beer and co-workers found that a dicationic [2]rotaxane selectively bound its templating anion, chloride, in 65:35 d_6-acetone/D_2O, with no binding of acetate or dihydrogen phosphate observed (**Figure 1.29**).[203] This selectivity was attributed to the complementary size and shape of the binding pocket of the rotaxane to the halide anion. In contrast, the larger size of the oxoanions prevents their full encapsulation within the interlocked host structure.

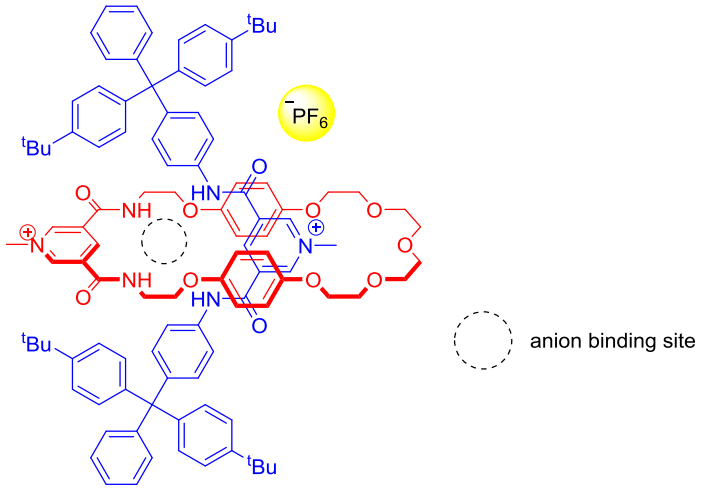

Figure 1.29: Beer's chloride selective [2]rotaxane[203]

Interlocked molecules may also be used as anion sensors through the incorporation of a reporter group into their structure. Several examples of rotaxanes appended with luminescent transition metal motifs have demonstrated sensing properties, such as Beer's halogen bonding, Ru(II)-bipyridyl containing system, which showed an enhancement in its MLCT emission upon the addition of iodide in pure water (**Figure 1.30**).[204]

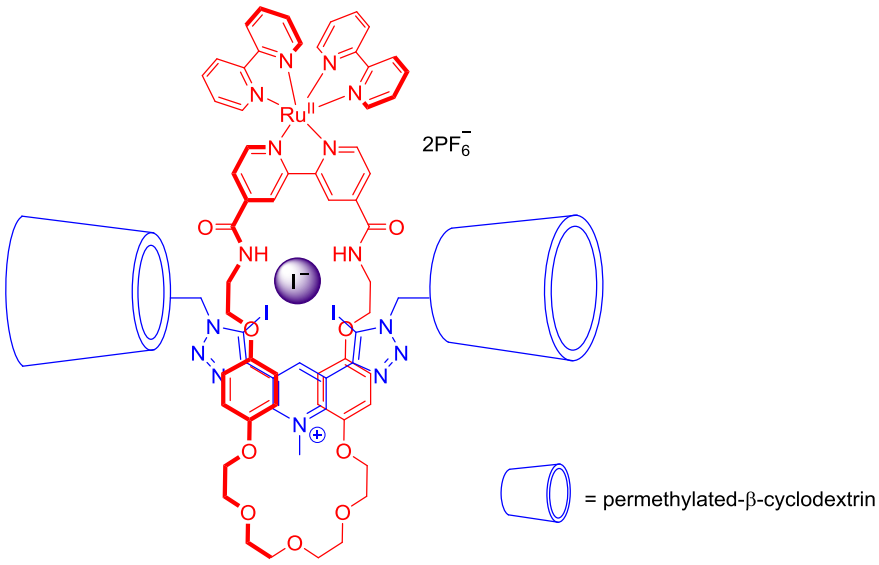

Figure 1.30: Beer's luminescent Ru(II)bipyridyl containing iodide sensor[204]

The inclusion of organic fluorophores into interlocked architectures has also been used to generate optical anion sensors. Lin reported a [2]rotaxane containing the diketopyrollopyrolle motif that selectively senses fluoride by a colorimetric and luminescent response in DMSO

(**Figure 1.31a**).[205] Similarly, Smith used a squaraine-based [2]rotaxane to sense chloride in $CHCl_3$.[206] In the presence of the halide anion, translocation of the macrocycle component away from the central dye unit of the axle towards the triazole motif results in a dramatic increase in the emission intensity of the dye (**Figure 1.31b**).

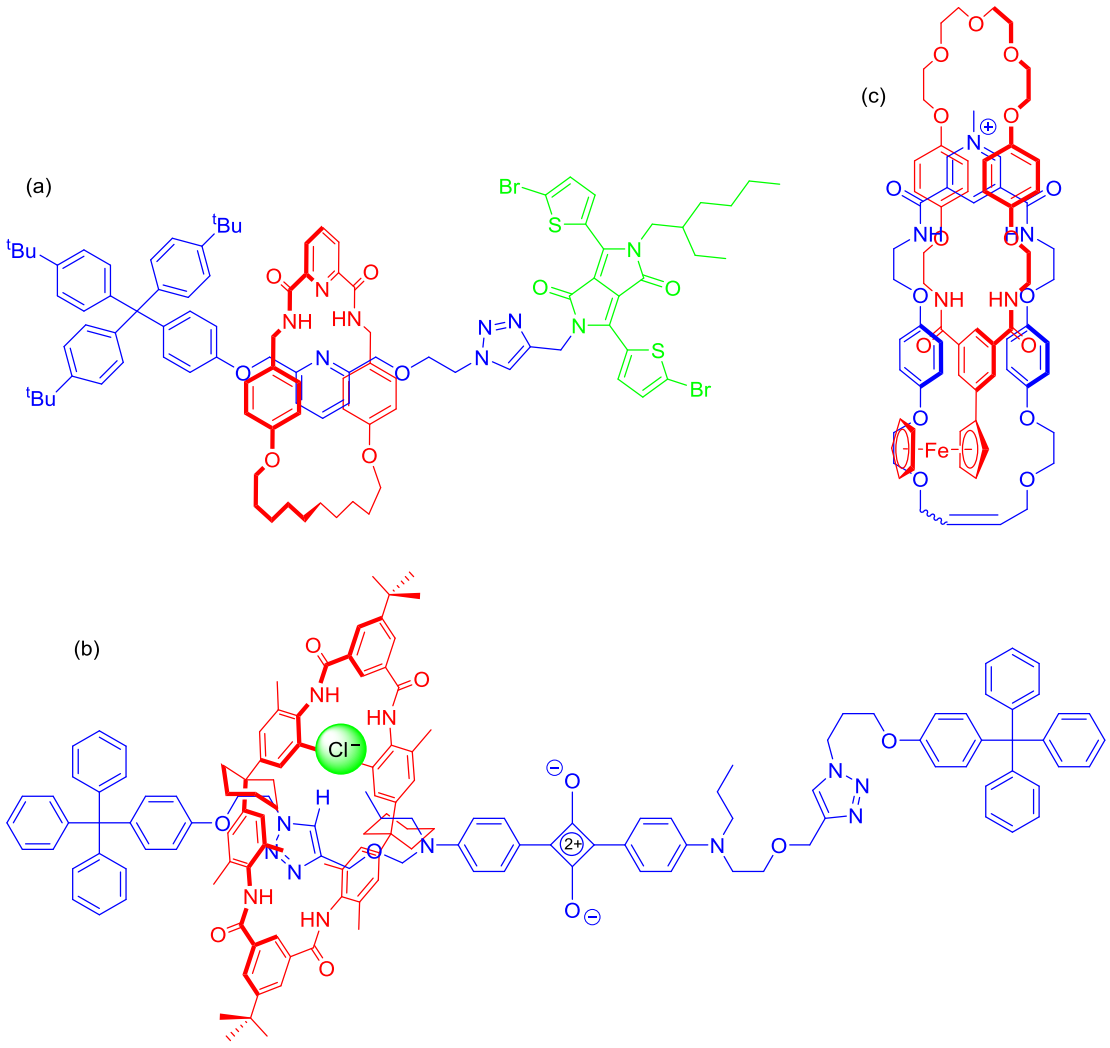

Figure 1.31: Anion sensing interlocked structures: (a) Lin's fluoride sensor,[205] (b) Smiths's chloride sensing [2]rotaxane shuttle,[206] (c) Beer's ferrocene containing [2]catenane[207]

Beer and co-workers have prepared a series of redox-active interlocked hosts incorporating ferrocene motifs,[207–211] such as a [2]catenane which showed a 20 mV cathodic shift in its ferrocene/ferrocenium redox couple upon addition of one equivalent of chloride in 1:1 CH_2Cl_2/CH_3CN (**Figure 1.31c**).[207]

1.3.6 Other applications of interlocked molecules

Over the last few years, the fabrication of nanoscale devices that exploit the dynamic behavior of interlocked molecules has attracted much attention. In catenanes, this motion is purely rotational, whereas in rotaxanes both shuttling and rotary motion are possible. Importantly, these movements can be controlled through the use of external stimuli as demonstrated by Kaifer and co-workers, who prepared a [2]rotaxane in which the shuttling motion of a $CBPQT^{4+}$ macrocycle along an axle containing benzidine and biphenol motifs could be controlled by addition of acid or base or electrochemically (**Figure 1.32**).[212] Stimuli controlled motion has since been used in the construction of more elaborate, functional molecular machines and switches such as logic gates,[213,214] nanomotors,[215–217] ratchets,[218,219] artificial molecular muscles[220,221] and a sequence-specific peptide synthesizer.[222]

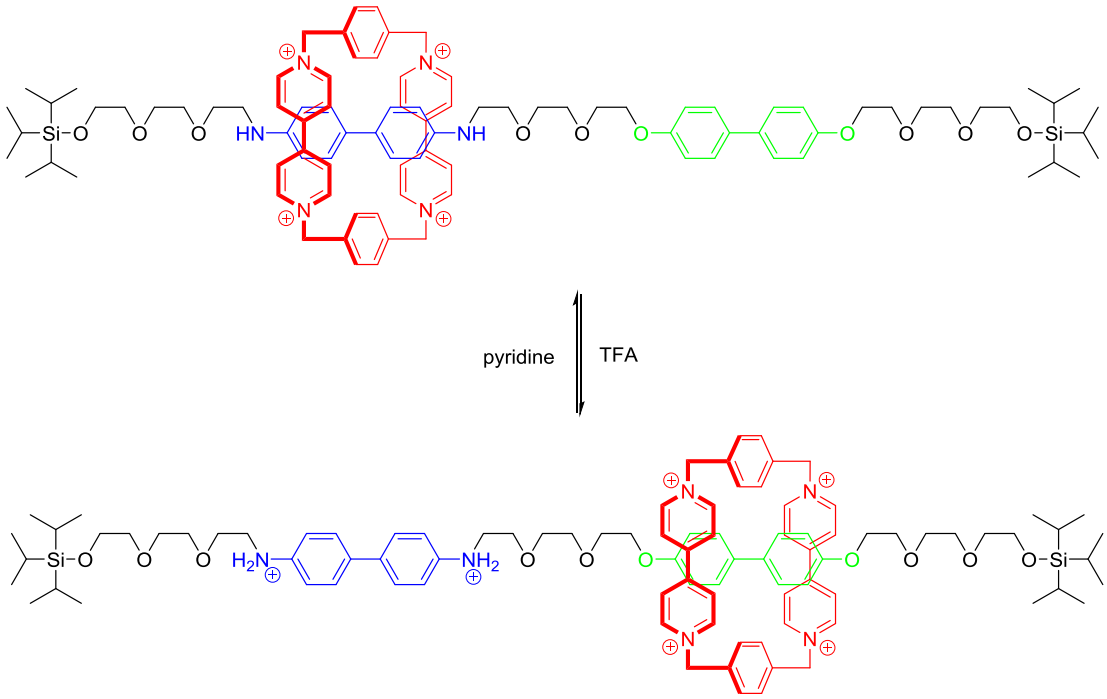

Figure 1.32: Kaifer's pH and electrochemical responsive [2]rotaxane[212]

Interlocked molecules have also been used in the field of supramolecular catalysis, where their constrained environments and dynamic motions have been used to control the reactivity of catalytic groups incorporated into their structures.[223] For example, Leigh and co-workers

very recently reported the first use of an interlocked structure as a ligand for asymmetric transition metal catalysis. Coordination of a Ni(II)-ion to a [2]rotaxane was used to catalyse the enantioselective Michael addition reaction of diethyl malonate with trans-β-nitrostyrene (**Scheme 1.9**).[224] The enantiomeric excess of the reaction was significantly reduced when an acyclic ligand system was used, highlighting the importance of the more structurally defined binding pocket of the rotaxane.

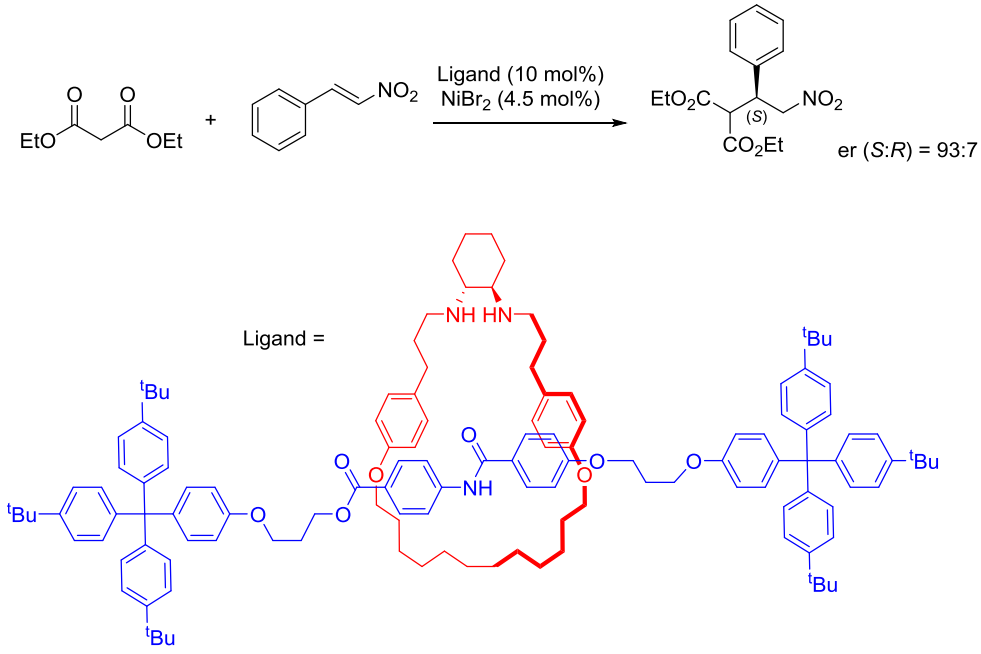

Scheme 1.9: Leigh's asymmetric catalysis using a [2]rotaxane ligand[224]

1.4 Project Outline

The work in this thesis is broadly concerned with the preparation of acyclic, macrocyclic and interlocked receptors for the recognition of anions in competitive organic and aqueous solvent media. Particular attention is paid to comparing the anion binding properties of hosts containing the halogen bonding 5-iodo-1,2,3-triazole motif and their hydrogen bonding prototriazole analogues, with the aim of further investigating the differences between these two interactions. Interlocked receptors incorporating Lewis acidic triarylborane anion binding motifs are also investigated.

Chapter Two discusses the preparation of pyridinium-based acyclic and interlocked receptors. Investigations into the anion selectivity trends of halogen and hydrogen bonding hosts are undertaken using ^{1}H NMR titration experiments. Substitution of the pyridinium unit of these receptors with a fluorescent quinolinium motif is also undertaken to afford luminescent anion sensors.

Chapter Three concerns the synthesis of acyclic and macrocyclic receptors containing the dicationic 1,2-bis(pyridinium)ethane motif. Attempts towards the preparation of interlocked receptors containing the motif are also discussed.

Chapter Four focuses on a series of water soluble receptors based around functionalised α-cyclodextrins. Isothermal titration calorimetry experiments are used to investigate differences in the thermodynamics of anion binding to halogen bonding and hydrogen bonding analogues.

Chapter Five details the preparation of a [2]rotaxane containing an axle component with a triarylborane motif as a stopper group. Investigations into its anion binding properties are conducted using multinuclear NMR and UV-visible spectroscopies.

1.5 References

1 C. H. Park and H. E. Simmons, *J. Am. Chem. Soc.*, 1968, **90**, 2431–2432.
2 C. J. Pedersen, *Angew. Chem. Int. Ed. Engl.*, 1988, **27**, 1021–1027.
3 J.-M. Lehn, *Angew. Chem. Int. Ed. Engl.*, 1988, **27**, 89–112.
4 D. J. Cram, *Angew. Chem. Int. Ed. Engl.*, 1988, **27**, 1009–1020.
5 N. H. Evans and P. D. Beer, *Angew. Chem. Int. Ed.*, 2014, **53**, 11716–11754.
6 J. L. Sessler, P. Gale, W.-S. Cho, J. F. Stoddart, S. J. Rowan, T. Aida and A. E. Rowan, *Anion Receptor Chemistry*, The Royal Society of Chemistry, 2006.
7 A. L. Berger, C. O. Randak, L. S. Ostedgaard, P. H. Karp, D. W. Vermeer and M. J. Welsh, *J. Biol. Chem.*, 2005, **280**, 5221–5226.
8 R. J. Carton, *Fluoride*, 2006, **39**, 163–172.
9 F. J. Baud, *Hum. Exp. Toxicol.*, 2007, **26**, 191–201.
10 V. H. Smith, G. D. Tilman and J. C. Nekola, *Environ. Pollut.*, 1999, **100**, 179–196.
11 E. A. Katayev, G. V. Kolesnikov and J. L. Sessler, *Chem. Soc. Rev.*, 2009, **38**, 1572–1586.
12 F. Hofmeister, *Arch. Für Exp. Pathol. Pharmakol.*, 1888, **24**, 247–260.
13 M. Boiocchi, L. Del Boca, D. E. Gómez, L. Fabbrizzi, M. Licchelli and E. Monzani, *J. Am. Chem. Soc.*, 2004, **126**, 16507–16514.
14 V. Amendola, D. Esteban-Gómez, L. Fabbrizzi and M. Licchelli, *Acc. Chem. Res.*, 2006, **39**, 343–353.
15 P. A. Gale, *Acc. Chem. Res.*, 2006, **39**, 465–475.

16 T. Gunnlaugsson, M. Glynn, G. M. Tocci (née Hussey), P. E. Kruger and F. M. Pfeffer, *Coord. Chem. Rev.*, 2006, **250**, 3094–3117.
17 H. Juwarker, J. M. Lenhardt, J. C. Castillo, E. Zhao, S. Krishnamurthy, R. M. Jamiolkowski, K.-H. Kim and S. L. Craig, *J. Org. Chem.*, 2009, **74**, 8924–8934.
18 Y. Hua, R. O. Ramabhadran, E. O. Uduehi, J. A. Karty, K. Raghavachari and A. H. Flood, *Chem. – Eur. J.*, 2011, **17**, 312–321.
19 J. L. Sessler, D. E. Gross, W.-S. Cho, V. M. Lynch, F. P. Schmidtchen, G. W. Bates, M. E. Light and P. A. Gale, *J. Am. Chem. Soc.*, 2006, **128**, 12281–12288.
20 D. B. Varshey, J. R. G. Sander, T. Friščić and L. R. MacGillivray, in *Supramolecular Chemistry*, John Wiley & Sons, Ltd, 2012.
21 G. R. Desiraju, P. S. Ho, L. Kloo, A. C. Legon, R. Marquardt, P. Metrangolo, P. Politzer, G. Resnati and K. Rissanen, *Pure Appl. Chem.*, 2013, **85**, 1711–1713.
22 A. C. Legon, *Angew. Chem. Int. Ed.*, 1999, **38**, 2686–2714.
23 P. Metrangolo, F. Meyer, T. Pilati, G. Resnati and G. Terraneo, *Angew. Chem. Int. Ed.*, 2008, **47**, 6114–6127.
24 C. A. Hunter, *Angew. Chem. Int. Ed.*, 2004, **43**, 5310–5324.
25 J. L. Cook, C. A. Hunter, C. M. R. Low, A. Perez-Velasco and J. G. Vinter, *Angew. Chem. Int. Ed.*, 2007, **46**, 3706–3709.
26 T. Clark, M. Hennemann, J. S. Murray and P. Politzer, *J. Mol. Model.*, 2006, **13**, 291–296.
27 R. Cabot and C. A. Hunter, *Chem. Commun.*, 2009, 2005.
28 M. G. Sarwar, B. Dragisic, L. J. Salsberg, C. Gouliaras and M. S. Taylor, *J. Am. Chem. Soc.*, 2010, **132**, 1646–1653.
29 M. G. Chudzinski and M. S. Taylor, *J. Org. Chem.*, 2012, **77**, 3483–3491.
30 L. J. McAllister, D. W. Bruce and P. B. Karadakov, *J. Phys. Chem. A*, 2012, **116**, 10621–10628.
31 C. C. Robertson, R. N. Perutz, L. Brammer and C. A. Hunter, *Chem. Sci.*, 2014, **5**, 4179–4183.
32 K. Rissanen, *CrystEngComm*, 2008, **10**, 1107–1113.
33 C. B. Aakeröy, N. R. Champness and C. Janiak, *CrystEngComm*, 2009, **12**, 22–43.
34 R. Bertani, P. Sgarbossa, A. Venzo, F. Lelj, M. Amati, G. Resnati, T. Pilati, P. Metrangolo and G. Terraneo, *Coord. Chem. Rev.*, 2010, **254**, 677–695.
35 P. Metrangolo and G. Resnati, *Cryst. Growth Des.*, 2012, **12**, 5835–5838.
36 P. Metrangolo, G. Resnati, T. Pilati, R. Liantonio and F. Meyer, *J. Polym. Sci. Part Polym. Chem.*, 2007, **45**, 1–15.
37 D. W. Bruce, P. Metrangolo, F. Meyer, T. Pilati, C. Präsang, G. Resnati, G. Terraneo, S. G. Wainwright and A. C. Whitwood, *Chem. – Eur. J.*, 2010, **16**, 9511–9524.
38 F. Meyer and P. Dubois, *CrystEngComm*, 2013, **15**, 3058–3071.
39 A. Priimagi, G. Cavallo, P. Metrangolo and G. Resnati, *Acc. Chem. Res.*, 2013, **46**, 2686–2695.
40 A. Bruckmann, M. Pena and C. Bolm, *Synlett*, 2008, **2008**, 900–902.
41 O. Coulembier, F. Meyer and P. Dubois, *Polym. Chem.*, 2010, **1**, 434–437.
42 S. M. Walter, F. Kniep, E. Herdtweck and S. M. Huber, *Angew. Chem. Int. Ed.*, 2011, **50**, 7187–7191.
43 F. Kniep, S. H. Jungbauer, Q. Zhang, S. M. Walter, S. Schindler, I. Schnapperelle, E. Herdtweck and S. M. Huber, *Angew. Chem. Int. Ed.*, 2013, **52**, 7028–7032.
44 C. J. Serpell, N. L. Kilah, P. J. Costa, V. Félix and P. D. Beer, *Angew. Chem. Int. Ed.*, 2010, **49**, 5322–5326.
45 N. L. Kilah, M. D. Wise, C. J. Serpell, A. L. Thompson, N. G. White, K. E. Christensen and P. D. Beer, *J. Am. Chem. Soc.*, 2010, **132**, 11893–11895.
46 L.-Y. You, S.-G. Chen, X. Zhao, Y. Liu, W.-X. Lan, Y. Zhang, H.-J. Lu, C.-Y. Cao and Z.-T. Li, *Angew. Chem. Int. Ed.*, 2012, **51**, 1657–1661.
47 O. Dumele, N. Trapp and F. Diederich, *Angew. Chem. Int. Ed.*, 2015, **54**, 12339–12344.
48 M. Llinàs-Brunet, M. D. Bailey, N. Goudreau, P. K. Bhardwaj, J. Bordeleau, M. Bös, Y. Bousquet, M. G. Cordingley, J. Duan, P. Forgione, M. Garneau, E. Ghiro, V. Gorys, S. Goulet, T. Halmos, S. H. Kawai, J. Naud, M.-A. Poupart and P. W. White, *J. Med. Chem.*, 2010, **53**, 6466–6476.

49 L. A. Hardegger, B. Kuhn, B. Spinnler, L. Anselm, R. Ecabert, M. Stihle, B. Gsell, R. Thoma, J. Diez, J. Benz, J.-M. Plancher, G. Hartmann, D. W. Banner, W. Haap and F. Diederich, *Angew. Chem. Int. Ed.*, 2011, **50**, 314–318.
50 H. T. Chifotides and K. R. Dunbar, *Acc. Chem. Res.*, 2013, **46**, 894–906.
51 D. Quiñonero, C. Garau, C. Rotger, A. Frontera, P. Ballester, A. Costa and P. M. Deyà, *Angew. Chem. Int. Ed.*, 2002, **41**, 3389–3392.
52 S. Demeshko, S. Dechert and F. Meyer, *J. Am. Chem. Soc.*, 2004, **126**, 4508–4509.
53 P. de Hoog, P. Gamez, I. Mutikainen, U. Turpeinen and J. Reedijk, *Angew. Chem. Int. Ed.*, 2004, **43**, 5815–5817.
54 R. E. Dawson, A. Hennig, D. P. Weimann, D. Emery, V. Ravikumar, J. Montenegro, T. Takeuchi, S. Gabutti, M. Mayor, J. Mareda, C. A. Schalley and S. Matile, *Nat. Chem.*, 2010, **2**, 533–538.
55 A. Frontera, *Coord. Chem. Rev.*, 2013, **257**, 1716–1727.
56 Y. Zhao, Y. Domoto, E. Orentas, C. Beuchat, D. Emery, J. Mareda, N. Sakai and S. Matile, *Angew. Chem. Int. Ed.*, 2013, **52**, 9940–9943.
57 M. Giese, M. Albrecht and K. Rissanen, *Chem. Rev.*, 2015, **115**, 8867–8895.
58 C. R. Wade, A. E. J. Broomsgrove, S. Aldridge and F. P. Gabbaï, *Chem. Rev.*, 2010, **110**, 3958–3984.
59 H. Zhao, L. A. Leamer and F. P. Gabbaï, *Dalton Trans.*, 2013, **42**, 8164–8178.
60 M. Newcomb, J. H. Horner and M. T. Blanda, *J. Am. Chem. Soc.*, 1987, **109**, 7878–7879.
61 M. Newcomb and M. T. Blanda, *Tetrahedron Lett.*, 1988, **29**, 4261–4264.
62 M. T. Blanda, J. H. Horner and M. Newcomb, *J. Org. Chem.*, 1989, **54**, 4626–4636.
63 M. T. Blanda and M. A. Herren, *Chem. Commun.*, 2000, 343–344.
64 M. Schulte, M. Schürmann and K. Jurkschat, *Chem. – Eur. J.*, 2001, **7**, 347–355.
65 T. J. Wedge and M. F. Hawthorne, *Coord. Chem. Rev.*, 2003, **240**, 111–128.
66 K. I. Tugashov, D. A. Gribanyov, F. M. Dolgushin, A. F. Smol'yakov, A. S. Peregudov, M. K. Minacheva, B. N. Strunin, I. A. Tikhonova and V. B. Shur, *J. Organomet. Chem.*, 2013, **747**, 167–173.
67 Y. Agnus, R. Louis and R. Weiss, *J. Am. Chem. Soc.*, 1979, **101**, 3381–3384.
68 S. L. Tobey and E. V. Anslyn, *J. Am. Chem. Soc.*, 2003, **125**, 14807–14815.
69 A. Brugnara, F. Topić, K. Rissanen, A. de la Lande, B. Colasson and O. Reinaud, *Chem. Sci.*, 2014, **5**, 3897–3904.
70 H. T. Ngo, X. Liu and K. A. Jolliffe, *Chem. Soc. Rev.*, 2012, **41**, 4928–4965.
71 J. Pouessel, N. L. Bris, A. Bencini, C. Giorgi, B. Valtancoli and R. Tripier, *Dalton Trans.*, 2012, **41**, 10521–10532.
72 W. Xu, J. J. Vittal and R. J. Puddephatt, *J. Am. Chem. Soc.*, 1993, **115**, 6456–6457.
73 N. L. S. Yue, M. C. Jennings and R. J. Puddephatt, *Inorg. Chem.*, 2005, **44**, 1125–1131.
74 M. A. Yawer, V. Havel and V. Sindelar, *Angew. Chem. Int. Ed.*, 2015, **54**, 276–279.
75 M. Lisbjerg, B. E. Nielsen, B. O. Milhøj, S. P. A. Sauer and M. Pittelkow, *Org. Biomol. Chem.*, 2014, **13**, 369–373.
76 K. I. Assaf, M. S. Ural, F. Pan, T. Georgiev, S. Simova, K. Rissanen, D. Gabel and W. M. Nau, *Angew. Chem. Int. Ed.*, 2015, **54**, 6852–6856.
77 M. J. Langton, C. J. Serpell and P. D. Beer, *Angew. Chem. Int. Ed.*, 2016, **55**, 1974–1987.
78 E. Fischer, *Berichte Dtsch. Chem. Ges.*, 1894, **27**, 2985–2993.
79 D. E. Koshland, *Angew. Chem. Int. Ed. Engl.*, 1995, **33**, 2375–2378.
80 F. P. Schmidtchen, *Angew. Chem. Int. Ed. Engl.*, 1977, **16**, 720–721.
81 F. P. Schmidtchen, *Chem. Ber.*, 1981, **114**, 597–607.
82 K. N. Trueblood, C. B. Knobler, E. Maverick, R. C. Helgeson, S. B. Brown and D. J. Cram, *J. Am. Chem. Soc.*, 1981, **103**, 5594–5596.
83 D. J. Cram, *Angew. Chem. Int. Ed. Engl.*, 1986, **25**, 1039–1057.
84 M. P. Hughes and B. D. Smith, *J. Org. Chem.*, 1997, **62**, 4492–4499.
85 G. Schwarzenbach, *Helv. Chim. Acta*, 1952, **35**, 2344–2359.
86 D. K. Cabbiness and D. W. Margerum, *J. Am. Chem. Soc.*, 1969, **91**, 6540–6541.
87 A. E. Martell, R. D. Hancock and R. J. Motekaitis, *Coord. Chem. Rev.*, 1994, **133**, 39–65.
88 H. Luecke and F. A. Quiocho, *Nature*, 1990, **347**, 402–406.
89 J. W. Pflugrath and F. A. Quiocho, *J. Mol. Biol.*, 1988, **200**, 163–180.

90 J. M. Llinares, D. Powell and K. Bowman-James, *Coord. Chem. Rev.*, 2003, **240**, 57–75.
91 J. M. Lehn, E. Sonveaux and A. K. Willard, *J. Am. Chem. Soc.*, 1978, **100**, 4914–4916.
92 B. Dietrich, J. Guilhem, J.-M. Lehn, C. Pascard and E. Sonveaux, *Helv. Chim. Acta*, 1984, **67**, 91–104.
93 R. J. Motekaitis, A. E. Martell, I. Murase, J. M. Lehn and M. W. Hosseini, *Inorg. Chem.*, 1988, **27**, 3630–3636.
94 B. Dietrich, B. Dilworth, J.-M. Lehn, J.-P. Souchez, M. Cesario, J. Guilhem and C. Pascard, *Helv. Chim. Acta*, 1996, **79**, 569–587.
95 C. Bazzicalupi, A. Bencini, C. Giorgi, B. Valtancoli, V. Lippolis and A. Perra, *Inorg. Chem.*, 2011, **50**, 7202–7216.
96 E. Fan, S. A. Van Arman, S. Kincaid and A. D. Hamilton, *J. Am. Chem. Soc.*, 1993, **115**, 369–370.
97 V. D. Jadhav and F. P. Schmidtchen, *J. Org. Chem.*, 2008, **73**, 1077–1087.
98 K. Kavallieratos, S. R. de Gala, D. J. Austin and R. H. Crabtree, *J. Am. Chem. Soc.*, 1997, **119**, 2325–2326.
99 S. O. Kang, J. M. Llinares, D. Powell, D. VanderVelde and K. Bowman-James, *J. Am. Chem. Soc.*, 2003, **125**, 10152–10153.
100 S. O. Kang, D. VanderVelde, D. Powell and K. Bowman-James, *J. Am. Chem. Soc.*, 2004, **126**, 12272–12273.
101 S. Kubik, R. Goddard, R. Kirchner, D. Nolting and J. Seidel, *Angew. Chem. Int. Ed.*, 2001, **40**, 2648–2651.
102 S. Kubik, R. Kirchner, D. Nolting and J. Seidel, *J. Am. Chem. Soc.*, 2002, **124**, 12752–12760.
103 F. Sommer and S. Kubik, *Org. Biomol. Chem.*, 2014, **12**, 8851–8860.
104 V. Blažek Bregović, N. Basarić and K. Mlinarić-Majerski, *Coord. Chem. Rev.*, 2015, **295**, 80–124.
105 C. Jia, B. Wu, S. Li, X. Huang, Q. Zhao, Q.-S. Li and X.-J. Yang, *Angew. Chem. Int. Ed.*, 2011, **50**, 486–490.
106 J. L. Sessler, S. Camiolo and P. A. Gale, *Coord. Chem. Rev.*, 2003, **240**, 17–55.
107 I. Saha, J. T. Lee and C.-H. Lee, *Eur. J. Org. Chem.*, 2015, **2015**, 3859–3885.
108 S. K. Kim, J. Lee, N. J. Williams, V. M. Lynch, B. P. Hay, B. A. Moyer and J. L. Sessler, *J. Am. Chem. Soc.*, 2014, **136**, 15079–15085.
109 V. V. Rostovtsev, L. G. Green, V. V. Fokin and K. B. Sharpless, *Angew. Chem. Int. Ed.*, 2002, **41**, 2596–2599.
110 J. Cai and J. L. Sessler, *Chem. Soc. Rev.*, 2014, **43**, 6198–6213.
111 Y. Li and A. H. Flood, *J. Am. Chem. Soc.*, 2008, **130**, 12111–12122.
112 R. O. Ramabhadran, Y. Liu, Y. Hua, M. Ciardi, A. H. Flood and K. Raghavachari, *J. Am. Chem. Soc.*, 2014, **136**, 5078–5089.
113 A. Caballero, F. Zapata, L. González, P. Molina, I. Alkorta and J. Elguero, *Chem. Commun.*, 2014, **50**, 4680–4682.
114 Z. Xu, N. J. Singh, J. Lim, J. Pan, H. N. Kim, S. Park, K. S. Kim and J. Yoon, *J. Am. Chem. Soc.*, 2009, **131**, 15528–15533.
115 L. C. Gilday, S. W. Robinson, T. A. Barendt, M. J. Langton, B. R. Mullaney and P. D. Beer, *Chem. Rev.*, 2015, **115**, 7118–7195.
116 A. Mele, P. Metrangolo, H. Neukirch, T. Pilati and G. Resnati, *J. Am. Chem. Soc.*, 2005, **127**, 14972–14973.
117 M. G. Sarwar, B. Dragisic, S. Sagoo and M. S. Taylor, *Angew. Chem. Int. Ed.*, 2010, **49**, 1674–1677.
118 M. G. Chudzinski, C. A. McClary and M. S. Taylor, *J. Am. Chem. Soc.*, 2011, **133**, 10559–10567.
119 F. Zapata, A. Caballero, N. G. White, T. D. W. Claridge, P. J. Costa, V. Félix and P. D. Beer, *J. Am. Chem. Soc.*, 2012, **134**, 11533–11541.
120 R. Tepper, B. Schulze, M. Jäger, C. Friebe, D. H. Scharf, H. Görls and U. S. Schubert, *J. Org. Chem.*, 2015, **80**, 3139–3150.
121 D. F. Shriver and M. J. Biallas, *J. Am. Chem. Soc.*, 1967, **89**, 1078–1081.
122 M. Hirai and F. P. Gabbaï, *Chem. Sci.*, 2014, **5**, 1886–1893.
123 C.-W. Chiu, Y. Kim and F. P. Gabbaï, *J. Am. Chem. Soc.*, 2009, **131**, 60–61.

124 V. Amendola, M. Bonizzoni, D. Esteban-Gómez, L. Fabbrizzi, M. Licchelli, F. Sancenón and A. Taglietti, *Coord. Chem. Rev.*, 2006, **250**, 1451–1470.
125 J. W. Steed, *Chem. Soc. Rev.*, 2009, **38**, 506–519.
126 R. Custelcean, *Chem. Soc. Rev.*, 2014, **43**, 1813–1824.
127 M. Lisbjerg, B. M. Jessen, B. Rasmussen, B. E. Nielsen, A. Ø. Madsen and M. Pittelkow, *Chem. Sci.*, 2014, **5**, 2647–2650.
128 C. L. D. Gibb and B. C. Gibb, *J. Am. Chem. Soc.*, 2011, **133**, 7344–7347.
129 Y. Zhou, J. F. Zhang and J. Yoon, *Chem. Rev.*, 2014, **114**, 5511–5571.
130 N. Busschaert, C. Caltagirone, W. Van Rossom and P. A. Gale, *Chem. Rev.*, 2015, **115**, 8038–8155.
131 X. Zhuang, W. Liu, J. Wu, H. Zhang and P. Wang, *Spectrochim. Acta. A. Mol. Biomol. Spectrosc.*, 2011, **79**, 1352–1355.
132 R. Gotor, A. M. Costero, S. Gil, M. Parra, R. Martínez-Máñez, F. Sancenón and P. Gaviña, *Chem. Commun.*, 2013, **49**, 5669–5671.
133 K. Ghosh, A. R. Sarkar, A. Samadder and A. R. Khuda-Bukhsh, *Org. Lett.*, 2012, **14**, 4314–4317.
134 K.-C. Chang, S.-S. Sun, M. O. Odago and A. J. Lees, *Coord. Chem. Rev.*, 2015, **284**, 111–123.
135 S. J. Butler and D. Parker, *Chem. Soc. Rev.*, 2013, **42**, 1652–1666.
136 H.-J. Mo, Y. Shen and B.-H. Ye, *Inorg. Chem.*, 2012, **51**, 7174–7184.
137 T. Gunnlaugsson, P. E. Kruger, T. C. Lee, R. Parkesh, F. M. Pfeffer and G. M. Hussey, *Tetrahedron Lett.*, 2003, **44**, 6575–6578.
138 S. R. Bayly, P. D. Beer and G. Z. Chen, in *Ferrocenes*, ed. P. Š. F. of Science, John Wiley & Sons, Ltd, 2008, pp. 281–318.
139 Y. Willener, K. M. Joly, C. J. Moody and J. H. R. Tucker, *J. Org. Chem.*, 2008, **73**, 1225–1233.
140 K. A. Nielsen, J. O. Jeppesen, E. Levillain and J. Becher, *Angew. Chem. Int. Ed.*, 2003, **42**, 187–191.
141 S. F. M. van Dongen, S. Cantekin, J. A. A. W. Elemans, A. E. Rowan and R. J. M. Nolte, *Chem. Soc. Rev.*, 2013, **43**, 99–122.
142 A. Caballero, F. Zapata and P. D. Beer, *Coord. Chem. Rev.*, 2013, **257**, 2434–2455.
143 M. J. Langton and P. D. Beer, *Acc. Chem. Res.*, 2014, **47**, 1935–1949.
144 A. Affeld, G. M. Hübner, C. Seel and C. A. Schalley, *Eur. J. Org. Chem.*, 2001, **2001**, 2877–2890.
145 C.-W. Chiu, C.-C. Lai and S.-H. Chiu, *J. Am. Chem. Soc.*, 2007, **129**, 3500–3501.
146 I. Yoon, M. Narita, T. Shimizu and M. Asakawa, *J. Am. Chem. Soc.*, 2004, **126**, 16740–16741.
147 S.-Y. Hsueh, J.-L. Ko, C.-C. Lai, Y.-H. Liu, S.-M. Peng and S.-H. Chiu, *Angew. Chem. Int. Ed.*, 2011, **50**, 6643–6646.
148 E. Wasserman, *J. Am. Chem. Soc.*, 1960, **82**, 4433–4434.
149 I. T. Harrison and S. Harrison, *J. Am. Chem. Soc.*, 1967, **89**, 5723–5724.
150 D. H. Busch, *J. Incl. Phenom. Mol. Recognit. Chem.*, 1992, **12**, 389–395.
151 M. Xue, Y. Yang, X. Chi, X. Yan and F. Huang, *Chem. Rev.*, 2015, **115**, 7398–7501.
152 G. Gil-Ramírez, D. A. Leigh and A. J. Stephens, *Angew. Chem. Int. Ed.*, 2015, **54**, 6110–6150.
153 C. O. Dietrich-Buchecker, J. P. Sauvage and J. P. Kintzinger, *Tetrahedron Lett.*, 1983, **24**, 5095–5098.
154 C. O. Dietrich-Buchecker, J. P. Sauvage and J. M. Kern, *J. Am. Chem. Soc.*, 1984, **106**, 3043–3045.
155 D. A. Leigh, P. J. Lusby, S. J. Teat, A. J. Wilson and J. K. Y. Wong, *Angew. Chem. Int. Ed.*, 2001, **40**, 1538–1543.
156 A. I. Prikhod′ko and J.-P. Sauvage, *J. Am. Chem. Soc.*, 2009, **131**, 6794–6807.
157 S. M. Goldup, D. A. Leigh, P. J. Lusby, R. T. McBurney and A. M. Z. Slawin, *Angew. Chem. Int. Ed.*, 2008, **47**, 6999–7003.
158 A.-M. L. Fuller, D. A. Leigh, P. J. Lusby, A. M. Z. Slawin and D. B. Walker, *J. Am. Chem. Soc.*, 2005, **127**, 12612–12619.
159 A.-M. L. Fuller, D. A. Leigh and P. J. Lusby, *Angew. Chem. Int. Ed.*, 2007, **46**, 5015–5019.
160 C. Hamann, J.-M. Kern and J.-P. Sauvage, *Inorg. Chem.*, 2003, **42**, 1877–1883.
161 D. A. Leigh, R. G. Pritchard and A. J. Stephens, *Nat. Chem.*, 2014, **6**, 978–982.

162 F. Zapata, O. A. Blackburn, M. J. Langton, S. Faulkner and P. D. Beer, *Chem. Commun.*, 2013, **49**, 8157–8159.
163 C. Lincheneau, B. Jean-Denis and T. Gunnlaugsson, *Chem. Commun.*, 2014, **50**, 2857–2860.
164 S.-T. Tung, C.-C. Lai, Y.-H. Liu, S.-M. Peng and S.-H. Chiu, *Angew. Chem. Int. Ed.*, 2013, **52**, 13269–13272.
165 T.-H. Ho, C.-C. Lai, Y.-H. Liu, S.-M. Peng and S.-H. Chiu, *Chem. – Eur. J.*, 2014, **20**, 4563–4567.
166 V. Aucagne, J. Berná, J. D. Crowley, S. M. Goldup, K. D. Hänni, D. A. Leigh, P. J. Lusby, V. E. Ronaldson, A. M. Z. Slawin, A. Viterisi and D. B. Walker, *J. Am. Chem. Soc.*, 2007, **129**, 11950–11963.
167 K. D. Hänni and D. A. Leigh, *Chem. Soc. Rev.*, 2010, **39**, 1240–1251.
168 Y. Sato, R. Yamasaki and S. Saito, *Angew. Chem. Int. Ed.*, 2009, **48**, 504–507.
169 H. Lahlali, K. Jobe, M. Watkinson and S. M. Goldup, *Angew. Chem. Int. Ed.*, 2011, **50**, 4151–4155.
170 B. L. Allwood, H. Shahriari-Zavareh, J. F. Stoddart and D. J. Williams, *J. Chem. Soc. Chem. Commun.*, 1987, 1058–1061.
171 P. R. Ashton, E. J. T. Chrystal, P. T. Glink, S. Menzer, C. Schiavo, N. Spencer, J. F. Stoddart, P. A. Tasker, A. J. P. White and D. J. Williams, *Chem. – Eur. J.*, 1996, **2**, 709–728.
172 C. Zhang, S. Li, J. Zhang, K. Zhu, N. Li and F. Huang, *Org. Lett.*, 2007, **9**, 5553–5556.
173 W. Jiang, H. D. F. Winkler and C. A. Schalley, *J. Am. Chem. Soc.*, 2008, **130**, 13852–13853.
174 K. Kim, *Chem. Soc. Rev.*, 2002, **31**, 96–107.
175 S. Liu, C. Ruspic, P. Mukhopadhyay, S. Chakrabarti, P. Y. Zavalij and L. Isaacs, *J. Am. Chem. Soc.*, 2005, **127**, 15959–15967.
176 Y. H. Ko, E. Kim, I. Hwang and K. Kim, *Chem. Commun.*, 2007, 1305–1315.
177 V. Kolman, M. S. A. Khan, M. Babinský, R. Marek and V. Sindelar, *Org. Lett.*, 2011, **13**, 6148–6151.
178 J. M. Spruell, W. F. Paxton, J.-C. Olsen, D. Benítez, E. Tkatchouk, C. L. Stern, A. Trabolsi, D. C. Friedman, W. A. Goddard and J. F. Stoddart, *J. Am. Chem. Soc.*, 2009, **131**, 11571–11580.
179 G. Barin, A. Coskun, M. M. G. Fouda and J. F. Stoddart, *ChemPlusChem*, 2012, **77**, 159–185.
180 F. Vögtle, S. Meier and R. Hoss, *Angew. Chem. Int. Ed. Engl.*, 1992, **31**, 1619–1622.
181 C. A. Hunter, *J. Am. Chem. Soc.*, 1992, **114**, 5303–5311.
182 J. J. Gassensmith, J. M. Baumes and B. D. Smith, *Chem. Commun.*, 2009, 6329–6338.
183 D. M. D'Souza, D. A. Leigh, L. Mottier, K. M. Mullen, F. Paolucci, S. J. Teat and S. Zhang, *J. Am. Chem. Soc.*, 2010, **132**, 9465–9470.
184 A. Altieri, V. Aucagne, R. Carrillo, G. J. Clarkson, D. M. D'Souza, J. A. Dunnett, D. A. Leigh and K. M. Mullen, *Chem. Sci.*, 2011, **2**, 1922–1928.
185 R. Ahmed, A. Altieri, D. M. D'Souza, D. A. Leigh, K. M. Mullen, M. Papmeyer, A. M. Z. Slawin, J. K. Y. Wong and J. D. Woollins, *J. Am. Chem. Soc.*, 2011, **133**, 12304–12310.
186 Y. Akae, H. Okamura, Y. Koyama, T. Arai and T. Takata, *Org. Lett.*, 2012, **14**, 2226–2229.
187 H. Y. Au-Yeung, G. D. Pantoş and J. K. M. Sanders, *Proc. Natl. Acad. Sci.*, 2009, **106**, 10466–10470.
188 G. T. Spence and P. D. Beer, *Acc. Chem. Res.*, 2013, **46**, 571–586.
189 G. M. Hübner, J. Gläser, C. Seel and F. Vögtle, *Angew. Chem. Int. Ed.*, 1999, **38**, 383–386.
190 J. A. Wisner, P. D. Beer, M. G. B. Drew and M. R. Sambrook, *J. Am. Chem. Soc.*, 2002, **124**, 12469–12476.
191 K. M. Mullen and P. D. Beer, *Chem. Soc. Rev.*, 2009, **38**, 1701–1713.
192 K. M. Mullen, J. Mercurio, C. J. Serpell and P. D. Beer, *Angew. Chem. Int. Ed.*, 2009, **48**, 4781–4784.
193 M. J. Langton, L. C. Duckworth and P. D. Beer, *Chem. Commun.*, 2013, **49**, 8608–8610.
194 M. J. Langton and P. D. Beer, *Chem. Commun.*, 2014, **50**, 8124–8127.
195 M. J. Langton, O. A. Blackburn, T. Lang, S. Faulkner and P. D. Beer, *Angew. Chem. Int. Ed.*, 2014, **53**, 11463–11466.
196 N. G. White and P. D. Beer, *Chem. Commun.*, 2012, **48**, 8499–8501.
197 N. G. White and P. D. Beer, *Org. Biomol. Chem.*, 2013, **11**, 1326–1333.

198 N. G. White, P. J. Costa, S. Carvalho, V. Félix and P. D. Beer, *Chem. – Eur. J.*, 2013, **19**, 17751–17765.
199 N. G. White, H. G. Lovett and P. D. Beer, *RSC Adv.*, 2014, **4**, 12133–12147.
200 N. G. White, A. R. Colaço, I. Marques, V. Félix and P. D. Beer, *Org. Biomol. Chem.*, 2014, **12**, 4924–4931.
201 G. T. Spence, C. J. Serpell, J. Sardinha, P. J. Costa, V. Félix and P. D. Beer, *Chem. – Eur. J.*, 2011, **17**, 12955–12966.
202 M. K. Chae, J. Suk and K.-S. Jeong, *Tetrahedron Lett.*, 2010, **51**, 4240–4242.
203 L. M. Hancock, L. C. Gilday, S. Carvalho, P. J. Costa, V. Félix, C. J. Serpell, N. L. Kilah and P. D. Beer, *Chem. – Eur. J.*, 2010, **16**, 13082–13094.
204 M. J. Langton, I. Marques, S. W. Robinson, V. Félix and P. D. Beer, *Chem. – Eur. J.*, 2016, **22**, 185–192.
205 M. V. R. Raju and H.-C. Lin, *Org. Lett.*, 2013, **15**, 1274–1277.
206 J. J. Gassensmith, S. Matthys, J.-J. Lee, A. Wojcik, P. V. Kamat and B. D. Smith, *Chem. – Eur. J.*, 2010, **16**, 2916–2921.
207 N. H. Evans, H. Rahman, A. V. Leontiev, N. D. Greenham, G. A. Orlowski, Q. Zeng, R. M. J. Jacobs, C. J. Serpell, N. L. Kilah, J. J. Davis and P. D. Beer, *Chem. Sci.*, 2012, **3**, 1080–1089.
208 N. H. Evans and P. D. Beer, *Org. Biomol. Chem.*, 2010, **9**, 92–100.
209 N. H. Evans, C. J. Serpell, N. G. White and P. D. Beer, *Chem. – Eur. J.*, 2011, **17**, 12347–12354.
210 N. H. Evans, C. J. Serpell and P. D. Beer, *Chem. Commun.*, 2011, **47**, 8775–8777.
211 J. Y. C. Lim, M. J. Cunningham, J. J. Davis and P. D. Beer, *Dalton Trans.*, 2014, **43**, 17274–17282.
212 R. A. Bissell, E. Córdova, A. E. Kaifer and J. F. Stoddart, *Nature*, 1994, **369**, 133–137.
213 C. P. Collier, E. W. Wong, M. Belohradský, F. M. Raymo, J. F. Stoddart, P. J. Kuekes, R. S. Williams and J. R. Heath, *Science*, 1999, **285**, 391–394.
214 D.-H. Qu, Q.-C. Wang and H. Tian, *Angew. Chem. Int. Ed.*, 2005, **44**, 5296–5299.
215 D. A. Leigh, J. K. Y. Wong, F. Dehez and F. Zerbetto, *Nature*, 2003, **424**, 174–179.
216 J. V. Hernández, E. R. Kay and D. A. Leigh, *Science*, 2004, **306**, 1532–1537.
217 V. Balzani, M. Clemente-León, A. Credi, B. Ferrer, M. Venturi, A. H. Flood and J. F. Stoddart, *Proc. Natl. Acad. Sci.*, 2006, **103**, 1178–1183.
218 M. N. Chatterjee, E. R. Kay and D. A. Leigh, *J. Am. Chem. Soc.*, 2006, **128**, 4058–4073.
219 V. Serreli, C.-F. Lee, E. R. Kay and D. A. Leigh, *Nature*, 2007, **445**, 523–527.
220 Y. Liu, A. H. Flood, P. A. Bonvallet, S. A. Vignon, B. H. Northrop, H.-R. Tseng, J. O. Jeppesen, T. J. Huang, B. Brough, M. Baller, S. Magonov, S. D. Solares, W. A. Goddard, C.-M. Ho and J. F. Stoddart, *J. Am. Chem. Soc.*, 2005, **127**, 9745–9759.
221 C. Romuald, A. Ardá, C. Clavel, J. Jiménez-Barbero and F. Coutrot, *Chem. Sci.*, 2012, **3**, 1851–1857.
222 B. Lewandowski, G. D. Bo, J. W. Ward, M. Papmeyer, S. Kuschel, M. J. Aldegunde, P. M. E. Gramlich, D. Heckmann, S. M. Goldup, D. M. D'Souza, A. E. Fernandes and D. A. Leigh, *Science*, 2013, **339**, 189–193.
223 D. A. Leigh, V. Marcos and M. R. Wilson, *ACS Catal.*, 2014, **4**, 4490–4497.
224 S. Hoekman, M. O. Kitching, D. A. Leigh, M. Papmeyer and D. Roke, *J. Am. Chem. Soc.*, 2015, **137**, 7656–7659.

Chapter Two

Pyridinium- and quinolinium-based halogen and hydrogen bonding hosts for anion recognition

2.1 Introduction

As discussed in Chapter 1, the use of halogen bonding (XB) interactions for the purpose of solution phase anion recognition is still very much in its infancy. Much of the work conducted in this area thus far has aimed to gauge the anion binding strength and selectivity of receptors incorporating different XB donor motifs. Several reports have emerged where the anion binding properties of these XB receptors have been directly compared with their hydrogen bonding (HB) analogues, which have generally demonstrated the XB receptors to be the more effective hosts. For example, Taylor and co-workers prepared a receptor containing a central urea motif functionalised with two iodotetrafluorophenyl XB donors, which was found to bind chloride (K_a = 2400 M^{-1}) more strongly than bromide, iodide and a variety of oxoanions in CD_3CN (**Figure 2.1a**).[1] The HB analogue of this receptor bound chloride substantially more weakly (K_a = 86 M^{-1}) and displayed no anion selectivity in the same solvent system. Similarly, Resnati and co-workers demonstrated that a monodentate 2-iodoimidazolium-based XB receptor binds dihydrogen phosphate significantly more strongly than its HB analogue (K_a = 1100 M^{-1} and K_a = 26 M^{-1}, respectively) in d_6-DMSO (**Figure 2.1b**),[2] whilst Molina and co-workers have shown that a receptor containing two iodo-triazolium XB donors binds hydrogen pyrophosphate more strongly than an analogous mixed XB and HB receptor (K_a = 9800 M^{-1} and K_a = 1700 M^{-1}, respectively) in 9:1 CD_3CN/CD_3OD (**Figure 2.1c**).[3]

The stronger anion association exhibited by XB receptors can potentially be ascribed to the covalent character of XB-anion interactions. In a recent seminal report by Beer and co-workers, X-Ray absorption spectroscopy was used to quantify the degree of covalency in the interaction between chloride anions and a range of organic XB donors containing iodotriazole and iodotriazolium motifs.[4] Analysis of the spectroscopic data suggested that the level of covalency is similar to that of a transition-metal coordinate bond.

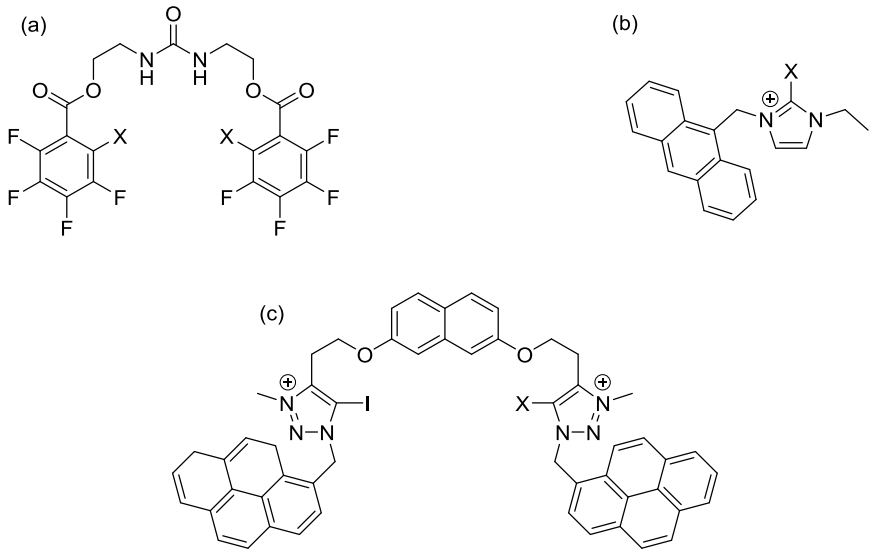

Figure 2.1: (a) Taylor's urea-based receptors, (b) Resnati's imidazolium receptors and (c) Molina's triazolium containing receptors. X = I or H.

Several interlocked host structures incorporating XB donor motifs into their binding cavities have also been reported.[4–11] The strong anion affinities displayed by these hosts have allowed binding studies to be conducted in highly competitive organic and even aqueous solvent media. For example, Beer and co-workers have recently reported a [2]catenane containing a 3,5-bis-iodotriazole-pyridinium XB donor motif, which was found to bind bromide and iodide strongly (K_a > 10^4 M^{-1}) in a 45:45:10 $CDCl_3/CD_3OD/D_2O$ solvent mixture (**Figure 2.2**).[4] Substantially weaker binding of chloride (K_a = 1850 M^{-1}) and no binding of acetate and dihydrogen phosphate was observed in the same solvent mixture. This selectivity preference, towards the heavier halides, has been observed for other XB interlocked anion receptors.[5,7,10] In contrast, the analogous all HB [2]catenane displayed significantly weaker association of all anions investigated in a less competitive 1:1 $CDCl_3/CD_3OD$ solvent mixture.

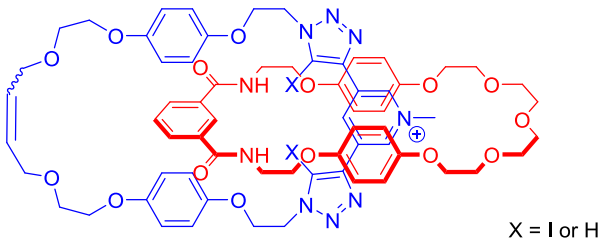

Figure 2.2: Beer's XB and HB [2]catenanes

2.1.1 Chapter aims

With the aim of further probing the differences between the XB and HB interactions, this chapter describes the preparation of a series of new acyclic and interlocked pyridinium-based anion receptors containing either XB iodotriazole or HB prototriazole functionality. The structures of the binding motifs present in these hosts are based on the pyridinium nicotinamide motif (**Figure 2.3a**), which has previously been incorporated into anion receptors, such as Beer's sulfate selective [2]catenane (**Figure 2.3b**).[12] Comparisons of the hosts' anion recognition properties are made in competitive solvent media.

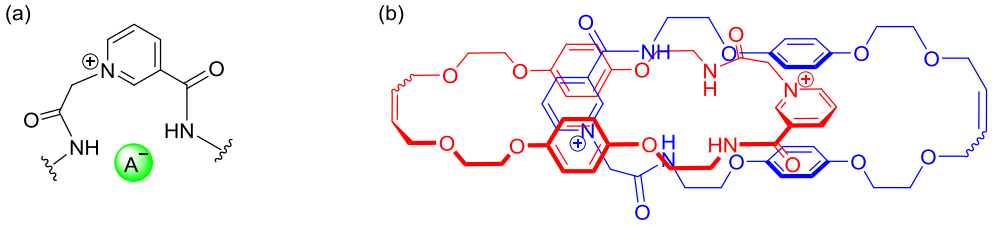

Figure 2.3: (a) The pyridinium-nicotinamide anion binding motif and (b) Beer's pyridinium-nicotinamide-based [2]catenane

The preparation and anion sensing capabilities of related receptors containing a fluorescent quinolinium motif are also discussed.

2.2 Acyclic halogen and hydrogen bonding pyridinium receptors

Initial work focused on the synthesis of acyclic receptors containing a single 1,3-substituted pyridinium unit, functionalised with an amide HB donor and either an XB iodotriazole or HB prototriazole group (**Figure 2.4**).

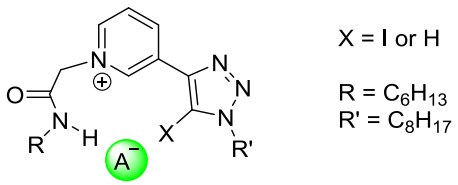

Figure 2.4: Structure of target acyclic pyridinium receptors

2.2.1 Synthesis of acyclic receptors

The first step in the synthesis of both target acyclic receptors involved a Cu(I)-catalysed azide-alkyne cycloaddition (CuAAC) reaction between 3-ethynyl pyridine and 1-azidooctane,[13] to give triazole derivatives **1** and **2** (**Scheme 2.1**). To prepare **1**, a recently reported 'one-pot' synthetic procedure was used in which the iodotriazole group is formed in a concerted fashion starting from a proto-alkyne, rather than through the initial isolation of an iodo-alkyne intermediate.[14,15] In this reaction, $Cu(ClO_4)_2{\cdot}6H_2O$ is reduced by NaI to generate both the active Cu(I) catalyst and the triiodide anion, an electrophilic iodine source. DBU is used as a base, to deprotonate the proto-alkyne starting material and TBTA is added to stabilise the Cu(I) ion. Interestingly, when THF was used as the solvent, formation of prototriazole **2** as a side-product was observed, which proved to be inseparable from the target material using chromatographic techniques. Exclusive formation of iodotriazole was achieved using a 1:1 THF/MeCN solvent mixture, with the product isolated in a 92% yield. Prototriazole **2** was prepared in a 98% yield using conventional CuAAC conditions, with $[Cu(MeCN)_4][PF_6]$ used as the source of Cu(I).[16]

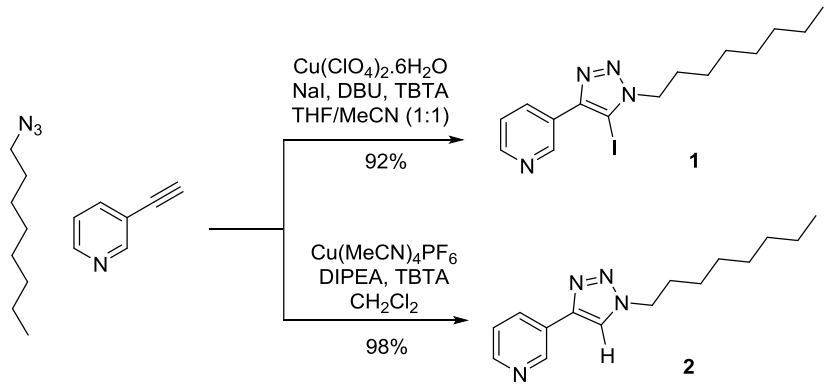

Scheme 2.1: Synthesis of triazole derivatives **1** and **2** *via* CuAAC reactions

Reaction of bromoacetylbromide with hexylamine yielded alkyl bromide derivative **3**, which was used to alkylate compounds **1** and **2** in the presence of a catalytic amount of NaI. Following purification by column chromatography, the pyridinium species obtained were

anion exchanged by washing with $NH_4PF_{6(aq)}$ to give the target XB and HB acyclic receptors **4·PF$_6$** and **5·PF$_6$** in respective yields of 39% and 64% (**Scheme 2.2**).

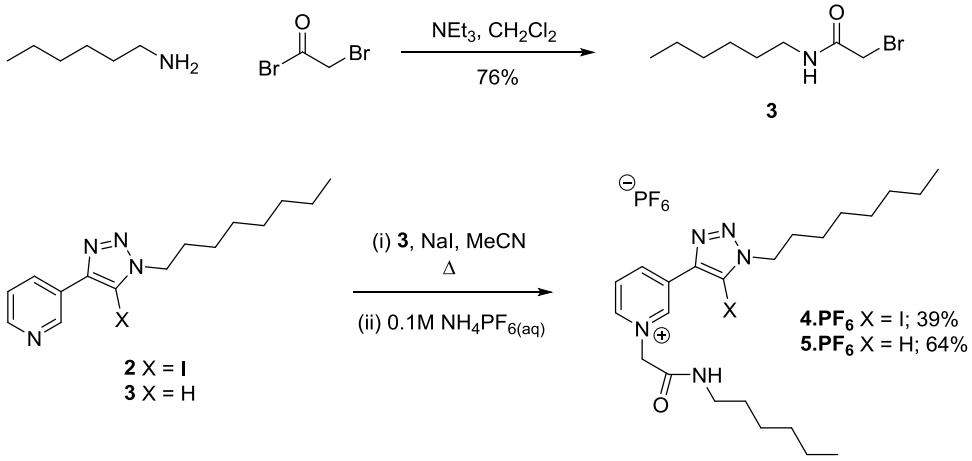

Scheme 2.2: Synthesis of acyclic receptors **4·PF$_6$** and **5·PF$_6$**

2.2.2 Anion binding investigations

The anion binding properties of the acyclic receptors were investigated using ^{1}H NMR titration experiments, performed in a competitive 1:1 $CDCl_3/CD_3OD$ solvent mixture. The chemical shifts of the respective receptors' proton resonances were monitored upon addition of increasing quantities of chloride, bromide, dihydrogen phosphate and acetate, as their TBA salts. A more detailed description of this procedure is given in section 6.3.

For HB receptor **5·PF$_6$**, significant downfield perturbations of the resonances of pyridinium proton *a* and triazole proton *e* were observed with all of the anions added, indicating these protons are directly involved in HB interactions (**Figure 2.4**). The magnitude of these shifts was larger in the halide titrations than in the oxoanion titration experiments. It should be noted that the resonance of the amide proton *f* could not be observed due to hydrogen-deuterium exchange.

Interestingly, none of the proton resonances of XB receptor **4·PF$_6$** shifted substantially upon addition of any of the anions and hence no quantitative binding data could be calculated for this receptor. It is possible that, in this case, anion association is mediated purely through a XB interaction, which would explain the lack of observable shifts in the ^{1}H NMR spectra.

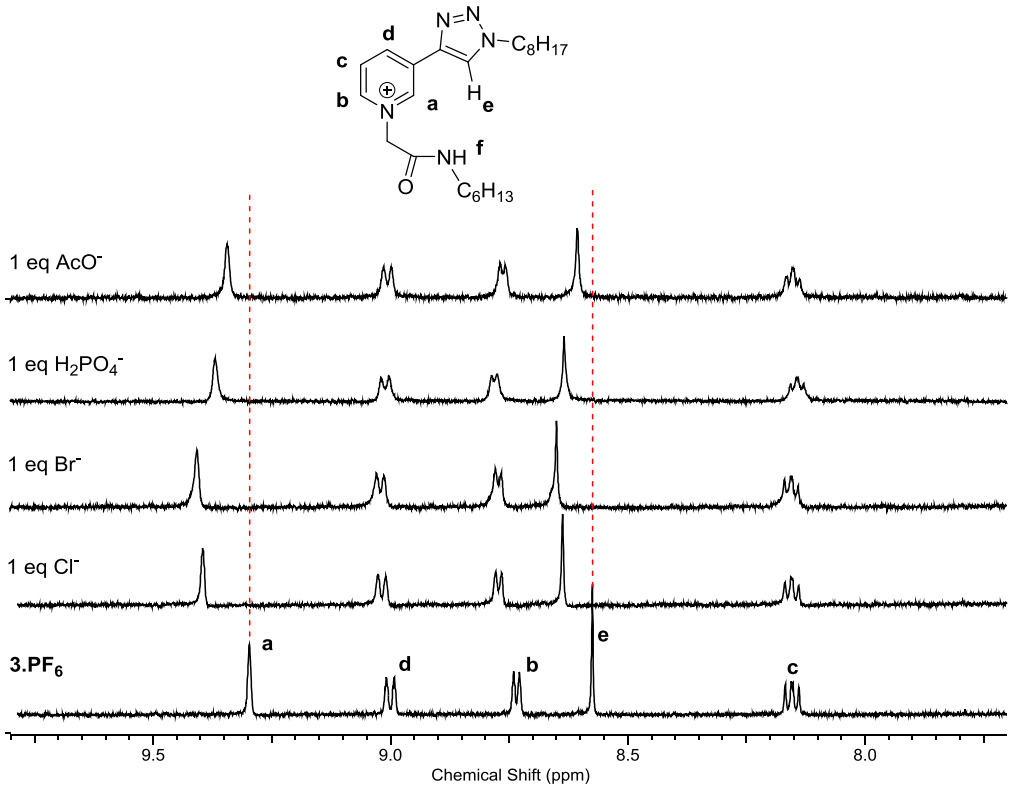

Figure 2.4: Truncated ^{1}H NMR spectra of receptor **5·PF$_6$** before and after addition of 1 eq. of various anions (1:1 $CDCl_3/CD_3OD$, 298 K, 500 MHz).

The titration data collected for receptor **5·PF$_6$** was analysed using the WinEQNMR software package.[17] Through monitoring the chemical shift of proton *a* (**Figure 2.5**), 1:1 stoichiometric association constants were determined (**Table 2.1**), the magnitudes of which reveal that all the anions were bound with moderate affinities. However, the selectivity of the receptor is relatively modest with only a 2·5-fold difference between the association constants of the most strongly bound anion (dihydrogen phosphate) and the most weakly bound anion (acetate). It is important to note that the selectivity trend observed through the calculated association constants cannot be simply derived from visual inspection of the chemical shift plots. The magnitude of the change in chemical shift of the monitored proton provides no information regarding the strength of the interaction between the host and a given anion.

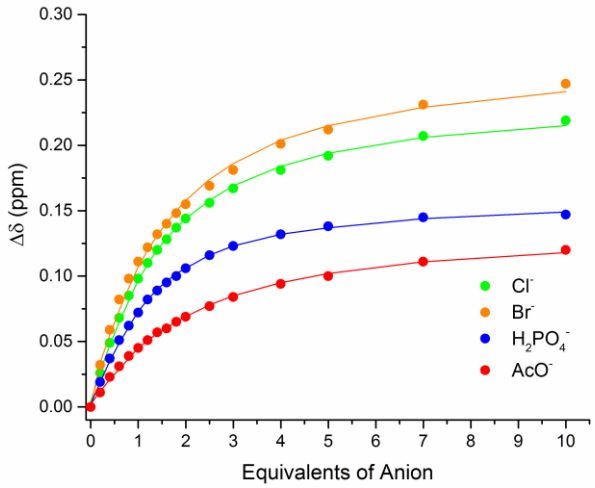

Figure 2.5: Experimental titration data (points) and calculated 1:1 binding isotherms (lines) for the addition of TBA salts of various anions to **5·PF$_6$**, monitoring proton *a* (1:1 $CDCl_3/CD_3OD$, 298 K, 500 MHz)

Table 2.1: Association constants (K_a) determined for **5·PF$_6$** with various anions (1:1 $CDCl_3/CD_3OD$, 298 K, 500 MHz).

Anion	**K_a (M^{-1})**[a]
Cl^-	520
Br^-	450
$H_2PO_4^-$	710
AcO^-	290

[a] Calculated using chemical shift of proton *a*. Estimated errors within ±10%.

The integration of the XB and HB anion binding motifs of acyclic receptors **4·PF$_6$** and **5·PF$_6$** into the axle components of [2]rotaxanes was subsequently targeted. It was hoped that the constrained three-dimensional binding pockets of such hosts would increase anion association strength and also enhance selectivity.

2.2.3 Pseudorotaxane assembly studies

An initial investigation was undertaken to assess the ability of **4·PF$_6$** and **5·PF$_6$** to form interpenetrated pseudorotaxane assemblies with an isophthalamide macrocycle, in the presence of a templating anion. Previous work by Beer demonstrated that a variety of XB and HB acyclic receptors are capable of this, including a species containing the pyridinium

nicotinamide motif discussed in section 2.1.1.[5,18–20] The macrocycle used in the investigations was prepared using a previously reported synthetic procedure (**Scheme 2.3**).[21]

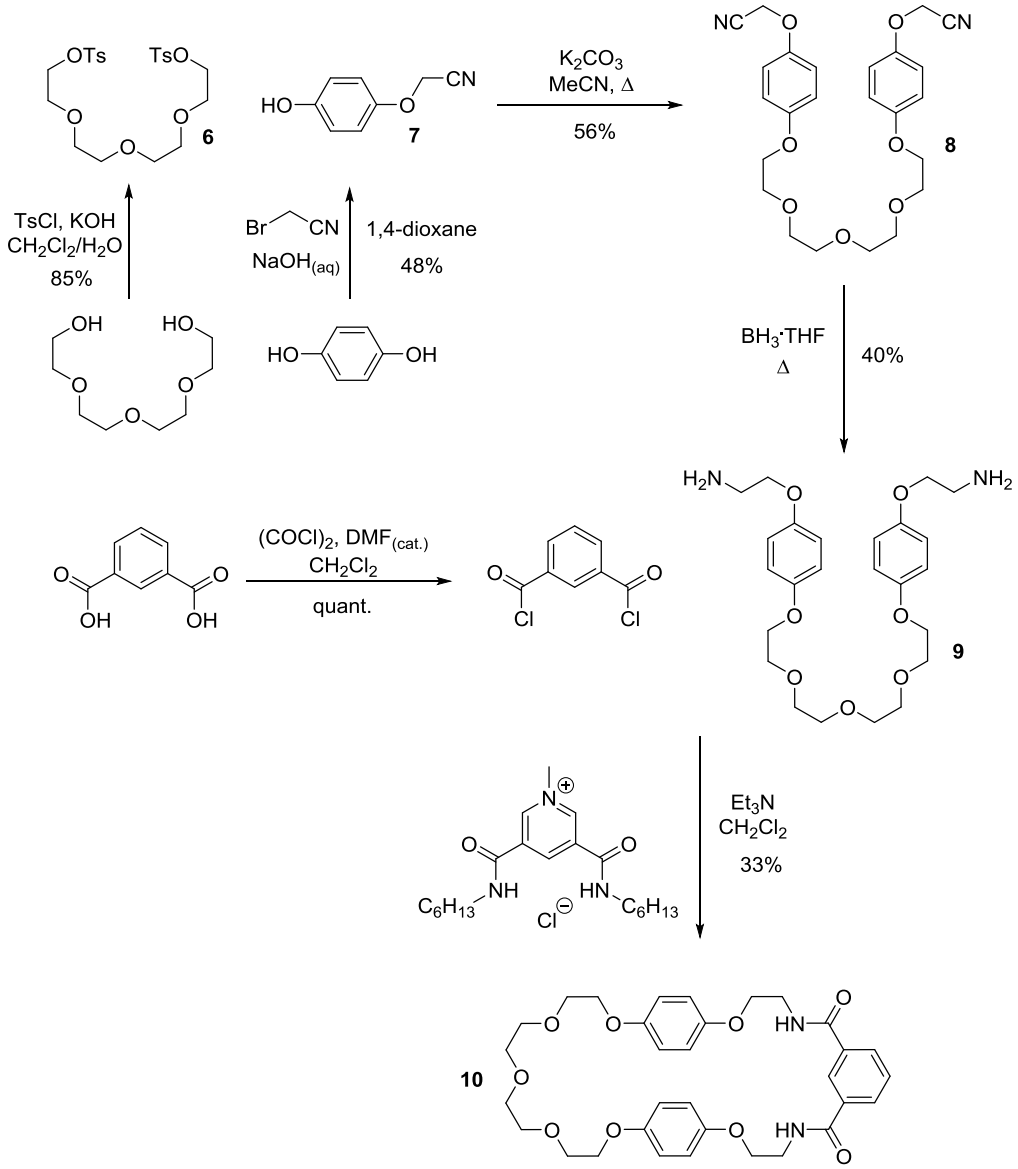

Scheme 2.3: Preparation of isophthalamide macrocycle **10**

Tetraethylene glycol was reacted with *p*-toluenesulfonyl chloride to give bis-tosylate **6** and hydroquinone was reacted with bromoacetonitrile to give compound **7**. The reaction of two equivalents of **7** with one equivalent of **6** in the presence of K_2CO_3 afforded bis-nitrile compound **8**, which was reduced using a 1M solution of borane in THF, to give bis-amine **9**. Macrocycle formation was achieved through condensation of isophthaloyl chloride with **9** in

the presence of a templating pyridinium chloride species.[22] Following purification by column chromatography, the target macrocycle **10** was isolated in a 33% yield.

^{1}H NMR spectroscopy was used to undertake qualitative pseudorotaxane assembly studies. An equimolar mixture of macrocycle **10**, TBACl and either **4·PF$_6$** or **5·PF$_6$** in $CDCl_3$ solution was prepared (**Scheme 2.4**) and the ^{1}H NMR spectrum obtained was compared with spectra of the individual components. In both cases the resonances for hydroquinone protons *5* and *6* of the macrocycle were split and underwent a significant upfield shift. This is diagnostic of pseudorotaxane formation and is due to the desymmetrisation of these proton environments and the favourable π-π aromatic donor-acceptor interactions between the electron-rich rings and the electron-deficient pyridinium unit of threads **4·PF$_6$** and **5·PF$_6$**.

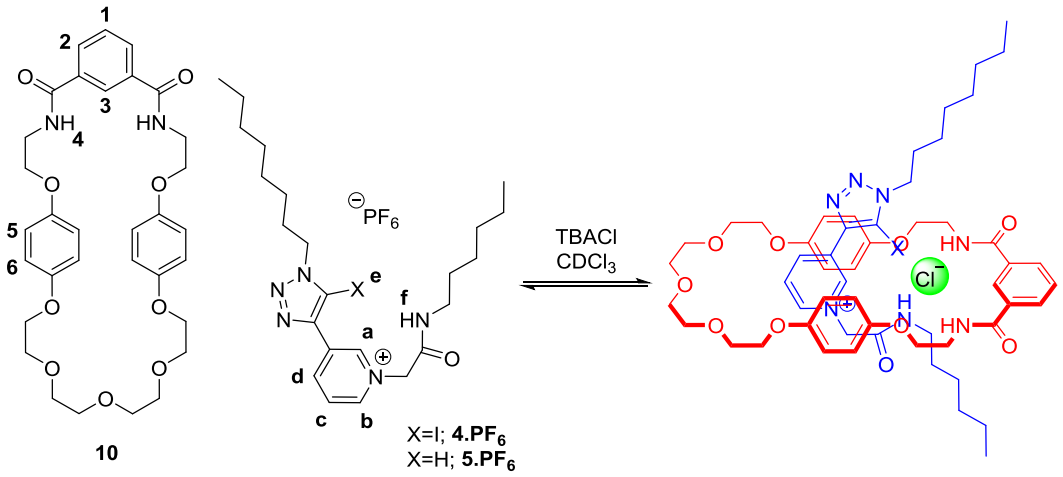

Scheme 2.4: Pseudorotaxane formation between **4·PF$_6$**/**5·PF$_6$** and macrocycle **10** in the presence of a templating chloride anion

Substantial downfield shifts of amide proton *f*, pyridinium proton *a* and triazole proton *e* (Δδ = 1.92 ppm, 0.83 ppm and 0.29 ppm respectively) were also observed for the assembly formed with **5·PF$_6$** (**Figure 2.6**). In the case of XB **4·PF$_6$** a similarly large downfield shift of amide proton *f* occurred ($\Delta\delta$ = 2.23 ppm), however minimal movement of pyridinium proton *a* was observed, suggesting this proton does not form any direct HB interactions with the anion.

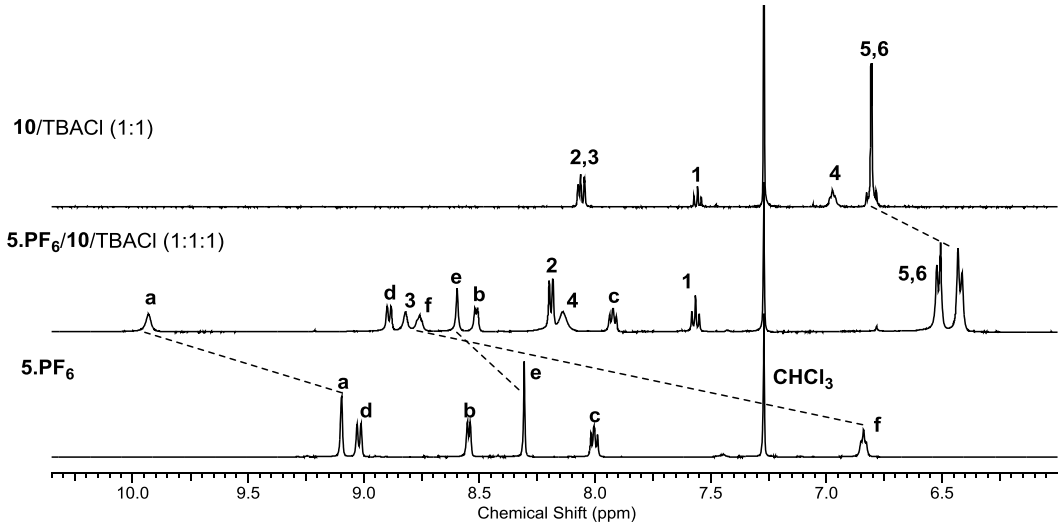

Figure 2.6: ^{1}H NMR spectra of: (a) an equimolar mixture of **10** and TBACl, (b) an equimolar mixture of **5.PF$_6$**, **10** and TBACl and (c) **5.PF6** ($CDCl_3$, 298 K).

Repeating both experiments in the absence of TBACl resulted in no perturbations of the hydroquinone resonances, implying that no interpenetrated assemblies had formed. This highlights the crucial templating role played by the chloride anion in the pseudorotaxane assembly process.

2.3 Halogen and hydrogen bonding rotaxanes

Encouraged by the success of the pseudorotaxane formation studies, the preparation of [2]rotaxanes containing the XB and HB pyridinium anion binding motifs, as axle components, was attempted using a chloride templated 'clipping' methodology. This necessitated the initial synthesis of appropriate axle components and a macrocycle precursor.

2.3.1 Synthesis of axle components

A bulky terphenyl propyl-azide stopper derivative **14** was prepared using a previously reported synthetic procedure (**Scheme 2.5**).[23] Reaction of 1-bromo-4-*tert*-butylbenzene with magnesium turnings in the presence of a catalytic amount of iodine generated a Grignard reagent, which was reacted with diethylcarbonate to give alcohol **11**. This was dissolved in a mixture of molten phenol and concentrated HCl to afford terphenyl-alcohol **12**. Reaction of

12 with 1,3-dibromopropane gave propyl bromide **13**, which was then reacted with NaN_3 to give the target propyl-azide stopper **14**.

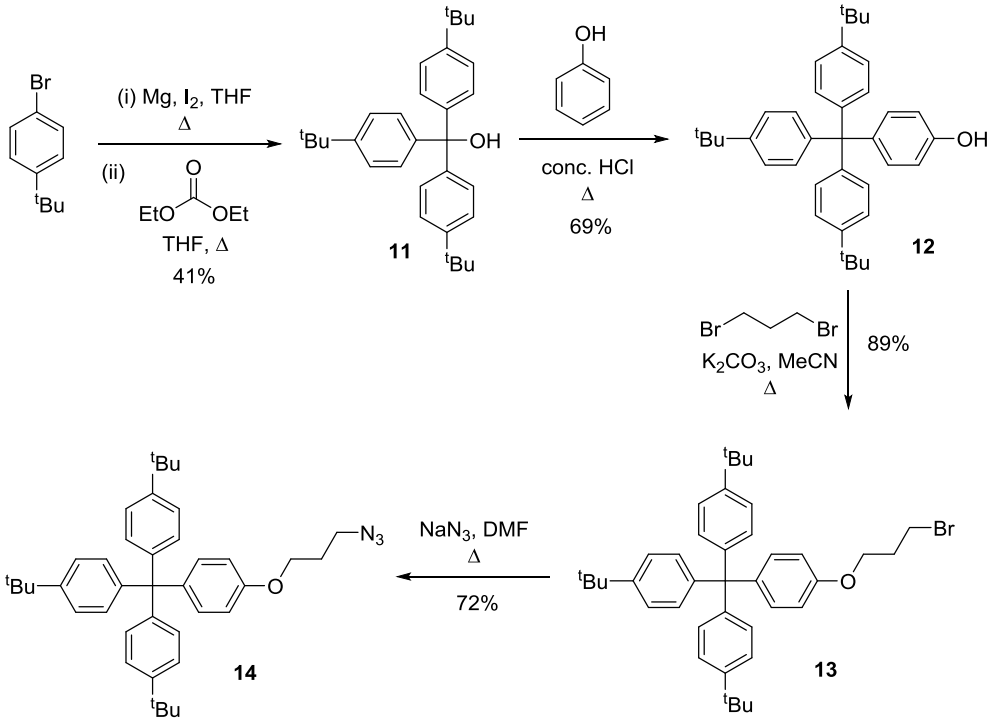

Scheme 2.5: Synthesis of propyl-azide terphenyl stopper **14**.

To prepare an alkyl bromide-appended terphenyl stopper, alcohol **11** was reacted with acetyl chloride to form a carbocation intermediate, which was then reacted with aniline to give terphenyl-amine **15**.[24] A condensation reaction between **15** and bromoacetyl bromide afforded the target stopper **16** in a 90% yield (**Scheme 2.6**).

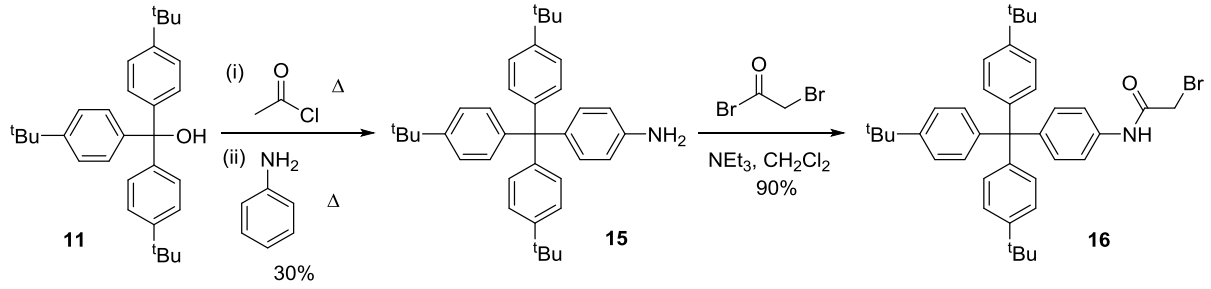

Scheme 2.6: Synthesis of alkyl bromide-appended stopper **16**.

Reaction of azide **14** with 3-ethynylpyridine under CuAAC conditions gave the iodo- and proto-triazole derivatives **17** and **18** in yields of 85% and 93%, respectively. The conditions used for these reactions were identical to those used in the preparation of triazole derivatives **1**

and **2**. Compounds **17** and **18** were alkylated with alkyl bromide-appended stopper **16**, in the presence of a catalytic amount of NaI. Following purification by column chromatography the pure products were converted to their chloride salts by washing with aqueous ammonium chloride, to give target axles **19·Cl** and **20·Cl** in yields of 63% and 28%, respectively (**Scheme 2.7**).

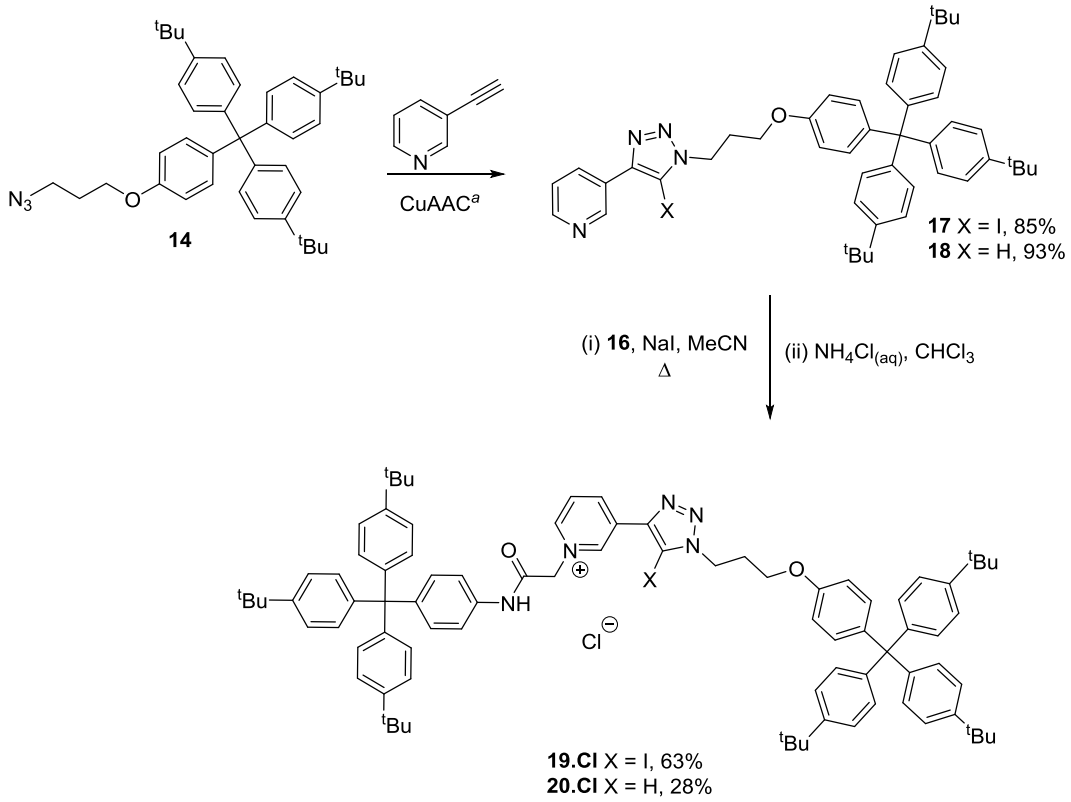

Scheme 2.7: Synthesis of XB and HB axle components **19·Cl** and **20·Cl**. [a] For X = I: $Cu(ClO_4)_2 \cdot 6H_2O$, NaI, DBU, TBTA, THF/MeCN, dark; For X = H: $[Cu(MeCN)_4][PF_6]$, DIPEA, TBTA, CH_2Cl_2.

2.3.2 Synthesis of macrocycle precursor

Bis-vinyl appended macrocycle precursor **25** was prepared using a literature procedure (**Scheme 2.8**).[25] 2-Allyloxyethanol was reacted with *p*-toluenesulfonyl chloride to give tosylate **21**, which was then reacted with hydroquinone to give **22**. Reaction of **22** with bromoacetonitrile afforded nitrile derivative **23**, which was reduced with $LiAlH_4$ to give amine **24**. Two equivalents of **24** were condensed with one equivalent of 5-nitroisophthaloyl dichloride to give **25** in a 69% yield.

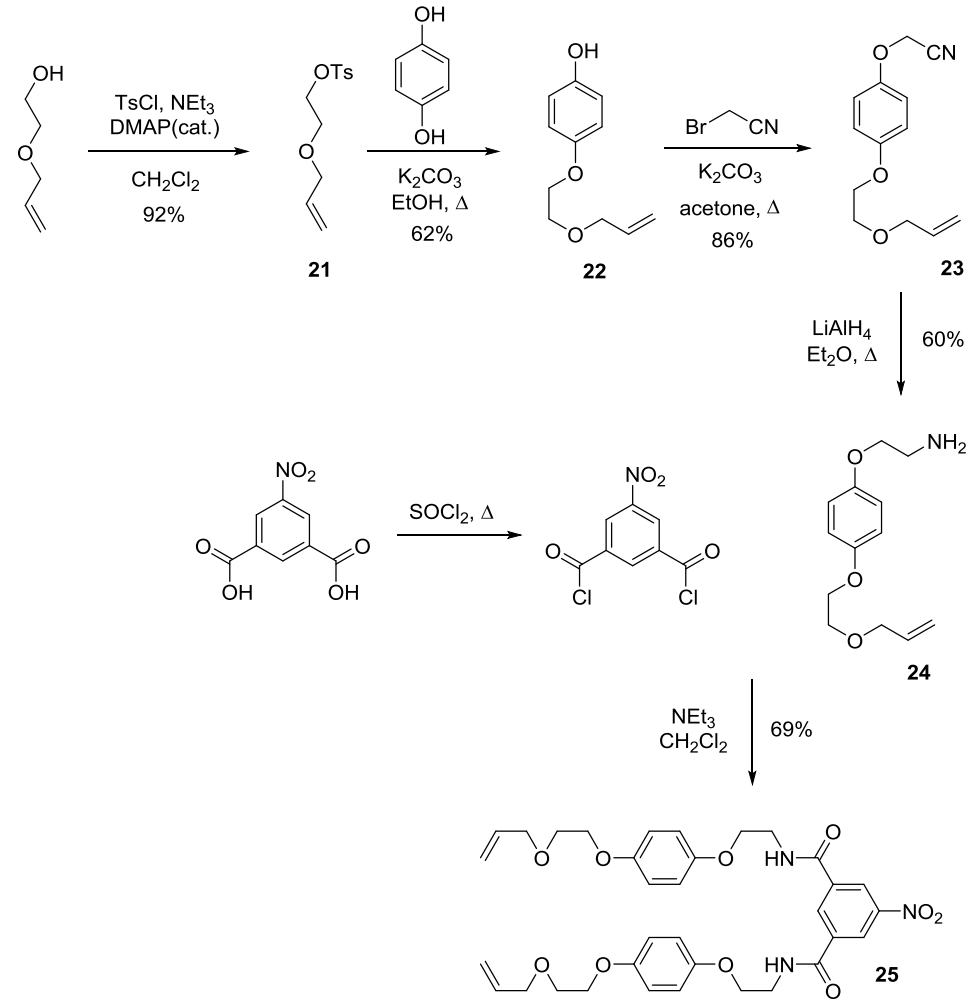

Scheme 2.8: Preparation of bis-vinyl-appended macrocycle precursor **25**

2.3.3 Synthesis of rotaxanes

Rotaxane formation was achieved using a clipping procedure by combining an equimolar mixture of macrocycle precursor **25** and either XB axle **19·Cl** or HB axle **20·Cl** in dry CH_2Cl_2, with the chloride counter anion of the axle component acting as a template. Subsequent addition of Grubbs' second generation catalyst led to a ring closing metathesis (RCM) reaction of **25** around the axles affording the interlocked products. Following purification by preparative thin layer chromatography and exchange of the templating chloride anion for a non-coordinating hexafluorophosphate anion, the target XB and HB [2]rotaxanes **26·PF$_6$** and **27·PF$_6$** were isolated in comparable yields of 22% and 18%,

respectively (**Scheme 2.9**). Both rotaxanes were fully characterised by ^{1}H, ^{13}C, ^{19}F and ^{31}P NMR spectroscopy and high resolution ESI mass spectrometry.

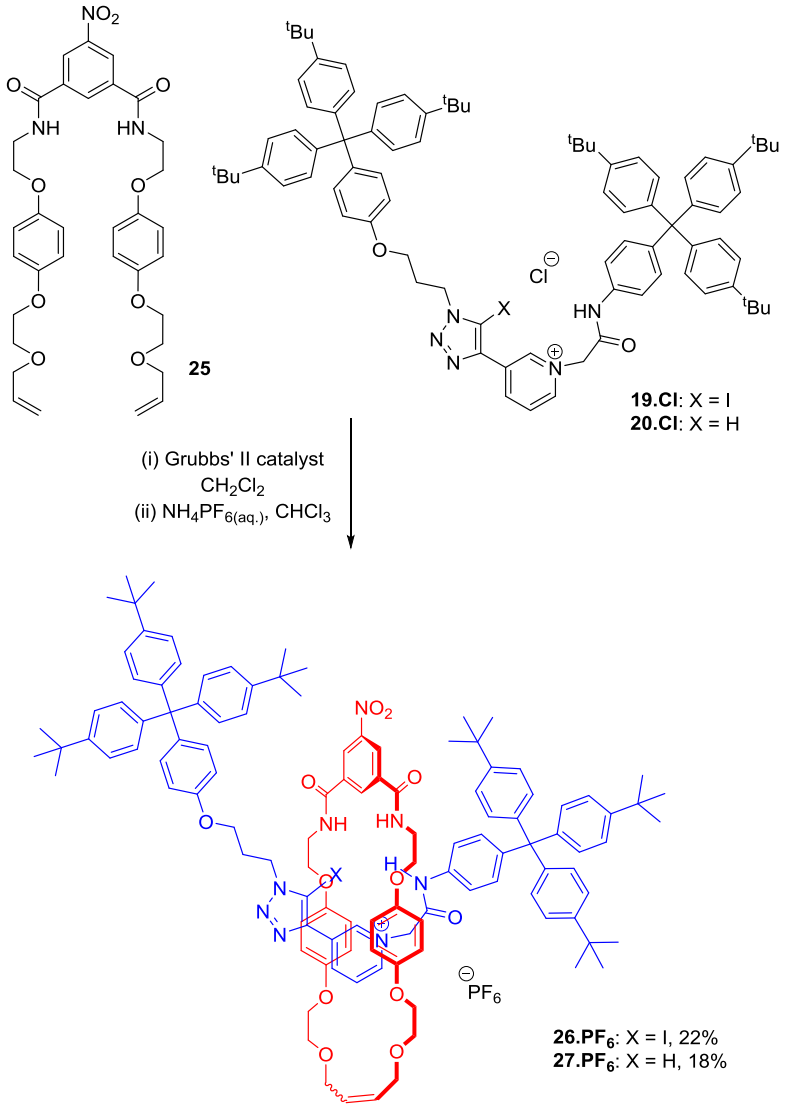

Scheme 2.9: Synthesis of rotaxanes **26·PF$_6$** and **27·PF$_6$**

Evidence for the formation of the HB interlocked product can be seen through comparison of the ^{1}H NMR spectra of **27·Cl** with those of axle **20·Cl** and macrocycle precursor **25** (**Figure 2.7)**. Upon formation of the rotaxane, the hydroquinone resonances of the macrocycle component (*4* and *5*) shift upfield and split, indicative of the π-π aromatic donor-acceptor interactions formed with the axle component and the desymmetrisation of the proton environments. Substantial downfield shifts of the internal aromatic proton *2* and the amide

protons *3* of the macrocycle are also observed due to the HB interactions these protons have with the chloride anion. The loss of the resonance for the terminal alkene protons *7* confirms that the ring closing metathesis reaction has occurred. Similar shifts were also observed in the formation of XB rotaxane **26·Cl**.

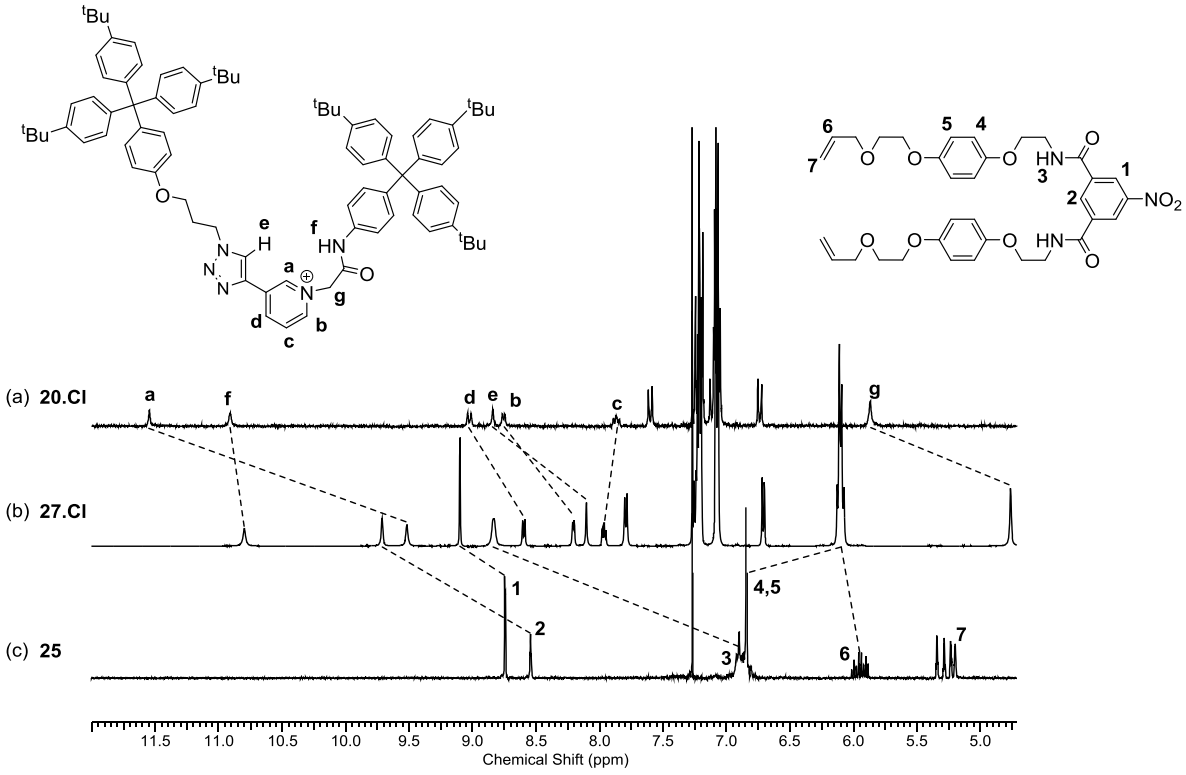

Figure 2.7: Truncated ^{1}H NMR spectra of: (a) HB axle **20·Cl**, (b) HB rotaxane **27·Cl** and (c) macrocycle precursor **25** ($CDCl_3$, 298 K)

Further evidence for the interlocked nature of rotaxanes **26·PF$_6$** and **27·PF$_6$** was obtained from two-dimensional ^{1}H-^{1}H ROESY NMR spectroscopy (**Figure 2.8**).

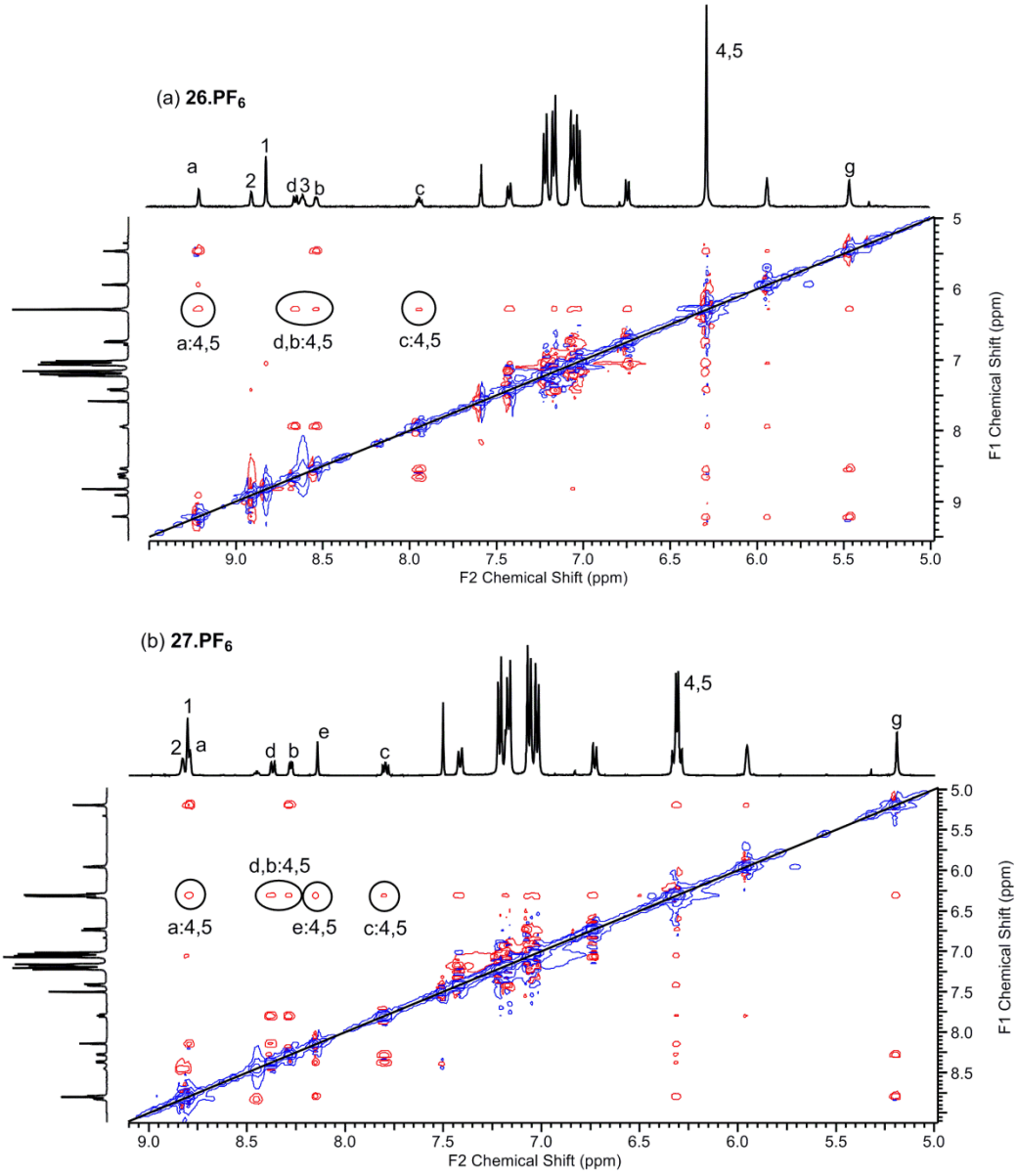

Figure 2.8: Truncated ^{1}H-^{1}H ROESY NMR spectra of; (a) XB rotaxane **26·PF$_6$** and (b) HB rotaxane **27·PF$_6$** (1:1 $CDCl_3$/CD_3OD, 298 K, 500 MHz).

In the spectra of both rotaxanes, cross peaks are observed between the resonances of hydroquinone protons *4* and *5* of the macrocycle and pyridinium protons *a*, *b*, *c* and *d* of the axle, implying that these protons are in close proximity to each other. In the HB rotaxane **27·PF$_6$** an additional cross-peak for the interaction between the hydroquinone protons and triazole proton *e* of the axle is also observed.

2.3.4 Anion binding properties of rotaxanes

The anion binding properties of rotaxanes **26·PF$_6$** and **27·PF$_6$** were investigated using ^{1}H NMR titration experiments performed in the 1:1 $CDCl_3$/CD_3OD solvent mixture. The internal cavity protons of the interlocked structures were monitored upon addition of chloride, bromide, iodide, dihydrogen phosphate and acetate TBA salts.

For both rotaxanes, the macrocycle's internal aromatic proton *2* and axle proton *a* shifted downfield upon addition of ten equivalents of the halides and dihydrogen phosphate, with triazole proton *e* also moving downfield in HB rotaxane **27·PF$_6$**, indicative of HB interactions between these protons and the anionic guests. In XB rotaxane **26·PF$_6$**, macrocycle proton *2* underwent the most significant shift for all anions, with chloride causing the largest magnitude change (0.45 ppm) followed by bromide (0.34 ppm), iodide (0.29 ppm) and dihydrogen phosphate (0.27 ppm). A similar trend was observed for axle proton *a*, however the magnitude of chemical shift perturbation was notably smaller; chloride (0.14 ppm) > bromide (0.13 ppm) > iodide (0.11 ppm) > dihydrogen phosphate (0.04 ppm). Addition of TBAOAc resulted in minimal shifts in any of the resonances of **26·PF$_6$**, implying that the rotaxane binds acetate very weakly.

Conversely, for HB rotaxane **27·PF$_6$**, axle proton *a* undergoes the largest change in chemical shift, with chloride again causing the largest magnitude of change (0.65ppm) followed by bromide (0.49 ppm), dihydrogen phosphate (0.47 ppm), iodide (0.30 ppm) and acetate (0.04 ppm). For macrocycle proton *2* the trend observed mirrored that seen for **26.PF$_6$**; chloride (0.32 ppm) > bromide (0.27 ppm) > iodide (0.22 ppm) > dihydrogen phosphate (0.12 ppm) > acetate (0.10 ppm).

WinEQNMR analysis[17] of the titration data, monitoring macrocycle proton *2* for each rotaxane (**Figure 2.9**), determined 1:1 stoichiometric association constants shown in **Table 2.2**.

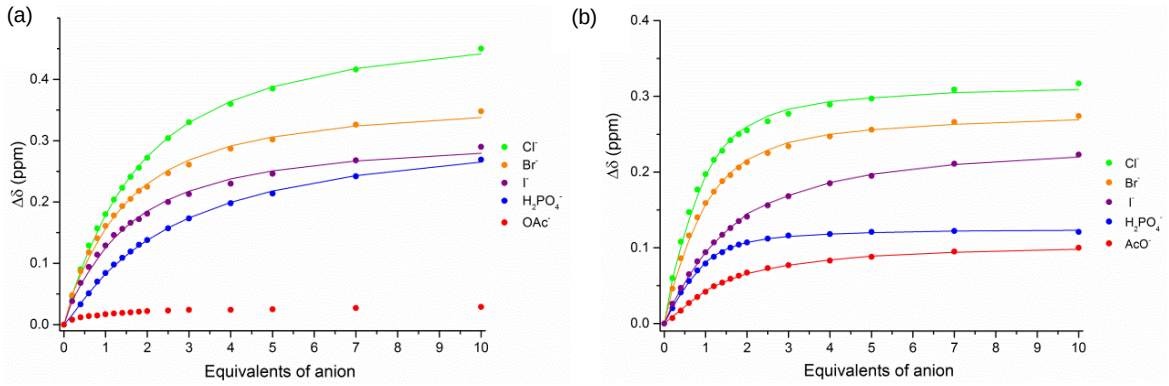

Figure 2.9: Experimental titration data (points) and calculated 1:1 binding isotherms (lines) for the addition of TBA salts of various anions to: (a) **26·PF$_6$** and (b) **27·PF$_6$**, monitoring macrocycle proton *2* (1:1 $CDCl_3/CD_3OD$, 298 K, 500 MHz).

Table 2.2: Association constants (K_a) determined for **26·PF6**, **27·PF6** and **5·PF6** with various anions (1:1 $CDCl_3/CD_3OD$, 298 K, 500 MHz).

Anion	K_a **(M^{-1})**[a]		
	26·PF$_6$	**27·PF$_6$**	**5·PF$_6$**
Cl^-	380	1830	520
Br^-	530	1300	450
I^-	470	450	–[c]
$H_2PO_4^-$	210	2400	710
AcO^-	–[b]	540	290

[a] Calculated using chemical shift of proton *2*. Estimated errors within ±10%. [b] Shifts too small to determine K_a. [c] Titration not performed.

HB rotaxane **27·PF$_6$** binds all of the anions, with the exception of iodide, significantly more strongly than XB rotaxane **26·PF$_6$**. This contradicts previous studies comparing the recognition properties of analogous XB and HB interlocked hosts, which have generally shown the XB system to bind anions with greater affinities.[4,5,7] One possible explanation is the XB-anion interaction of rotaxane **26·PF$_6$** causes the complexed anion to be held further away from the positive charge of the pyridinium group than in **27·PF$_6$**, which as a result substantially reduces the electrostatic contribution to the binding process.

Also of note are the contrasting anion selectivity trends of the two rotaxanes. XB rotaxane **26·PF$_6$** displays a preference for the halides over the more basic oxoanions, however, selectivity between the halides is relatively modest. In contrast, HB rotaxane **27·PF$_6$** forms the

strongest interaction with dihydrogen phosphate, followed by chloride, bromide, acetate and iodide. With the exception of acetate, this trend mirrors anion basicity. It is noteworthy that selectivity towards dihydrogen phosphate is unprecedented for an interlocked host, suggesting that the size and topology of the three-dimensional binding pocket of **27·PF$_6$** is highly complementary to the tetrahedral oxoanion.

Comparison of the association constants of rotaxane **27·PF$_6$** with those of HB acyclic receptor **5·PF$_6$** shows that the interlocked structure binds all of the anions more strongly, as expected. A greater degree of selectivity between the anions is also observed for the rotaxane. For example, the association constant calculated for dihydrogen phosphate association is approximately five times greater than that calculated for acetate association with the rotaxane, whilst only a 2.5-fold difference in these association constants is seen with the acyclic system.

2.4 Rotaxane containing a bis-iodotriazole pyridinium axle component

Following the anion binding studies performed with **26·PF$_6$** and **27·PF$_6$**, the effects of increasing the number of XB donors in the rotaxane's binding pocket on anion association strength and selectivity were investigated. Hence, the preparation of a rotaxane containing a pyridinium axle component with two iodotriazole motifs was undertaken.

2.4.1 Synthesis of bis-iodotriazole pyridinium axle

To prepare the bis-iodotriazole containing axle component, the previously prepared iodotriazole derivative **17** was firstly alkylated with propargyl bromide to give alkyne **28·Br**, which then underwent a CuAAC reaction with propyl-azide terphenyl stopper **14**. Following purification by preparative thin layer chromatography, the product was washed with aqueous ammonium chloride to give target axle **29·Cl** in a reasonable yield of 49% (**Scheme 2.10**).

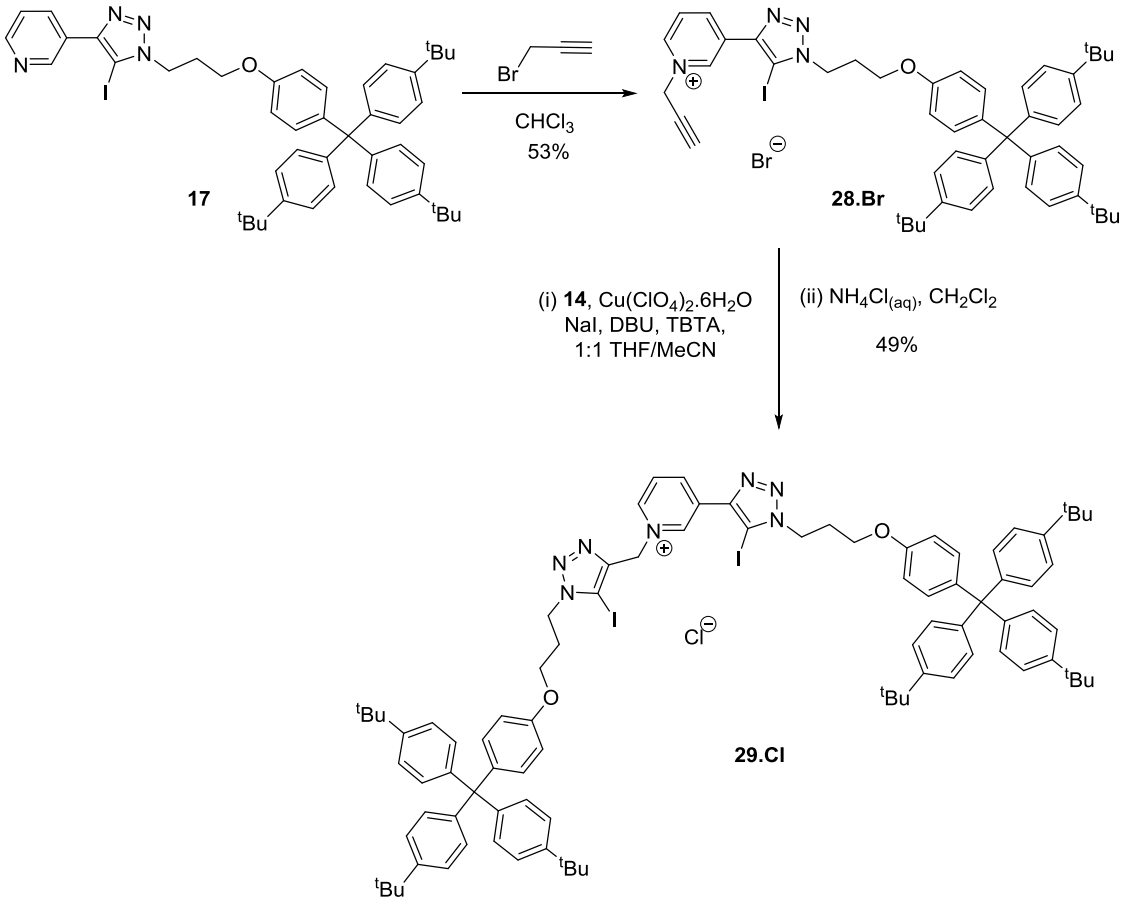

Scheme 2.10: Synthesis of bis-iodo-triazole axle **29·Cl**

2.4.2 Synthesis of rotaxane

Formation of the desired rotaxane was achieved using an identical 'clipping' procedure to the one used in the preparation of rotaxanes **26·PF$_6$** and **27·PF$_6$**, with a ring closing metathesis reaction of macrocycle precursor **25** around axle **29·Cl** giving the interlocked product **30·Cl**. The crude material was purified using a combination of preparative thin layer chromatography and size exclusion chromatography, after which the pure rotaxane was anion exchanged to give the hexafluorophosphate salt **30·PF$_6$**, in an isolated yield of 11%. In an attempt to improve this modest yield an analogous rotaxane formation procedure was performed using bromide as the templating species, however a similar isolated yield of 10% was obtained (**Scheme 2.11**). The modest yields obtained for both reactions can in part be attributed to the challenging chromatographic purification of the interlocked product.

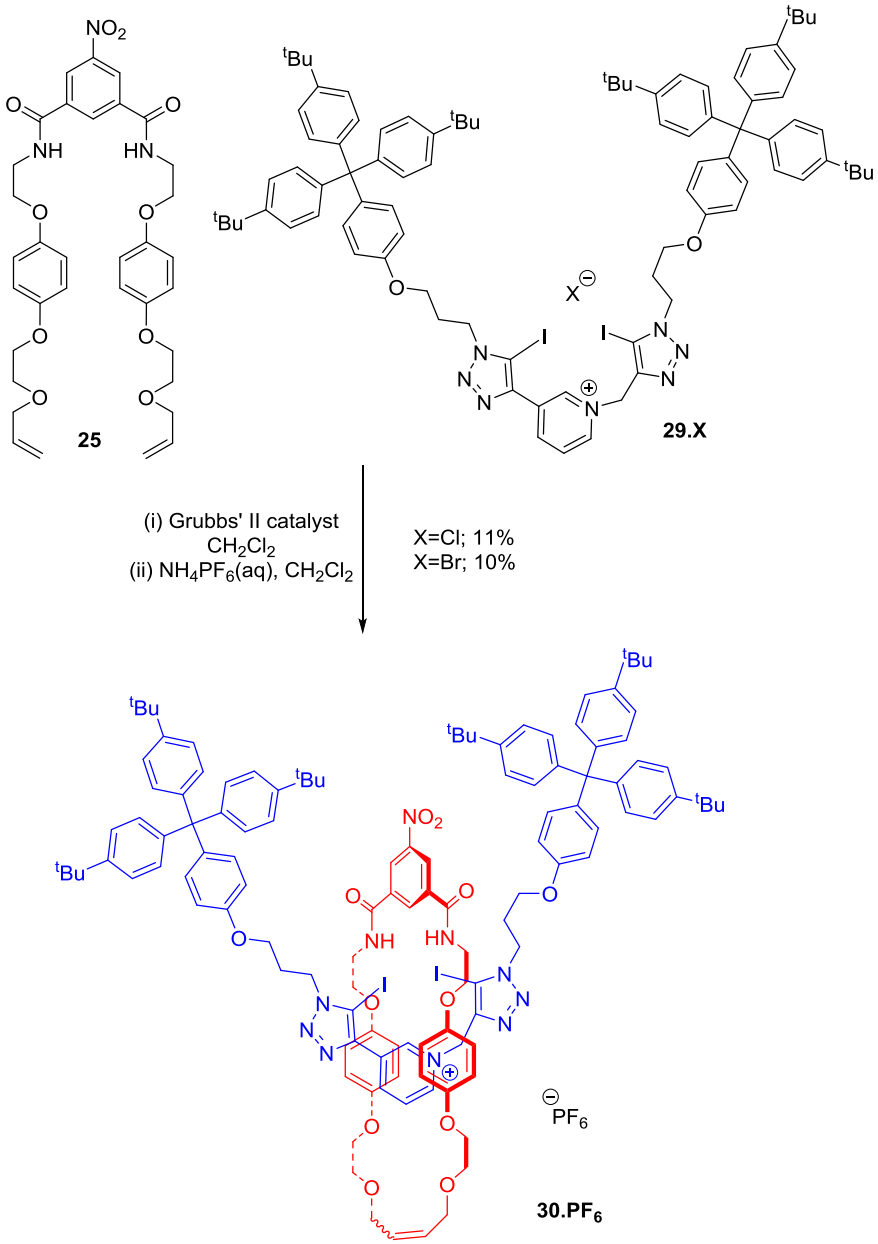

Scheme 2.11: Synthesis of rotaxane **30·PF$_6$**

The interlocked receptor **30·PF$_6$** was fully characterised using ^{1}H (**Figure 2.10**), ^{13}C, ^{19}F and ^{31}P NMR spectroscopy, high-resolution ESI mass spectrometry, and two-dimensional ^{1}H-^{1}H ROESY NMR.

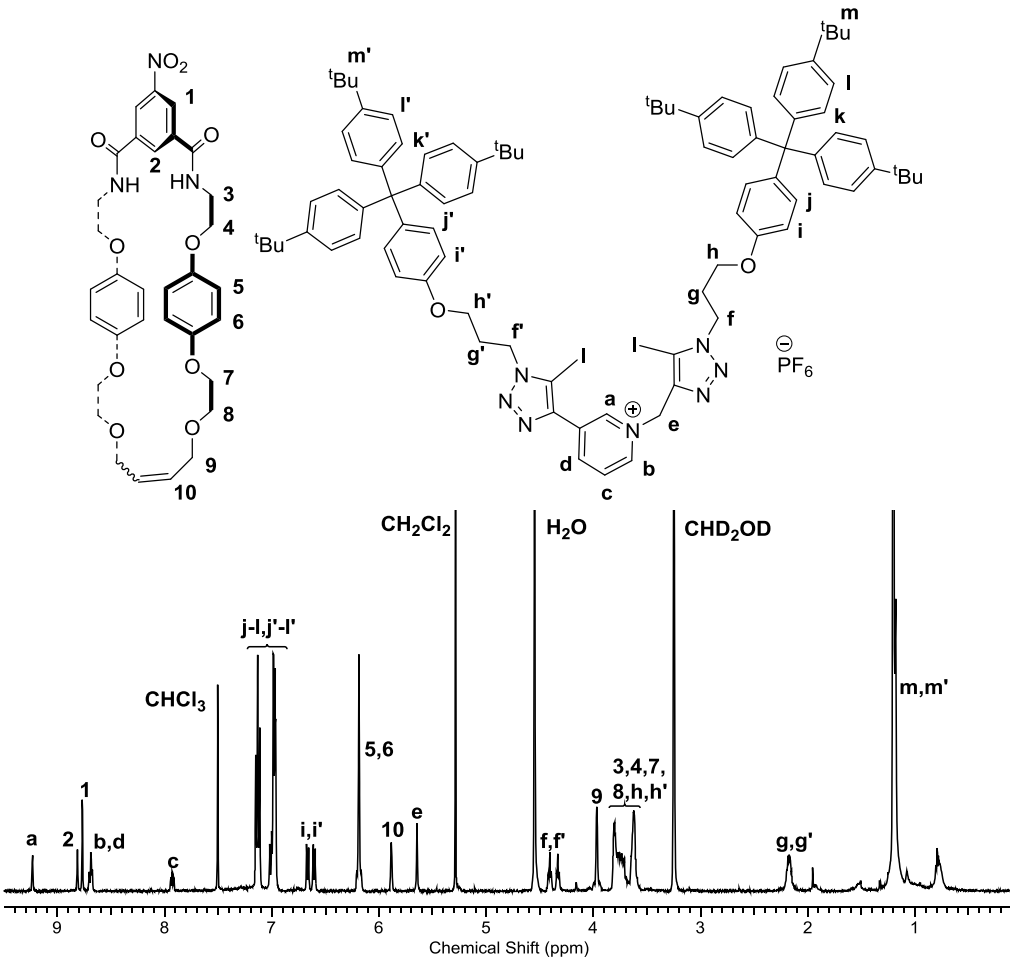

Figure 2.10: ^{1}H NMR spectrum of rotaxane **30·PF$_6$** (1:1 $CDCl_3/CD_3OD$, 298 K, 500MHz).

2.4.3 Anion binding properties of rotaxane 30·PF$_6$

As with **26.PF$_6$** and **27.PF$_6$**, the anion binding properties of **30·PF$_6$** were investigated in a 1:1 $CDCl_3/CD_3OD$ solvent mixture. Protons within the binding cavity of the rotaxane were monitored as increasing equivalents of chloride, bromide (**Figure 2.11**), iodide and dihydrogen phosphate anions were added as their TBA salts. Owing to the small amount of material isolated, no titration was performed with TBAOAc. A significant downfield perturbation of the macrocycle proton *2* was observed upon addition of all anions, indicating a HB interaction with the anionic guests. The largest magnitude shifts were seen with chloride and bromide (~ 0.4 ppm), with smaller shifts observed with iodide and dihydrogen phosphate (0.27 ppm and 0.14 ppm, respectively). Divergence of the resonances of hydroquinone protons *5* and *6* was also observed with all four anions. Furthermore, a substantial upfield

shift of pyridinium proton *a* of the axle component was observed upon addition of the halide salts. The nature of this shift suggests that this proton does not form an HB interaction with the anions, implying that their association with the axle component is mediated through XB and electrostatic interactions. Interestingly, no perturbation of this resonance was observed when dihydrogen phosphate was added, implying that the oxoanion does not form any XB interactions with the axle component.

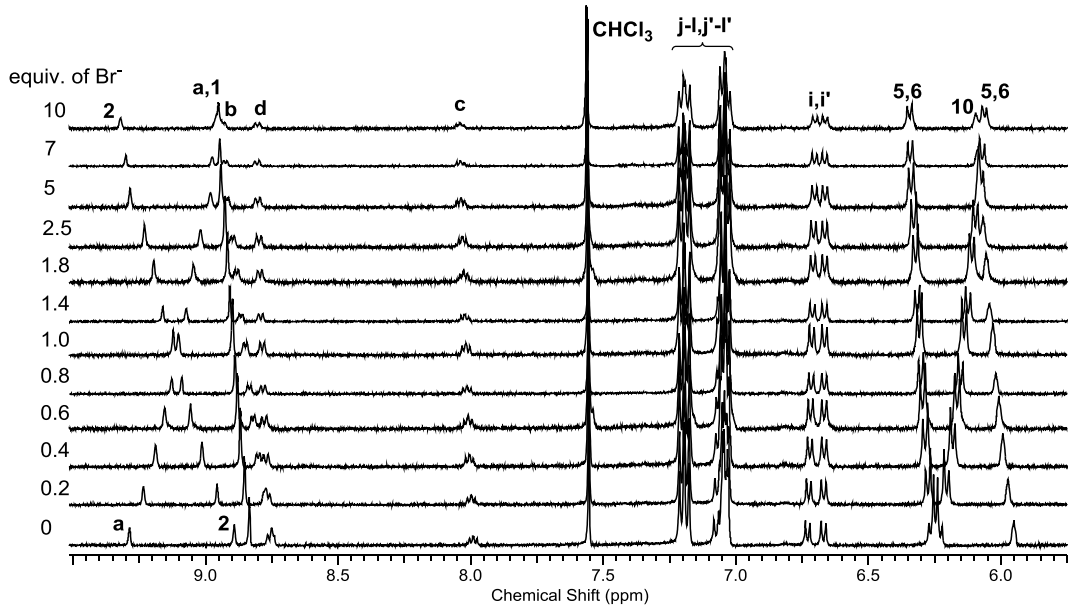

Figure 2.11: Truncated ^{1}H NMR spectra of **30·PF$_6$** upon addition of increasing equivalents of TBABr (1:1 $CDCl_3/CD_3OD$, 298 K, 500 MHz).

WinEQNMR analysis[17] of the titration data allowed the calculation of 1:1 stoichiometric association constants. For the halides, consistent values were obtained by monitoring the chemical shifts of several protons within the binding pocket (protons *2*, *5*, *6* and *a*), suggesting that these anions are fully encapsulated within the interlocked host. Comparison of the values obtained (**Table 2.3**) by monitoring proton *2* (**Figure 2.12**), shows that **30·PF$_6$** displays a preference towards the halides over dihydrogen phosphate, with the association constants of bromide and iodide approximately twenty times greater than that for the oxoanion. A modest preference for the larger halide anions, bromide and iodide, over chloride is also observed.

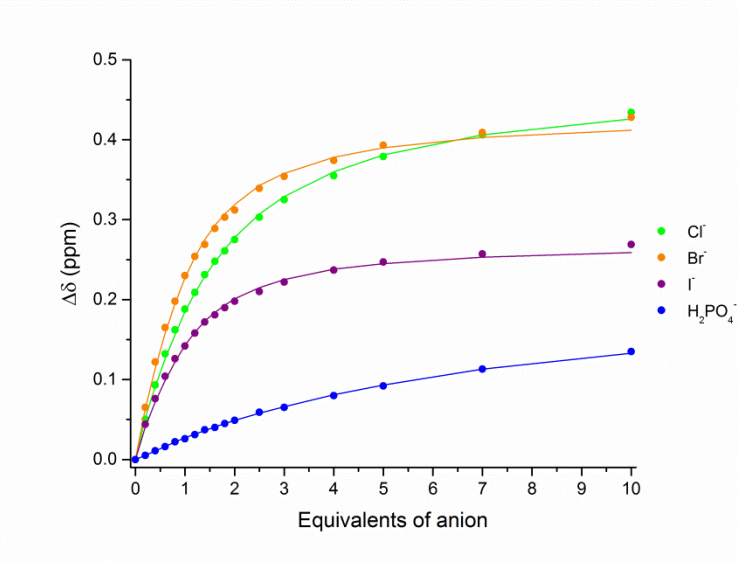

Figure 2.12: Experimental titration data (points) and calculated 1:1 binding isotherms (lines) for the addition of TBA salts of various anions to **30·PF$_6$**, monitoring macrocycle proton *2* (1:1 $CDCl_3/CD_3OD$, 298 K, 500 MHz)

Table 2.3: Association constants (K_a) determined for rotaxanes **30·PF$_6$**, **26·PF$_6$** and **27·PF$_6$** with various anions (1:1 $CDCl_3/CD_3OD$, 298 K, 500 MHz).

Anion	K_a **(M^{-1})**[a]		
	30·PF$_6$	**26·PF$_6$**	**27·PF$_6$**
Cl^-	460	380	1830
Br^-	1070	530	1300
I^-	1060	470	450
$H_2PO_4^-$	55	210	2400
AcO^-	–[b]	–[c]	540

[a] Calculated using chemical shift of proton *2*. Estimated errors within ±10%. [b] Titration not performed. [c] Shifts too small to determine K_a.

Comparing the anion association constants of all three rotaxanes **26·PF$_6$**, **27·PF$_6$** and **30·PF$_6$** (**Table 2.3**), demonstrates that substituting HB donors for XB donors in a rotaxane's binding pocket can have drastic effects on the anion selectivity trends observed. All-HB rotaxane **27·PF$_6$** displayed selectivity mirroring the basicity trend of the anions, with the association constant of dihydrogen phosphate (the most basic) approximately five times greater than that of iodide (the least basic). As the number of XB donors within the axle component is increased, a reversal of this selectivity trend was observed. Rotaxane **26·PF$_6$**, which contains a

single XB donor, shows a modest selectivity for the halides over the oxoanion, whilst rotaxane **30·PF$_6$**, containing two XB donors, shows a further enhancement to this selectivity, with the larger halides (bromide and iodide) being bound significantly more strongly. These results suggest that the XB interactions formed by **26·PF$_6$** and **30·PF$_6$** favour the association of more polarisable anions, which may be a consequence of the covalent character of the XB-anion interaction.

Further evidence of the anion binding mode of the rotaxane was provided by single crystal X-ray structural analysis of the chloride and bromide salts, **30·Cl** and **30·Br**. Small crystals of both salts were obtained by cooling a 1:1 $CDCl_3$/CD_3OD solution of **30·PF$_6$** containing either TBACl or TBABr to 253 K, with the structures determined by Jason Lim and Dr. Asha Brown.

Both structures (**Figure 2.13**) reveal that the halide anions are fully encapsulated within the three-dimensional binding pocket of the rotaxane by an array of five complementary receptor···anion XB and HB interactions in the solid state. The I···X$^-$ distances between the axle iodotriazole iodine atoms and the halide anions are 3.206(4) Å and 3.173(3) Å in **30·Cl** (∠C-I···Cl$^-$ = 172.4(4)°, 171.3(3)°), and 3.367(2) Å and 3.260(1) Å in **30·Br** (∠C-I···Br$^-$ = 170.6(3)°, 173.2(4)°). These distances are substantially shorter than the sum of the van der Waal's radii of the elements (%$VdW_{I,X}$ = 85–88),[26] while the C-I···X$^-$ angles are accordant with the expected linear XB geometry, which verifies the existence of strong, directional XB interactions in the solid state. Three DH···X$^-$ (D = N, C) short contacts between the macrocycle isophthalamide group and the halide anion are also observed in each structure, with D···X$^-$ distances ranging from 3.24–3.47 Å (for **30·Cl**) and 3.31–3.57 Å (for **30·Br**), and DH···X$^-$ angles ranging from 138–170°. In the structure of **30·Cl** and additional CH···Cl$^-$ HB interaction between the chloride anion and a chloroform solvent molecule is also observed.

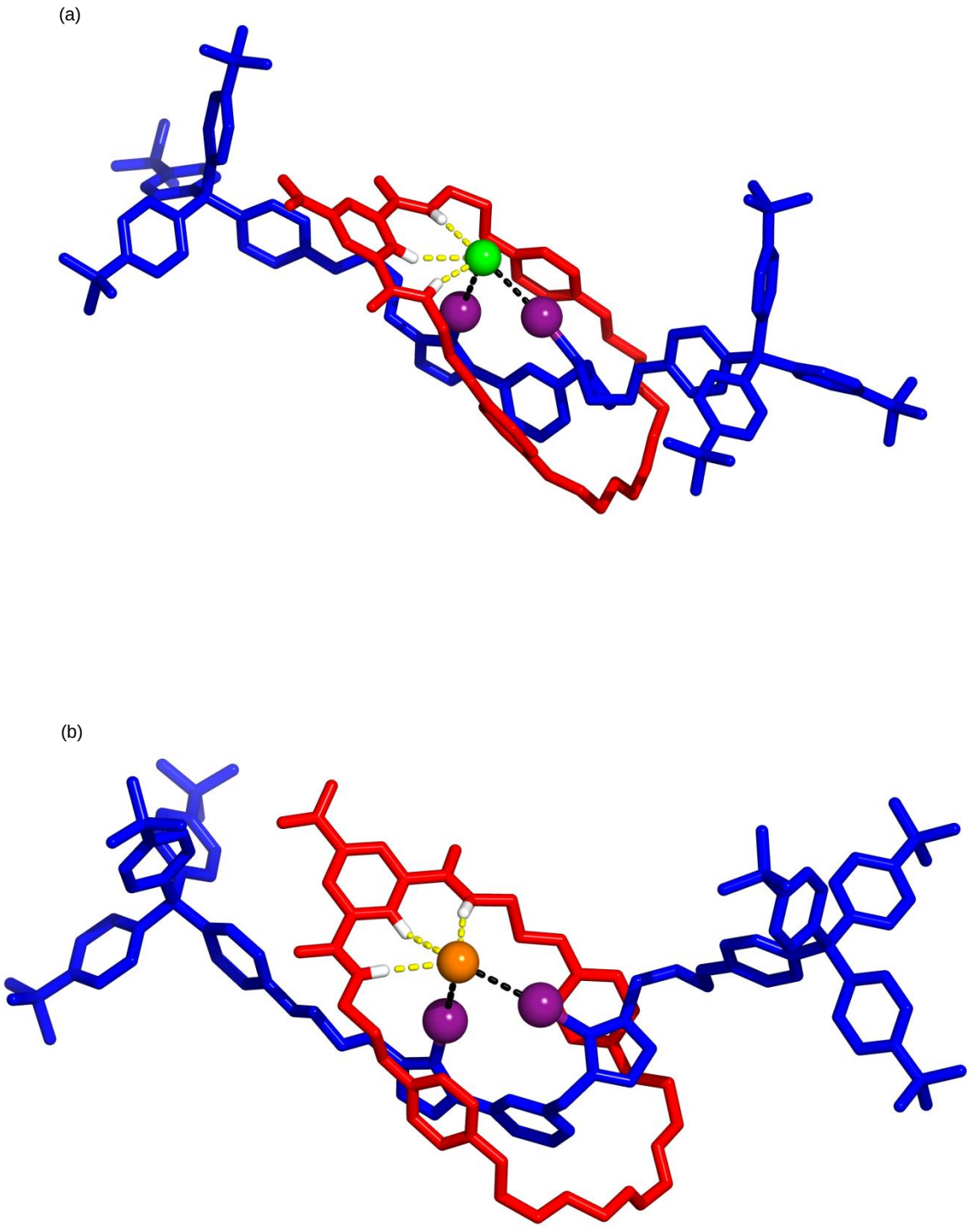

Figure 2.13: Solid-state X-Ray structures of: (a) **30·Cl** and (b) **30·Br** (solvent molecules and all non-hydrogen bonding hydrogen atoms omitted for clarity). HB interactions shown as yellow dashed lines; XB interactions shown as black dashed lines.

2.5 Acyclic and interlocked hydrogen bonding quinolinium receptors

Having demonstrated the anion recognition capabilities of the acyclic and interlocked hosts discussed above, analogous receptors with the potential of sensing anions through an optical response were prepared. To achieve this, the pyridinium motif was substituted with a fluorescent quinolinium motif.

The quinolinium fluorophore has been extensively used for sensing applications. Several examples of sensors for biological molecules, such as proteins[27] and saccharides,[28] have been reported which incorporate quinolinium motifs as signalling units. In the field of anion sensing, simple quinolinium derivatives are known to undergo a "turn-off" fluorescence response in the presence of negatively charged species. The reduction in emission intensity observed is caused by collisions between the fluorophore and anions and is referred to as dynamic quenching. This has led to applications, such as the use of 6-methoxy-1-methylquinolinium in the measurement of intracellular chloride concentrations.[29–31] A handful of hydrogen bonding anion receptors that incorporate the quinolinium motif have also been reported.[32–34] For example, Fabbrizzi and co-workers prepared a tricationic tripodal receptor containing three quinolinium groups, which undergoes a "turn-off" fluorescence response upon addition of a variety of anions in MeCN (**Figure 2.14a**),[32] whilst Yatsimirsky and co-workers reported a series of bis-quinolinium pyridine-2,6-dicarboxamide receptors that show the same response in water (**Figure 2.14b**).[34] In such receptors, the quenching of the fluorescence is caused by both binding of the anion (static quenching) and by collisions of the anion with the fluorophore (dynamic quenching).

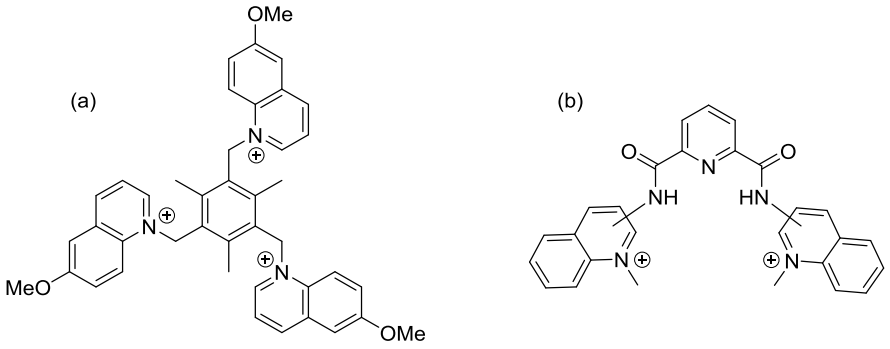

Figure 2.14: HB anion sensors containing the quinolinium fluorophore: (a) Fabbrizzi's tripodal receptor,[32] (b) Yatsimirsky's family of pyridine-2,6-dicarboaxmide receptors[34]

The following sections describe the preparation, anion binding and anion sensing properties of quinolinium containing analogues of the HB acyclic receptor **5·PF$_6$** and interlocked receptor **27·PF$_6$**.

2.5.1 Synthesis of acyclic receptor

The target acyclic receptor was prepared using an analogous procedure to that used in the synthesis of pyridinium receptor **5·PF$_6$** (**Scheme 2.12**). 3-Bromoquinoline was reacted with ethynyltrimethylsilane under Sonogashira coupling conditions to give a trimethylsilyl-protected alkyne, which was subsequently deprotected with KOH in MeOH to afford 3-ethynylquinoline **31**. A CuAAC reaction between **31** and 1-azidooctane gave prototriazole derivative **32** which, after alkylation with **3**, purification by column chromatography and anion exchange by washing with aqueous NH_4PF_6, afforded the target receptor **33·PF$_6$** in 54% yield.

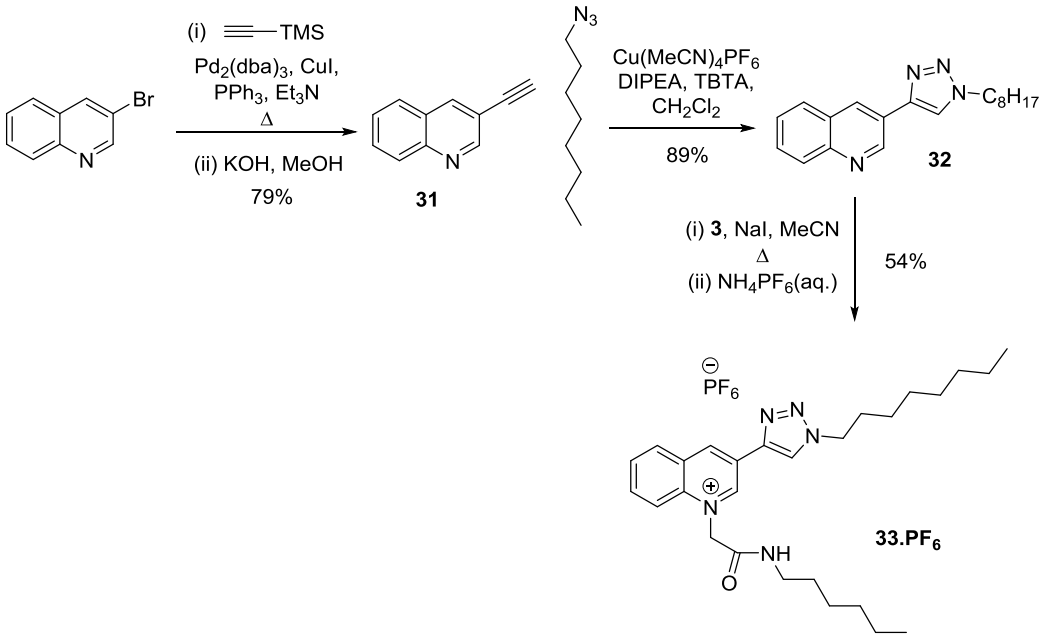

Scheme 2.12: Synthesis of acyclic receptor **33·PF$_6$**.

2.5.2 Anion binding properties of acyclic receptor 33·PF$_6$

Initial investigations into the anion binding properties of receptor **33·PF$_6$** were conducted using ^{1}H NMR titration experiments performed in 1:1 $CDCl_3/CD_3OD$ solution. Addition of chloride, bromide (**Figure 2.15**) and dihydrogen phosphate TBA salts resulted in significant downfield shifts of quinolinium proton *a* and triazole proton *g*. For proton *a*, the perturbations were of a similar magnitude in both halide titrations (~ 0.2 ppm), with a smaller shift caused by dihydrogen phosphate (0.12 ppm). A titration with TBA acetate was also performed; however as equivalents of the anion increased additional resonances began to appear in the aromatic region of the spectra, suggesting an anion induced decomposition of the receptor. Owing to the highly basic nature of the acetate anion, this most likely occurs through a deprotonation pathway.

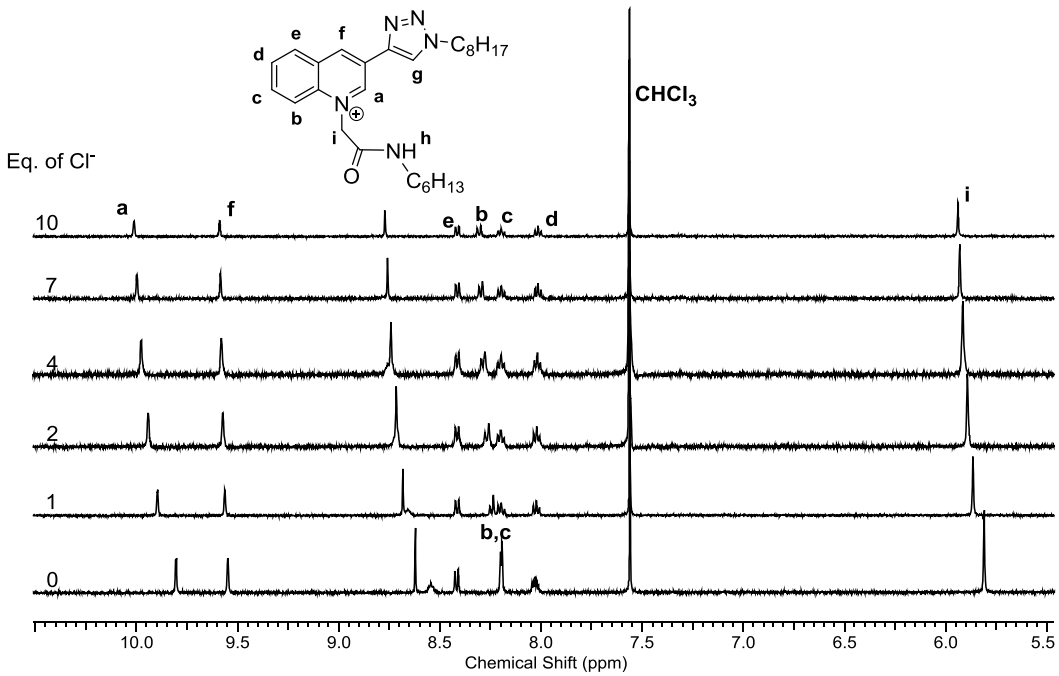

Figure 2.15: Truncated ^{1}H NMR spectra of **33·PF$_6$** upon addition of increasing equivalents of TBACl (1:1 $CDCl_3/CD_3OD$, 298 K, 500 MHz).

WinEQNMR analysis[17] of the titration data, monitoring the shift of proton *a* (**Figure 2.16**), determined 1:1 stoichiometric association constants (**Table 2.4**). As with HB pyridinium receptor **5·PF$_6$**, a modest selectivity between the anions was observed, with dihydrogen phosphate bound the most strongly.

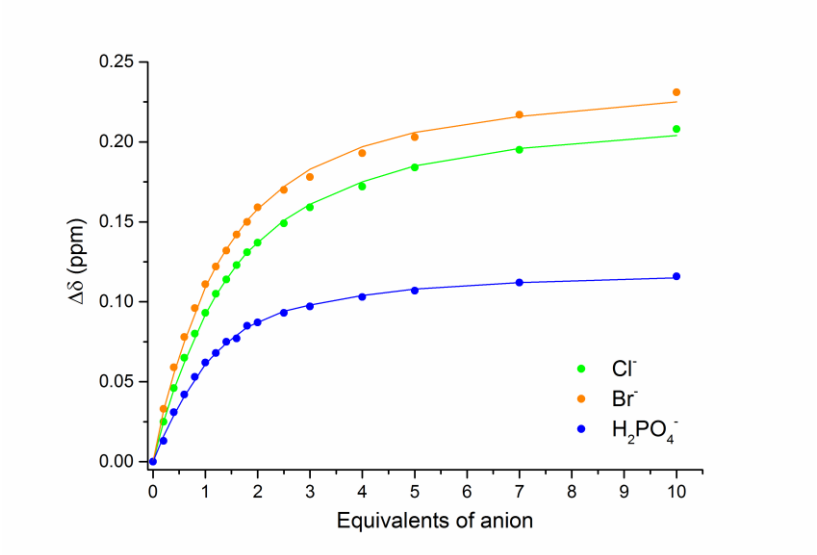

Figure 2.16: Experimental titration data (points) and calculated 1:1 binding isotherms (lines) for the addition of TBA salts of various anions to **33·PF$_6$**, monitoring proton *a* (1:1 $CDCl_3/CD_3OD$, 298 K, 500 MHz)

Table 2.4: Association constants (K_a) determined for acyclic receptors **33·PF$_6$** and **5·PF$_6$** with various anions (1:1 $CDCl_3/CD_3OD$, 298 K, 500 MHz).

Anion	K_a (M^{-1})[a]	
	33·PF$_6$	**5·PF$_6$**
Cl^-	530	520
Br^-	630	450
$H_2PO_4^-$	970	710
AcO^-	–[b]	290

[a] Calculated using chemical shift of proton *a*. Estimated errors within ±10%. [b] No value calculated due to decomposition of receptor

2.5.3 UV-visible and fluorescence anion titration experiments

The ability of **33·PF$_6$** to act as an optical anion sensor was investigated using UV-visible and fluorescence titration experiments.

Minimal changes in the absorption spectra of the receptor were observed after addition of up to two-hundred equivalents of chloride (**Figure 2.17**), bromide and dihydrogen phosphate in a 1:1 $CHCl_3/CH_3OH$ solvent mixture. Similar responses have been reported for other HB quinolinium anion receptors.[34]

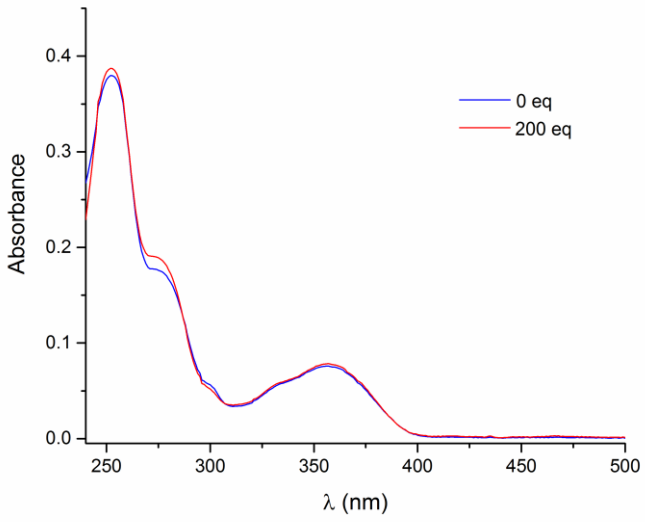

Figure 2.17: UV-visible absorption spectra of **33·PF$_6$** (10 μM concentration) before (blue line) and after (red line) addition of 200 equivalents of TBACl (1:1 $CHCl_3/CH_3OH$, 293K).

In contrast, substantial changes in the emission spectrum of **33·PF$_6$** were observed in the same solvent system. Addition of up to four-hundred equivalents of the same three anions resulted in a quenching of the emission intensity, with the magnitude of reduction similar in all cases (~ 60%) (**Figure 2.18a**, bromide titration).

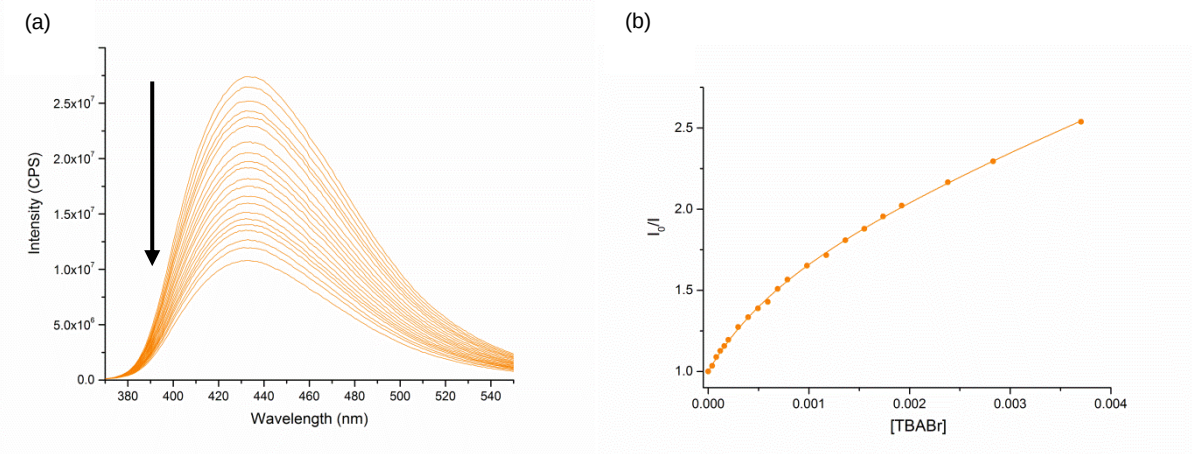

Figure 2.18: (a) Changes in the emission spectrum of **33·PF$_6$** (10 μM concentration) on addition of up to 400 equivalents of TBABr (1:1 $CHCl_3/CH_3OH$, λ_{ex} = 358 nm), (b) Stern-Volmer plot of fluorescence quenching of **33·PF$_6$** by TBABr (λ_{ex} = 358 nm, λ_{em} = 432 nm). Experimental data represented by points and calculated 1:1 binding isotherm represented by line.

A plot of I_0/I *vs.* [anion] (where I_0 and I correspond to the emission intensity measured in the absence and in the presence of the anion, respectively) was used to obtain more information about the fluorescence quenching mechanism. The plots showed downward curvature initially and became linear as the amount of anion increases (**Figure 2.18b**, bromide titration). This suggests that at low anion concentrations the quenching mechanism has both static and dynamic components, whilst at high anion concentrations, when the amount of unbound receptor present is negligible, a dynamic quenching mechanism becomes dominant. This has previously been observed in systems where association of the anion causes only a partial decrease in the receptor's emission intensity, rather than complete quenching (**Figure 2.19**).[32]

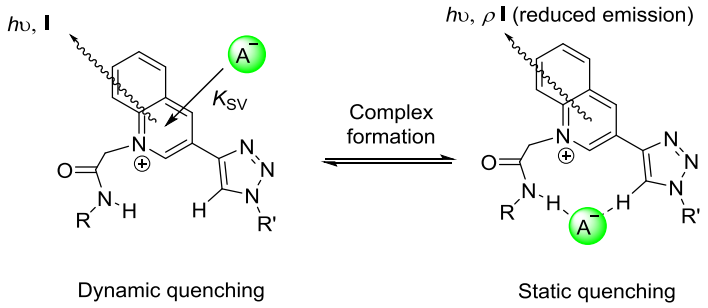

Figure 2.19: Quenching mechanism of receptor **33·PF$_6$** by anions

Plots of this nature can be represented by **Equation 1**, where K_a is the ground state association constant, K_{SV} is the Stern-Volmer constant for dynamic quenching and ρ is the factor by which fluorescence is reduced upon anion complexation.

$$\frac{I_0}{I} = \frac{(1+K_a[A^-])(1+K_{SV}[A^-])}{1+\rho K_a[A^-]} \qquad \textbf{Equation 1}$$

Fitting of the experimental data to this 1:1 binding isotherm, using the Origin™ software package, afforded values for K_a, K_{SV} and ρ (**Table 2.5**).

Table 2.5: Calculated association constants (K_a), Stern-Volmer constants (K_{SV}) and static quenching factors (ρ) for acyclic receptor **33·PF$_6$** with various anions (1:1 $CHCl_3/CH_3OH$, 293 K).

Anion	K_a (M^{-1})^a	K_{SV} (M^{-1})^a	ρ^a
Cl^-	2560	160	0.58
Br^-	1910	120	0.50
$H_2PO_4^-$	1400	70	0.39

a Calculated monitoring emission intensity at 358 nm. Estimated errors within ±10%.

Despite the quality of the fit between the experimental and calculated data, it is likely that the values obtained are unreliable. For instance, a reversal of the anion selectivity trend is observed compared to the ^{1}H NMR titration results. In addition, the largest K_{SV} value was obtained for chloride (160 M^{-1}), which contradicts earlier studies with related quinolinium receptors, which have generally shown K_{SV} values to be greater for the heavier halides. This

has been ascribed to the 'heavy-atom effect'.[35] These discrepancies suggest that the model used to describe the quenching mechanism of **33·PF$_6$** is not accurate, which is potentially due to the assumptions that are made in the derivation of **Equation 1**. These include the use of a single K_{SV} value and a single rate of photoexcitation for both complexed and uncomplexed forms of the fluorophore. Removal of these assumptions results in an expression with a larger number of adjustable parameters, which is difficult to fit reliably. The data obtained from the ^{1}H NMR titration experiments most likely provides a more accurate estimate of the strength of anion association.

2.5.4 Synthesis of a quinolinium containing [2]rotaxane

The anion binding quinolinium motif was then incorporated into the axle component of a [2]rotaxane. This was attempted using the same chloride-templated 'clipping' strategy as used in the synthesis of the previously discussed pyridinium containing rotaxanes. The preparation of a quinolinium-containing axle was undertaken using a synthetic procedure analogous to that used for pyridinum axle **20·Cl** (**Scheme 2.13**). 3-Ethynyl quinoline **31** was reacted with propyl-azide stopper **14** under CuAAC conditions to give prototriazole derivative **34**, which was then alkylated with alkyl-bromide appended stopper **16** in the presence of NaI. Following purification and anion exchange to the chloride salt, the target axle **35·Cl** was isolated in a 40% yield.

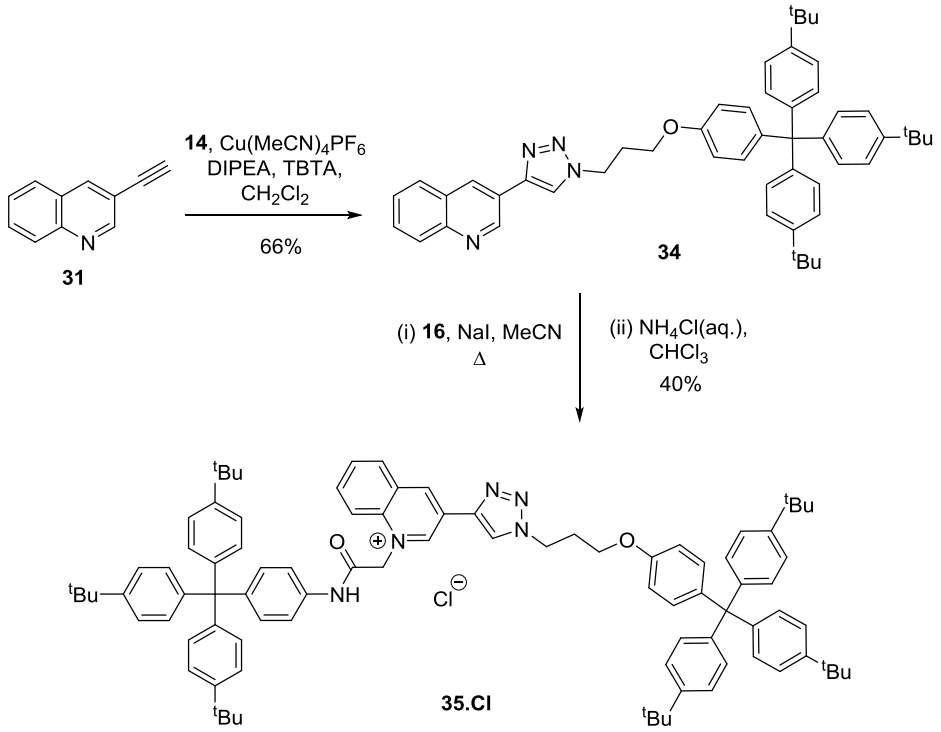

Scheme 2.13: Synthesis of quinolinium axle **35·Cl**

The target rotaxane was then prepared as shown in **Scheme 2.14**. Extensive chromatographic purification was required to isolate the pure product, after which anion exchange, by washing with aqueous NH_4PF_6, gave **36·PF$_6$** in a modest yield of 7%.

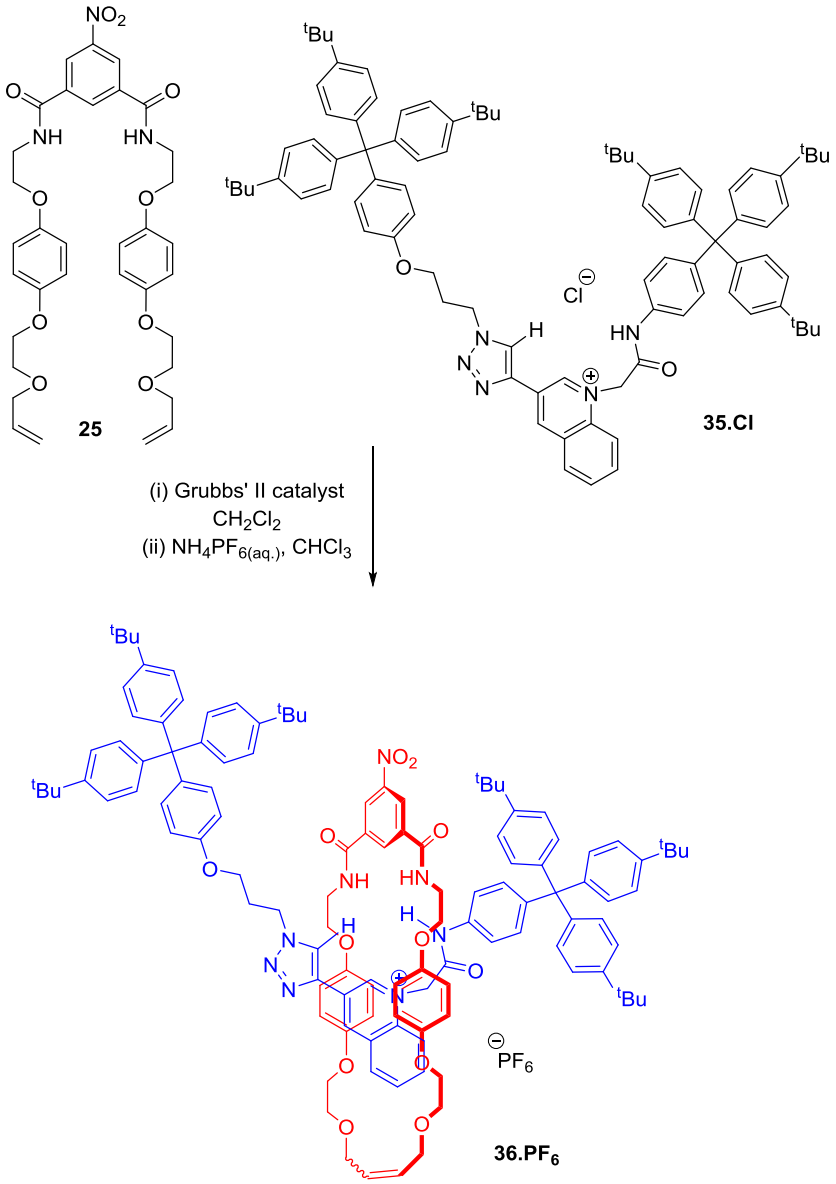

Scheme 2.14: Synthesis of rotaxane **36·PF$_6$**

The interlocked receptor **36.PF$_6$** was fully characterised using ^{1}H (**Figure 2.20**), ^{13}C, ^{19}F and ^{31}P NMR spectroscopy and high resolution ESI mass spectrometry. Comparison of the ^{1}H NMR spectrum of **36·PF$_6$** with that of the analogous HB pyridinum containing rotaxane **27·PF$_6$**, shows that the hydroquinone resonances are shifted further upfield in rotaxane **36·PF$_6$** (δ = 6.14 ppm for **36.PF$_6$**; δ = 6.34 ppm for **27.PF$_6$**), implying that there is a stronger π-π aromatic donor-acceptor interaction between axle and macrocycle in this rotaxane. This is most likely a result of the larger π-surface of the quinolinium motif relative to the pyridinium motif.

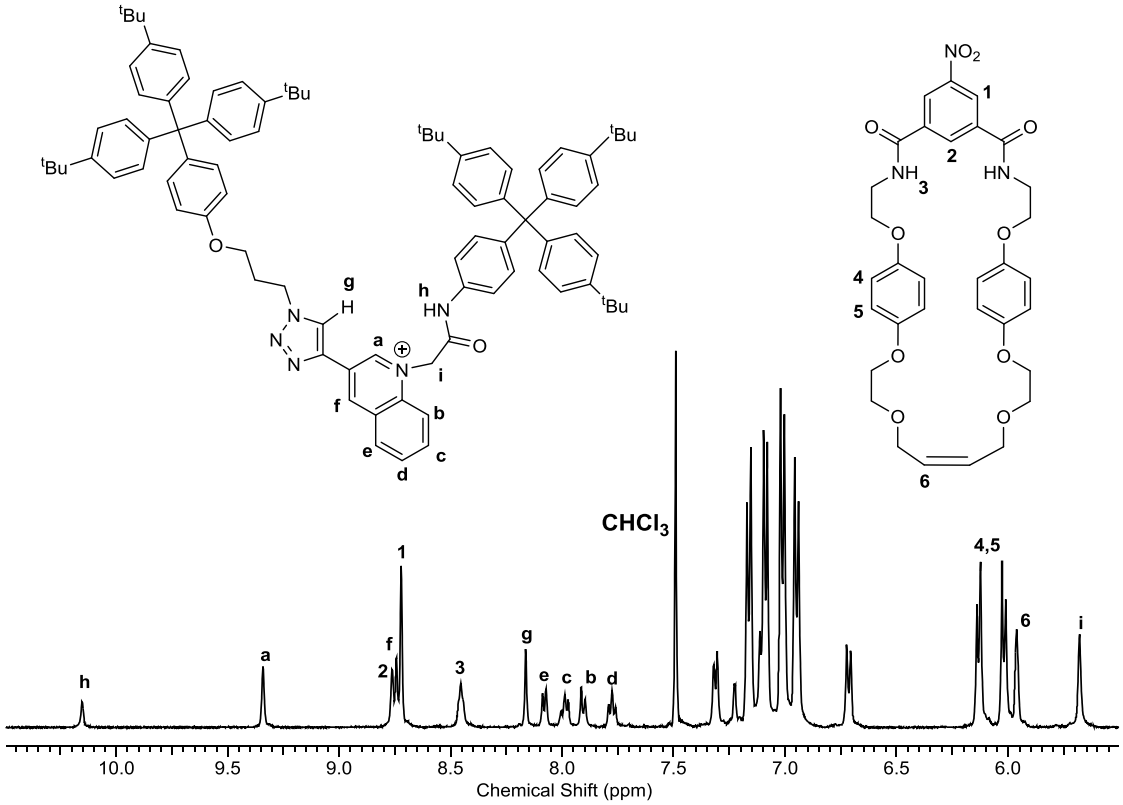

Figure 2.20: Truncated ^{1}H NMR spectrum of quinolinium rotaxane **36·PF$_6$** (1:1 $CDCl_3/CD_3OD$, 298 K, 500 MHz)

Two-dimensional ^{1}H-^{1}H ROESY NMR spectroscopy was used to confirm the interlocked nature of **36·PF$_6$** (**Figure 2.21**). Through-space interactions between protons *a*, *f* and *g* of the axle and hydroquinone protons *4* and *5* are observed, as well as an interaction between quinolinium proton *a* and macrocycle proton *2*.

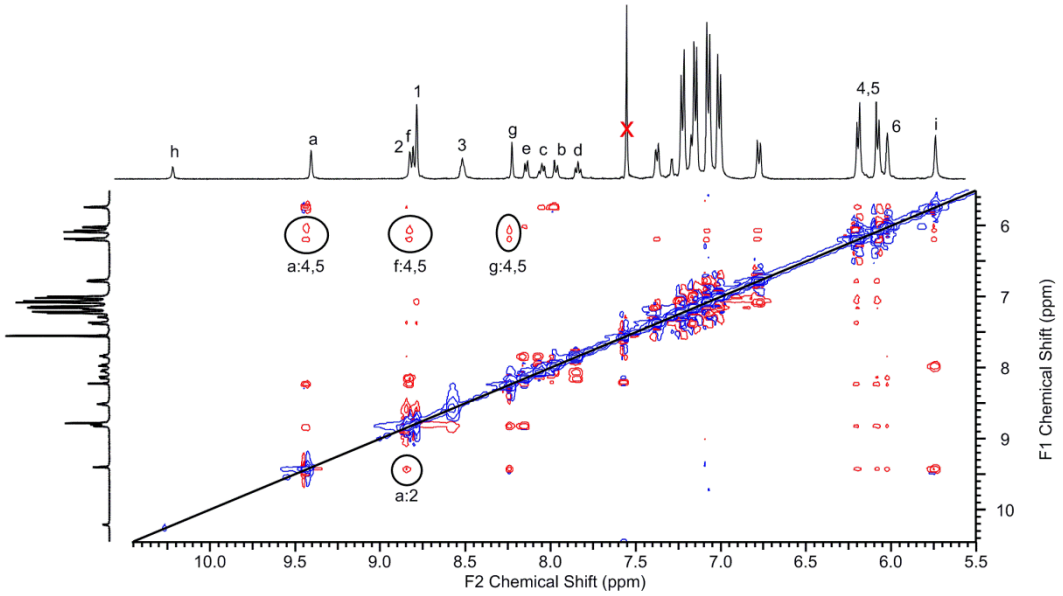

Figure 2.21: Truncated ^{1}H-^{1}H ROESY NMR spectrum of quinolinium rotaxane **36·PF$_6$** (1:1 $CDCl_3/CD_3OD$, 298 K, 500 MHz).

2.5.5 Anion binding properties of rotaxane 36·PF$_6$

The anion binding properties of rotaxane **36·PF$_6$** were investigated in a 1:1 $CDCl_3/CD_3OD$ solvent mixture. Addition of ten equivalents of chloride, bromide and dihydrogen phosphate TBA salts resulted in significant downfield perturbations of quinolinium proton *a*, triazole proton *g* and macrocycle proton *2*. For all three anions, proton *2* underwent the largest shift, with the greatest magnitude of change caused by chloride (0.57 ppm) followed by bromide (0.51 ppm) and dihydrogen phosphate (0.31 ppm). The same trend was observed for axle proton *a*; chloride (0.26 ppm) > bromide (0.22 ppm) > dihydrogen phosphate (0.09 ppm).

WinEQNMR analysis[17] of the titration data, monitoring proton *2* of the macrocycle component (**Figure 2.22**), gave 1:1 stoichiometric association constants (**Table 2.6**). Rotaxane **36·PF$_6$** displays a modest preference towards the halides over the more basic dihydrogen phosphate, with the association constant values calculated for chloride and bromide approximately three-times larger than that obtained for the oxoanion. Interestingly, this selectivity trend is the opposite of that observed with the analogous HB pyridinium rotaxane **27·PF$_6$**, which was found to bind dihydrogen phosphate more strongly than the

halides. This suggests that, unlike **27·PF$_6$**, the binding pocket of **36·PF$_6$** is not complementary to the size and shape of the tetrahedral anion, which is most likely due to a different orientation of the HB donor groups within the two rotaxanes. This lack of complementarity is verified further by the dihydrogen phosphate association constant of the acyclic quinolinium receptor **33·PF$_6$**, which is also larger than that calculated for rotaxane **36·PF$_6$**. In contrast, both halide anions are bound more strongly by the interlocked receptor, as would be expected.

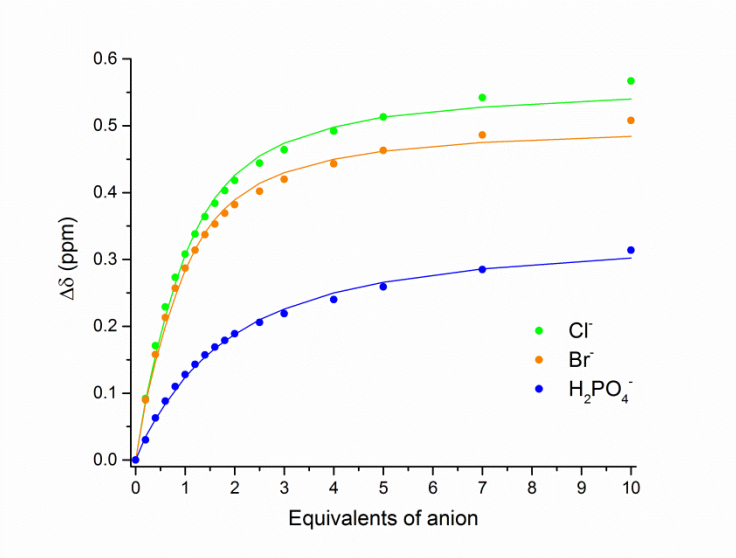

Figure 2.22: Experimental titration data (points) and calculated 1:1 binding isotherms (lines) for the addition of TBA salts of various anions to rotaxane **36·PF$_6$**, monitoring proton *2* (1:1 $CDCl_3/CD_3OD$, 298 K, 500 MHz)

Table 2.6: Association constants (K_a) determined for rotaxanes **36·PF$_6$** and **27·PF$_6$** and acyclic receptor **33·PF$_6$** with various anions (1:1 $CDCl_3/CD_3OD$, 298 K, 500 MHz).

Anion	K_a (M^{-1})[a]		
	36·PF$_6$	**27·PF$_6$**	**33·PF$_6$**
Cl^-	1190	1830	530
Br^-	1320	1300	630
$H_2PO_4^-$	380	2400	970

[a] Calculated using chemical shift of proton *2*. Estimated errors within ±10%.

Investigations into the optical response of rotaxane **36·PF$_6$** towards anion binding are yet to be conducted.

2.6 Conclusions and future work

The research work discussed in this chapter has demonstrated how substitution of HB donors for XB donors in anion receptors can have major effects on anion association strength and selectivity.

Initially acyclic receptors that contained a single XB iodotriazole or HB prototriazole motif were prepared. No binding interactions were observed between the XB derivative and a range of anions; however, the HB host was found to bind chloride, bromide, dihydrogen phosphate and acetate with reasonable affinity in a competitive 1:1 $CDCl_3/CD_3OD$ solvent mixture with a modest selectivity for dihydrogen phosphate.

Two novel [2]rotaxanes, XB **26·PF$_6$** and HB **27·PF$_6$**, containing the same anion binding motifs as these acyclic receptors within their axle components, were prepared by a chloride templated RCM 'clipping' procedure. Interestingly, the HB rotaxane **27·PF$_6$** bound all of the anions investigated more strongly than the XB rotaxane **26·PF$_6$**, with the exception of iodide, which was attributed to a greater electrostatic contribution to the binding interaction in **27·PF$_6$**. The rotaxanes displayed contrasting selectivity trends, with XB **26·PF$_6$** binding halides more strongly than dihydrogen phosphate and acetate, and HB **27·PF$_6$** showing an unprecedented selectivity towards dihydrogen phosphate.

A third novel rotaxane **30·PF$_6$** containing two iodotriazole XB donor motifs within its axle component exhibited an enhanced selectivity preference for the halides over dihydrogen phosphate relative to the mono-iodotriazole rotaxane **26·PF$_6$**. Particularly strong affinities were observed with the larger halides, bromide and iodide.

Fluorescent quinolinium analogues of HB receptors **5·PF$_6$** and **27·PF$_6$** were also prepared. Acyclic receptor **33·PF$_6$** was shown to have similar anion binding properties to its pyridinium analogue **5·PF$_6$**, with spectrofluorometric titration experiments revealing its ability to sense chloride, bromide and dihydrogen phosphate by a "turn-off" fluorescence response.

Interestingly, interlocked receptor **36·PF$_6$** displayed a different selectivity trend to that of the analogous pyridinium rotaxane **27·PF$_6$**, with the association constants for chloride and bromide of greater magnitude than that of the more basic dihydrogen phosphate anion. Analysis of the anion sensing properties of **36·PF$_6$** are yet to be conducted.

Future work in this area could involve investigations into the anion recognition properties of interlocked structures containing a larger number of XB donors within their binding pockets. This could be achieved by replacing the bis-amide binding motif of the macrocycle component with an XB bis-iodotriazole motif.

2.7 References

1 M. G. Chudzinski, C. A. McClary and M. S. Taylor, *J. Am. Chem. Soc.*, 2011, **133**, 10559–10567.
2 M. Cametti, K. Raatikainen, P. Metrangolo, T. Pilati, G. Terraneo and G. Resnati, *Org. Biomol. Chem.*, 2012, **10**, 1329–1333.
3 F. Zapata, A. Caballero, P. Molina, I. Alkorta and J. Elguero, *J. Org. Chem.*, 2014, **79**, 6959–6969.
4 S. W. Robinson, C. L. Mustoe, N. G. White, A. Brown, A. L. Thompson, P. Kennepohl and P. D. Beer, *J. Am. Chem. Soc.*, 2015, **137**, 499–507.
5 N. L. Kilah, M. D. Wise, C. J. Serpell, A. L. Thompson, N. G. White, K. E. Christensen and P. D. Beer, *J. Am. Chem. Soc.*, 2010, **132**, 11893–11895.
6 A. Caballero, F. Zapata, N. G. White, P. J. Costa, V. Félix and P. D. Beer, *Angew. Chem. Int. Ed.*, 2012, **51**, 1876–1880.
7 M. J. Langton, S. W. Robinson, I. Marques, V. Félix and P. D. Beer, *Nat. Chem.*, 2014, **6**, 1039–1043.
8 L. C. Gilday and P. D. Beer, *Chem. – Eur. J.*, 2014, **20**, 8379–8385.
9 B. R. Mullaney, B. E. Partridge and P. D. Beer, *Chem. – Eur. J.*, 2015, **21**, 1660–1665.
10 B. R. Mullaney, A. L. Thompson and P. D. Beer, *Angew. Chem. Int. Ed.*, 2014, **53**, 11458–11462.
11 M. J. Langton, I. Marques, S. W. Robinson, V. Félix and P. D. Beer, *Chem. – Eur. J.*, 2016, **22**, 185–192.
12 B. Huang, S. M. Santos, V. Felix and P. D. Beer, *Chem. Commun.*, 2008, 4610–4612.
13 S. G. Alvarez and M. T. Alvarez, *Synthesis*, 1997, **1997**, 413–414.
14 W. S. Brotherton, R. J. Clark and L. Zhu, *J. Org. Chem.*, 2012, **77**, 6443–6455.
15 D. N. Barsoum, N. Okashah, X. Zhang and L. Zhu, *J. Org. Chem.*, 2015, **80**, 9542–9551.
16 V. V. Rostovtsev, L. G. Green, V. V. Fokin and K. B. Sharpless, *Angew. Chem. Int. Ed.*, 2002, **41**, 2596–2599.
17 M. J. Hynes, *J. Chem. Soc. Dalton Trans.*, 1993, 311–312.
18 M. R. Sambrook, P. D. Beer, J. A. Wisner, R. L. Paul, A. R. Cowley, F. Szemes and M. G. B. Drew, *J. Am. Chem. Soc.*, 2005, **127**, 2292–2302.
19 C. J. Serpell, N. L. Kilah, P. J. Costa, V. Félix and P. D. Beer, *Angew. Chem. Int. Ed.*, 2010, **49**, 5322–5326.
20 N. G. White, H. G. Lovett and P. D. Beer, *RSC Adv.*, 2014, **4**, 12133–12147.
21 L. M. Hancock and P. D. Beer, *Chem. – Eur. J.*, 2009, **15**, 42–44.
22 J. A. Wisner, P. D. Beer and M. G. B. Drew, *Angew. Chem.*, 2001, **113**, 3718–3721.
23 H. Zheng, W. Zhou, J. Lv, X. Yin, Y. Li, H. Liu and Y. Li, *Chem. – Eur. J.*, 2009, **15**, 13253–13262.
24 H. W. Gibson, S. H. Lee, P. T. Engen, P. Lecavalier, J. Sze, Y. X. Shen and M. Bheda, *J. Org. Chem.*, 1993, **58**, 3748–3756.

25 M. R. Sambrook, P. D. Beer, M. D. Lankshear, R. F. Ludlow and J. A. Wisner, *Org. Biomol. Chem.*, 2006, **4**, 1529–1538.
26 A. Bondi, *J. Phys. Chem.*, 1964, **68**, 441–451.
27 Hong, Soo-Yeon; Yoon, Seung-Soo; Kang, Chul-Hun; Suh, Myung-Koo, *Bull. Korean Chem. Soc.*, 2004, **25**, 345–346.
28 R. Badugu, J. R. Lakowicz and C. D. Geddes, *Bioorg. Med. Chem.*, 2005, **13**, 113–119.
29 S. Jayaraman and A. S. Verkman, *Biophys. Chem.*, 2000, **85**, 49–57.
30 C. D. Geddes, K. Apperson, J. Karolin and D. J. S. Birch, *Anal. Biochem.*, 2001, **293**, 60–66.
31 L. Baù, F. Selvestrel, M. Arduini, I. Zamparo, C. Lodovichi and F. Mancin, *Org. Lett.*, 2012, **14**, 2984–2987.
32 V. Amendola, L. Fabbrizzi and E. Monzani, *Chem. – Eur. J.*, 2004, **10**, 76–82.
33 A. N. Swinburne, M. J. Paterson, A. Beeby and J. W. Steed, *Org. Biomol. Chem.*, 2010, **8**, 1010–1016.
34 A. Dorazco-González, M. F. Alamo, C. Godoy-Alcántar, H. Höpfl and A. K. Yatsimirsky, *RSC Adv.*, 2013, **4**, 455–466.
35 J. C. Koziar and D. O. Cowan, *Acc. Chem. Res.*, 1978, **11**, 334–341.

Chapter Three

Halogen and hydrogen bonding anion receptors incorporating the 1,2-bis(pyridinium)ethane motif

3.1 Introduction

Derivatives of the 1,2-bis(pyridinium)ethane motif have been extensively exploited by the Loeb group in the preparation of a variety of mechanically interlocked molecules.[1–11] The formation of these systems utilises the ability of the motif to form interpenetrated assemblies with 24-membered crown ethers as a templating interaction (**Figure 3.1**).[12] Solution and solid state evidence suggests that the association of the components is mediated by a combination of $N^+\cdots O$ ion-dipole interactions and a series of eight $CH\cdots O$ hydrogen bonding interactions.[13]

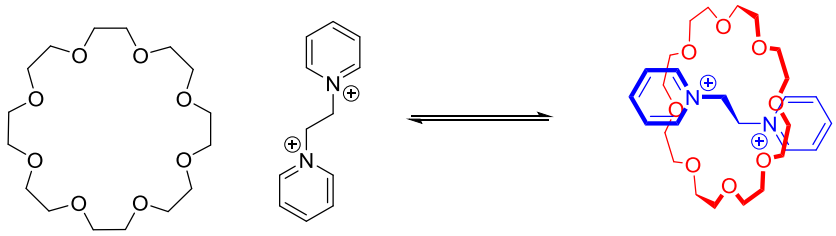

Figure 3.1: Complexation of 1,2-bis(pyridinium)ethane to 24-crown-8

Examples of interlocked structures prepared using this templation method include a [2]rotaxane formed *via* a stoppering reaction (**Figure 3.2a**)[11] and a [3]catenane synthesised using a clipping procedure (**Figure 3.2b**).[5] The interaction has also been used in the construction of more elaborate architectures such as molecular shuttles[14–16] and metal-organic rotaxane frameworks (MORFs).[17–20]

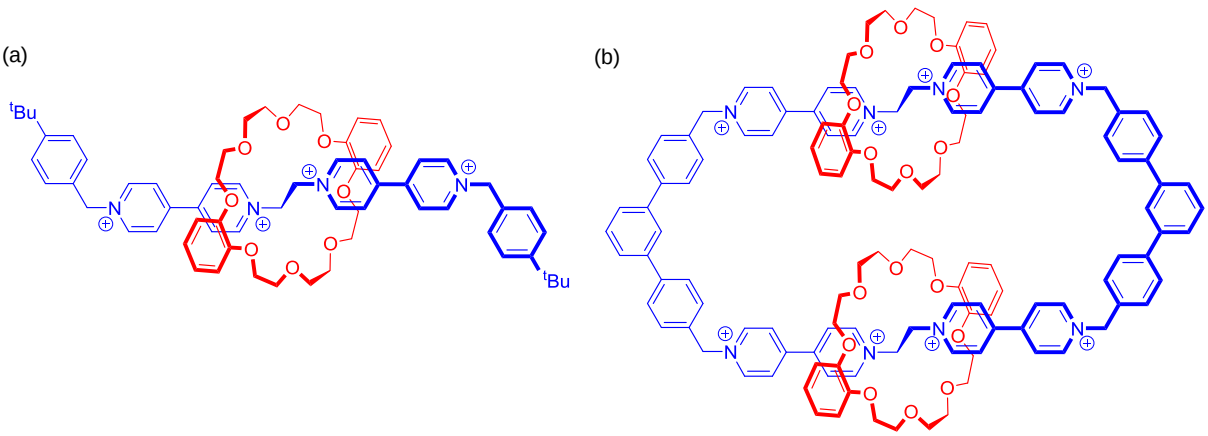

Figure 3.2: Interlocked molecules containing the 1,2-bis(pyridinium)ethane motif: (a) [2]rotaxane,[11] and (b) [3]catenane.[5]

The integration of the 1,2-bis(pyridinium)ethane motif into an anion receptor has yet to be reported, which is perhaps surprising considering its dicationic nature as well as its ability to act as a hydrogen bond donor.

3.1.1 Chapter aims

The aims of the work in this chapter were to synthesise novel acyclic and macrocyclic receptors containing a 1,2-bis(pyridinium)ethane motif functionalised with either XB iodotriazole or HB prototriazole groups (**Figure 3.3**) and investigate their anion binding capabilities. The attempted synthesis of interlocked structures incorporating these motifs is also discussed.

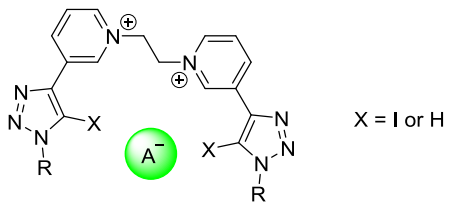

Figure 3.3: Structure of the anion binding motif incorporated into acyclic and macrocyclic receptors

3.2 Acyclic receptors

3.2.1 Synthesis

Initial attempts towards the preparation of the target acyclic receptors involved reaction of five equivalents of either iodotriazole derivative **1** or prototriazole derivative **2** with one equivalent of 1,2-dibromoethane (**Scheme 3.1**). After heating the reaction mixtures at reflux in MeCN for 2 days, no evidence of product formation was observed by TLC or mass spectrometry in either case. In an attempt to increase the reactivity of the alkylating agent, the reactions were repeated in the presence of a nucleophilic catalyst (NaI), however no products were detected.

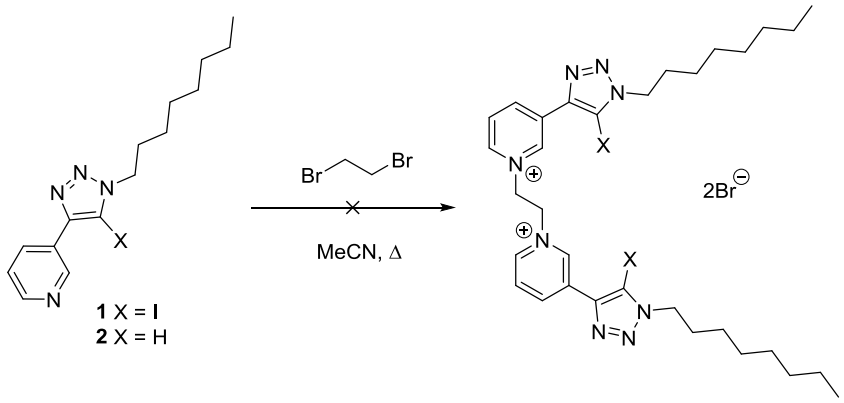

Scheme 3.1: Attempted synthesis of acyclic XB and HB receptors

A more potent alkylating agent, 1,2-bis(triflyloxy)ethane **37**, prepared by reaction of ethylene glycol with trifluoromethanesulfonic anhydride in the presence of pyridine,[21] was used in subsequent attempts. Two equivalents of **1** or **2** were stirred at room temperature with one equivalent of **37** in CH_2Cl_2 and the pure products precipitated from solution after 24 hours, as their triflate salts. Following anion exchange, by washing with aqueous NH_4PF_6, the target XB and HB anion receptors **38·2PF$_6$** and **39·2PF$_6$** were isolated in yields of 58% and 71% respectively (**Scheme 3.2**).

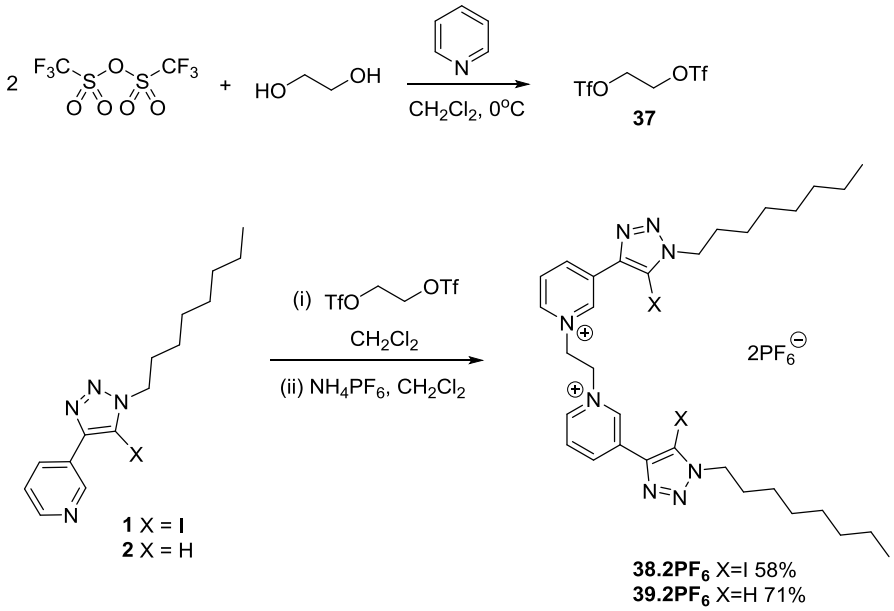

Scheme 3.2: Synthesis of acyclic receptors **38·2PF$_6$** and **39·2PF$_6$**

Both receptors were fully characterised by ^{1}H, ^{13}C, ^{19}F, and ^{31}P NMR spectroscopy and high resolution ESI mass spectrometry. Further confirmation of the structure of the HB receptor

was provided by single crystal X-ray structural analysis of the triflate salt **39·2OTf**, with crystals grown by diffusion of Et_2O into an MeCN solution of the compound. The structure, determined by Dr. Asha Brown (**Figure 3.4**), reveals both triflate counter-anions to be involved in a number of C-H···O hydrogen bonding interactions with the pyridinium and triazole protons of the host. Analysis of the crystal packing reveals an offset intermolecular parallel stacking interaction between the pyridinium-triazole units of adjacent molecules, with a distance between mean-planes of 3.253 Å (**Figure 3.4b**).

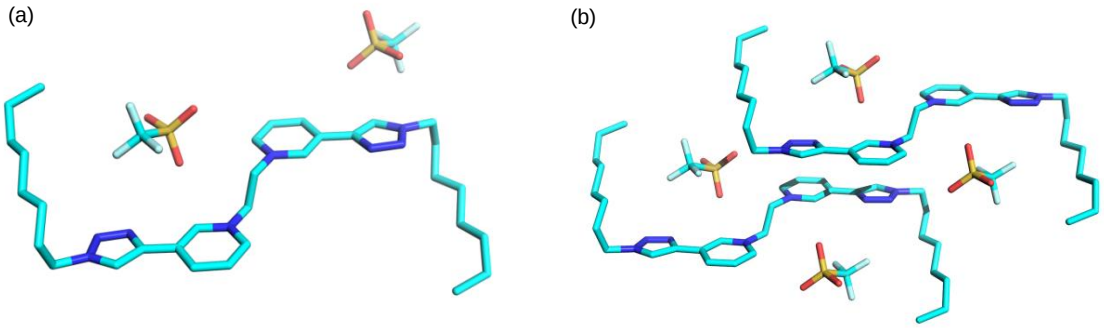

Figure 3.4: (a) Solid-state structure of **39·2OTf**; (b) solid-state crystal packing

3.2.2 Pseudorotaxane assembly studies

Thermodynamic parameters for the interpenetrative complexation of a variety of simple 1,2-bis(pyridinium)ethane derivatives with 24-membered crown ether macrocycles were determined by Loeb and co-workers using ^{1}H NMR experiments in CD_3CN.[13] The strongest binding was observed when electron-withdrawing substituents were attached to the pyridinium units of the threading component, which was attributed to the greater acidity of the aromatic protons of these species. Furthermore, the association constants calculated when dibenzo-24-crown-8 (DB24C8) was used as the macrocycle component were higher than those with 24-crown-8. ^{1}H NMR data and X-ray structural analysis showed that this is due to the formation of π-π aromatic donor-acceptor interactions between the electron-deficient

pyridinium rings of the threading component and the electron-rich catechol ether groups of the DB24C8 macrocycle.

Investigations into the ability of compounds **38·2PF$_6$** and **39·2PF$_6$** to form pseudorotaxane assemblies with DB24C8 were undertaken using analogous ^{1}H NMR experiments in CD_3CN. In the case of HB **39·2PF$_6$** a [2]pseudorotaxane was formed in slow exchange on the NMR timescale, with two sets of peaks observed, relating to the complexed and uncomplexed species (**Figure 3.5**). Upon complexation the resonances of pyridinium protons *b* and *c*, and the ethylene protons *a* are shifted downfield due to HB interactions with the macrocycle, whilst the signals of pyridinium protons *d* and *e*, and triazole protons *f* are shifted upfield, implying there is an aromatic π-stacking interaction between the threading species and the catechol ether units of the macrocycle. The slow kinetics of the association can be attributed to the steric bulk of the substituents attached to the pyridinium units. Using the single point method,[22,23] an association constant of 2075 M^{-1} was calculated, which is similar in magnitude to the values calculated by Loeb for other 1,2-bis(pyridinium)ethane motifs attached to electron withdrawing groups.[13]

By contrast, there appears to be no interaction between XB **38·2PF$_6$** and DB24C8, with no change observed in the chemical shift of any protons of the two species upon combining them. This is most likely a consequence of the steric bulk of the iodotriazole groups of **38·2PF$_6$**, which prevent threading from occurring.

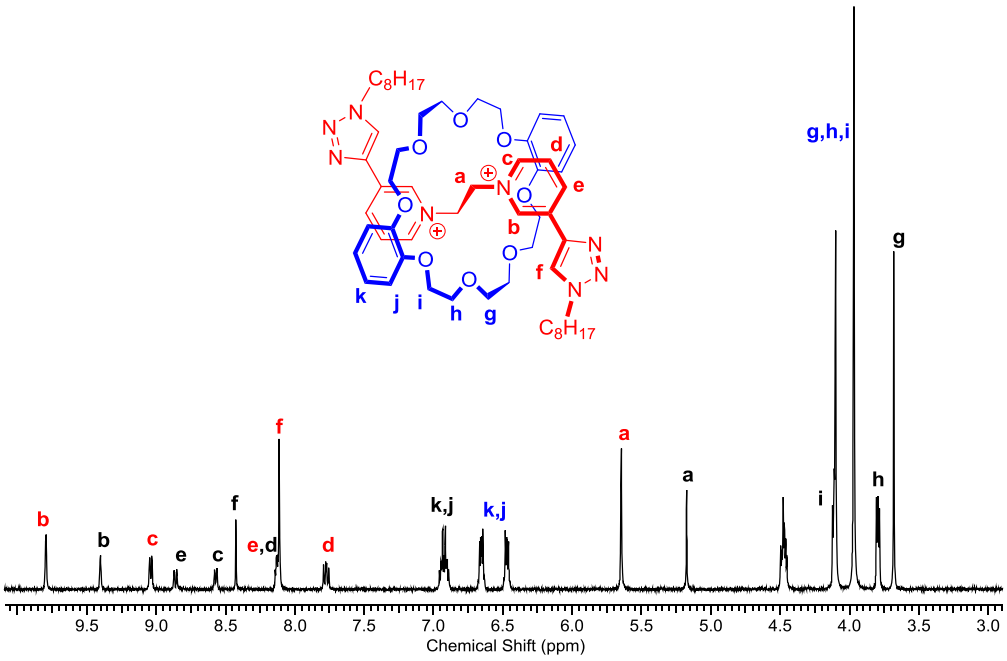

Figure 3.5: Truncated ^{1}H NMR spectrum of an equimolar mixture of **39·2PF$_6$** and DB24C8 (CD_3CN, 298 K, 400 MHz)

3.2.3 Anion binding properties

The anion binding properties of the XB and HB receptors were investigated using ^{1}H NMR titration experiments performed in a competitive aqueous solvent mixture (45:45:10 $CDCl_3/CD_3OD/D_2O$). The chemical shifts of the respective receptors' proton resonances were monitored upon addition of up to ten equivalents of chloride, bromide, iodide, dihydrogen phosphate, acetate and sulfate as their TBA salts.

For XB receptor **38·2PF$_6$** substantial downfield perturbations of pyridinium protons *c* were observed in the titrations with chloride, bromide and the oxoanions, with the largest magnitude of shift caused by sulfate (0.46 ppm), followed by bromide (0.25 ppm), dihydrogen phosphate (0.23 ppm), chloride (0.22 ppm) and acetate (0.12 ppm). The signal for ethylene protons *a* also underwent a downfield shift, however the magnitude of change was similar for all anions (~ 0.1 ppm). Minimal changes to pyridinium protons *b* were observed, indicating that they are not directly involved in anion association (**Figure 3.6**).

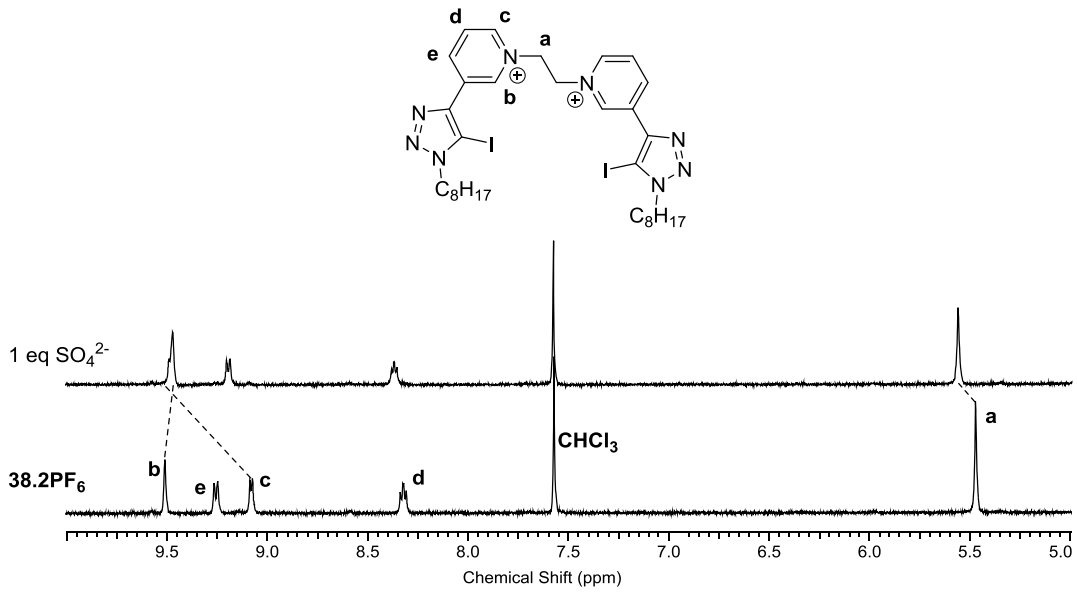

Figure 3.6: Truncated ^{1}H NMR spectra of **38·2PF$_6$** before and after addition of one equivalent of $(TBA)_2SO_4$ (45:45:10 $CDCl_3/CD_3OD/D_2O$, 298 K, 500 MHz)

For HB receptor **39·2PF$_6$** substantial downfield shifts of pyridinium protons *b* and *c*, and triazole protons *f* occurred upon addition of all of the anions investigated, with protons *b* undergoing the largest change in chemical shift in all cases. The greatest magnitude of shift was observed with iodide (0.66 ppm), followed by bromide (0.63 ppm), sulfate (0.54 ppm), chloride (0.48 ppm), dihydrogen phosphate (0.18 ppm) and acetate (0.16 ppm). This trend is surprising, considering that iodide is the least basic of the anions studied and so would be expected to form the weakest HB interaction. Similarly to receptor **38·2PF$_6$**, ethylene protons *a* also underwent a small downfield shift (0.1 – 0.2 ppm) with all of the anions (**Figure 3.7**).

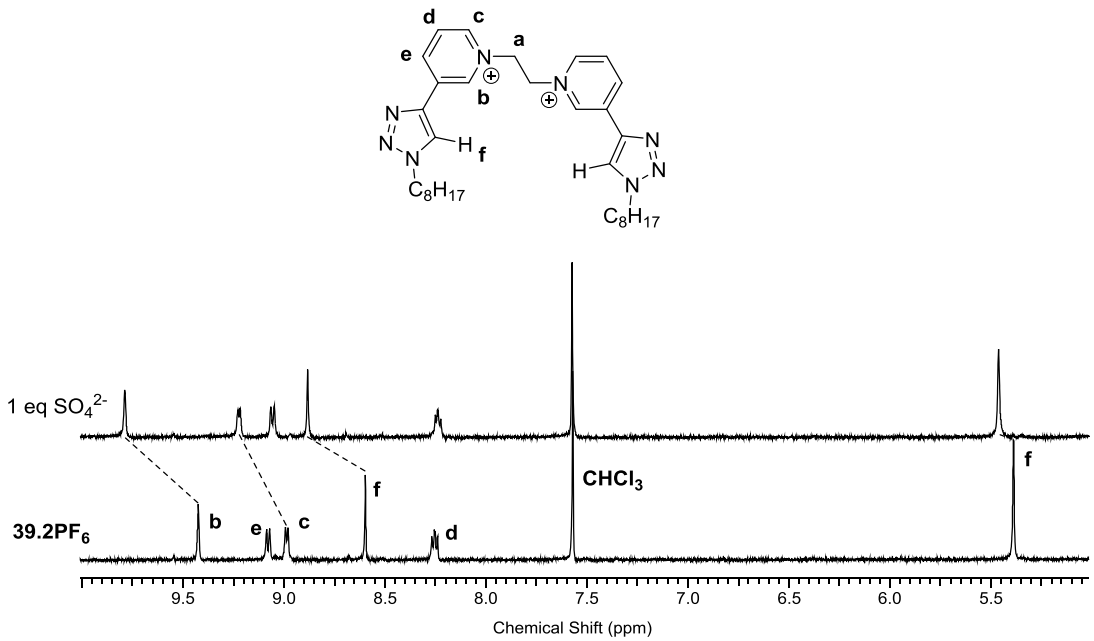

Figure 3.7: Truncated ^{1}H NMR spectra of **39.2PF$_6$** before and after addition of one equivalent of $(TBA)_2SO_4$ (45:45:10 $CDCl_3/CD_3OD/D_2O$, 298 K, 500 MHz)

The titration data obtained for both receptors was analysed using WinEQNMR software.[24] For XB host **38·2PF$_6$**, 1:1 stoichiometric association constants were calculated (**Table 3.1**) by monitoring the change in the chemical shift of proton *c* (**Figure 3.8a**). These revealed that sulfate was bound significantly more strongly than the other anions investigated, which can be attributed to the dianionic nature of the oxoanion. Indeed, sulfate binding was too strong (K_a > 10^4 M^{-1}) to allow an accurate determination of its association constant. Amongst the singly charged anions, binding strength was in the order Br^- > $H_2PO_4^-$ > Cl^- > AcO^-, however the differences between the association constant values were relatively modest.

For HB receptor **39·2PF$_6$**, the titration data was analysed monitoring the change in chemical shifts of pyridinium protons *b* (**Figure 3.8b**) and triazole protons *f*, with the association constants calculated independent of the proton used. The resonance of proton *c* could not be followed due to its overlap with the signal of protons *e* for a substantial proportion of the titration. Fitting of the curves revealed that the halides and acetate bound with a 1:1 stoichiometry, whilst dihydrogen phosphate and sulfate formed 1:2 (host:guest) complexes. As with XB receptor **38·2PF$_6$**, sulfate was found to bind most strongly (K_{11} > 10^4 M^{-1}), with

the association constants of the singly charged anions at least two orders of magnitude smaller. Again only modest selectivity preferences between the singly charged anions was observed, with the halides and dihydrogen phosphate bound slightly more strongly than acetate (**Table 3.1**).

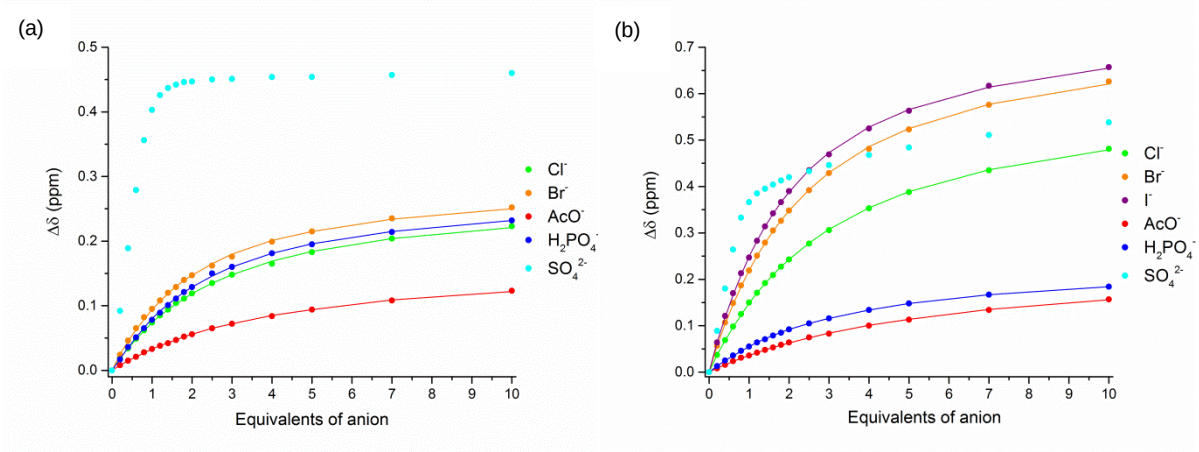

Figure 3.8: Experimental titration data (points) and calculated binding isotherms (lines) for the addition of TBA salts of various anions to: (a) and **38·2PF$_6$** and (b) **39·2PF$_6$**, monitoring protons *c* and *b*, respectively (45:45:10 $CDCl_3/CD_3OD/D_2O$, 298 K, 500 MHz).

Table 3.1: Association constants (K_a) determined for **38·2PF$_6$** and **39·2PF$_6$** with various anions (45:45:10 $CDCl_3/CD_3OD/D_2O$, 298 K, 500 MHz).

Anion	K_a **(M^{-1})**[a]	
	38·PF$_6$	**39·PF$_6$**
Cl^-	220	180
Br^-	310	260
I^-	-[b]	320
AcO^-	120	75
$H_2PO_4^-$	260	K_{11} = 320 K_{12} = 45
SO_4^{2-}	> 10^4	K_{11} > 10^4

[a] Calculated using chemical shift of proton *2*. Estimated errors within ±10%. [b] No value calculated due to precipitation of receptor

The lack of notable selectivity displayed by either receptor towards the singly charged anions is most likely a consequence of their lack of preorganisation. The shifts observed in the ^{1}H NMR titration experiments suggest that multiple modes of anion binding are available to the acyclic systems, which presumably allows the effective association of anions of various

geometries and sizes (**Figure 3.9**). Also of note is the similarity between the K_a values calculated for both receptors. This implies that the XB/HB interactions provided by the triazole groups have little effect on the strength of anion binding. Owing to the dicationic nature of the receptors, it is likely that anion association is primarily driven by electrostatic interactions.

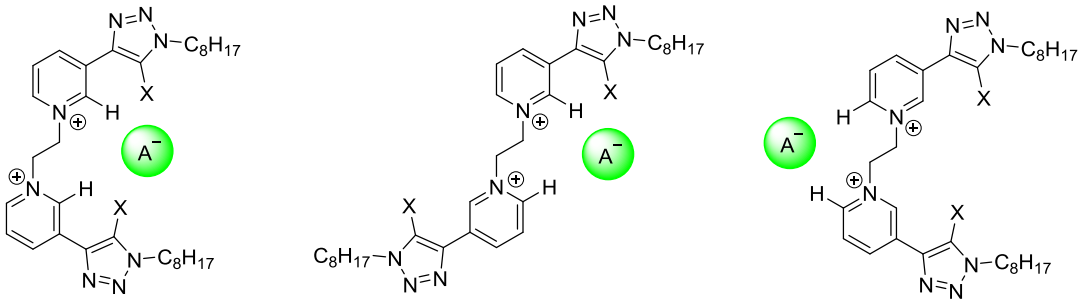

Figure 3.9: Possible anion binding modes of acyclic receptors **38·2PF$_6$** and **39·2PF$_6$**

3.3 Macrocyclic receptors

Attempts were made to construct macrocyclic analogues of the acyclic receptor systems in the expectation that a greater level of preorganisation would result in increased anion association strength and a higher degree of selectivity. The target macrocycles were designed so that they could also potentially be used in the anion-templated formation of interlocked structures.

3.3.1 Synthesis of macrocycles

To prepare the target XB and HB macrocyclic receptors, previously synthesised bis-amine **9** was initially reacted with the hydrogen sulfate salt of the diazotransfer reagent imidazolium sulfonylazide[25,26] in the presence of K_2CO_3 and a catalytic amount of $CuSO_4{\cdot}5H_2O$, to give bis-azide **40**.[27] This was reacted with two equivalents of either 3-(iodoethynyl)pyridine or 3-ethynylpyridine under CuAAC conditions to afford bis-iodotriazole and bis-prototriazole derivatives **41** and **42**, respectively, in good yields. Macrocycle formation was achieved by addition of one equivalent of bis-triflate **37** to a dilute CH_2Cl_2 solution (~ 3 mM) of either **41** or **42**. After stirring the mixtures at room temperature for 24 hours, the crude materials were

purified using column chromatography, dissolved in hot water (~ 70 °C) and upon addition of a saturated aqueous solution of NH_4PF_6 the target XB and HB receptors **43·2PF$_6$** and **44·2PF$_6$** were isolated in yields of 28% and 44%, respectively (**Scheme 3.3**).

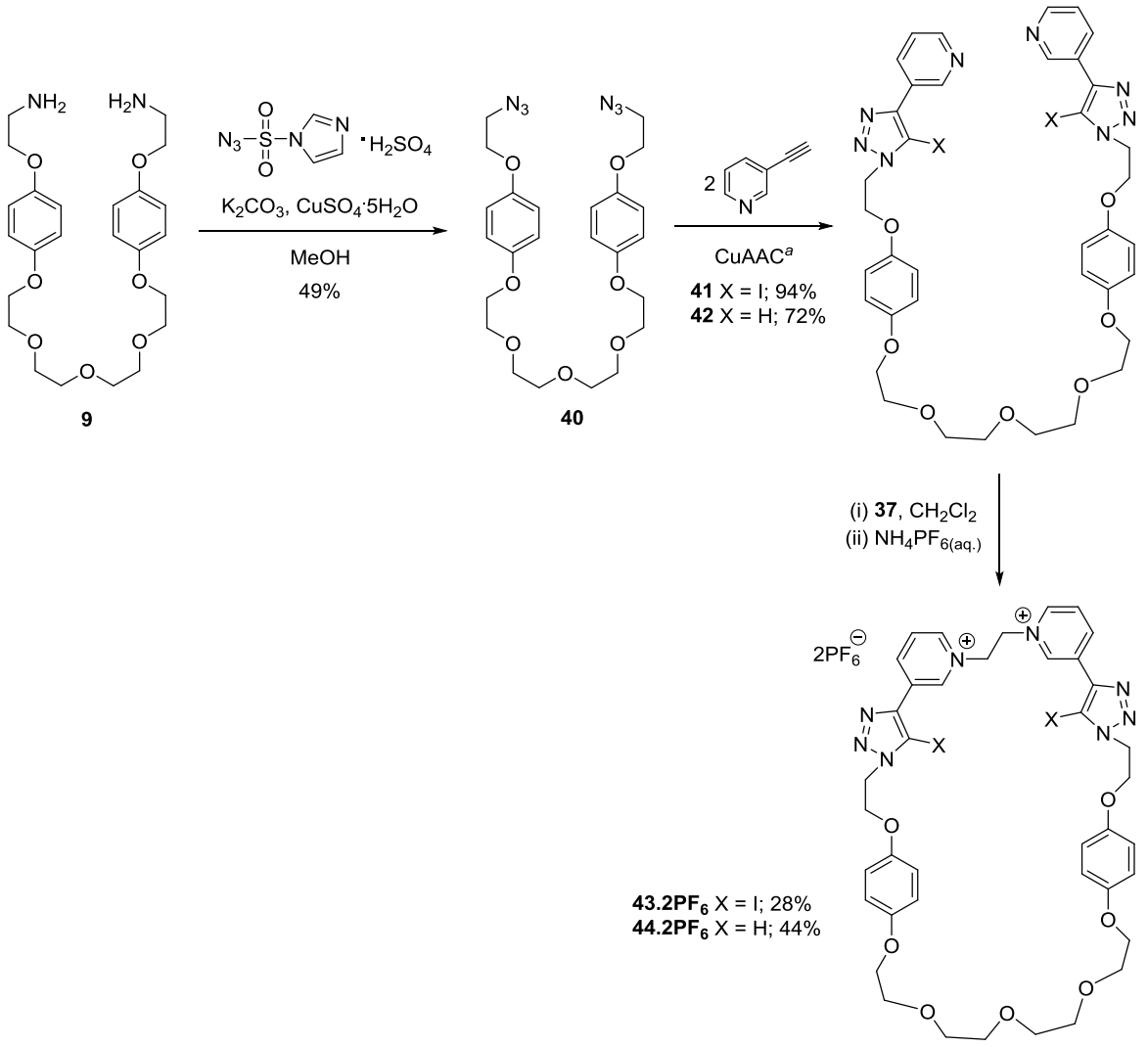

9 **40**

Scheme 3.3: Synthesis of XB and HB macrocyclic receptors **43·2PF$_6$** and **44·2PF$_6$**. [a] For X = I: $Cu(ClO_4)_2·6H_2O$, NaI, DBU, TBTA, THF/MeCN, dark; for X = H: $[Cu(MeCN)_4][PF_6]$, DIPEA, TBTA, CH_2Cl_2.

Both macrocycles were fully characterised using ^{1}H (**Figure 3.10**, **44·2PF$_6$**), ^{13}C, ^{19}F and ^{31}P NMR spectroscopy and high resolution ESI mass spectrometry.

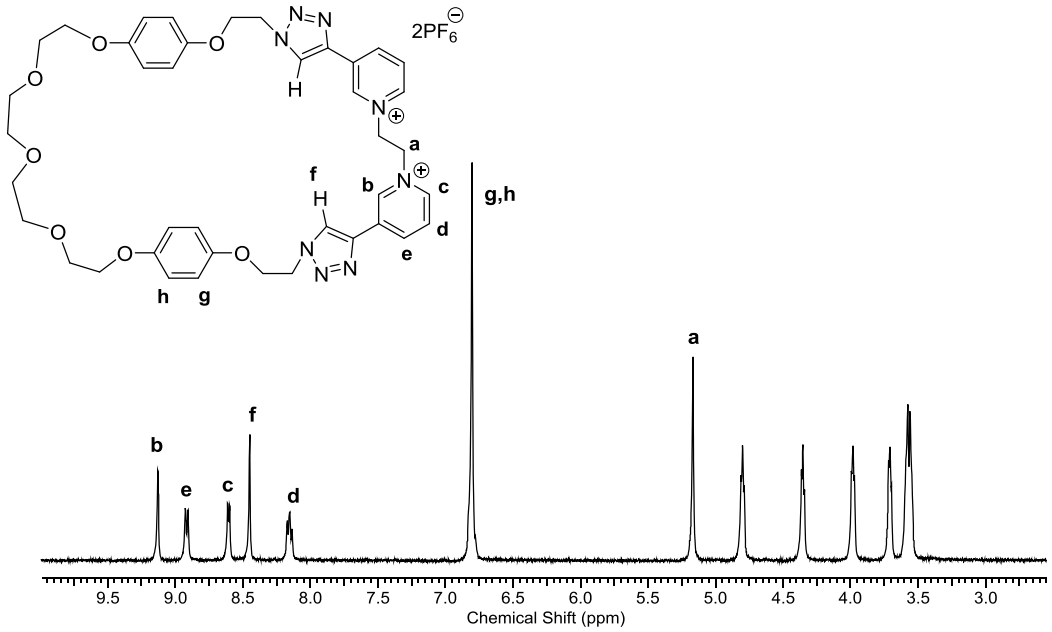

Figure 3.10: Truncated ^{1}H NMR spectrum of HB macrocycle **44·2PF$_6$**

3.3.2 Anion binding studies

Investigations into the anion binding properties of the two macrocyclic receptors were initially undertaken using ^{1}H NMR titrations in 45:45:10 $CDCl_3/CD_3OD/D_2O$. However, the poor solubility of both hosts in this solvent system precluded the determination of any quantitative data. The same problem was also encountered using an alternative aqueous solvent mixture (9:1 CD_3CN/D_2O). Improved levels of solubility were observed in d_6-DMSO, which allowed titrations with TBA salts of various singly charged anions to be conducted.

For XB macrocycle **43·2PF$_6$**, the addition of chloride and bromide led to downfield perturbations of pyridinium protons *c* (0.18 ppm and 0.07 ppm, respectively), with minimal shifts of the other protons within the host observed. However, no quantitative data could be obtained by monitoring the signal of proton *c* due to its overlap with the signal of proton *e* for a substantial proportion of both titrations.

For HB macrocycle **44·2PF$_6$**, significant downfield shifts of pyridinium protons *b* and *c*, and triazole protons *f* were seen in the chloride and bromide titration experiments. Internal pyridinium protons *b* underwent the largest change in chemical shift, with chloride causing a

larger magnitude of change (0.44 ppm) than bromide (0.14 ppm). The titration data was analysed using WinEQNMR software,[24] monitoring the shift of protons *b* (**Figure 3.11**), which afforded relatively modest 1:1 association constants of 97(1) M^{-1} for chloride and 54(1) M^{-1} for bromide.

For both macrocycles, the shifts observed in titrations with nitrate and iodide were minimal, suggesting these anions are bound very weakly, whilst addition of acetate and dihydrogen phosphate led to decomposition of the hosts. Owing to the high basicity of these anions in DMSO, this most likely occurs through deprotonation of the acidic pyridinium protons of the macrocycle.

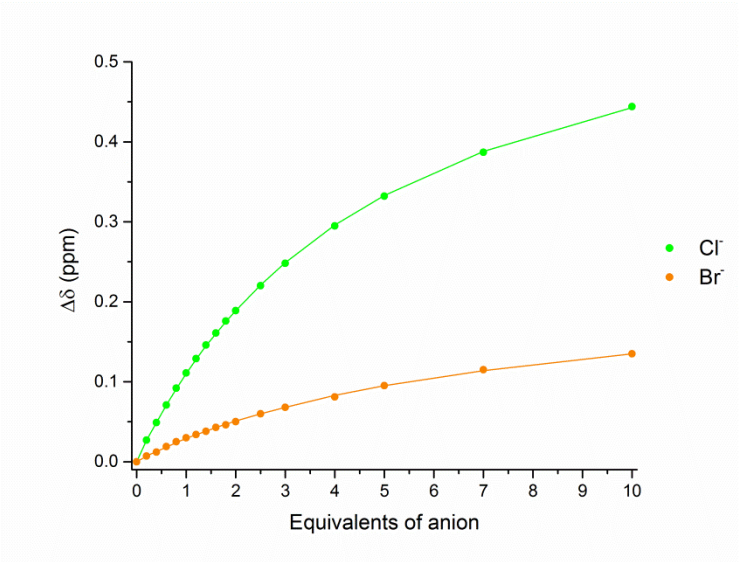

Figure 3.11: Experimental titration data (points) and calculated 1:1 binding isotherms (lines) for the addition of the TBA salts of chloride and bromide to **44·2PF$_6$**, monitoring proton *b* (d_6-DMSO, 298 K, 500 MHz).

Solid-state characterisation of **44·2Cl** provided evidence of the mode by which chloride is bound within the HB macrocycle. Crystals suitable for X-ray analysis were grown by slow evaporation of an MeCN solution of **44·2Cl**, with the structure solved by Dr. Asha Brown (**Figure 3.12a**). Analysis of the structure reveals that one of the chloride counter-anions is located within the central cavity of the macrocycle and forms short C-H···Cl^- contacts with both internal pyridinium protons (2.54 Å and 2.89 Å) and one of the triazole protons (2.72 Å).

The crystal packing structure shows that a water molecule bridges between the encapsulated chloride anions of adjacent macrocycles, forming an infinite HB chain (**Figure 3.12b**). Both pyridinium-triazole units of the macrocycle are involved in intermolecular stacking interactions, with distances between the mean-planes of 3.140 Å and 3.535 Å.

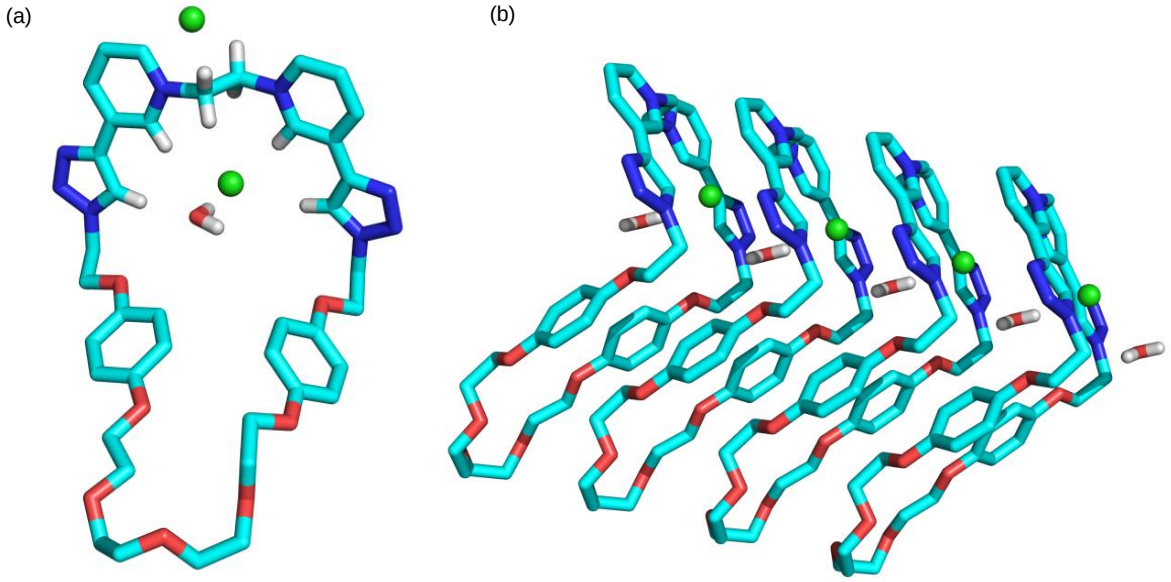

Figure 3.12: (a) Solid-state structure of macrocycle **44·2Cl**; (b) solid-state crystal packing

As the titration experiments with the macrocyclic and acyclic receptors were performed in different solvent systems, their anion association constants could not be directly compared. Hence, the chloride and bromide titrations with HB acyclic receptor **39·2PF$_6$** were repeated in d_6-DMSO (**Figure 3.13**). WinEQNMR analysis[24] determined 1:1 stoichiometric association constant values of similar magnitude to those obtained for the macrocyclic receptor, with chloride bound slightly more strongly than bromide (**Table 3.2**). This suggests that increasing the preorganisation of this binding motif through its incorporation within a macrocycle has little effect on the strength of halide binding.

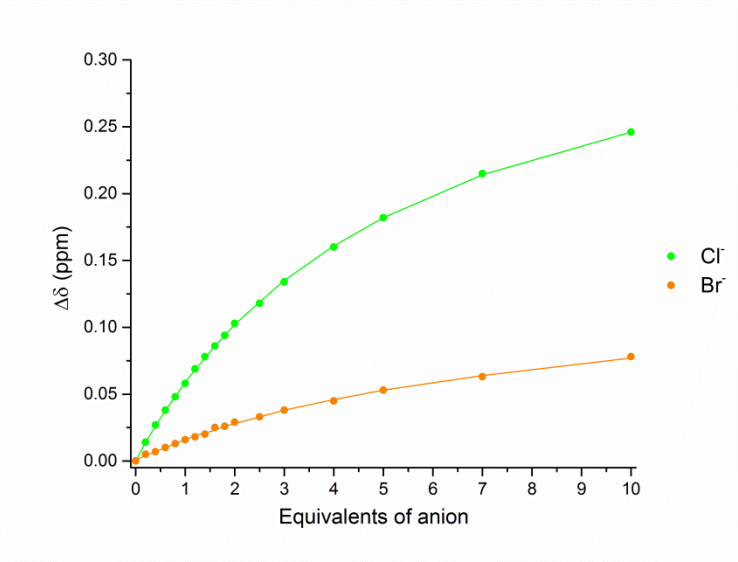

Figure 3.13: Experimental titration data (points) and calculated 1:1 binding isotherms (lines) for the addition of the TBA salts of chloride and bromide to **39·2PF$_6$**, monitoring proton *b* (d_6-DMSO, 298 K, 500 MHz).

Table 3.2: Association constants (K_a) determined for **39·2PF$_6$** and **44·2PF$_6$** with various anions (d_6-DMSO, 298 K, 500 MHz).

Anion	K_a **(M^{-1})**[a]	
	39·2PF$_6$	**44·2PF$_6$**
Cl^-	84	97
Br^-	44	54

[a] Calculated using chemical shift of proton *2*. Estimated errors within ±10%.

3.3.3 Pseudorotaxane assembly studies

In order to assess the viability of preparing interlocked structures containing macrocycles **43·2PF$_6$** and **44·2PF$_6$** *via* anion templated synthesis, qualitative pseudorotaxane assembly studies were conducted with a XB 3,5-bis-iodotriazole pyridinium chloride threading component **45·Cl**[28] (provided by Sean Robinson), using ^{1}H NMR. An equimolar mixture of **45·Cl** and either **43·2PF$_6$** or **44·2PF$_6$** was prepared in 1:1 $CDCl_3$/CD_3CN (**Scheme 3.4**), and the ^{1}H NMR spectrum obtained was compared with those of the individual components. The mixed solvent system used was required for both components to be soluble.

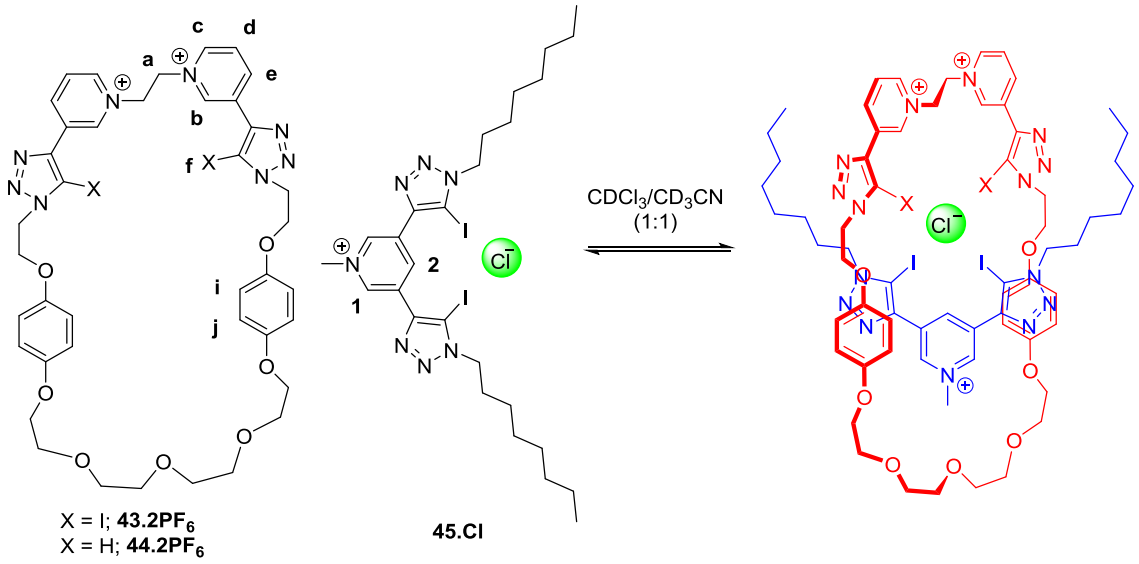

Scheme 3.4: Pseudorotaxane formation between **43·2PF$_6$**/**44·2PF$_6$** and **45·Cl**

In the spectrum obtained with the HB macrocycle (**Figure 3.14**), pseudorotaxane formation was inferred from the upfield shift and splitting of the hydroquinone proton resonances *i* and *j*. The relatively small shift observed (~ 0.05 ppm) suggests that the π-π aromatic donor-acceptor interactions with the pyridinium unit of the thread are weak, which is most likely due to the large separation between the hydroquinone units of the macrocycle. Substantial downfield shifts of macrocycle protons *b* and *f* were also observed, confirming that the templating chloride anion is bound within the macrocycle's central cavity.

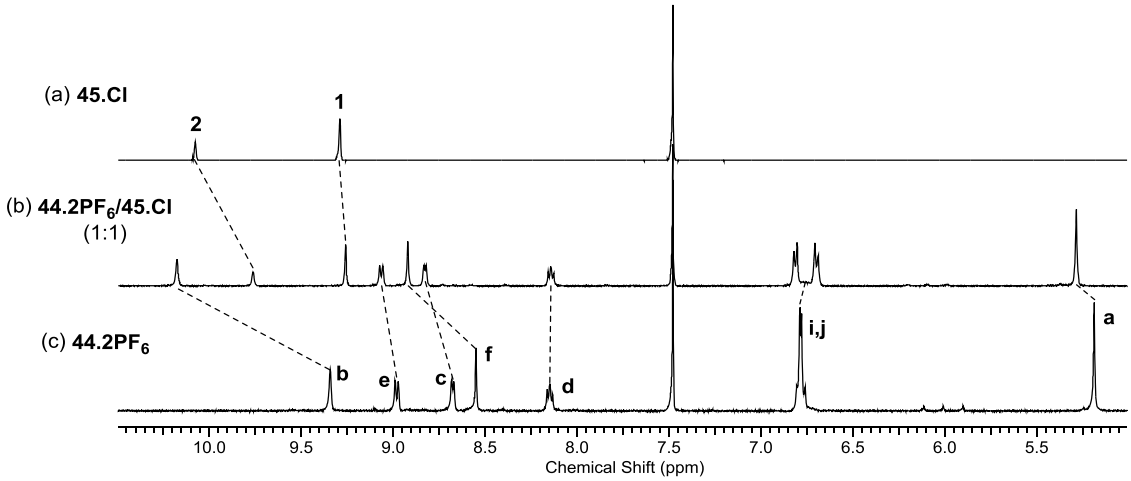

Figure 3.14: Truncated ^{1}H NMR spectra of: (a) **45·Cl**, (b) an equimolar mixture of **45·Cl** and **44·2PF$_6$**, and (c) **44·2PF$_6$** (1:1 $CDCl_3/CD_3CN$, 298 K, 500 MHz)

In the analogous experiment performed with XB macrocycle **43·2PF$_6$**, no upfield shift or splitting of the hydroquinone resonances was observed in the presence of the threading component, indicating that an interpenetrated assembly does not form. Instead, it is likely that an orthogonal assembly is formed between the components outside the cavity of **43·2PF$_6$** (**Figure 3.15**), which is implied by the downfield shift of the signal of pyridinium proton *c* of the macrocycle (0.28 ppm).

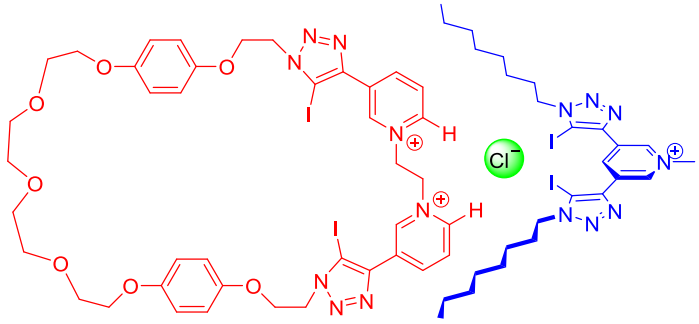

Figure 3.15: Possible structure of an orthogonal assembly formed between **43·2PF$_6$** and **45·Cl**

3.4 Attempted synthesis of interlocked receptors

Following on from the pseudorotaxane studies, the preparation of a [2]rotaxane containing HB macrocycle **44·2PF$_6$** was targeted. This was attempted using a chloride-templated 'click-stoppering' methodology (**Scheme 3.5**), which necessitated the initial synthesis of a bis-azide appended analogue of threading component **45·Cl** and an alkyne-appended stopper derivative. As macrocycle **44·2PF$_6$** possesses a large central cavity it was anticipated that the terphenyl derivatives, prepared in Chapter 2, would be too small to act as stopper groups. It was therefore decided to employ permethylated-β-cyclodextrin-based stoppers, which have previously been incorporated into interlocked structures for this purpose.[29,30] In addition to the added steric bulk provided by these derivatives, it was hoped that they would also impart the target rotaxane with aqueous solubility and potentially allow anion binding studies to be

conducted in pure water. A more detailed discussion of the properties of cyclodextrin derivatives can be found in Chapter 4.

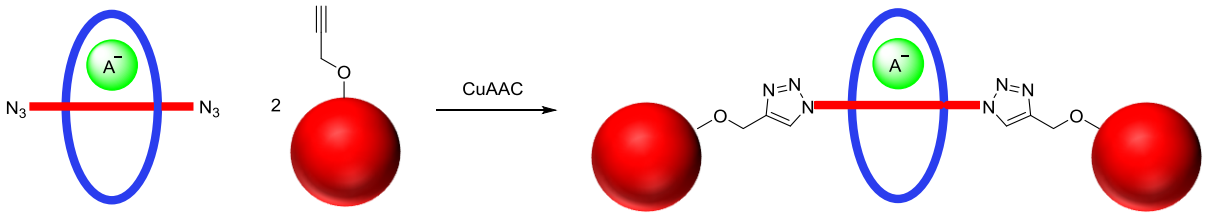

Scheme 3.5: Cartoon representation of an anion templated 'click-stoppering' rotaxane formation reaction

3.4.1 Synthesis of axle precursor

The multi-step preparation of the bis-azide functionalised 3,5-bis-iodotriazole pyridinium axle precursor was achieved as shown in **Scheme 3.6**. Commercially avaialable 3,5-dibromopyridine was reacted with ethynyltrimethylsilane under Sonogashira coupling conditions to give a trimethylsilyl-protected bis-alkyne, which was subsequently deprotected using KOH to give 3,5-diethynylpyridine **46**.[31] Addition of *n*-BuLi followed by iodine gave bis-iodoalkyne **47**. 3-Bromopropan-1-ol was reacted with sodium azide and then with *para*-toluenesulfonyl chloride to afford 3-tosyl-1-azidopropane **48**. Two equivalents of azide **48** were then reacted with one equivalent of bis-alkyne **47** under CuAAC conditions to give bis-iodotriazole derivative **49**, in an 86% yield. Compound **49** was then converted to bis-azide **50**, through reaction with sodium azide, after which it was heated under reflux in a 9:1 mixture of $CHCl_3$/MeI, causing pyridinium derivative **51·I** to precipitate from solution as an orange solid. This was converted to its chloride salt, by washing with aqueous NH_4Cl, to afford the target axle precursor **51·Cl** in 11% yield. The low yield obtained for the final synthetic step can be attributed to the poor solubility of **51·I**, which made the anion exchange procedure difficult to perform.

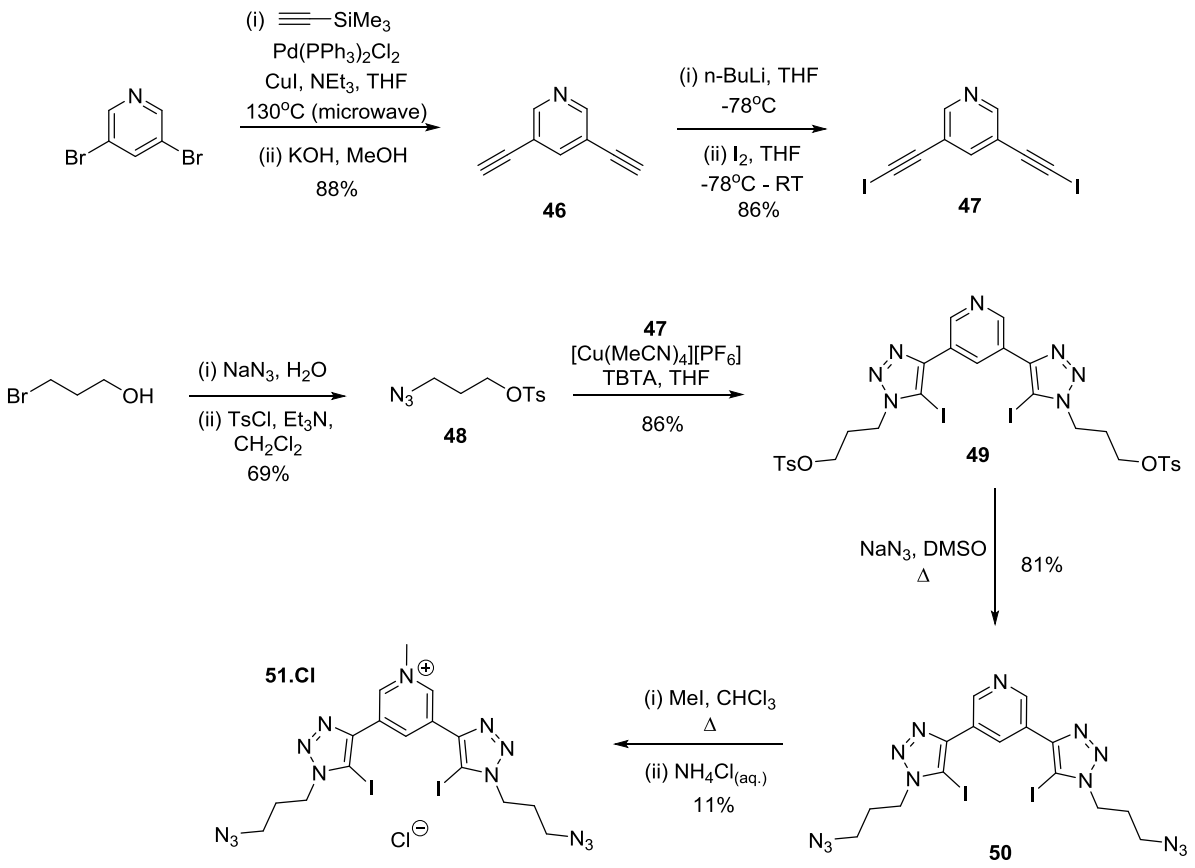

Scheme 3.6: Synthesis of the 3,5-bis-iodotriazole pyridinium axle precursor **51·Cl**

3.4.2 Synthesis of alkyne-appended stopper

The target alkyne-appended permethylated-β-cyclodextrin stopper derivative was prepared using previously reported synthetic procedures (**Scheme 3.7**).[32,33] Commercially available β-cyclodextrin was reacted with *p*-toluenesulfonic anhydride in the presence of NaOH to give mono-tosylate **52**. The remaining hydroxyl groups of **52** were then methylated through reaction with a 3.5-fold excess of methyl iodide and a 7-fold excess of sodium hydride to afford **53**, which was subsequently reacted with a large excess of propargyl alcohol and sodium hydride (50 equivalents and 40 equivalents, respectively) to afford the alkyne derivative **54** in a 65% yield.[33]

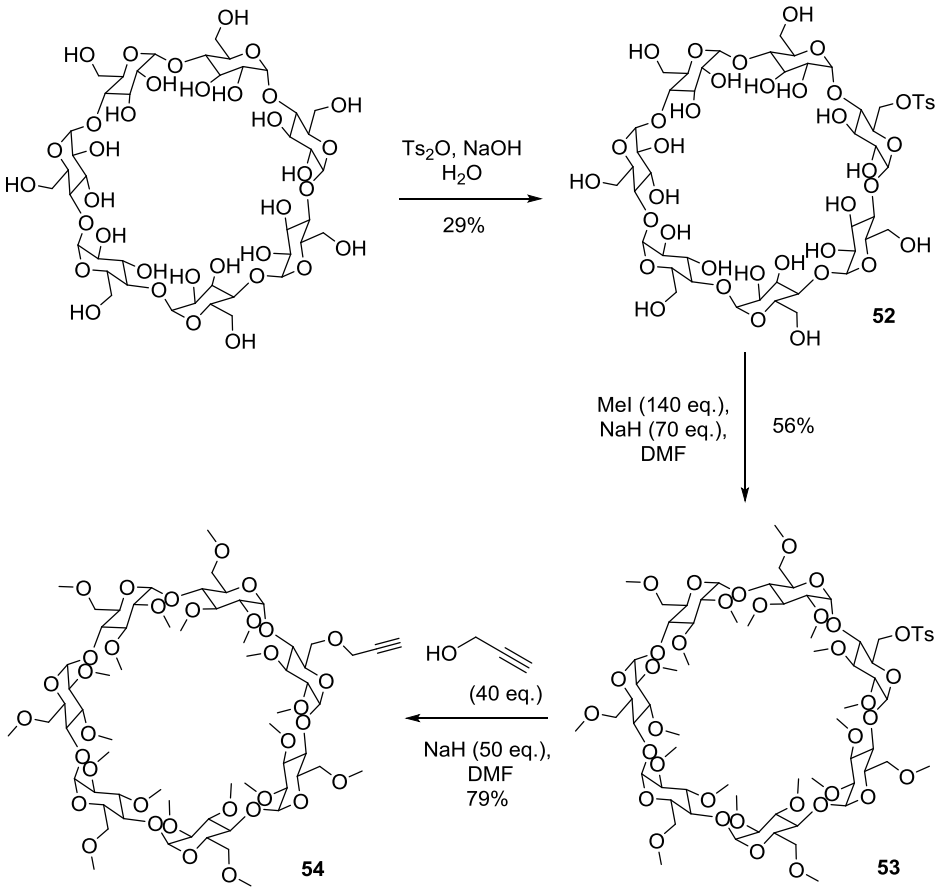

Scheme 3.7: Synthesis of alkyne-appended stopper **54**

3.4.3 Attempted synthesis of [2]rotaxane

Rotaxane formation was attempted *via* the 'click-stoppering' methodology (**Scheme 3.8**). Initially, an equimolar mixture of axle precursor **51·Cl** and macrocycle **44·2PF$_6$** was prepared in 1:1 CH_2Cl_2/MeCN, to produce a chloride-templated interpenetrative assembly. Subsequently, two equivalents of the alkyne-appended stopper derivative **54**, and catalytic amounts of TBTA and $[Cu(MeCN)_4][PF_6]$ were added. The resulting mixture was stirred at room temperature, with progress of the reaction monitored using TLC. After 48 hours both the axle precursor and stopper starting materials had been consumed and the crude product mixture was analysed using ESI mass spectrometry. Surprisingly, this showed peaks corresponding to multiple axle and rotaxane species, which differed only by the ratio of prototriazole and iodotriazole units they contained. This suggested that a hydrogen-iodine exchange process had occurred during the reaction. No evidence of this exchange was

observed within the macrocycle component, with only the bis-prototriazole stating material **44·2PF$_6$** seen in the mass spectrum. Purification of the crude mixture, using preparative TLC, was attempted; however it proved impossible to isolate any pure products.

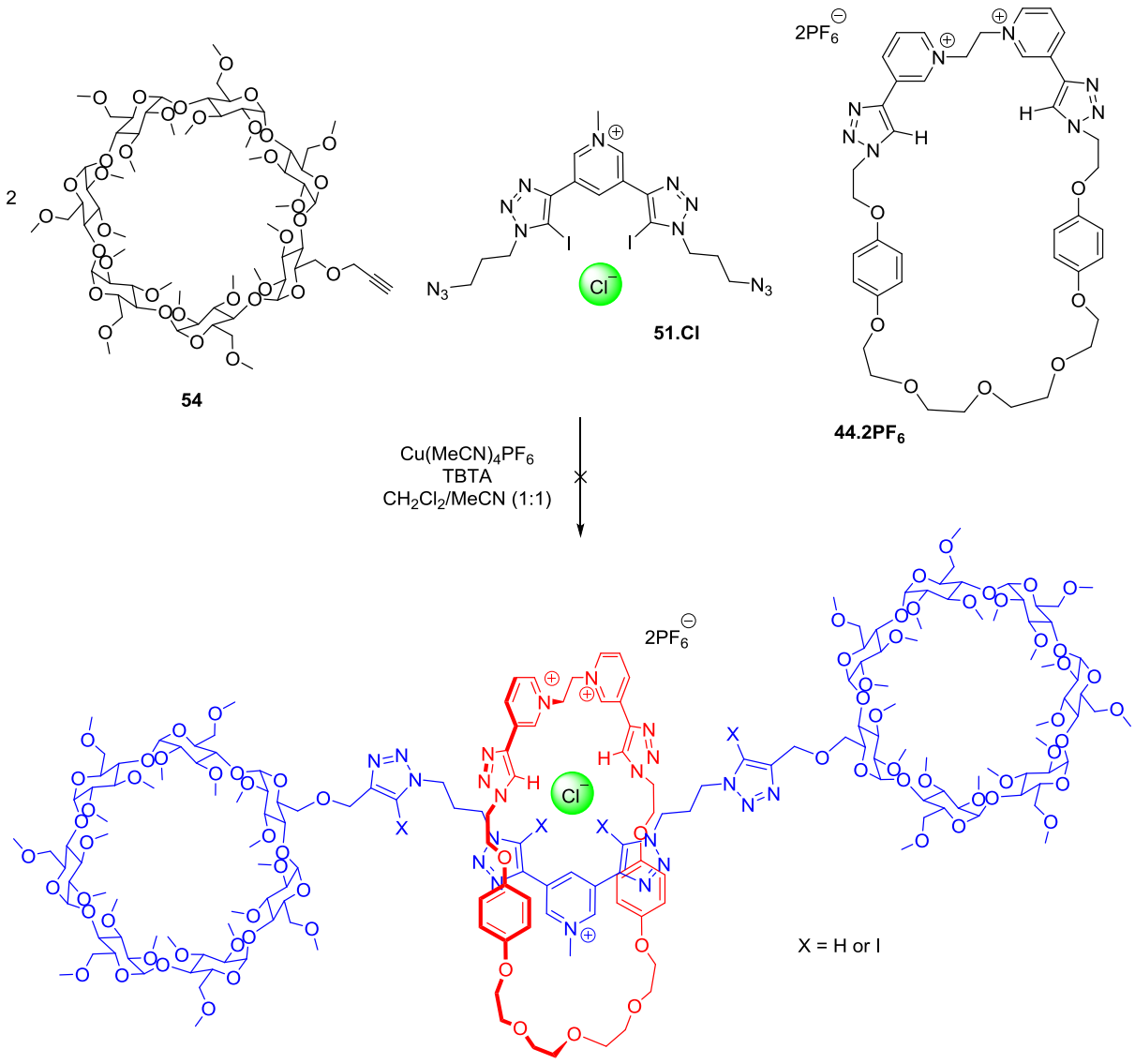

Scheme 3.8: Attempted synthesis of [2]rotaxane

To further investigate the hydrogen-iodine exchange observed by ESI mass spectrometry, a CuAAC reaction was performed between two equivalents of alkyne-appended terphenyl derivative **55** (provided by Dr. Lydia Gilday) and one equivalent of **51·Cl** (**Figure 3.16a**). As with the rotaxane formation reaction above, ESI mass spectrometry analysis of the crude product mixture showed that species containing varying numbers of proto- and iodotriazole groups had formed (**Figure 3.16b**). This demonstrates that the exchange process does not

require the presence of macrocycle **44·2PF$_6$** or the cyclodextrin-based stopper **54**. Instead, it most likely occurs through insertion of the Cu(I)-ions present in the reaction into the highly polarised C-I bond of the iodotriazole motifs.

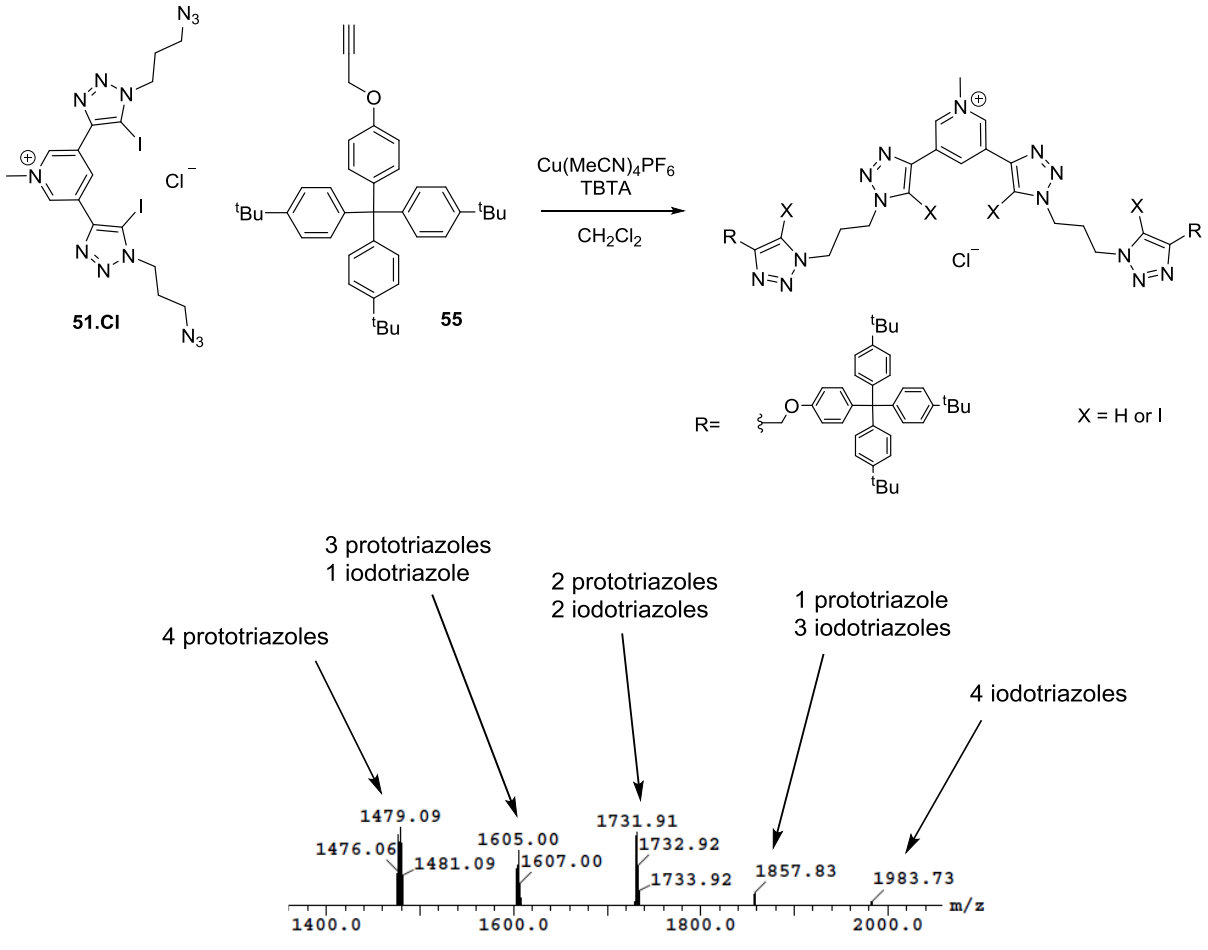

Figure 3.16: (a) Reaction between **51·Cl** and terphenyl alkyne **55**; (b) Truncated ESI mass spectrum of crude reaction mixture showing distribution of mixed proto- and iodotriazole products

3.4.4 Attempted synthesis of an all HB rotaxane

Taking into account the difficulties encountered with the rotaxane formation reaction using XB axle precursor **51·Cl**, subsequent attempts to prepare an interlocked structure containing macrocycle **44·2PF$_6$** utilised a pyridinium bis-amide axle precursor, which has previously been used in the preparation of a rotaxane by the 'click-stoppering' methodology.[34] This was prepared by alkylating pyridine derivative **56** (provided by Dr. Asha Brown) with methyl iodide to give **57·I**, which was anion exchanged to produce **57·Cl** (**Scheme 3.9**).

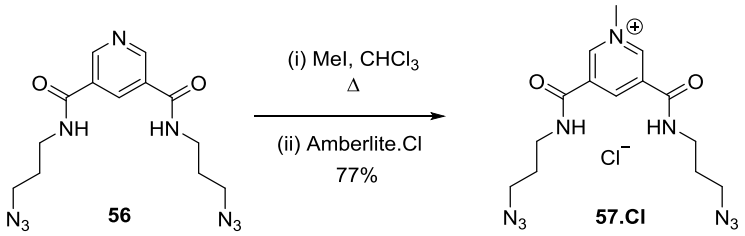

Scheme 3.9: Synthesis of bis-amide axle precursor **57·Cl**

Rotaxane formation was attempted *via* an analogous synthetic procedure to one used with XB axle precursor **51·Cl** (**Scheme 3.10**). A less competitive 2:1 CH_2Cl_2/MeCN solvent mixture was used with the aim of increasing the strength of the templating interaction. Initially, the reaction was found to progress very slowly and hence two equivalents of DIPEA were added to increase the rate of reaction through proton abstraction. After TLC had indicated that both **57·Cl** and stopper derivative **54** had all reacted, the crude product mixture was analysed using ESI mass spectrometry, which revealed that both the target [2]rotaxane as well as the free macrocycle and axle components were present. However, a ^{1}H NMR spectrum of the crude mixture (9:1 CD_3CN/CD_3OD) suggested a poor yield of the interlocked product. Nonetheless, preparative TLC was used in an attempt to isolate the rotaxane, but unfortunately only non-interlocked axle and cyclic products were isolated. This may indicate that the association between **57·Cl** and **44·2PF$_6$** is too weak to facilitate efficient rotaxane formation.

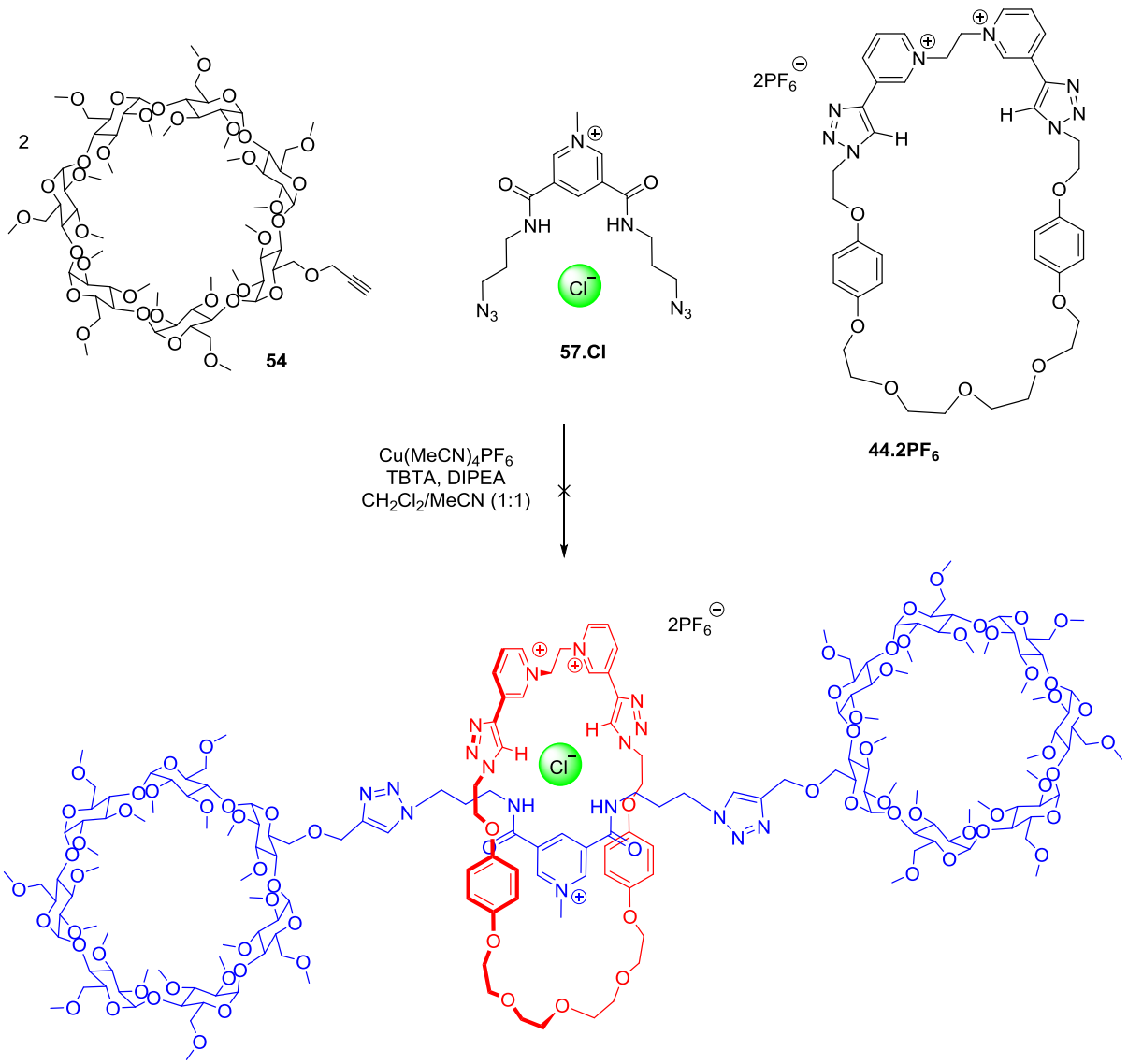

Scheme 3.10: Attempted synthesis of an all HB [2]rotaxane

3.5 Conclusions and future work

Two novel XB and HB acyclic receptors (**38·2PF$_6$** and **39·2PF$_6$**) containing the 1,2-bis(pyridinium)ethane motif were prepared. Anion binding investigations, in aqueous solvent media, revealed both receptors bound sulfate much more strongly than a range of singly charged anions, amongst which only modest selectivity was displayed. Surprisingly, there was little difference between the strength of anion association of the XB and HB receptors, which implies that the anion binding interactions with these acyclic hosts are primarily electrostatic in nature.

In an effort to increase anion association strength and obtain a higher degree of selectivity, analogous macrocyclic receptors (**43·2PF$_6$** and **44·2PF$_6$**) were synthesised. However, these hosts displayed disappointing anion binding properties, with only weak association of chloride and bromide, and no binding of other singly-charged anions, observed for both systems. Comparison of the association constants calculated for the HB acyclic and macrocyclic receptors showed that preorganisation of the binding motif through its incorporation within a macrocycle had little effect on the strength of anion association.

Attempts were then made to form interlocked structures containing macrocycles **43·2PF$_6$** and **44·2PF$_6$**. Preliminary pseudorotaxane studies revealed that HB macrocycle **44·2PF$_6$** formed an interpenetrated assembly with a bis-iodotriazole threading component **45·Cl**, whereas XB macrocycle **43·2PF$_6$** did not. Initial efforts to prepare a [2]rotaxane containing the HB macrocycle, by a 'click-stoppering' methodology, were hampered by halogen-hydrogen exchange within the axle component, however attempts to prepare an all HB rotaxane were also unsuccessful, which was attributed to the weakness of the templating interaction.

In summary, the anion binding investigations suggest that the bis-triazole functionalised 1,2-bis(pyridnium)ethane unit is an ineffective anion recognition motif. This may be a consequence of the motifs conformational flexibility. To overcome this, future work could

involve the preparation of a more rigid, preorganised analogue by replacing the ethylene spacer between the pyridinium units with a phenyl spacer (**Figure 3.17**).

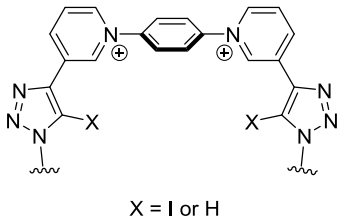

Figure 3.17: Alternative binding motif containing a phenyl spacer between the pyridinium units

3.6 References

1 S. J. Loeb and J. A. Wisner, *Chem. Commun.*, 1998, 2757–2758.
2 S. J. Loeb and J. A. Wisner, *Chem. Commun.*, 2000, 845–846.
3 G. J. E. Davidson, S. J. Loeb, N. A. Parekh and J. A. Wisner, *J. Chem. Soc. Dalton Trans.*, 2001, 3135–3136.
4 G. J. E. Davidson and S. J. Loeb, *Dalton Trans.*, 2003, 4319–4323.
5 A. L. Hubbard, G. J. E. Davidson, R. H. Patel, J. A. Wisner and S. J. Loeb, *Chem. Commun.*, 2004, 138–139.
6 N. Georges, S. J. Loeb, J. Tiburcio and J. A. Wisner, *Org. Biomol. Chem.*, 2004, **2**, 2751–2756.
7 S. J. Loeb and D. A. Tramontozzi, *Org. Biomol. Chem.*, 2005, **3**, 1393–1401.
8 G. J. E. Davidson, S. J. Loeb, P. Passaniti, S. Silvi and A. Credi, *Chem. – Eur. J.*, 2006, **12**, 3233–3242.
9 S. J. Loeb, *Chem. Soc. Rev.*, 2007, **36**, 226–235.
10 M. A. Bolla, J. Tiburcio and S. J. Loeb, *Tetrahedron*, 2008, **64**, 8423–8427.
11 D. J. Mercer, S. J. Vella, L. Guertin, N. D. Suhan, J. Tiburcio, V. N. Vukotic, J. A. Wisner and S. J. Loeb, *Eur. J. Org. Chem.*, 2011, **2011**, 1763–1770.
12 S. J. Loeb and J. A. Wisner, *Angew. Chem. Int. Ed.*, 1998, **37**, 2838–2840.
13 S. J. Loeb, J. Tiburcio, S. J. Vella and J. A. Wisner, *Org. Biomol. Chem.*, 2006, **4**, 667.
14 S. J. Loeb and J. A. Wisner, *Chem. Commun.*, 2000, 1939–1940.
15 A. M. Elizarov, S.-H. Chiu and J. F. Stoddart, *J. Org. Chem.*, 2002, **67**, 9175–9181.
16 S. J. Vella, J. Tiburcio and S. J. Loeb, *Chem. Commun.*, 2007, 4752–4754.
17 J. Tiburcio, G. J. E. Davidson and S. J. Loeb, *Chem. Commun.*, 2002, 1282–1283.
18 G. J. E. Davidson and S. J. Loeb, *Angew. Chem. Int. Ed.*, 2003, **42**, 74–77.
19 D. J. Hoffart and S. J. Loeb, *Angew. Chem. Int. Ed.*, 2005, **44**, 901–904.
20 V. N. Vukotic and S. J. Loeb, *Chem. Soc. Rev.*, 2012, **41**, 5896–5906.
21 M. F. Salomon and R. G. Salomon, *J. Am. Chem. Soc.*, 1979, **101**, 4290–4299.
22 J. C. Adrian and C. S. Wilcox, *J. Am. Chem. Soc.*, 1991, **113**, 678–680.
23 P. R. Ashton, E. J. T. Chrystal, P. T. Glink, S. Menzer, C. Schiavo, N. Spencer, J. F. Stoddart, P. A. Tasker, A. J. P. White and D. J. Williams, *Chem. – Eur. J.*, 1996, **2**, 709–728.
24 M. J. Hynes, *J. Chem. Soc. Dalton Trans.*, 1993, 311–312.
25 E. D. Goddard-Borger and R. V. Stick, *Org. Lett.*, 2007, **9**, 3797–3800.
26 N. Fischer, E. D. Goddard-Borger, R. Greiner, T. M. Klapötke, B. W. Skelton and J. Stierstorfer, *J. Org. Chem.*, 2012, **77**, 1760–1764.
27 N. G. White, H. G. Lovett and P. D. Beer, *RSC Adv.*, 2014, **4**, 12133–12147.
28 S. W. Robinson, C. L. Mustoe, N. G. White, A. Brown, A. L. Thompson, P. Kennepohl and P. D. Beer, *J. Am. Chem. Soc.*, 2015, **137**, 499–507.

29 M. J. Langton, S. W. Robinson, I. Marques, V. Félix and P. D. Beer, *Nat. Chem.*, 2014, **6**, 1039–1043.
30 M. J. Langton, I. Marques, S. W. Robinson, V. Félix and P. D. Beer, *Chem. – Eur. J.*, 2016, **22**, 185–192.
31 E. Bosch and C. L. Barnes, *Organometallics*, 2000, **19**, 5522–5524.
32 N. Zhong, H.-S. Byun and R. Bittman, *Tetrahedron Lett.*, 1998, **39**, 2919–2920.
33 J. A. Faiz, N. Spencer and Z. Pikramenou, *Org. Biomol. Chem.*, 2005, **3**, 4239–4245.
34 A. V. Leontiev, C. A. Jemmett and P. D. Beer, *Chem. – Eur. J.*, 2011, **17**, 816–825.

Chapter Four

Functionalised α-cyclodextrin hosts for anion recognition in pure water

4.1 Introduction

4.1.1 Anion recognition in pure water

The majority of the proposed applications of synthetic anion receptors are in the fields of biology, medicine and environmental science, making it a necessity that they can function in aqueous media.[1] Despite this, there are relatively few hosts capable of recognising anions in pure water, with the majority of examples reported to date operating in organic solvents or organic-aqueous solvent mixtures. This is primarily a consequence of the intrinsic properties anions possess, such as their pH dependence and high hydration energies (Section 1.1.2). However, the preparation of water-soluble receptors also presents a significant synthetic challenge, due to the poor solubility of many anion binding motifs.[2] Most reports of anion binding in water have utilised hosts containing a large number of positively charged HB groups, such as Lehn's polyammonium cryptands (Section 1.1.6).[3–5] Whilst these receptors have been shown to bind anions with very high affinities, they can only function over a narrow pH range, which restricts their applicability.

Recently, a handful of receptors that utilise a combination of the hydrophobic effect and HB interactions to bind anions in water have been described. The water solubilisation of these hosts is achieved through the attachment of several negatively charged carboxylate groups to their peripheries. Notable examples include Sindelar's bambusuril macrocycle (Section 1.1.9**)**,[6] Pittelkow's related biotin[6]uril macrocycle (**Figure 4.1a**)[7,8] and Gibb's cavitand host (**Figure 4.1b**).[9,10] All three of these receptors exhibit anion selectivity trends which mirror the Hofmeister series, with hydrophobic anions such as iodide and perchlorate (ClO_4^-) bound most strongly. Thermodynamic studies on the bambusuril and biotin[6]uril macrocycles revealed anion association to be entirely enthalpically driven, which is characteristic of a non-classical hydrophobic effect.[11]

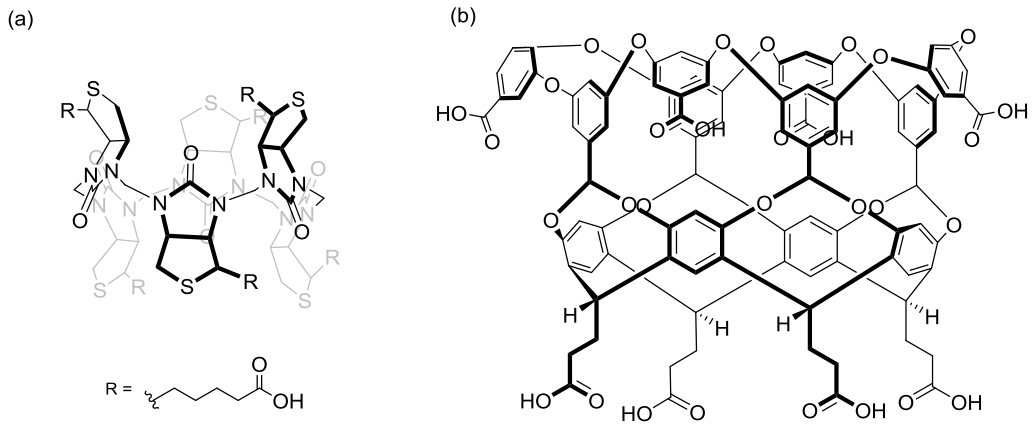

Figure 4.1: (a) Pittelkow's biotin[6]uril macrocycle[7] and (b) Gibb's cavitand[9]

Examples of XB receptors that can recognise anions in pure water are exceptionally rare; however those reported thus far have highlighted XB as a highly effective binding interaction in aqueous media. This is demonstrated by Beer's bis-iodotriazolium acyclic receptor containing hydrophilic tris-tetra(ethylene glycol) units (**Figure 4.2**),[12] which bound perrhenate (ReO_4^-) and iodide more strongly than other halides and the oxoanions perchlorate and sulfate, in D_2O. By contrast, the HB receptor analogue was incapable of binding perrhenate under the same conditions. Van't Hoff analysis of perrhenate binding by the XB host revealed the association to be enthalpically favoured and entropically disfavoured, suggesting that complexation is driven by the formation of strong XB-anion interactions.

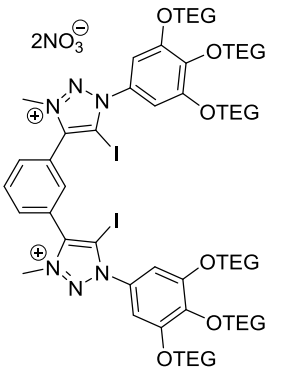

Figure 4.2: Beer's water-soluble acyclic XB receptor[12]

4.1.2 Cyclodextrins

Another method of imparting organic molecules with water solubility is through their inclusion within or attachment to cyclodextrins (CDs), which are naturally occurring cyclic oligosaccharides composed of 1-4 linked α-D-glucopyranose units. They are produced by an intramolecular transglycosylation reaction that occurs when starch is degraded by the CD glucanotransferase enzyme present in the bacterium *Bacilus macerans*. The most extensively studied forms are α-, β- and γ-CD, which contain six, seven and eight glucopyranose units, respectively (**Figure 4.3a**). All three homologues adopt a truncated-cone conformation and possess a hydrophobic internal cavity and a hydrophilic exterior (**Figure 4.3b**), with secondary hydroxyl groups (labelled 2-*O* and 3-*O*, **Figure 4.3c**) at the wider 2° rim and primary hydroxyl groups (labelled 6-*O*) at the narrower 1° rim. Various properties of the native (unfunctionalised) CDs are shown in **Table 4.1**.[13]

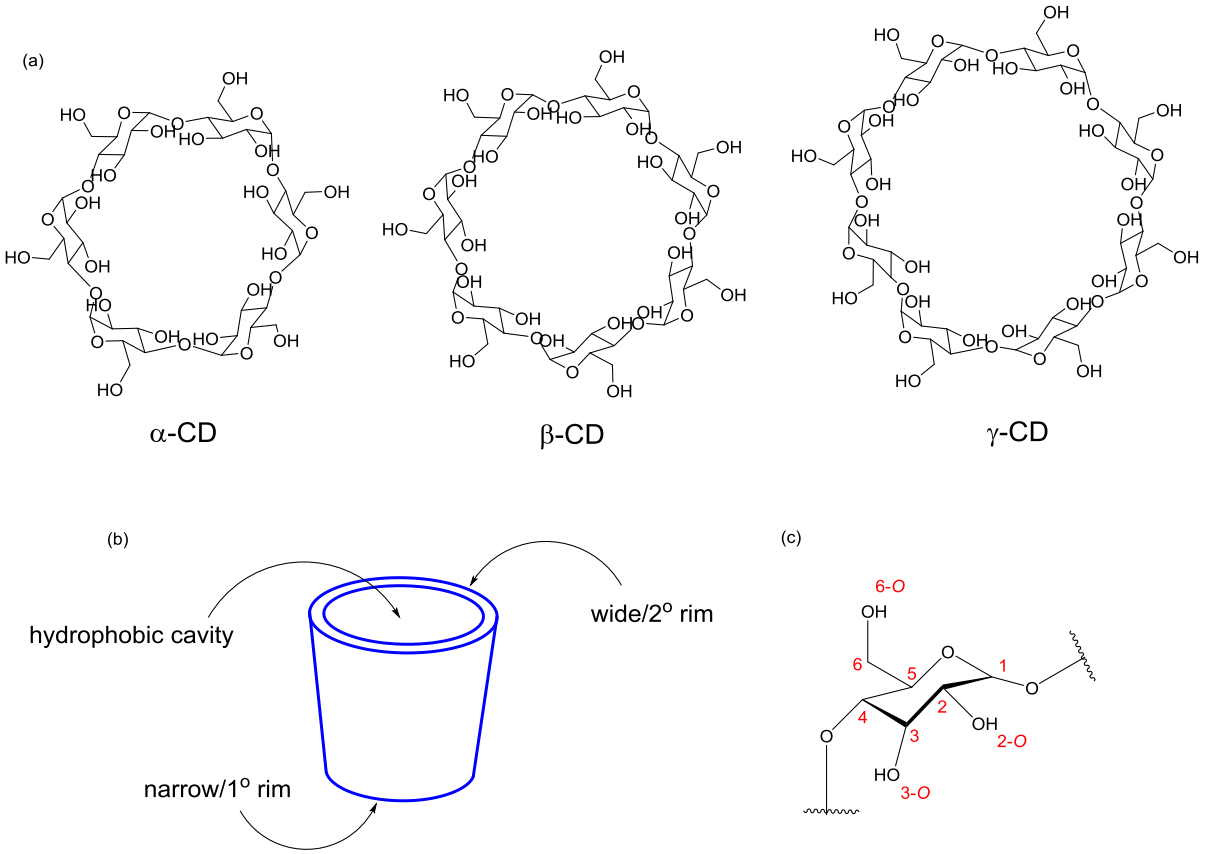

Figure 4.3: (a) α-, β-, and γ-CD, (b) 3D structure of CDs and (c) labelling of C and O atoms within one glucopyranose unit

Table 4.1: Properties of the three CD homolouges (reproduced from reference 14)

Properties	**α-CD**	**β-CD**	**γ-CD**
Molecular weight (g/mol)	972	1135	1297
Solubility in water at 298 K (g/L)	145	18.5	232
Cavity diameter (Å)	4.7-5.3	6.0-6.5	7.5-8.3
Outer diameter (Å)	14.6	15.4	17.5
Height of torus (Å)	7.9	7.9	7.9
Cavity volume ($Å^3$)	174	262	427

The ability of CDs to encapsulate hydrophobic organic guests within their central cavities in water[13–16] has led to their application in a variety of industries including drug delivery,[17] catalysis,[18] nanotechnology,[19] materials science, environmental protection,[20] molecular recognition[21] and chromatography.[13]

CDs have also been shown to form inclusion complexes with inorganic anions in aqueous solution.[22–24] In an early study by Laufer and co-workers, potentiometric titration experiments demonstrated that iodide, perchlorate and thiocyanate bind weakly within the cavity of α-CD (K_a = 19, 46 and 35 M^{-1}, respectively).[25] Very recently, Pursell and Pursell used UV-visible spectroscopy to investigate the inclusion of the triiodide anion (I_3^-) within α-CD.[26] Their results suggest that a 1:1 host-guest complex is formed with a very strong association constant (K_a = 1.45 x 10^5 at 293 K), whilst van't Hoff analysis revealed the association was enthalpically favourable and entropically disfavoured (ΔH = -31 kJ mol^{-1}, ΔS = -64 J K^{-1} mol^{-1}).

In addition, Nau and co-workers have shown that a range of dodecaborate anions ($[B_{12}X_{12}]^{2-}$; X = Cl, Br or I) form strong inclusion complexes with γ-CD.[27] Solid-state structural analysis showed the formation of a 2:1 (host:guest) complex (**Figure 4.4**), however solution-state ^1H NMR titration experiments in D_2O indicated 1:1 stoichiometric binding.

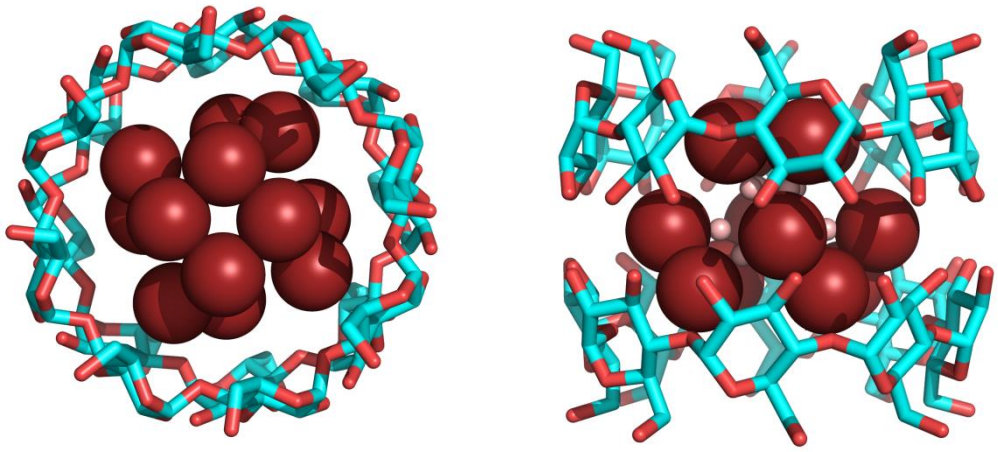

Figure 4.4: Solid-state X-ray structure of the 2:1 complex of native γ-CD and $[B_{12}Br_{12}]^{2-}$.[27]

Association constants determined using ITC and ^{1}H NMR titrations revealed $[B_{12}Br_{12}]^{2-}$ was bound most strongly (K_a = 9.6 x 10^5 M^{-1}), which was attributed, in part, to optimal dispersion interactions resulting from a favourable host-guest size match. Binding was again found to be enthalpically favoured and entropically disfavoured, which led the authors to suggest that the 'chaotropic effect' was also contributing to the strong association observed.[9,10,28,29] This relates to the disruption of the structure of the bulk water caused by solvation of the anions. Upon their inclusion within the cavity of the CD, hydrogen bonds are reformed between water molecules in the bulk solution resulting in an enthalpic gain and an entropic penalty. The larger the size of the anion the more pronounced this effect is.

Advances in the regioselective functionalisation of CDs has led to the construction of water-soluble anion receptors in which the CD is used as a scaffold to which XB or HB donors can be appended. This is exemplified by Beer's [2]rotaxane, which contains a XB 3,5-bis-iodotriazole pyridinium axle component with permethylated-β-CD stopper groups (**Figure 4.5a**).[30] The host displayed a remarkably high affinity for iodide in D_2O (K_a = 2200 M^{-1}), with chloride, bromide and sulfate bound substantially more weakly (K_a = 55 M^{-1}, 290 M^{-1} and 30 M^{-1}, respectively). Importantly, the iodide association constant of the analogous all-HB [2]rotaxane was two orders of magnitude smaller (K_a = 20 M^{-1}). Van't Hoff analysis showed

iodide association to be enthalpically driven with the XB host and entropically driven with the all-HB receptor.

Kim and co-workers described a hexacationic α-CD-based receptor, containing six prototriazolium groups attached to the 1° rim (**Figure 4.5b**), which bound a range of polyanionic species including phytic acid (K_a = 19 x 10^5 M^{-1}).[31]

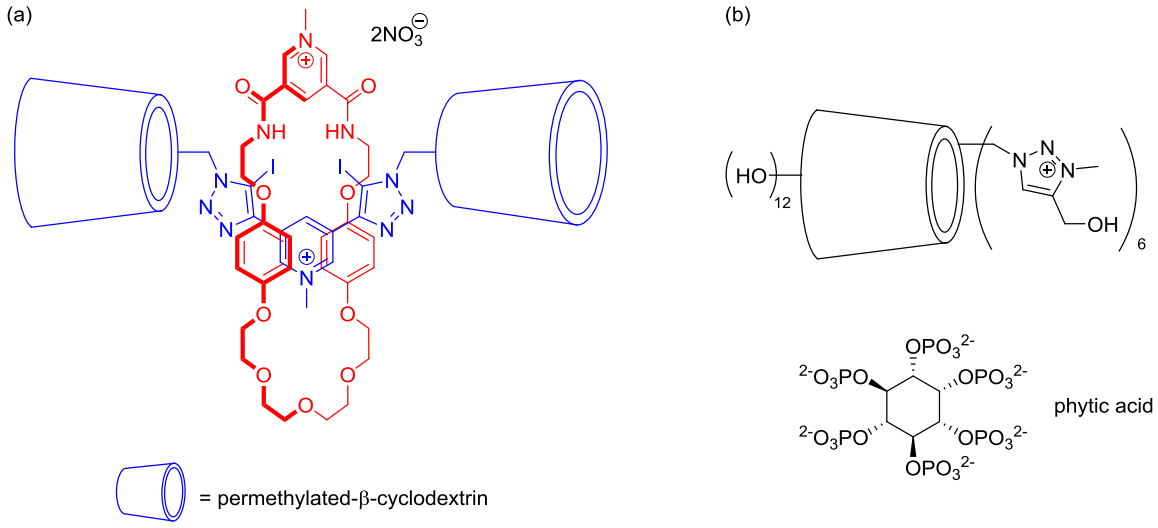

Figure 4.5: (a) Beer's XB [2]rotaxane[30] and (b) Kim's hexacationic α-CD based receptor.[31]

4.1.3 Chapter aims

The work in this chapter focuses on the preparation of a series of water-soluble anion receptors containing a permethylated-α-CD unit functionalised at the 1° rim with either XB or HB donor motifs. Initial work targeted the synthesis of host systems in which either two iodo- or proto-triazole pyridinium side-arms were attached to the 6 position of diametrically opposed glucopyranose units of the CD (positions 6^A and 6^D, **Figure 4.6a**).[#] Subsequently, the preparation of 'strapped' receptors containing a bis-iodo- or proto-triazole pyridinium motif bridging between the 6^A and 6^D positions of the α-CD (**Figure 4.6b**) is described. Investigations into the anion binding properties of these receptors were then conducted using ^{1}H NMR and ITC experiments.

By convention, in a mono-substituted α-CD derivative, the functionalised glucopyranose unit is denoted A, with the remaining units labelled B-F. $6^{A,D}$-substituted therefore means that Carbon 6 of glucopyranose units A and D are functionalised.

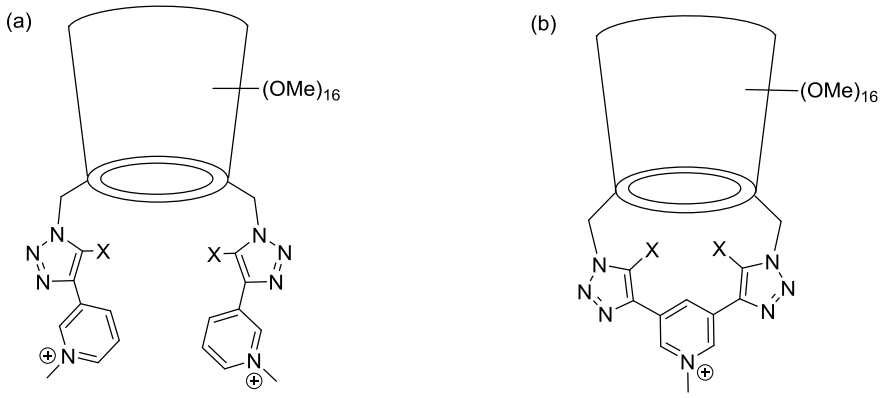

Figure 4.6: Target receptors containing (a) XB or HB triazole pyridinium side-arms and (b) XB or HB bis-triazole pyridinum 'strap'. X = I or H.

4.2 Synthesis of α-CD precursors

The preparation of all of the target receptors required the same bis-azide starting material ($6^{A,D}$-diazido-permethylated-α-CD). Importantly, the permethylated derivative was used due its greater solubility in organic solvents, relative to the non-methylated analogue, which significantly simplifies further functionalisation and purification.

Initially, native α-CD was reacted with excess benzyl chloride in the presence of sodium hydride to give perbenzylated-α-CD **58**. Subsequent regioselective de-*O*-benzylation gave $6^{A,D}$-dihydroxy-perbenzylated-α-CD **59**. The conditions used for this reaction were adapted from the procedure reported by Sinaÿ and co-workers, with **58** stirred at 50 ^{o}C overnight in sixty equivalents of DIBAL-H (1.5 M in toluene).[32] Following an acidic aqueous work-up, the target material was separated from small amounts of mono- and over-debenzylated side-products using column chromatography to afford **59** in a yield of 72% (**Scheme 4.1**).

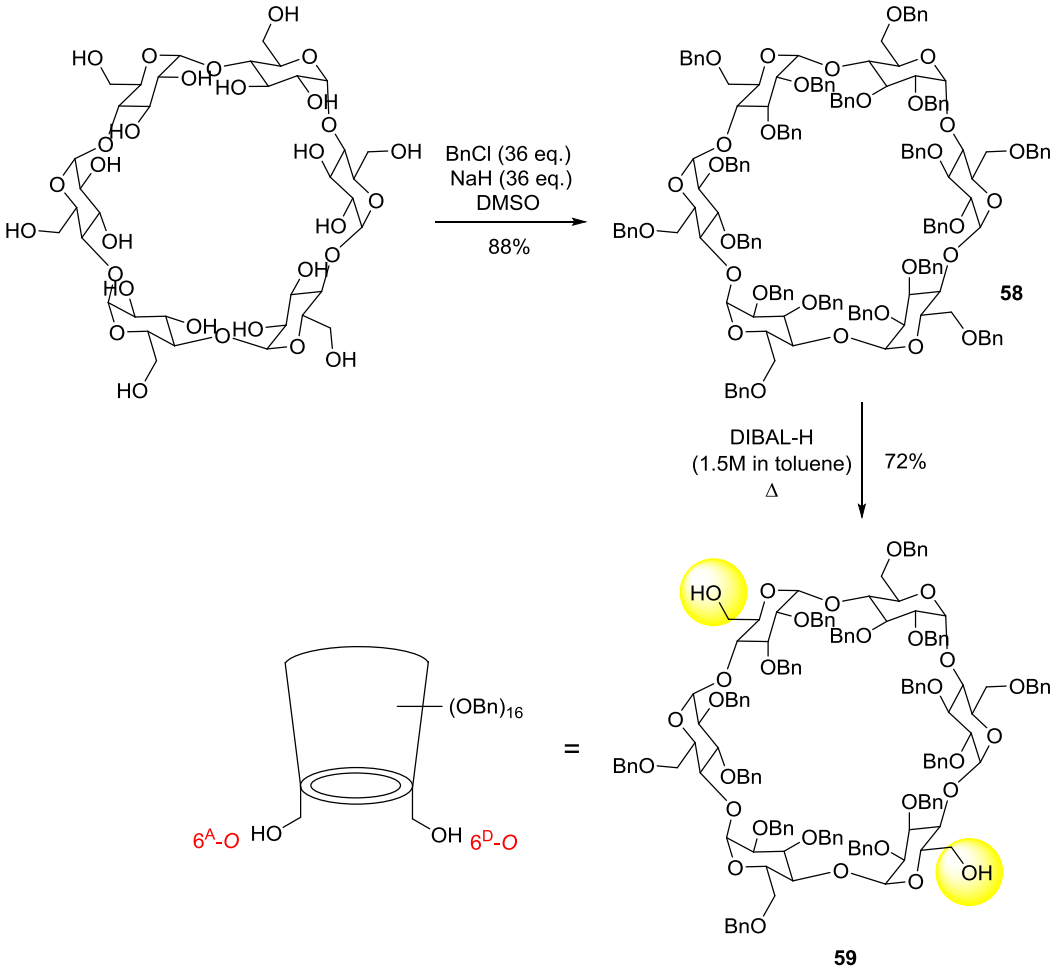

Scheme 4.1: Synthesis of precursor **59**.[32]

In the same report this procedure was obtained from, a number of experiments were performed to determine the origin of the regioselectivity of this reaction. It was concluded that the positions at which debenzylation occurs is controlled by sterics. In the mechanism proposed by the authors (**Scheme 4.2**), an initial mono-debenzylation occurs at the 1^{o} rim of **58** *via* coordination of two molecules of DIBAL-H to the 6-*O* position and the ring oxygen of one of the glucopyranose units. Importantly, this coordination cannot occur at the 2^{o} rim due to the greater density of benzyl groups. The aluminium alkoxide species generated in the first reaction sterically hinders the approach of a second pair of DIBAL-H molecules and hence they are directed towards the glucopyranose unit farthest away (unit D), where the second debenzylation reaction takes place.

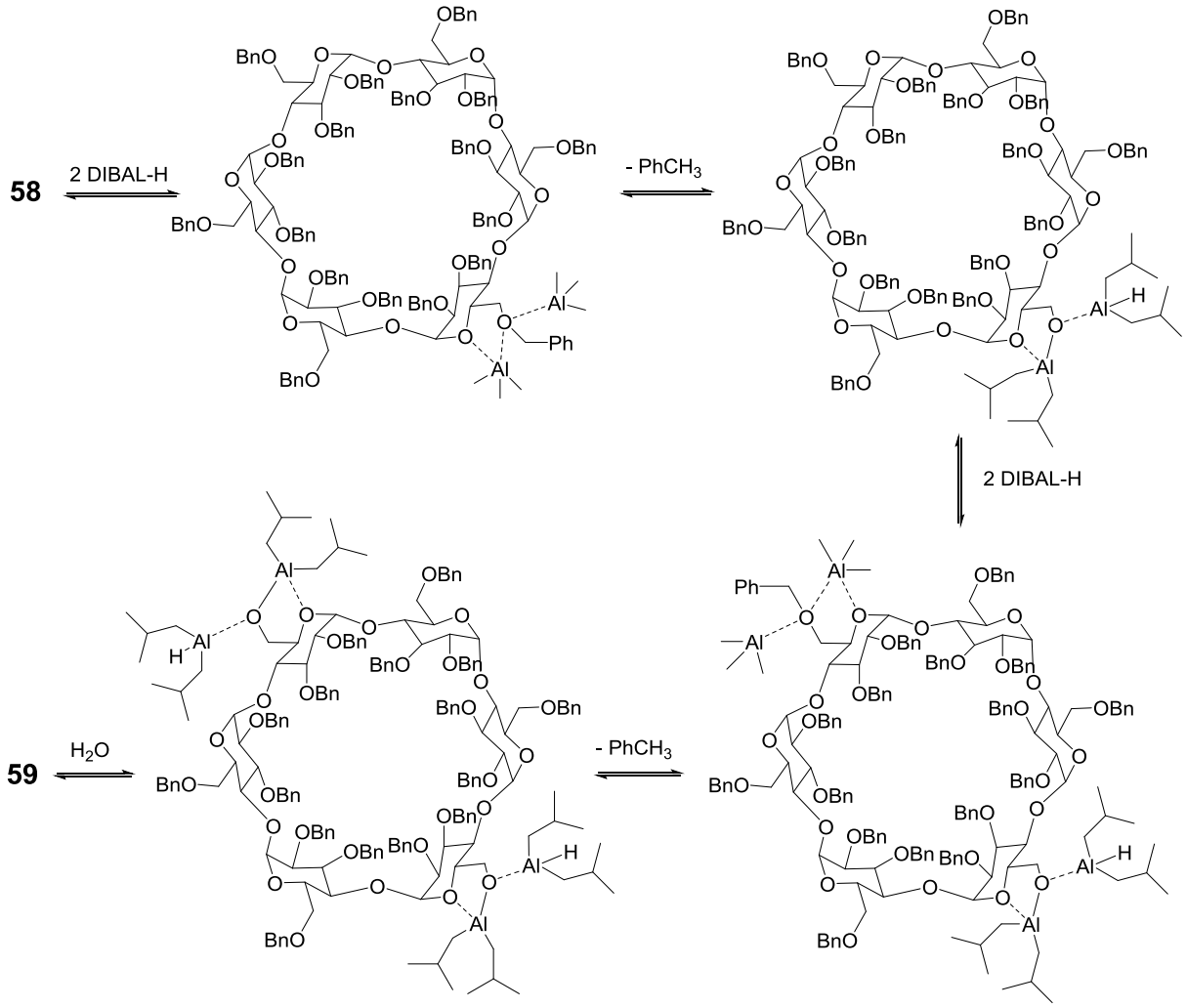

Scheme 4.2: Proposed mechanism of regioselective debenzylation of **58**.[32]

Confirmation that the product formed was the $6^{A,D}$-regioisomer was obtained from ^{1}H NMR spectroscopy, which showed the formation of an α-CD species with C_2 symmetry, as expected. The symmetry of the molecule results in the equivalence of protons in glucopyranose units opposite to each other (*i.e*, A=D, B=E and C=F), which is most clearly observed for the 1-*H* resonances, which appear as three distinct signals. It should be noted that DIBAL-H can also be used to de-*O*-methylate permethylated-CDs. However, the relatively smaller steric bulk of methoxy groups reduces the regioselectivity of these reactions leading to the formation of a mixture of products.[33] Hence, it is not possible to directly form $6^{A,D}$-dihydroxy-permethylated-α-CD.

Preparation of the target bis-azide derivative was then attempted by two different routes, starting from diol **59**. In the first route (**Scheme 4.3**) the hydroxyl groups of **59** were firstly mesylated through a reaction with methanesulfonyl chloride in the presence of triethylamine to give **60**,[34] which was subsequently fully debenzylated using Pd/C catalysed hydrogenolysis, to afford **61**.[35] Methylation of the sixteen hydroxyl groups of **61** was attempted using methyl iodide and sodium hydride. However, only partially methylated products were observed by ESI mass spectrometry, even when a large excess of the alkylating agent and base were used.

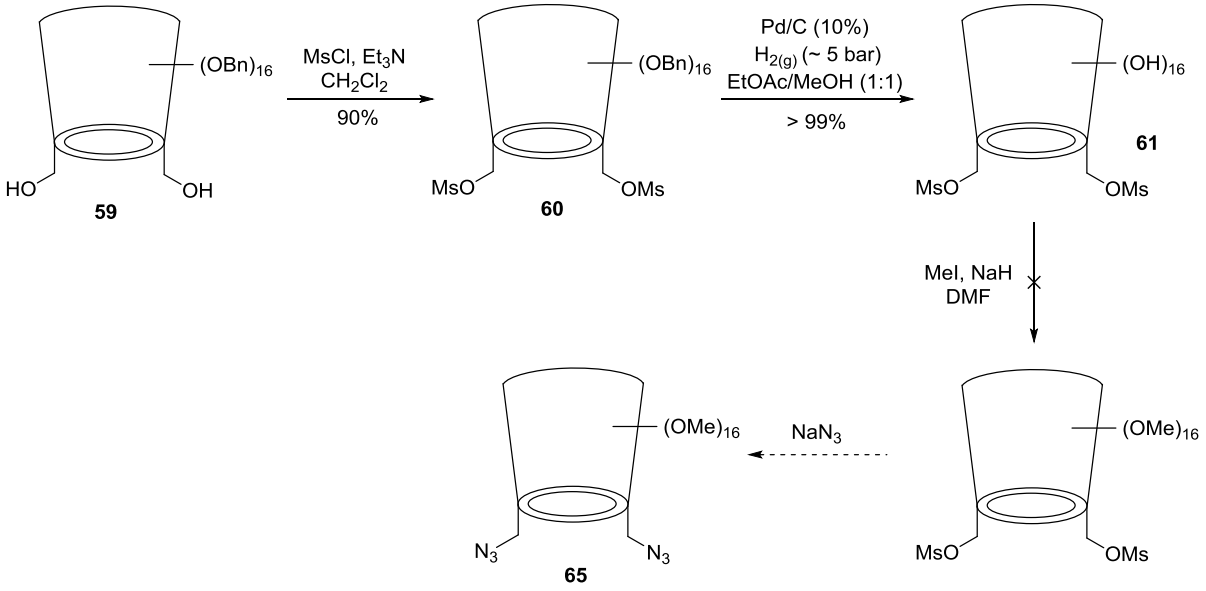

Scheme 4.3: Attempted synthesis of bis-azide **65**

An alternative route was therefore used, which was adapted from previously reported synthetic procedures (**Scheme 4.4**).[36,37] This involved the initial protection of the hydroxyl groups of **59** with tetrahydropyranyl (THP) functionality through a reaction with dihydropyran and a catalytic amount of camphorsulfonic acid to give **62**. Compound **62** was then debenzylated *via* Pd/C catalysed hydrogenolysis (~5 bar), and methylated using methyl iodide and sodium hydride. Hydrolysis of the THP groups, using an aqueous solution of acetic acid, afforded $6^{A,D}$-dihydroxy-permethylated-α-CD **63**. During the four synthetic steps used to convert **59** into diol **63**, the formation of the intermediates was monitored using ESI mass

spectrometry, which showed that partial cleavage of the THP protecting groups occurred in the debenzylation and methylation reactions. Owing to the instability of THP groups under acidic conditions, purification of these intermediate compounds using silica gel column chromatography was not attempted. As a consequence, the crude product mixture containing **63**, also contained substantial amounts of both mono-alcohol and fully methylated species as side products. Careful chromatographic purification afforded pure **63** in a 43% yield over the four steps, which is a significant improvement on the reported procedure.[37]

Reaction of **63** with methanesulfonyl chloride gave bis-mesylate **64** in quantitative yield, and conversion to the target $6^{A,D}$-diazido-permethylated-α-CD **65** was achieved *via* reaction with sodium azide.

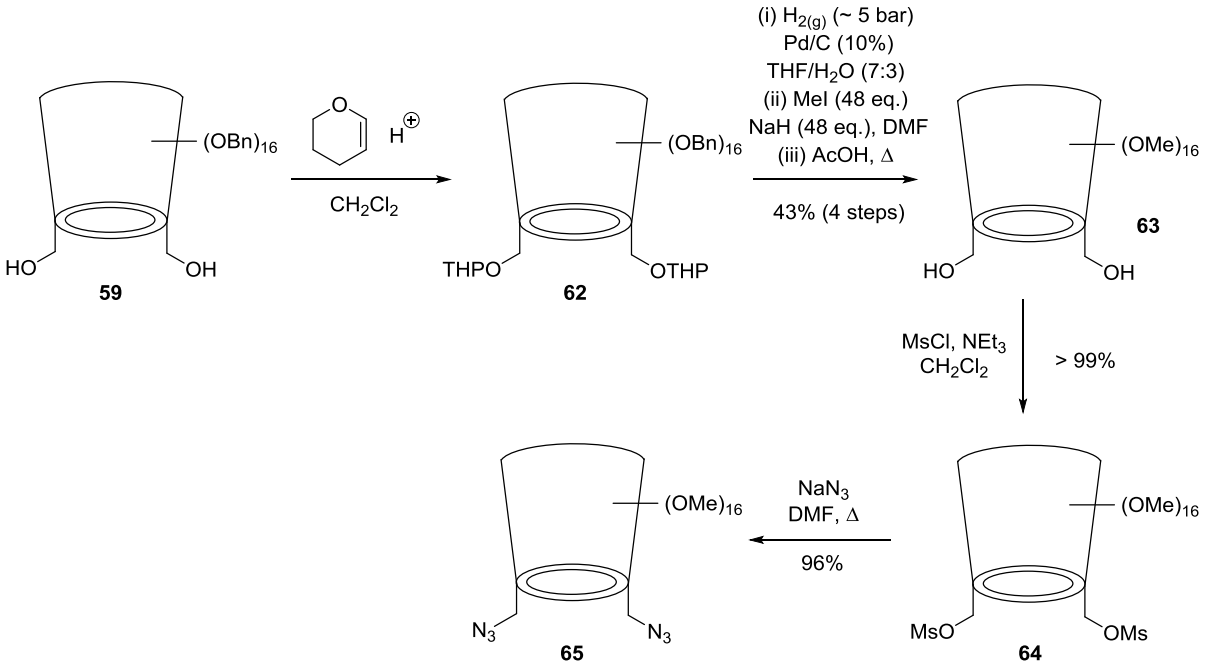

Scheme 4.4: Synthesis of bis-azide **65**

4.3 α-CD receptors containing halogen and hydrogen bonding side-arms

4.3.1 Synthesis

Having successfully prepared the bis-azide precursor **65**, the synthesis of dicationic receptors containing two iodo- or proto-triazole pyridinium side-arms was undertaken, as outlined in **Scheme 4.5**.

The reaction of **65** with two equivalents of either 3-(iodoethynyl)pyridine or 3-ethynylpyridine under CuAAC conditions gave bis-iodotriazole and bis-prototriazole derivatives **66** and **67**, respectively, in good yields. The pyridine units of both compounds were methylated using methyl iodide to afford **68·2I** and **69·2I**, which were anion exchanged to their nitrate salts using a nitrate-loaded Amberlite® column, to give the target water-soluble XB and HB receptors **68·2NO$_3$** and **69·2NO$_3$.** The conversion of the hosts to their nitrate salts was based on the weakly coordinating nature of this anion in water along with the good solubility it provides.[12,30,38] In addition, nitrate forms very weak inclusion complexes with α-CD (K_a ~ 2 M^{-1}) and hence it should not compete with other anions for association to either of the receptors.[25]

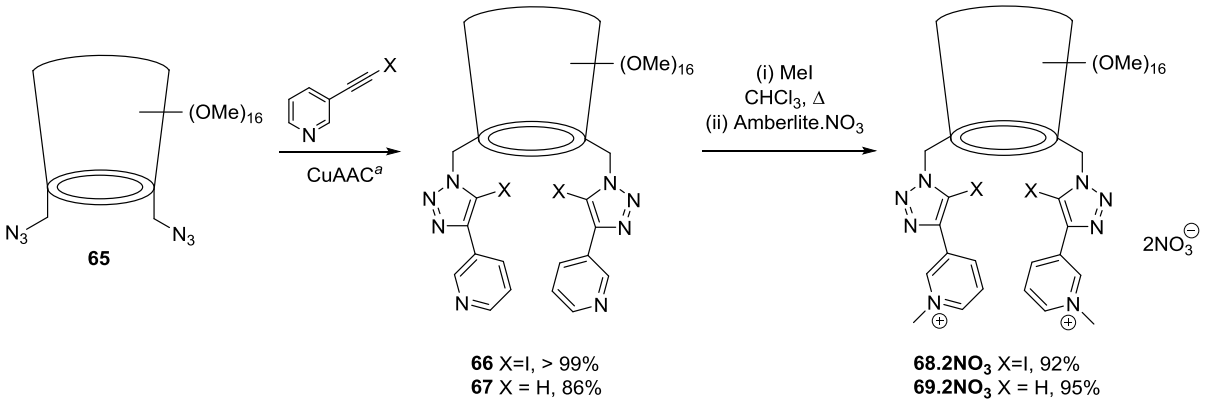

Scheme 4.5: Synthesis of XB and HB receptors **68·2NO$_3$** and **69·2NO$_3$**. [a] For X = I: $[Cu(MeCN)_4][PF_6]$, TBTA, THF; for X = H: $[Cu(MeCN)_4][PF_6]$, DIPEA, TBTA, CH_2Cl_2.

The receptors were characterised by ^{1}H (**Figure 4.7**, **68·2NO$_3$**) and ^{13}C NMR spectroscopy, and high-resolution ESI mass spectrometry, with the assignment of the resonances in the ^{1}H

spectra requiring the use of 2D COSY, 2D ROESY and 1D TOCSY NMR. For both systems the corresponding protons of each triazole pyridinium side-arm are equivalent, with only one set of resonances observed in the aromatic region of the spectra. Also of note are the 6-*H* protons of the glucopyranose units attached to the triazole group (units A and D), which are diastereotopic and hence appear as two distinct signals (*g* and *g*').

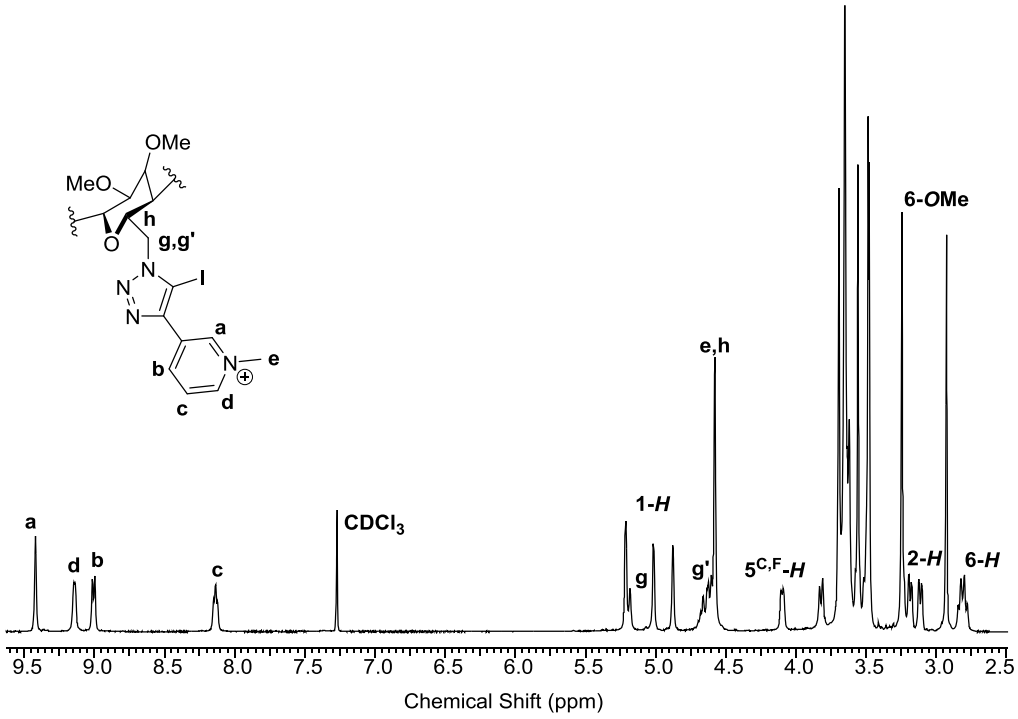

Figure 4.7: ^{1}H NMR spectrum of XB receptor **68·2NO$_3$** ($CDCl_3$, 298 K, 500 MHz)

4.3.2 Anion binding properties of 68·2NO$_3$ and 69·2NO$_3$

Preliminary investigations into the anion binding properties of the XB and HB receptors were conducted using ^{1}H NMR titration experiments performed in pure D_2O, with the protons of the two hosts monitored upon addition of up to 120 equivalents of chloride, bromide, iodide, sulfate, perchlorate (ClO_4^-) and perrhenate (ReO_4^-), as their sodium salts.

In the case of XB host **68·2NO$_3$**, the addition of iodide, perchlorate and perrhenate resulted in significant downfield shifts of the *h* and $5^{C,F}$-*H* protons, all of which are located within the central cavity of the CD, at the 1^{o} rim (**Figure 4.8**). Furthermore, pyridinium protons *d* also shifted downfield in the perchlorate and perrhenate titrations (0.18 ppm and 0.45 ppm,

respectively), along with protons *a* in the perrhenate titration (0.14 ppm). Only minimal perturbations to any of the pyridinium resonances were seen in the iodide titration. These observations suggest all three anions are bound within the cavity of the CD, with only the oxoanions forming significant interactions with the iodotriazole pyridinium groups.

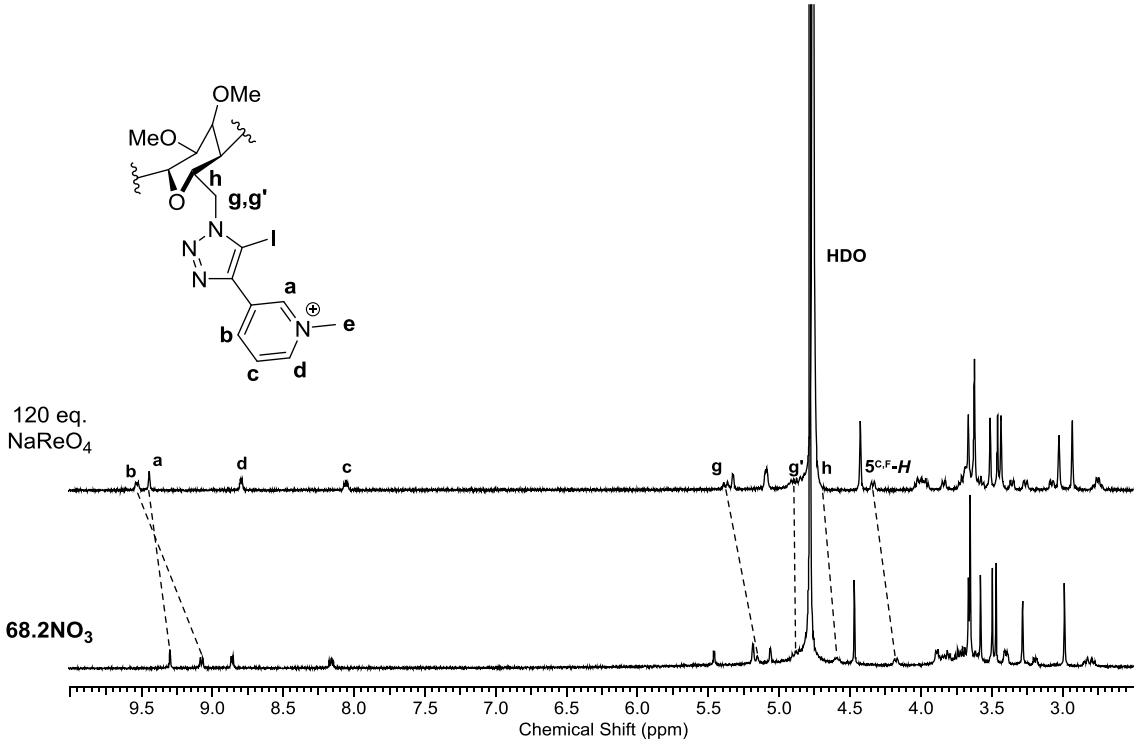

Figure 4.8: Truncated ^{1}H NMR spectra of XB receptor **68·2NO$_3$** before and after addition of 120 equivalents of $NaReO_4$ (D_2O, 298 K, 500 MHz).

Downfield shifts of the *h* and $5^{C,F}$-*H* protons were again observed in analogous titrations with HB receptor **69·2NO$_3$** (**Figure 4.9**), with the addition of iodide and perrhenate also resulting in a downfield shift of triazole protons *f* (0.24 ppm and 0.08 ppm, respectively). However, minimal perturbations to these protons were seen in the perchlorate titration and none of the pyridinium protons (*a*-*d*) shifted substantially in any of the titrations performed. As with the XB host, it appears that all three anions are encapsulated within the cavity of the CD, but in this case only iodide and perrhenate form significant interactions with the prototriazole HB donor groups.

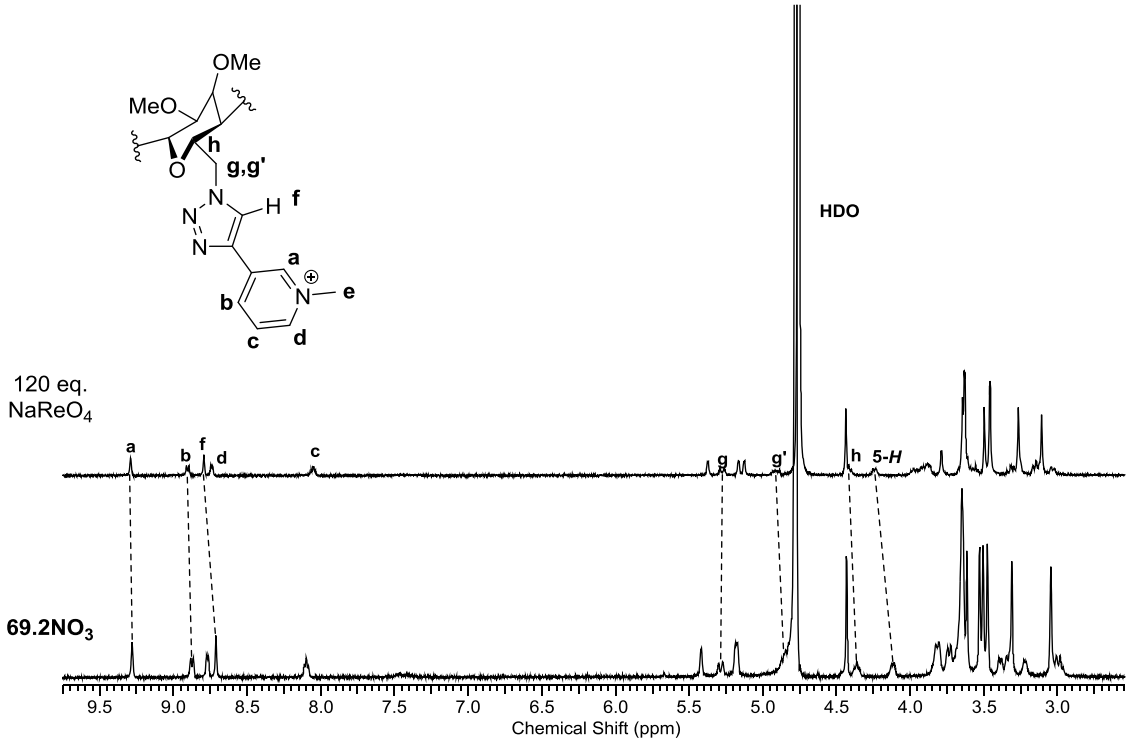

Figure 4.9: Truncated ^{1}H NMR spectra of HB receptor **69·2NO$_3$** before and after addition of 120 equivalents of $NaReO_4$ (D_2O, 298 K, 500 MHz).

By contrast, minimal perturbations to the resonances of either receptor were seen in the titrations with chloride, bromide and sulfate, implying that these anions are bound very weakly. This is perhaps unsurprising considering their high hydration energies, which must be overcome to allow binding to occur.

WinEQNMR analysis of the iodide, perchlorate and perrhenate titration data,[39] monitoring the shift of the $5^{C,F}$-*H* protons for both hosts (**Figure 4.10**), determined 1:1 stoichiometric association constants (**Table 4.1**).

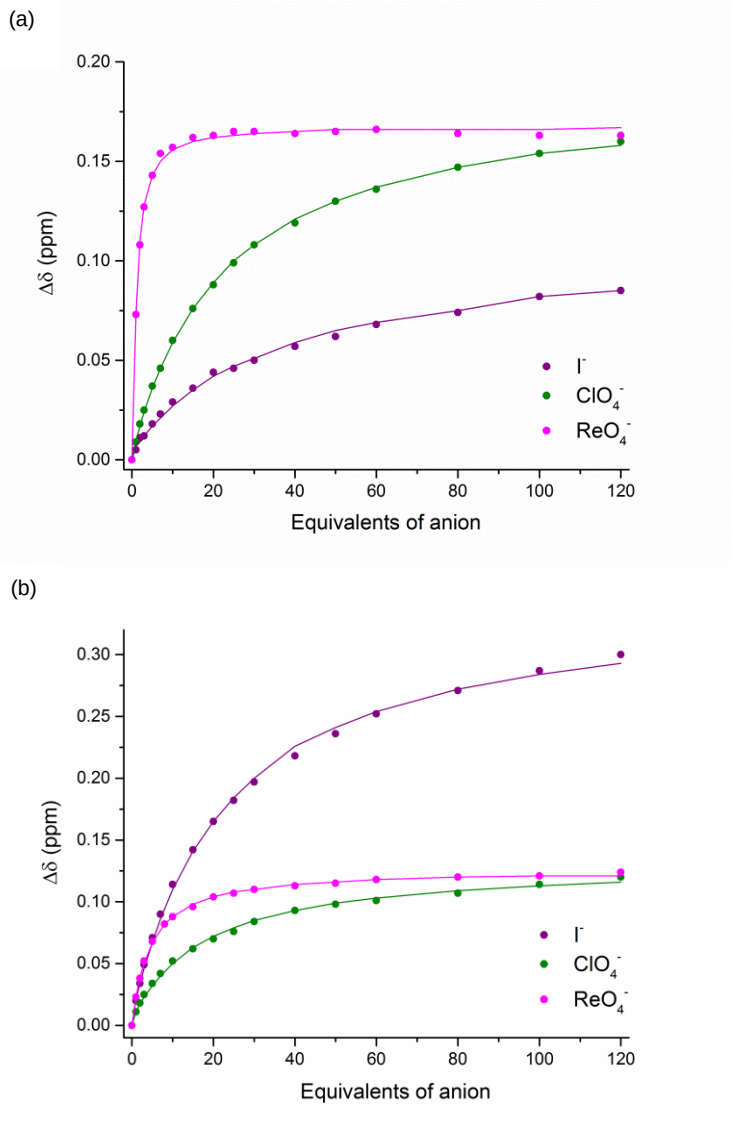

Figure 4.10: Experimental titration data (points) and calculated 1:1 binding isotherms (lines) for the addition of sodium salts of various anions to: (a) **68·2NO$_3$** and (b) **69·2NO$_3$**, monitoring protons 5^{C,F}-*H* (D_2O, 298 K, 500 MHz)

Table 4.2: Association constants (K_a) determined for receptors **68·2NO$_3$** and **69·2NO$_3$** with various anions (D_2O, 298 K, 500 MHz), along with properties of these anions.

Anion	K_a **(M^{-1})**[a]		ΔG_{hyd} **(kJ/mol)**	**Ionic Radius (nm)**[40]
	68·2NO$_3$	**69·2NO$_3$**		
I^-	18	27	-275[41]	0.22
ClO_4^-	27	36	-205[41]	0.25
ReO_4^-	950	170	-330[42]	0.26

[a] Calculated using chemical shift of 5^{C,F}-*H* protons. Estimated errors within ±10%.

Both receptors display selectivity towards perrhenate, with the association constants of iodide and perchlorate an order of magnitude less. As the hydration energy of perrhenate is the largest of the three anions (**Table 4.2**), it is unlikely that the observed selectivity is a consequence of a hydrophobic effect. Instead, it is possible that the strong binding is, in part, a result of a favourable size match between the cavity of the CD and the oxoanion, which allows the formation of strong dispersion forces between them. The relatively smaller size of iodide and perchlorate presumably reduces the strength of these dispersion forces, resulting in a weaker association. Importantly, there is a large difference between the magnitudes of the perrhenate association constants of the two receptors, with the value calculated for the XB host approximately five-times greater than that of the HB host. This implies that the XB interactions formed between the anion and **68·2NO$_3$** are significantly stronger than the HB interactions formed by **69·2NO$_3$**, which is consistent with the results obtained for the acyclic receptors discussed in Section 4.1.1.[12]

The strong association observed with **69·2NO$_3$** is particularly noteworthy as perrhenate is commonly used as a model for the highly toxic, radioactive pertechnetate anion, due to their similar sizes and hydration energies.[42] As pertechnetate is an environmental pollutant,[43,44] the production of hosts capable of selectively binding and/or sensing perrhenate in aqueous media has been highlighted as an important challenge for supramolecular chemists.[45] Despite this, only a handful of receptors capable of binding this oxoanion in pure water have been reported,[12,46,47] with the majority of examples functioning in organic solvent systems.[48–51] The most effective host known to date is Amendola's hexacationic azacryptand (log K = 5.22, pH 2, 303 K),[46] however the strong association observed requires low pH and hence reduces this receptors applicability. The pH independent XB receptor **68·2NO$_3$** therefore constitutes the most effective host currently known for perrhenate recognition in neutral water and further

highlights the utility of the XB interaction for the purpose of anion recognition in aqueous media.

A titration between native α-CD and sodium perrhenate was also undertaken to assess the stability of the inclusion complex formed in the absence of the additional XB/HB binding groups. By monitoring the shift of the 3-*H* protons, which are directed towards the centre of the CDs cavity, a 1:1 stoichiometric association constant of 96(2) M^{-1} was determined, implying that the HB arms of receptor **69·2NO$_3$** play a modest contribution to the binding of perrhenate. Interestingly, the iodide and perchlorate association constants of both receptors are of a similar magnitude to the values reported for the binding of these anions to native α-CD (K_a = 19 M^{-1} and K_a = 46 M^{-1}).[25] This suggests that the additional binding interactions provided by either host contribute minimally towards the association of these anions.

4.3.3 ITC investigations of perrhenate binding

In order to further investigate the origins of the perrhenate selectivity displayed by XB **68·2NO$_3$** and HB **69·2NO$_3$**, isothermal titration calorimetry (ITC) experiments were performed in water. During these experiments aliquots of a solution of sodium perrhenate were added to a solution of each of the receptors at regular intervals, with the heat pulses generated (**Figure 4.11a** and **b**) integrated with respect to time to produce curves of Δ*H* vs. concentration of anion (**Figure 4.11c** and **d**). Fitting of these isotherms to a 1:1 stoichiometric binding model using a non-linear least-squares squares regression method afforded the thermodynamic parameters of the binding events along with the association constants (**Table 4.3**). It should be noted that the heat outputs observed for each addition to HB **69·2NO$_3$** were small, making the errors associated with the fitting process large. The calculated values for this receptor are therefore only rough estimates. Further details of the experimental conditions used in the titrations can be found in section 6.6.

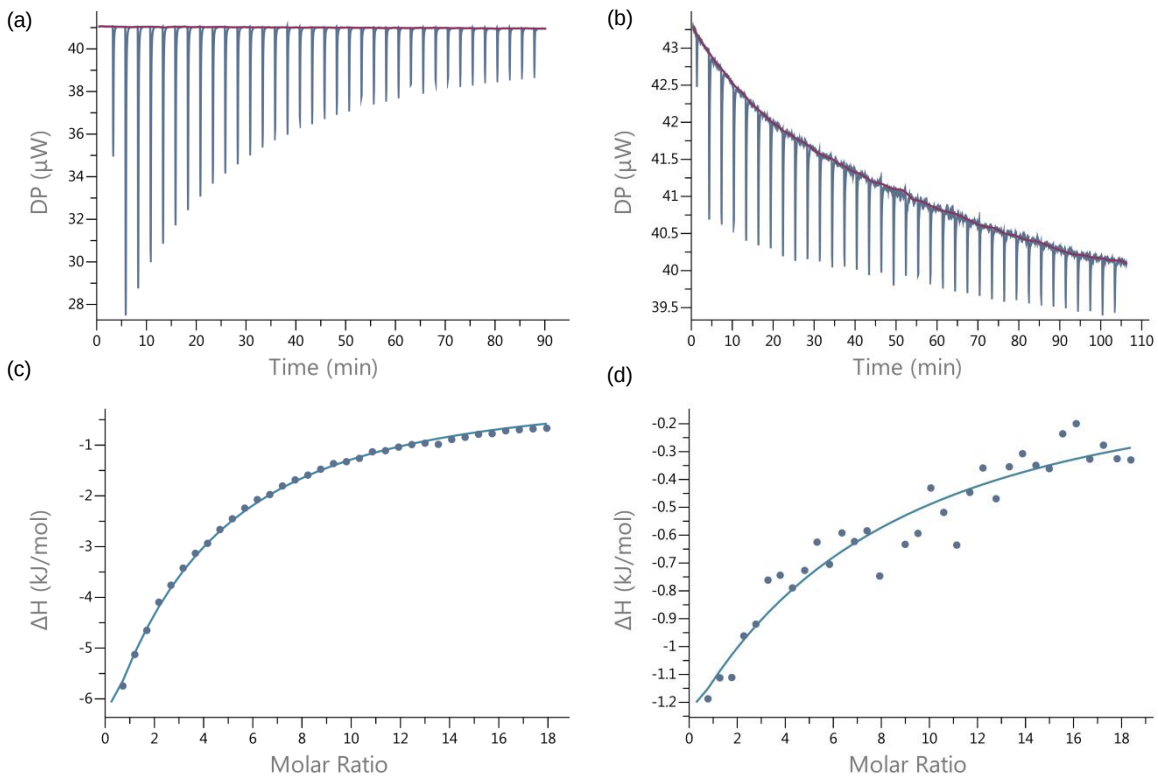

Figure 4.11: (a and b) Raw ITC data for the sequential addition of $NaReO_4$ to **68·2NO$_3$** and **69·2NO$_3$**, respectively (H_2O, 298 K); (c and d) Integrated heat plots obtained from titrations with **68·2NO$_3$** and **69·2NO$_3$**, respectively.

Table 4.3: Association constants and thermodynamic parameters determined for **68·2NO$_3$** and **69·2NO$_3$** with $NaReO_4$ (H_2O, 298K). Errors in parentheses.

	68·2NO$_3$	**69·2NO$_3$**
K_a **(M^{-1})**	650(10)	290(100)
Δ*G* (kJ/mol)	-16.1	-14.0
Δ*H* (kJ/mol)	-54.0(0.4)	-21.9(8.5)
-*T*Δ*S* (kJ/mol)	37.9	7.8

In both titrations, association was found to be enthalpically favoured and entropically disfavoured and, in agreement with the results obtained in the ^{1}H NMR titration experiments, the XB receptor exhibited a higher perrhenate affinity than the HB host. This can be attributed to the significantly larger enthalpic contribution to binding with **68·2NO$_3$**, which presumably is a consequence of the strong XB-anion interactions formed. Indeed, in the two other reports where thermodynamic investigations of anion binding with an XB host in water were

conducted, a large enthalpic contribution to association was also found.[12,30] As previously discussed, the association of perrhenate with HB **69·2NO$_3$** is almost entirely mediated by the inclusion of the anion within the cavity of the CD. Therefore, the thermodynamic parameters calculated in the titration with this receptor imply that the driving forces for anion recognition may be similar to those Nau and co-workers proposed for the inclusion of the dodecaborate anions within native γ-CD.[27] That is a combination of the strong dispersion forces formed due to the favourable size match between the cavity of the CD and the perrhenate anion, along with a contribution from the 'chaotropic effect'. This is perhaps unsurprising, considering the relatively large size of the perrhenate anion.

4.4 'Strapped' halogen and hydrogen bonding α-CD receptors

Following the encouraging results obtained with receptors **68·2NO$_3$** and **69·2NO$_3$** it was decided to prepare analogous host systems in which the XB or HB donors were appended to a 'strap' connecting the 6^A and 6^D positions of a permethylated α-CD (see **Figure 4.6b**). It was hoped that the greater preorganisation of these receptors would lead to stronger anion association and potentially alter their selectivity.

Several examples of 'strapped' α-CD species have been reported to date. These include Sinaÿ's 6^{A,D}-oligomethylinic strapped α-CDs, prepared by ring closing metathesis reactions (**Figure 4.12a**)[52], and Kraus' 6^{A,D}-disulfide strapped permethylated-α-CD, synthesised *via* the oxidative linkage of a disulfanyl precursor (**Figure 4.12b**).[53] Recently, Chambron and co-workers described a more elaborate system in which permethylated-α-CD is capped with a cyclotriveratrylene unit *via* the formation of three disulfide linkages at the 6^A, 6^C and 6^E positions of the CD (**Figure 4.12c**).[54] However, there are currently no examples of strapped CD species prepared using CuAAC reactions.

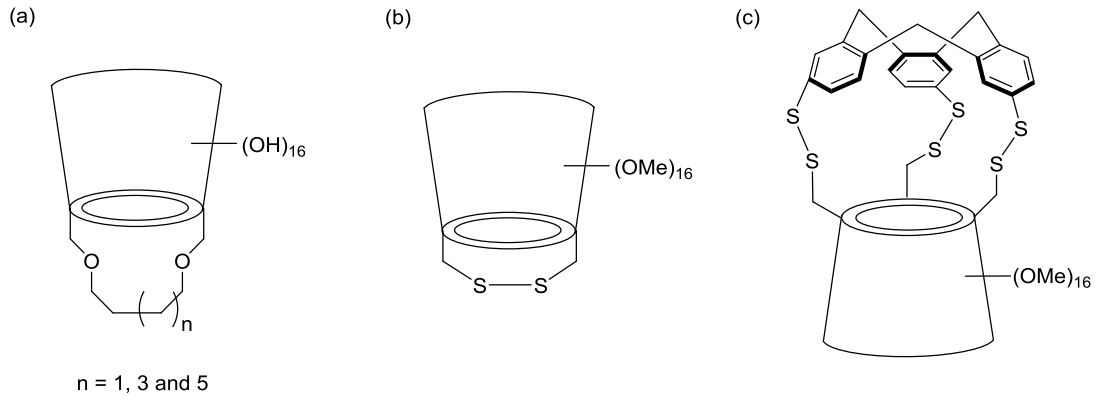

Figure 4.12: (a) Sinaÿ's oligomethylinic strapped α-CDs,[52] (b) Kraus' disulfide strapped permethylated-α-CD[53] and (c) Chambron's cyclotriveratrylene capped permethylated-α-CD.[54]

4.4.1 Synthesis

To prepare both the HB and XB systems, a double CuAAC reaction was initially performed between one equivalent of bis-azide **65** and one equivalent of either 3,5-diethynyl pyridine **46** or 3,5-bis(iodoethynyl)pyridine **47** (**Schemes 4.6** and **4.7**). Dilute conditions were used (5 mM concentration) to disfavour the formation of oligomeric species.

For the HB derivative, TLC analysis of the crude reaction mixture revealed that both starting materials had been fully consumed after four days and that only one α-CD-containing species was present, which ESI mass spectrometry confirmed as the target product **70**. However, it proved difficult to separate **70** from TBTA and hence an isolated yield of only 46% was obtained.

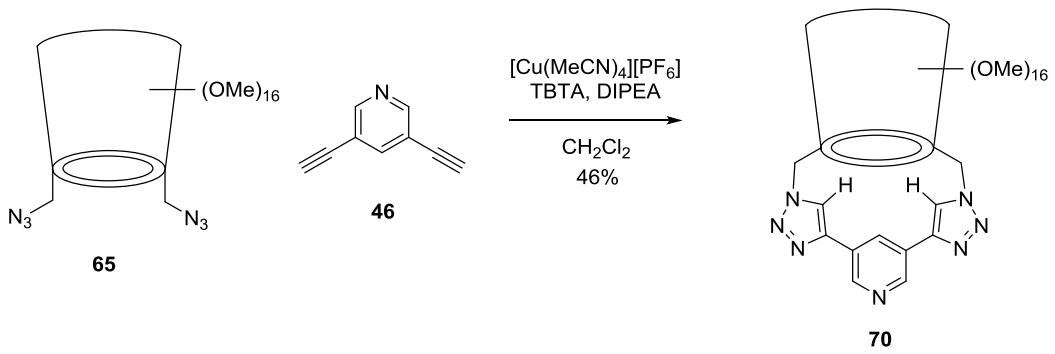

Scheme 4.6: Synthesis of strapped α-CD derivative **70**

Conversely, for the XB derivative, TLC analysis showed that three α-CD-containing species were present in the crude reaction mixture, two of which were identified by ESI mass

spectrometry as the target 'strapped' derivative **71**, and the corresponding dimeric species **72**. Presumably, the third species is a larger oligomeric structure. Purification of the crude material, by preparative TLC, afforded the target material **71** in a 22% yield and the dimeric product **72** in a 9% yield.

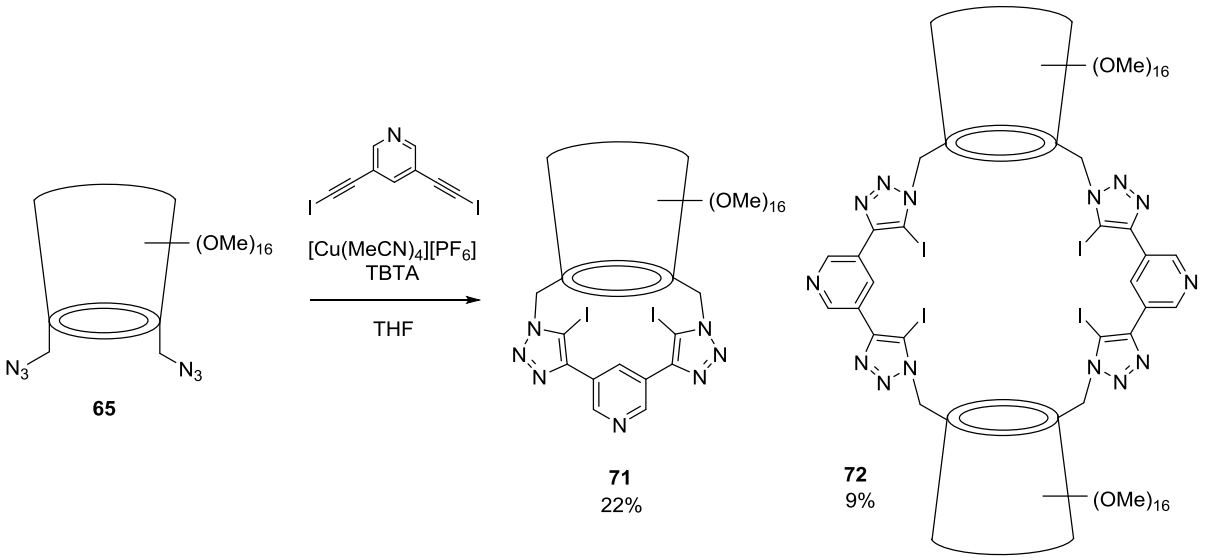

Scheme 4.7: Synthesis of strapped and dimeric α-CD derivatives **71** and **72**

Comparison of the ^{1}H NMR spectra of **71** and **72** (**Figure 4.13**), confirmed that they are different species. This is most evident from inspection of the aromatic regions of the spectra, which are clearly distinct. In both compounds the CD units have C_2 symmetry, as evident from the three separate signals corresponding to the 1-*H* protons.

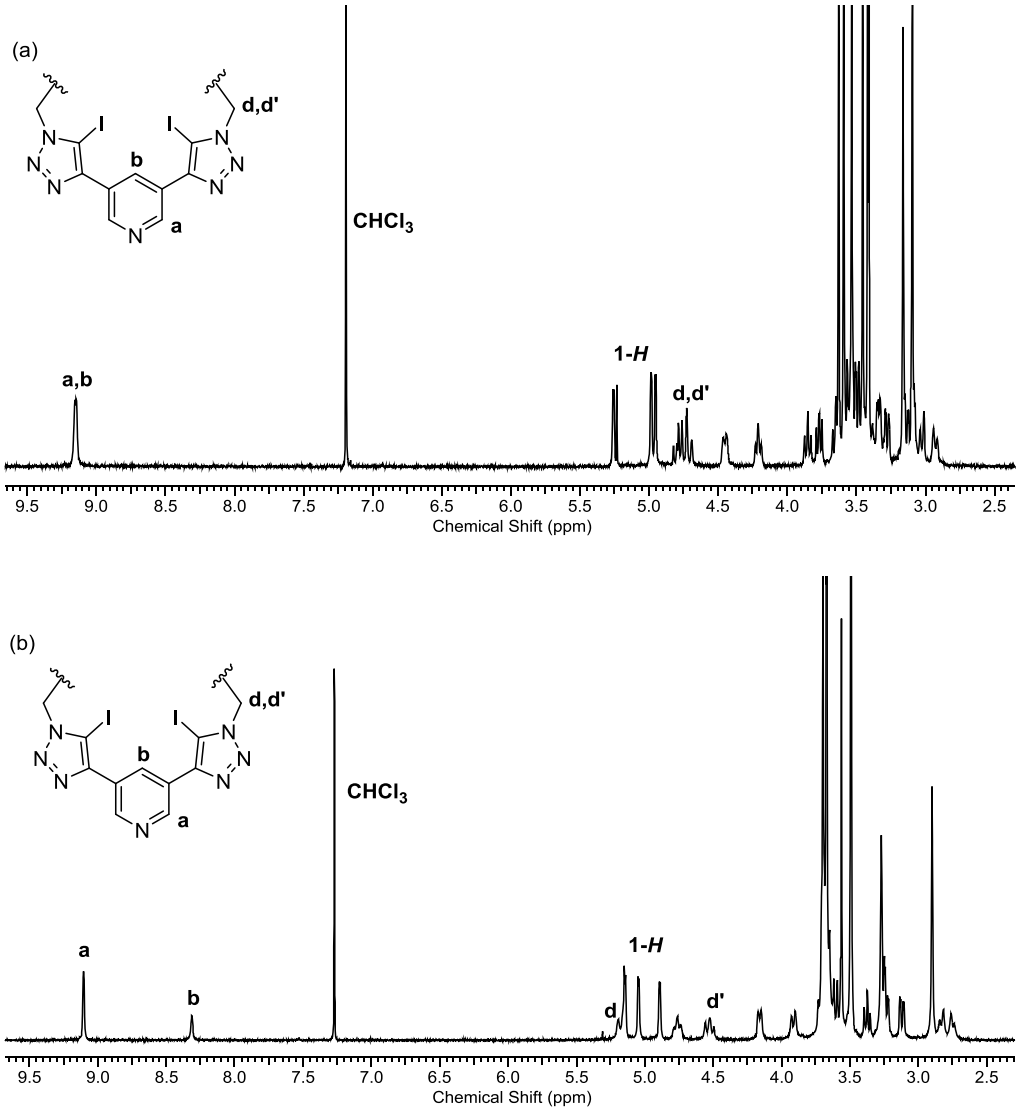

Figure 4.13: Truncated ^{1}H NMR spectra of: (a) **71** and (b) **72** ($CDCl_3$, 298 K, 500 MHz)

The difference in the products obtained in the two reactions suggests that the formation of **71** is less favourable than the formation of **70**. This is most likely a consequence of the steric bulk of the iodines present in **71**, which presumably hinder the second intramolecular 'click' reaction, allowing an intermolecular reaction to occur as well.

Methylation of **70** and **71**, with methyl iodide, followed by anion exchange afforded the target HB and XB receptors **73·NO_3** and **74·NO_3** (**Scheme 4.8**), which were characterised by ^{1}H and ^{13}C NMR spectroscopy and high resolution ESI mass spectrometry.

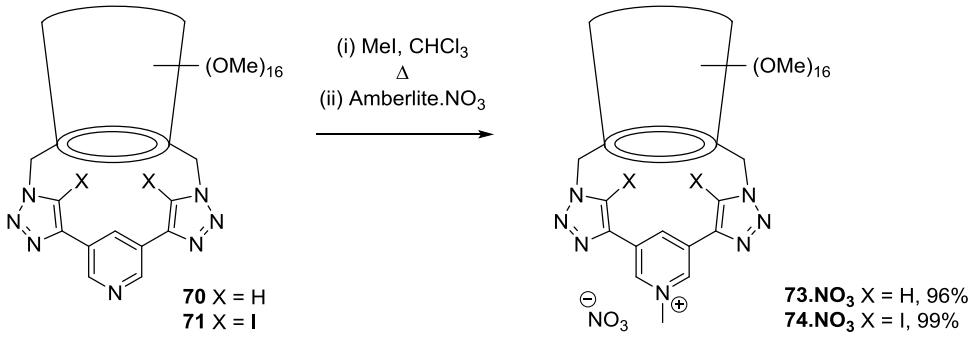

Scheme 4.8: Synthesis of HB and XB strapped receptors **73·NO_3** and **74·NO_3**

4.4.2 Anion binding properties of 73·NO_3 and 74·NO_3

^{1}H NMR titration experiments were used to investigate the anion binding properties of **73·NO_3** and **74·NO_3** with chloride, bromide, iodide, perchlorate and perrhenate in pure D_2O.

In the case of HB receptor **73·NO_3**, substantial downfield perturbations of the pyridinium proton *b* and the triazole protons *c* were observed on addition of the halides, consistent with the formation of HB-anion interactions (**Figure 4.14**). In contrast, these protons shifted upfield with perchlorate and perrhenate, which suggests there is a difference in the binding mechanism of these anions relative to that of the halides. Also, large downfield shifts of the $5^{C,F}$-*H* protons, which are directed towards the centre of the CD cavity, were seen in all of the titrations performed, indicating that all the anions are encapsulated within the CD.

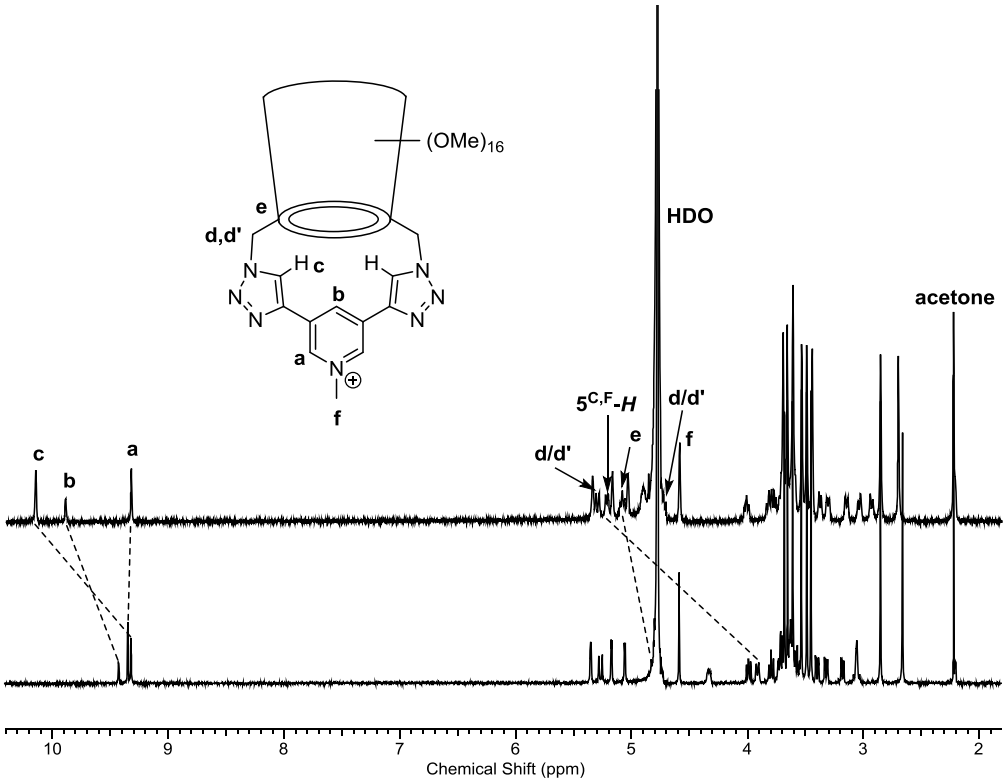

Figure 4.14: Truncated ^{1}H NMR spectra of HB receptor **73·NO$_3$** before and after the addition of ten equivalents of NaI (D_2O, 298 K, 500 MHz)

With the XB host **74·NO$_3$**, none of the protons underwent significant shifts with any of the anions investigated, implying that very weak association is occurring in all cases. This suggests that there is insufficient space to allow encapsulation of the anions within the cavity of the host, which is possibly due to the steric bulk of the iodotriazole groups.

WinEQNMR analysis[39] of the titration data obtained for HB host **73·NO$_3$**, monitoring the shift of the triazole protons *c* (**Figure 4.15**), gave 1:1 stoichiometric association constants (**Table 4.4**).

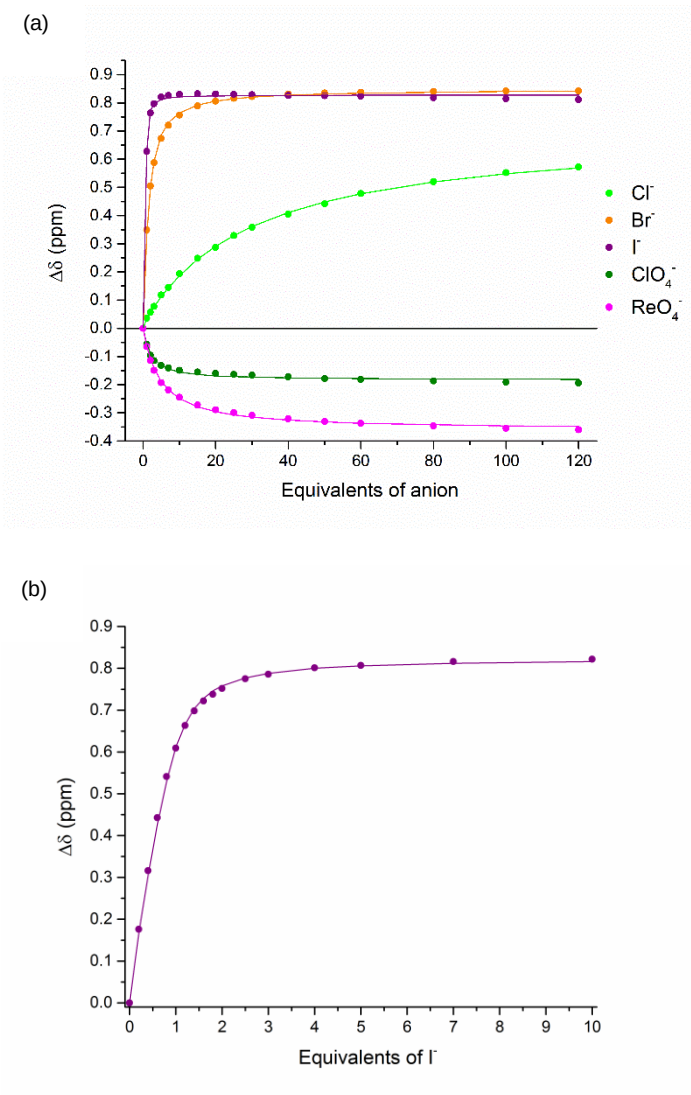

Figure 4.15: Experimental titration data (points) and calculated 1:1 binding isotherms (lines) for the addition of (a) 120 equivalents of various anions as their TBA salts to **73·NO$_3$** and (b) 10 equivalents of TBA iodide to **73·NO$_3$**, monitoring triazole protons *c* (D_2O, 298 K, 500 MHz).

Table 4.4: Association constants (K_a) determined for HB receptor **73.NO$_3$** with various anions (D_2O, 298 K, 500 MHz).

Anion	**K_a (M^{-1})**	
	73·NO$_3$[a]	**69·2NO$_3$**
Cl^-	20	-[d]
Br^-	660	-[d]
I^-	6900[b]	27
ClO_4^-	390[c]	36
ReO_4^-	150	170

[a] Calculated using chemical shift of triazole protons *c*. Estimated errors within ±10%.
[b] Calculated using alternative protocol in which only 10 equivalents of anion were added to receptor.
[c] Estimated error = ±15%. [d] Shifts too small to determine K_a.

The HB receptor displays a strong affinity and a high degree of selectivity towards iodide, with the association constant an order of magnitude greater than those for bromide, perchlorate and perrhenate, and two orders of magnitude greater than the value obtained for chloride. Indeed, iodide binding was so strong that an alternative titration protocol, involving addition of up to only 10 equivalents of the anion, had to be used to calculate a more accurate value than that obtained from the initial protocol used. The selectivity trend observed between the halides directly mirrors their hydration energies, with the most weakly solvated anion (iodide) bound most strongly. The host's higher affinity for bromide and iodide relative to perchlorate and perrhenate suggests that its binding pocket is better suited to the spherical anions than the tetrahedral oxoanions. This is most likely a result of the complementarity between the shape of the halides and the convergent orientation of the preorganised prototriazole HB donor groups of **73·NO$_3$**.

Comparison of the association constants of **73·NO$_3$** with those of the previously discussed HB receptor **69·2NO$_3$** reveals that the 'strapped' system is a substantially more effective host for all three halides and perchlorate. This is most notable for the halides, which are all bound very weakly by **69·2NO$_3$**, suggesting that the preorganised HB donor groups of **73·NO$_3$** are more ideally oriented to allow strong interactions with these anions. The more open nature of **69·2NO$_3$** presumably results in strong hydration of its triazole pyridinium arms, which reduces their HB donor ability. In contrast the HB donors within **73·NO$_3$** are potentially more shielded from the solvent, allowing them to form stronger interactions with the anions. Interestingly the perrhenate association constants of both receptors are similar to the value calculated for association of this anion to native α-CD (K_a = 96(2) M^{-1}), which implies that binding is primarily driven by inclusion of the anion within the cavity of the CD units.

4.5 Conclusions and future work

In conclusion, four novel anion receptors containing 1^o rim functionalised permethylated-α-CD have been prepared and their anion recognition properties investigated in pure water.

^{1}H NMR titration experiments showed that the dicationic XB and HB hosts **68·2NO$_3$** and **69·2NO$_3$** both displayed selectivity towards perrhenate, which was attributed to the good size match between the oxoanion and the central cavity of the CD unit. Importantly, the perrhenate association constant calculated for the XB receptor was approximately five-times greater than that obtained for the HB receptor, providing further evidence that XB is a more effective anion binding interaction than HB in water. ITC experiments were used to probe the thermodynamics of the perrhenate binding process for the two receptors and showed that association was enthalpically favoured and entropically disfavoured in both cases. This was ascribed to a number of factors including the 'chaotropic effect'; however the strong XB-anion interactions formed by **68·2NO$_3$** provided a notably large enthalpic contribution to binding.

The 'strapped' HB host **73·NO$_3$** exhibited a drastically different selectivity trend to **68·2NO$_3$** and **69·2NO$_3$**, with iodide bound substantially more strongly than the other halides, perchlorate and perrhenate. This is most likely due to the highly preorganised nature of the convergent HB donor groups present in **73·NO$_3$**, which are shielded from the solvent and create a binding pocket which is potentially more suited to the spherical halide anions than the tetrahedral oxoanions. XB receptor **74·NO$_3$** was found to bind all anions investigated very weakly. This is possibly a consequence of the steric bulk of the iodotriazole groups it contains, which presumably prevent anions from entering the cavity of the CD.

Ongoing work in this project will involve the use of ITC experiments to determine the thermodynamic parameters of anion association with **73·NO$_3$**. It would also be of interest to

investigate the anion binding properties of the methylated analogue of the dimeric derivative **72** (**Figure 4.16**).

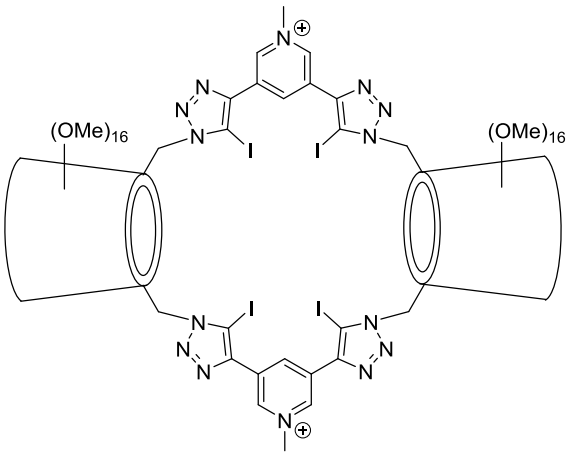

Figure 4.16: Methylated analogue of dimeric derivative **72**

4.6 References

1 N. H. Evans and P. D. Beer, *Angew. Chem. Int. Ed.*, 2014, **53**, 11716–11754.
2 M. J. Langton, C. J. Serpell and P. D. Beer, *Angew. Chem. Int. Ed.*, 2016, **55**, 1974–1987.
3 J. M. Lehn, E. Sonveaux and A. K. Willard, *J. Am. Chem. Soc.*, 1978, **100**, 4914–4916.
4 B. Dietrich, J. Guilhem, J.-M. Lehn, C. Pascard and E. Sonveaux, *Helv. Chim. Acta*, 1984, **67**, 91–104.
5 B. Dietrich, B. Dilworth, J.-M. Lehn, J.-P. Souchez, M. Cesario, J. Guilhem and C. Pascard, *Helv. Chim. Acta*, 1996, **79**, 569–587.
6 M. A. Yawer, V. Havel and V. Sindelar, *Angew. Chem. Int. Ed.*, 2015, **54**, 276–279.
7 M. Lisbjerg, B. M. Jessen, B. Rasmussen, B. E. Nielsen, A. Ø. Madsen and M. Pittelkow, *Chem. Sci.*, 2014, **5**, 2647–2650.
8 M. Lisbjerg, B. E. Nielsen, B. O. Milhøj, S. P. A. Sauer and M. Pittelkow, *Org. Biomol. Chem.*, 2014, **13**, 369–373.
9 C. L. D. Gibb and B. C. Gibb, *J. Am. Chem. Soc.*, 2011, **133**, 7344–7347.
10 R. S. Carnegie, C. L. D. Gibb and B. C. Gibb, *Angew. Chem. Int. Ed.*, 2014, **53**, 11498–11500.
11 D. B. Smithrud, T. B. Wyman and F. Diederich, *J. Am. Chem. Soc.*, 1991, **113**, 5420–5426.
12 J. Y. C. Lim and P. D. Beer, *Chem. Commun.*, 2015, **51**, 3686–3688.
13 E. M. M. Del Valle, *Process Biochem.*, 2004, **39**, 1033–1046.
14 M. V. Rekharsky and Y. Inoue, *Chem. Rev.*, 1998, **98**, 1875–1918.
15 G. Crini, *Chem. Rev.*, 2014, **114**, 10940–10975.
16 M. Delbianco, P. Bharate, S. Varela-Aramburu and P. H. Seeberger, *Chem. Rev.*, 2016, **116**, 1693–1752.
17 M. E. Davis and M. E. Brewster, *Nat. Rev. Drug Discov.*, 2004, **3**, 1023–1035.
18 M. Raynal, P. Ballester, A. Vidal-Ferran and P. W. N. M. van Leeuwen, *Chem. Soc. Rev.*, 2014, **43**, 1734–1787.
19 C. Y. Ang, S. Y. Tan, X. Wang, Q. Zhang, M. Khan, L. Bai, S. T. Selvan, X. Ma, L. Zhu, K. T. Nguyen, N. S. Tan and Y. Zhao, *J. Mater. Chem. B*, 2014, **2**, 1879–1890.
20 M. Lezcano, W. Al-Soufi, M. Novo, E. Rodríguez-Núñez and J. V. Tato, *J. Agric. Food Chem.*, 2002, **50**, 108–112.
21 A. Harada and Y. Takashima, *Chem. Rec.*, 2013, **13**, 420–431.

22 H. Schlenk and D. M. Sand, *J. Am. Chem. Soc.*, 1961, **83**, 2312–2320.
23 J. Taraszewska and J. Wójcik, *Supramol. Chem.*, 1993, **2**, 337–343.
24 R. V. Chamberlain, K. Slowinska, M. Majda, P. Bühlmann, H. Aoki and Y. Umezawa, *Langmuir*, 2000, **16**, 1388–1396.
25 R. I. Gelb, L. M. Schwartz, M. Radeos and D. A. Laufer, *J. Phys. Chem.*, 1983, **87**, 3349–3354.
26 J. L. Pursell and C. J. Pursell, *J. Phys. Chem. A*, 2016, **120**, 2144–2149.
27 K. I. Assaf, M. S. Ural, F. Pan, T. Georgiev, S. Simova, K. Rissanen, D. Gabel and W. M. Nau, *Angew. Chem. Int. Ed.*, 2015, **54**, 6852–6856.
28 K. Hamaguchi and E. P. Geiduschek, *J. Am. Chem. Soc.*, 1962, **84**, 1329–1338.
29 M. E. Deary, S. M. Mousa and D. M. Davies, *J. Incl. Phenom. Macrocycl. Chem.*, 2013, **78**, 127–136.
30 M. J. Langton, S. W. Robinson, I. Marques, V. Félix and P. D. Beer, *Nat. Chem.*, 2014, **6**, 1039–1043.
31 H. T. Le, S. C. Park, C. Kang, C. W. Lim and T. W. Kim, *Org. Biomol. Chem.*, 2015, **13**, 8291–8297.
32 T. Lecourt, A. Herault, A. J. Pearce, M. Sollogoub and P. Sinaÿ, *Chem. – Eur. J.*, 2004, **10**, 2960–2971.
33 S. Xiao, M. Yang, P. Sinaÿ, Y. Blériot, M. Sollogoub and Y. Zhang, *Eur. J. Org. Chem.*, 2010, **2010**, 1510–1516.
34 E. Deunf, E. Zaborova, S. Guieu, Y. Blériot, J.-N. Verpeaux, O. Buriez, M. Sollogoub and C. Amatore, *Eur. J. Inorg. Chem.*, 2010, **2010**, 4720–4727.
35 B. Bertino-Ghera, F. Perret, B. Fenet and H. Parrot-Lopez, *J. Org. Chem.*, 2008, **73**, 7317–7326.
36 T. Lecourt, J.-M. Mallet and P. Sinaÿ, *Carbohydr. Res.*, 2003, **338**, 2417–2419.
37 T. Hauch Fenger, J. Bjerre and M. Bols, *ChemBioChem*, 2009, **10**, 2494–2503.
38 M. J. Langton, I. Marques, S. W. Robinson, V. Félix and P. D. Beer, *Chem. – Eur. J.*, 2016, **22**, 185–192.
39 M. J. Hynes, *J. Chem. Soc. Dalton Trans.*, 1993, 311–312.
40 Y. Marcus, *J. Chem. Soc. Faraday Trans.*, 1991, **87**, 2995–2999.
41 A. Bianchi, K. Bowman-James and E. Garcia-Espana, *Supramolecular Chemistry of Anions*, Wiley-VCH, New York, 1997.
42 E. A. Katayev, G. V. Kolesnikov and J. L. Sessler, *Chem. Soc. Rev.*, 2009, **38**, 1572–1586.
43 R. Amano, A. Ando, T. Hiraki, H. Mori, H. Matsuda and K. Hisada, *Radioisotopes*, 1990, **39**, 585–586.
44 N. N. Popova, I. G. Tananaev, S. I. Rovnyi and B. F. Myasoedov, *Russ. Chem. Rev.*, 2003, **72**, 101–121.
45 B. M. Rambo and J. L. Sessler, *Chem. – Eur. J.*, 2011, **17**, 4946–4959.
46 R. Alberto, G. Bergamaschi, H. Braband, T. Fox and V. Amendola, *Angew. Chem. Int. Ed.*, 2012, **51**, 9772–9776.
47 V. Amendola, G. Bergamaschi, M. Boiocchi, R. Alberto and H. Braband, *Chem. Sci.*, 2014, **5**, 1820–1826.
48 J. A. Gawenis, K. T. Holman, J. L. Atwood and S. S. Jurisson, *Inorg. Chem.*, 2002, **41**, 6028–6031.
49 E. A. Katayev, N. V. Boev, V. N. Khrustalev, Y. A. Ustynyuk, I. G. Tananaev and J. L. Sessler, *J. Org. Chem.*, 2007, **72**, 2886–2896.
50 M. Saeki, Y. Sasaki, A. Nakai, A. Ohashi, D. Banerjee, A. C. Scheinost and H. Foerstendorf, *Inorg. Chem.*, 2012, **51**, 5814–5821.
51 E. A. Kataev, P. Pantos, E. Karnas, G. V. Kolesnikov, I. G. Tananaev, V. M. Lynch and J. L. Sessler, *Supramol. Chem.*, 2015, **27**, 346–356.
52 T. Lecourt, J.-M. Mallet and P. Sinaÿ, *Comptes Rendus Chim.*, 2003, **6**, 87–90.
53 L. Kumprecht, M. Buděšínský, P. Bouř and T. Kraus, *New J. Chem.*, 2010, **34**, 2254–2260.
54 F. Brégier, J. Lavalle and J.-C. Chambron, *Eur. J. Org. Chem.*, 2013, **2013**, 2666–2671.

Chapter Five

Fluoride recognition using a [2]rotaxane containing a Lewis acidic triarylborane motif

5.1 Introduction

The design of receptors which can selectively bind and sense fluoride has been highlighted as an important research goal owing to the numerous detrimental health implications associated with a chronic over exposure to this anion (Section 1.1.1).[1] However, the high basicity of fluoride in organic solvents, along with its high hydration enthalpy (ΔH^o = -504 kJ mol^{-1}) means that hydrogen bonding receptors are relatively ineffective for this purpose.[2–4] To this end, hosts containing Lewis acidic triarylborane groups have attracted much attention due to the strong dative B-F bonds they can form.[5] In particular, receptors containing the dimesitylborane motif have been widely investigated, as the steric protection the mesityl (Mes) substituents provide to the boron centre disfavours the coordination of large anions, greatly enhancing fluoride selectivity.[3,6–17] Such hosts are typically stable to both air and moisture, unlike many other borane derivatives. Also, the third substituent attached to the boron centre can be tailored to provide additional binding interactions, which invariably leads to a large cooperative enhancement in the strength of fluoride binding relative to the parent trimesitylborane (**Figure 5.1a**).[6] Another attractive feature of triarylboranes is their ability to act as anion sensors. The unoccupied p_π-orbital of the boron atom makes a large contribution to the LUMO of these systems, and hence coordination of fluoride can result in a substantial change to their photophysical properties allowing colorimetric or fluorescent detection to occur.[18]

A large variety of receptors of this nature have been reported, such as Gabbaï's bidentate Lewis acidic system (**Figure 5.1b**)[6] and hosts containing pendant cationic ammonium (**Figure 5.1c**)[7] and phosphonium groups (**Figure 5.1d**).[11] Impressively, the receptor containing the phosphonium functionality is capable of recognising fluoride even in pure water.

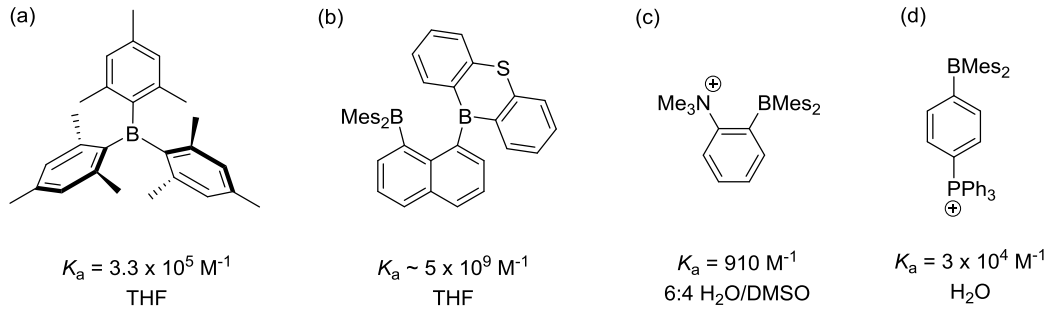

Figure 5.1: Borane-based fluoride receptors and their 1:1 association constants: (a) Trimesitylborane, (b) bidentate receptor,[6] (c) ammonium borane receptor[7] and (d) phosphonium borane receptor[11]

A handful of receptors that utilise a combination of Lewis acidic and hydrogen bonding interactions to bind fluoride have also been described. These include Gabbaï's trifluoroacetamide containing host[19] and Lee's phenol- and indole-based systems (**Figure 5.2**).[20]

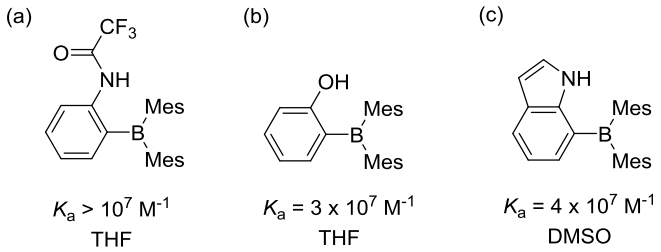

Figure 5.2: Hybrid borane/hydrogen bond donor receptors for fluoride and their 1:1 association constants: (a) Gabbaï's trifluoroacetamide-containing receptor,[19] (b) Lee's phenol-based host and (c) Lee's indole-based host.[20]

5.1.1 Chapter aims

This chapter describes the design and preparation of the first interlocked anion host to incorporate Lewis acidic borane functionality. Such a system is designed to selectively recognise fluoride and the target rotaxane structure was adapted from that of a [2]rotaxane previously reported by Beer and co-workers (**Figure 5.3a**), which displayed selectivity for the chloride anion.[21] The desired borane functionality was introduced through replacement of one of the rotaxane's terphenyl stoppers with a dimesitylborane motif (**Figure 5.3b**). Investigations into the chloride and fluoride binding properties of the rotaxane were undertaken using multinuclear NMR experiments and UV/vis spectroscopy.

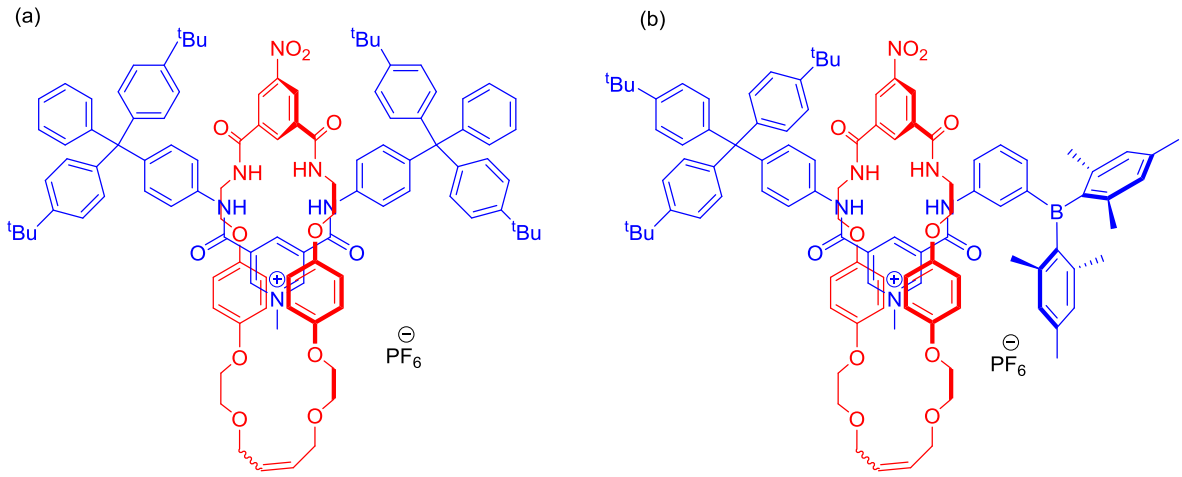

Figure 5.3: (a) Beer's chloride selective [2]rotaxane[21] and (b) target [2]rotaxane containing a dimesitylborane stopper group.

5.2 Synthesis

5.2.1 Synthesis of axle component

To prepare the target axle component, a dimesitylborane-functionalised aniline stopper derivative was initially synthesised using a literature procedure (**Scheme 5.1**).[22] Commercially available 3-bromoaniline was reacted with three equivalents of benzyl bromide in the presence of potassium carbonate to give the protected amine **75**. This was reacted with *n*-BuLi to give an organolithium intermediate, which was quenched with $FBMes_2$ (provided by Dr. Remi Tirfoin) to give the triarylborane derivative **76**. Deprotection of the amine functionality was achieved by Pd/C catalysed hydrogenolysis to afford aniline-stopper **77** in a 75% yield.

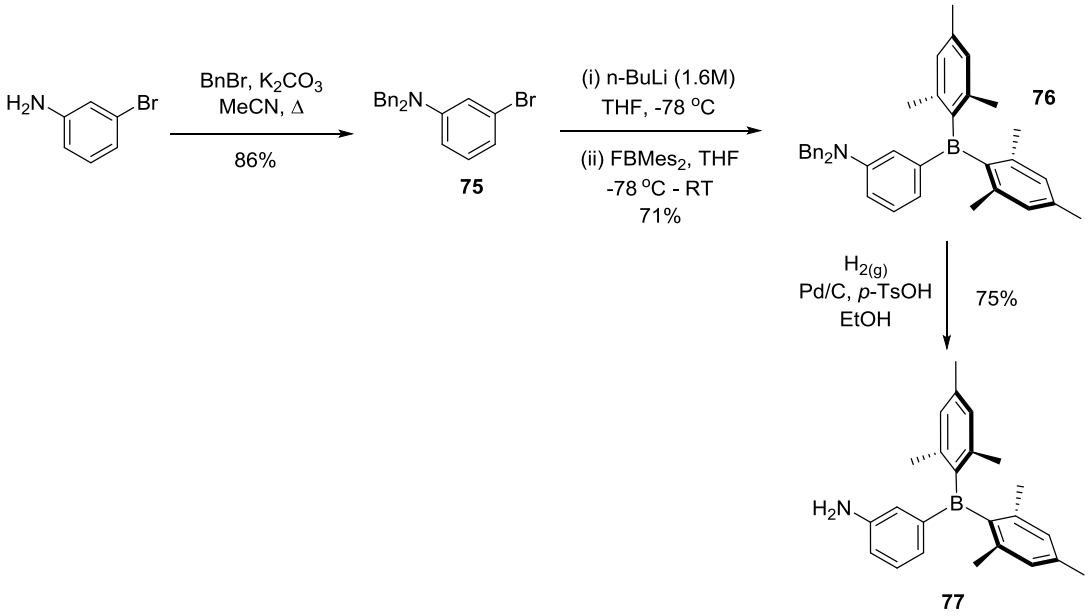

Scheme 5.1: Synthesis of dimesitylborane-functionalised stopper **77**[22]

Crystals of **76** suitable for X-ray structural analysis were formed by cooling a hexane/CH_2Cl_2 solution of the compound to -20 °C. Analysis of the structure (**Figure 5.4**), solved by Dr. Asha Brown, revealed that the dimesitylborane unit has a span of approximately 10.7 Å, which is comparable to that of the terphenyl stopper derivatives used in the synthesis of the rotaxanes in Chapter 2 (~ 11.8 Å). This, suggested that the dimesitylborane functionality is sterically bulky enough to act as a stopper group in a [2]rotaxane containing the isophthalamide macrocycle component shown in **Figure 5.3**.

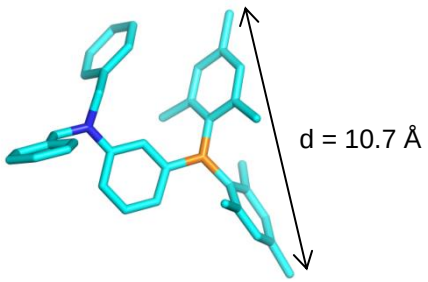

Figure 5.4: Solid-state structure of **76**

A mono-terphenyl-stoppered pyridine derivative **81** was prepared, using an adapted literature procedure (**Scheme 5.2**).[23] Commercially available 3,5-pyridine dicarboxylic acid was converted to dimethyl ester **78** by treatment with concentrated sulfuric acid in methanol.

Mono-ester hydrolysis of **78** *via* reaction with KOH afforded acid **79**, which was converted to the corresponding acid chloride, using oxalyl chloride, and reacted with terphenyl amine **15**[24] in the presence of triethylamine to give **80** in a 76% yield. Hydrolysis of the remaining ester group, under basic conditions, afforded the acid **81**.

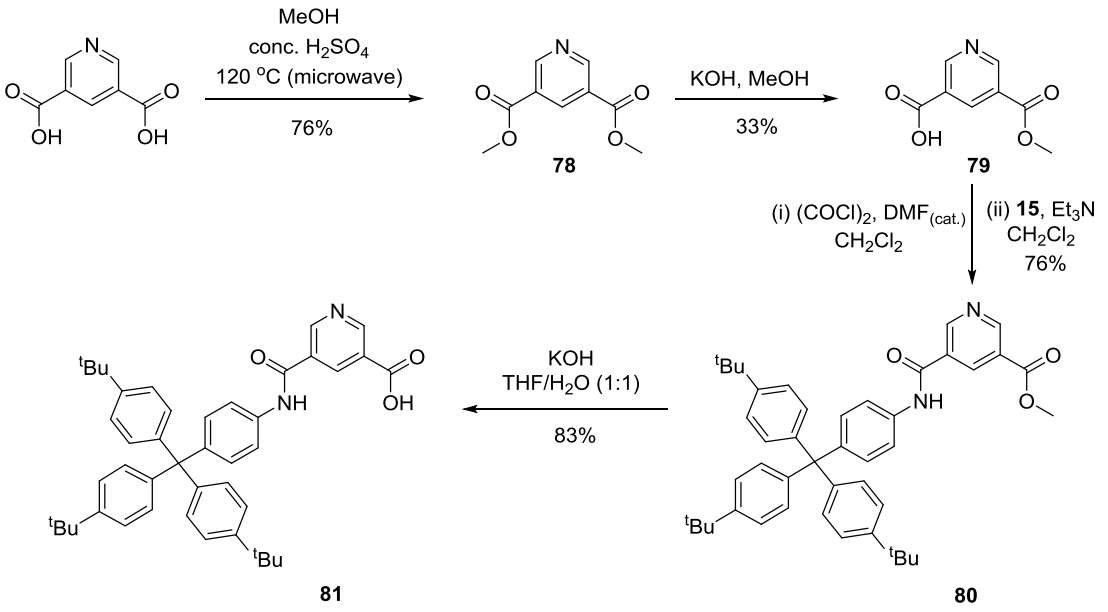

Scheme 5.2: Synthesis of mono-stoppered pyridine derivative **81**[23]

Acid **81** was reacted with oxalyl chloride to give the acid chloride intermediate, which was condensed with the dimesitylborane-functionalised aniline stopper **77** in the presence of trimethylamine. Purification of the crude reaction mixture required the use of preparative TLC, with the pure axle precursor **82** isolated in a modest yield of 39%. Methylation, using methyl iodide, followed by anion exchange, by washing with aqueous NH_4Cl, gave the target axle **83·Cl** in a 66% yield (**Scheme 5.3**).

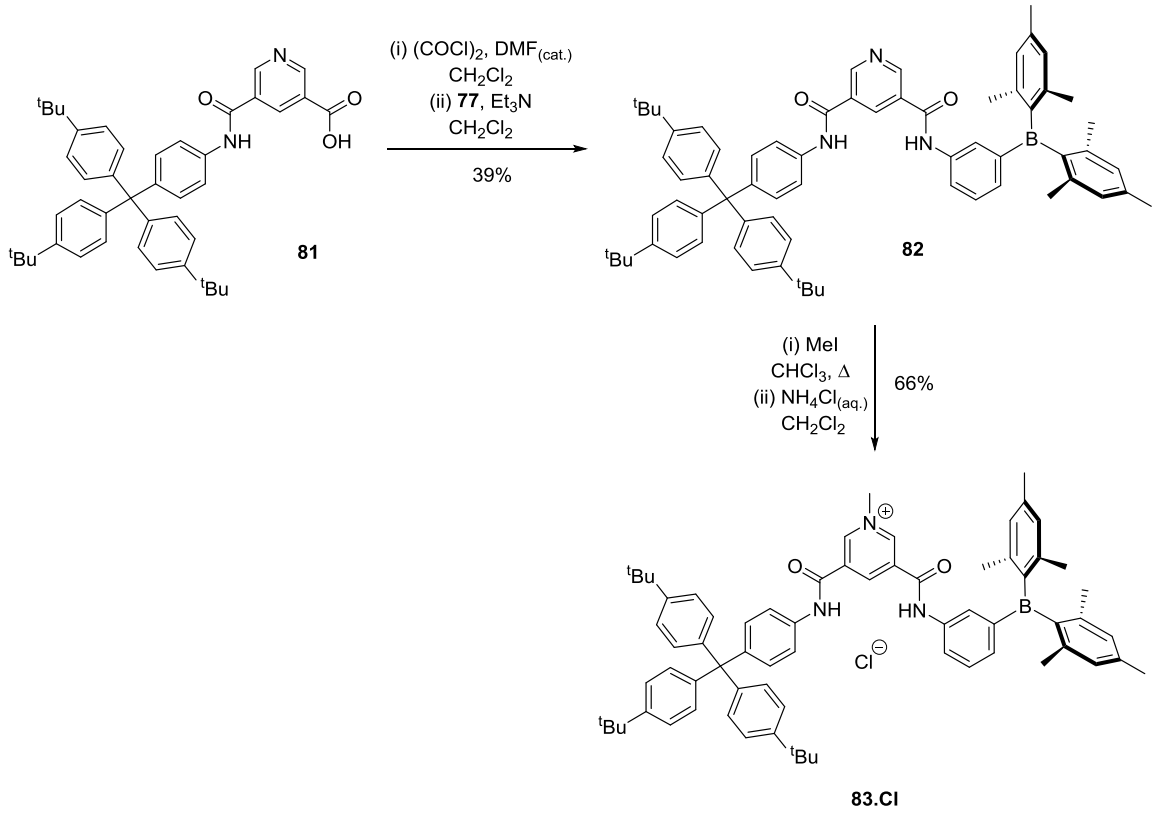

Scheme 5.3: Synthesis of axle component **83·Cl**

5.2.2 Synthesis of rotaxane

Rotaxane formation was achieved using a chloride-templated 'clipping' procedure (**Scheme 5.4**). An equimolar mixture of axle **83·Cl** and macrocycle precursor **25** was prepared in dry CH_2Cl_2, with the subsequent addition of Grubbs' second generation RCM catalyst affording the interlocked product. The crude material was purified using a combination of preparative TLC and size exclusion chromatography, following which, anion exchange gave the rotaxane **84·PF$_6$** in an isolated yield of 51%. The product was characterised by ^{1}H, ^{13}C, ^{19}F and ^{31}P NMR spectroscopy and high resolution ESI mass spectrometry.

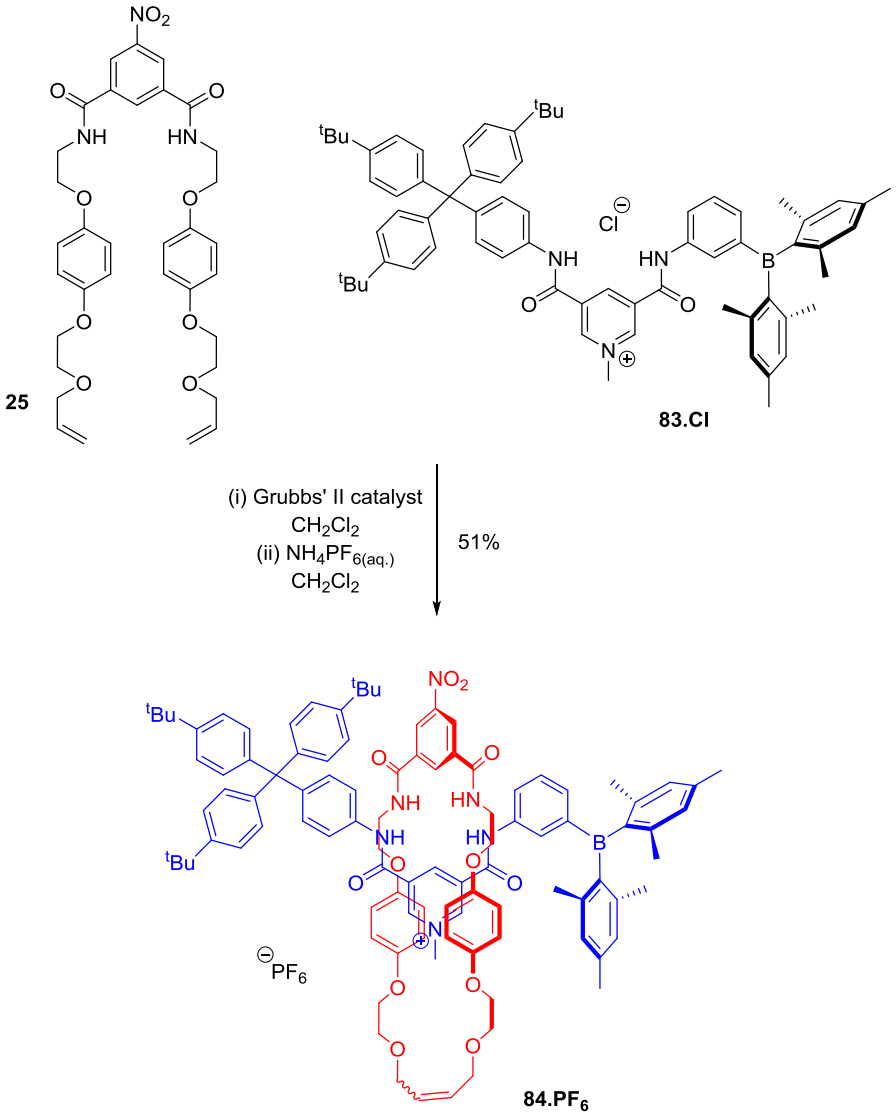

Scheme 5.4: Synthesis of rotaxane **84·PF$_6$**

Evidence for the formation of the interlocked product was provided by comparison of the ^{1}H NMR spectrum of **84·Cl** with those of axle **83·Cl** and macrocycle precursor **25** (**Figure 5.5**). In the spectrum of the rotaxane the signals of the hydroquinone protons of the macrocycle component (*4* and *5*) are shifted upfield and split due to the π-π aromatic donor-acceptor interactions formed with the pyridinium axle component. Substantial downfield shifts of the aromatic proton *2* and the amide protons *3* of the macrocycle are also observed, indicating that these protons participate in HB interactions with the templating chloride anion. No shifts of the mesityl aromatic protons *j* of the axle are seen, confirming that the borane unit is not involved in an anion binding interaction.

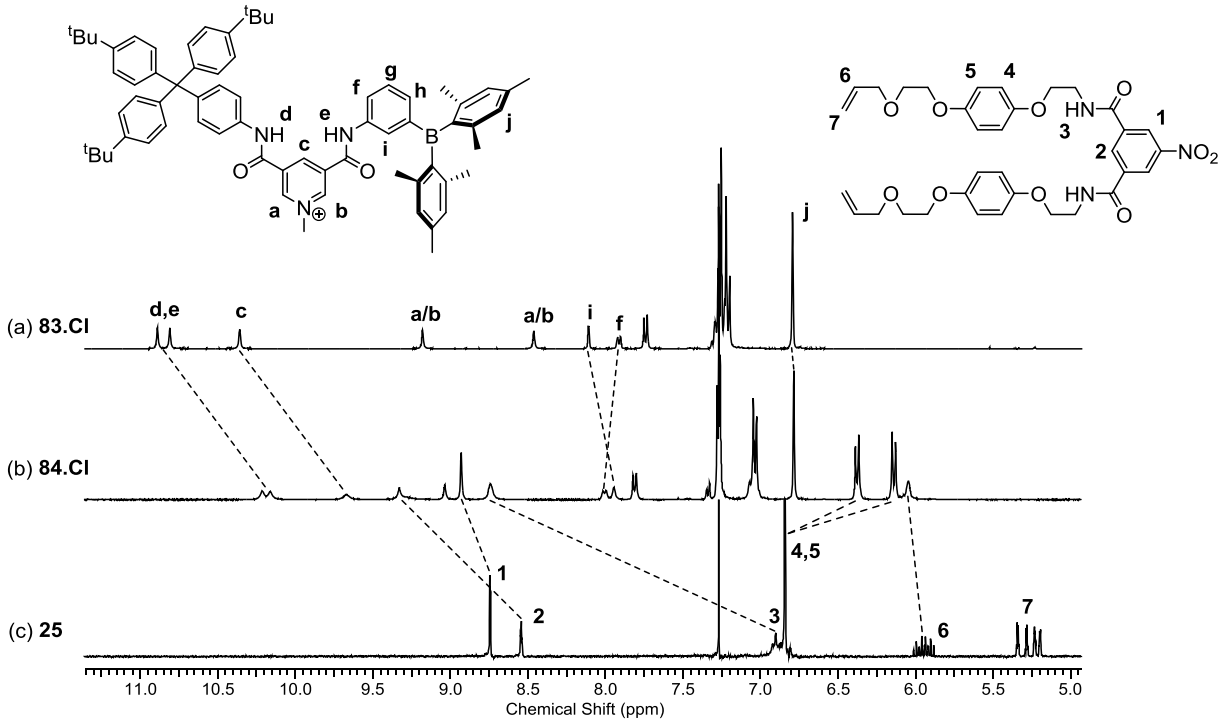

Figure 5.5: ^{1}H NMR spectra of: (a) axle **83·Cl**, (b) rotaxane **84·Cl** and (c) macrocycle precursor **25** ($CDCl_3$, 298 K)

A 2D ^{1}H-^{1}H ROESY NMR spectrum of **84·PF$_6$** was used to verify that the components of the rotaxane remained interlocked upon anion exchange (**Figure 5.6**). Through-space interactions were detected between hydroquinone protons *4* and *5* of the macrocycle and protons *a*, *b* and *c* of the axle component, along with an interaction between amide protons *3* and pyridinium proton *c*.

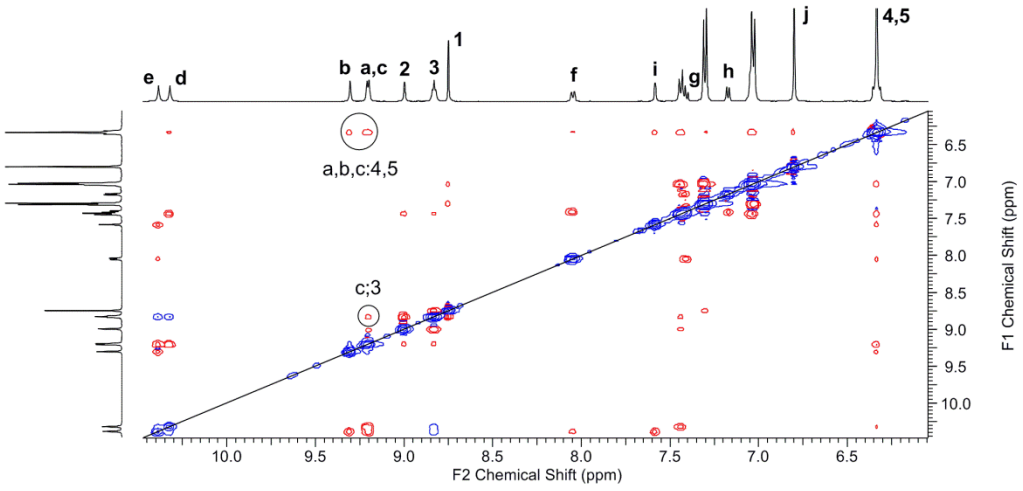

Figure 5.6: Truncated ^{1}H-^{1}H ROESY NMR spectrum of rotaxane **84·PF$_6$** (d_6-DMSO, 298 K, 500 MHz)

5.3 Fluoride binding properties of axle 83·PF_6

Before investigating the anion recognition properties of rotaxane **84·PF_6**, preliminary fluoride binding studies were performed with the hexafluorophosphate salt of the free axle component **83·PF_6** using a variety of spectroscopic techniques. It was anticipated that in the absence of the macrocycle component, the anion would exclusively interact with the borane group.

5.3.1 NMR studies

One equivalent of TBA fluoride trihydrate was added to a solution of **83·PF_6** in d_6-DMSO, with ^{1}H, ^{11}B and ^{19}F NMR spectra recorded before and after the addition. Comparison of the spectra revealed characteristic changes corresponding to the formation of the fluoroborate adduct **83·F** (**Scheme 5.5**).

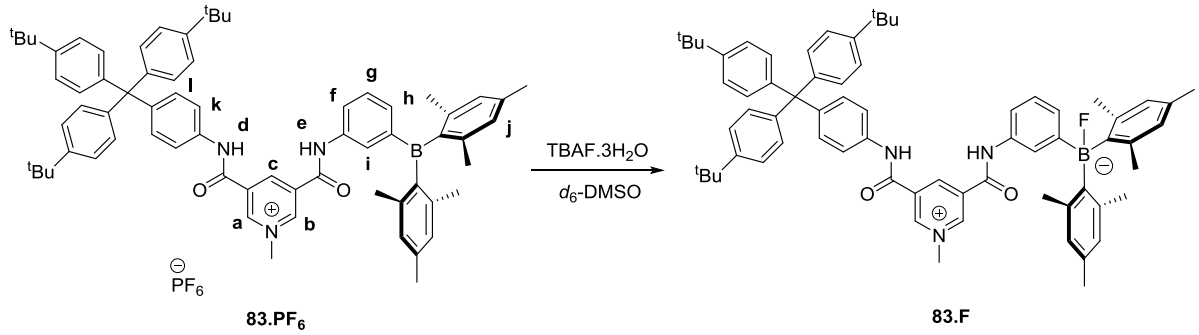

Scheme 5.5: Formation of fluoride adduct of **83·F**

In the ^{1}H NMR spectra, a substantial upfield shift of the mesityl aromatic protons *j* (from 6.84 ppm to 6.38 ppm) was observed (**Figure 5.7**), whilst in the ^{11}B NMR spectra, the broad signal of the triarylborane unit, at approximately 75 ppm, disappeared and a new, sharper resonance appeared at 4 ppm. A large perturbation of the ^{19}F NMR signal of free fluoride, at approximately -120 ppm, was also seen, with the signal corresponding to **83·F** observed at -174 ppm.

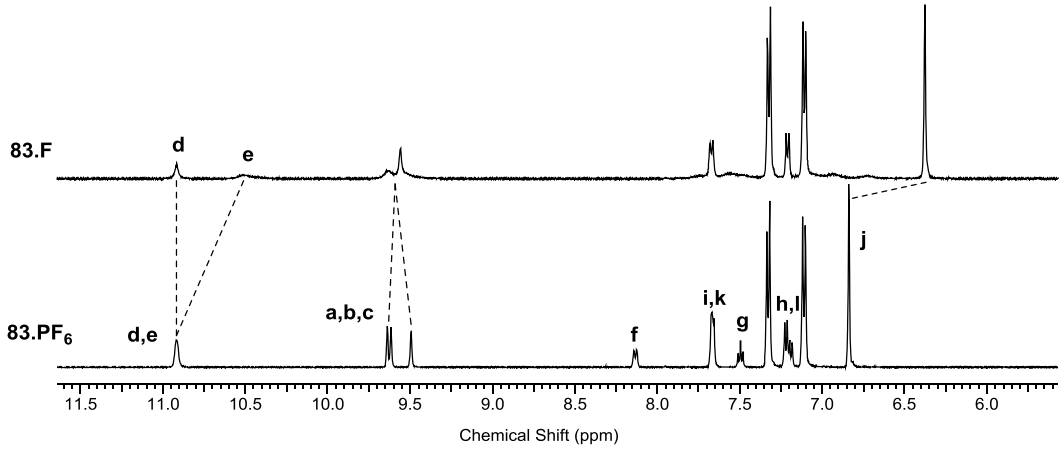

Figure 5.7: Truncated ^{1}H NMR spectra of axle **83·PF$_6$** before and after the addition of one equivalent of TBAF·3H$_2$O (d_6-DMSO, 298 K, 500 MHz)

Interestingly, conversion of **83·PF$_6$** to **83·F** was also accompanied by a naked-eye detectable colour change of the solution, from pale yellow to dark orange. A similar observation was made by Gabbaï and co-workers, who conducted fluoride binding studies with an analogous receptor containing similar functionality.[25] They ascribed this observation to an intramolecular charge-transfer interaction between the electron-rich fluoroborate group and the electron-poor pyridinium motif of their receptor. The presence of this interaction may provide an explanation for the broadening of the aromatic proton resonances *a-c* and *f-i* seen in the ^{1}H NMR spectrum of **83·F**. However, it is also possible that this is a result an aggregation process.

5.3.2 UV/vis studies

To further probe the fluoride binding properties of **83·PF$_6$**, as well as the origin of the observed colour change, a UV/visible titration experiment was performed in THF (**Figure 5.8**). The addition of up to one equivalent of TBA fluoride trihydrate resulted in a decrease in the intensity of the absorption band associated with the triarylborane unit at 320 nm, indicating the occupation of the vacant p_π-orbital of the boron atom. The formation of new absorption features, with maxima of 295 nm and 370 nm, was also observed, with the lower energy band presumably related to the charge-transfer interaction discussed above and the

cause of the colour change detected. The addition of the anion in excess of one equivalent led to spectral changes associated with a second equilibrium process, with a general decrease of the receptor's absorption observed. Owing to the highly basic nature of the fluoride anion in non-protic media, this was assumed to involve the deprotonation of **83·F**.

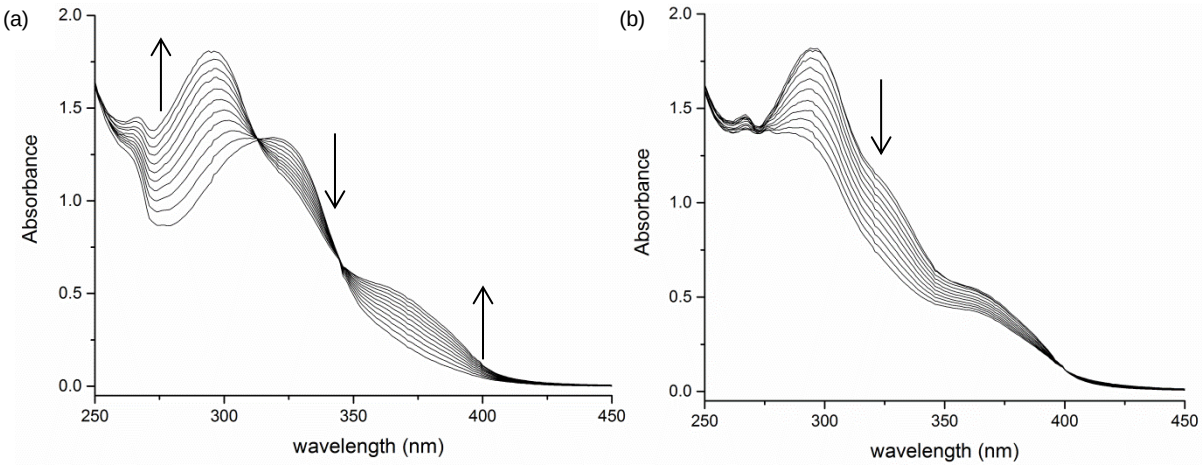

Figure 5.8: UV/visible absorption spectra of **83·PF$_6$** (50 μM concentration) upon addition of (a) 0-1 equivalent of TBAF·3H$_2$O and (b) 1-2 equivalents of TBAF·3H$_2$O (THF, 298 K)

Surprisingly, these spectral changes were still observed when the titration was repeated in THF/water mixtures (up to 20% water), in which the basicity of the anion is substantially reduced owing to competitive solvation effects. This suggests that the second process may involve the formation of a 2:1 (anion:host) complex rather than deprotonation. Despite this, attempts to fit the titration data were unsuccessful and hence no association constant values could be determined for the binding processes.

5.4 Anion binding properties of rotaxane 84·PF$_6$

5.4.1 NMR studies

The fluoride binding properties of **84·PF$_6$** were initially investigated using a ^{1}H NMR titration experiment, in which increasing equivalents of TBA fluoride trihydrate were added to a solution of the host in d_6-DMSO (**Figure 5.9**). Anion association was found to occur in slow exchange on the NMR timescale, with two sets of resonances observed in the spectra of the host containing less than one equivalent of the anion. Following the addition of one

equivalent, saturation was observed and only one set of signals, corresponding to the complexed species, remained. Based on the observation of strong 1:1 stoichiometric binding at the 2 mM concentration of the experiment, the lower limit of the association constant for complex formation can be estimated to be $\geq 10^4$ M^{-1}. Addition of fluoride in excess of one equivalent caused the resonances of **84·F** to become progressively broader, suggesting that the rotaxane was decomposing, presumably *via* a deprotonation pathway.

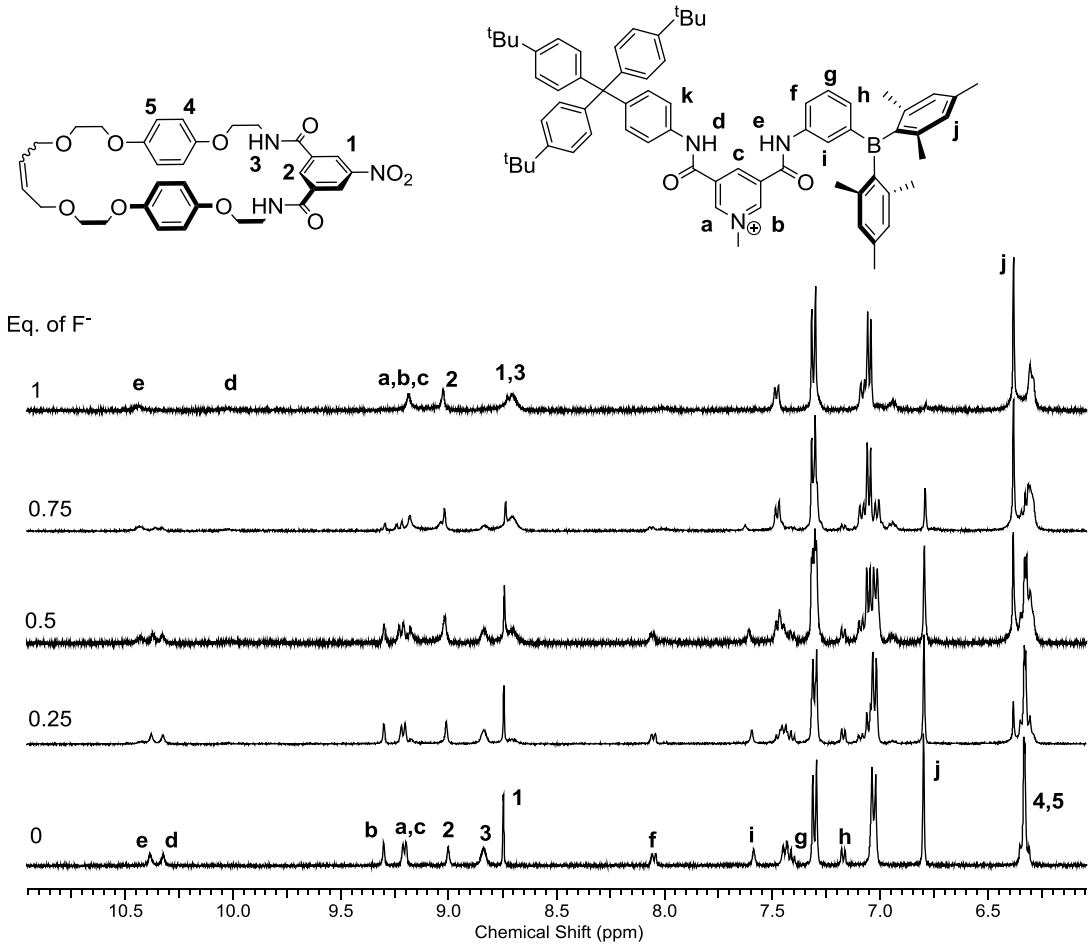

Figure 5.9: Truncated ^{1}H NMR spectra of **84·PF$_6$** upon addition of increasing equivalents of TBAF·3H$_2$O (d_6-DMSO, 298 K, 500 MHz)

The assignment of the proton resonances in the spectrum of the fluoride adduct **84·F** required the use of 2D ^{1}H-^{1}H ROESY NMR, with the addition of a drop of D_2O enabling assignment of the macrocycle amide protons *3*. Upon formation of **84·F**, the mesityl aromatic protons *j* shifted upfield from 6.80 ppm to 6.38 ppm, confirming that a fluoroborate species had

formed. Macrocycle amide protons *3* also underwent a modest upfield shift ($\Delta\delta$ = 0.05 ppm), implying that they may be involved in a HB interaction with the anion.

Evidence of an intramolecular charge-transfer interaction within the axle component of **84·F** was also observed, with addition of fluoride causing a noticeable colour change of the solution from yellow to yellow-orange. However, this was less pronounced than the colour change seen with the free axle **83·PF$_6$**. Substantial broadening of the resonances of aromatic protons *a-c* and *f-i* was also seen again.

Surprisingly, inspection of the $^{19}F\{^1H\}$ NMR spectrum of **84·F** revealed the presence of two fluorine containing species, with chemical shifts of -170 ppm and -174 ppm. Integration of their respective signals estimated an approximate 6:4 ratio of the two species. In a variable temperature ^{19}F NMR experiment in d_6-DMSO, the resonances were found to coalesce at approximately 75 ^oC (**Figure 5.10**), suggesting that **84·F** adopts two conformations, presumably due to a restricted rotation within the axle component of the rotaxane.

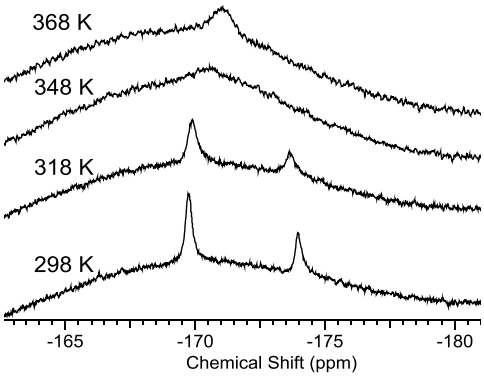

Figure 5.10: Truncated $^{19}F\{^1H\}$ NMR spectra of **84·F** at different temperatures (d_6-DMSO, 470 MHz)

The chemical shift of the minor species is similar to that of the fluoride-adduct of the free axle component **83·F**, whilst the shift of the major species is further downfield, implying that the fluoride is involved in an additional binding interaction.[19,20] Therefore, it is possible that the two conformations correspond to a cooperative and a non-cooperative fluoride binding mode (**Figure 5.11**), with the anion forming an HB interaction with the macrocycle amide protons *3* in the cooperative mode.

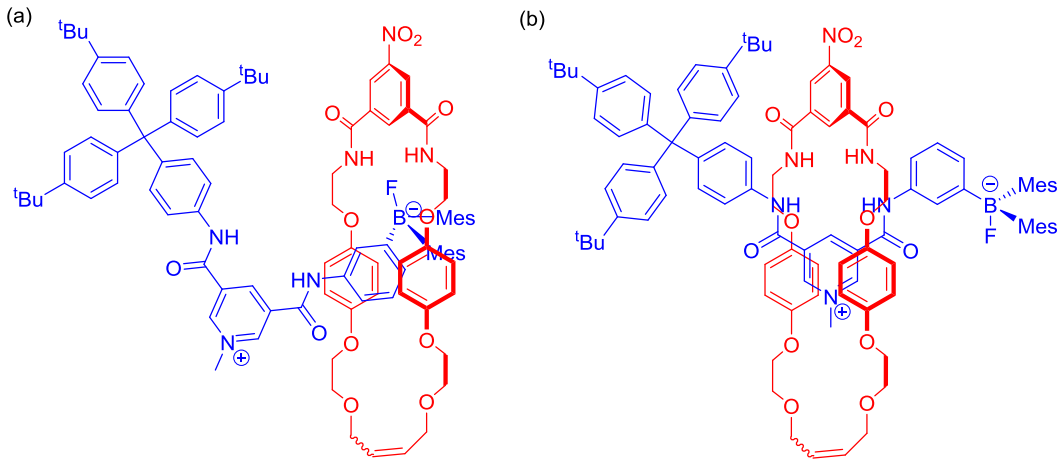

Figure 5.11: Possible conformations of **84·F**: (a) cooperative binding mode and (b) non-cooperative binding mode

As seen in **Figure 5.9** the ^{1}H NMR signals of the two conformations of **84·F** are not clearly resolved, which indicates that they are in the fast exchange limit. A variable temperature ^{1}H NMR experiment showed that the resonances associated with the macrocycle component significantly sharpened as temperature increased, as would be expected for a fluxional system (**Figure 5.12**).

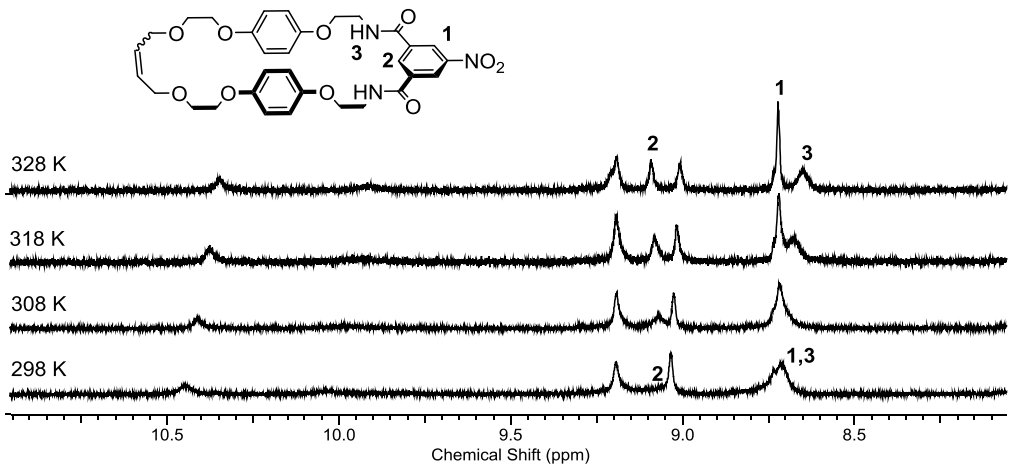

Figure 5.12: Truncated ^{1}H NMR spectra of **84·F** at different temperatures (d_6-DMSO, 500 MHz)

The chloride binding properties of **84·PF$_6$** were also investigated using a ^{1}H NMR titration experiment in which up to 10 equivalents of TBA chloride were added to a d_6-DMSO solution of the rotaxane. In this case, anion association was found to be in fast exchange on the NMR timescale. Large downfield perturbations of macrocycle proton *2* ($\Delta\delta$ = 0.40 ppm) and axle

proton *c* ($\Delta\delta$ = 0.32 ppm) were observed, indicating that the anion is encapsulated within the central HB binding pocket of the host. Surprisingly, amide protons *3*, *d* and *e* did not shift substantially during the titration, which may explain the small shift of the macrocycle amide protons seen on formation of **84·F**. Also, the mesityl protons *j* underwent a modest upfield shift ($\Delta\delta$ = 0.07 ppm), however this is most likely due to an inductive effect rather than association of the halide anion to the borane group. In contrast to the fluoride titration, no noticeable colour change was observed, which provides further evidence that the borane unit is not involved in the binding process.

WinEQNMR analysis[26] of the titration data, monitoring the shift of macrocycle proton *2* (**Figure 5.13**), afforded a 1:1 stoichiometric association constant of 1640(95) M^{-1}. This is at least an order of magnitude weaker than the fluoride association constant, confirming that the rotaxane displays an impressive selectivity for the smaller halide, as anticipated.

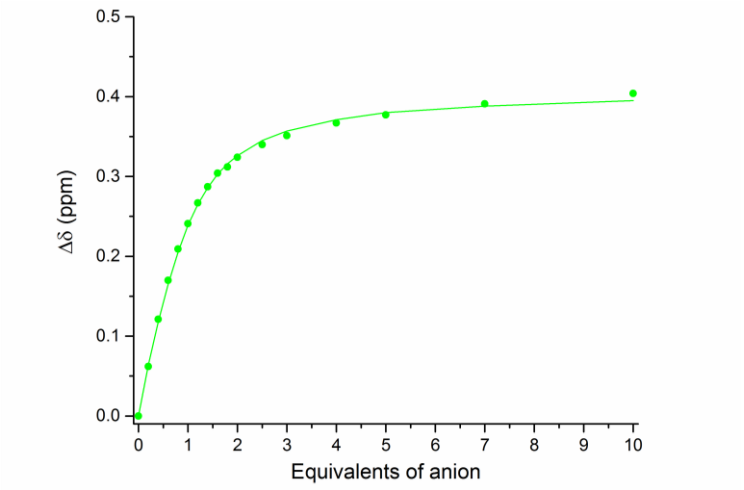

Figure 5.13: Experimental titration data (points) and calculated 1:1 binding isotherm (line) for the addition of 10 equivalents of TBA chloride to **84·PF$_6$**, monitoring macrocycle proton *2* (d_6-DMSO, 298 K, 400 MHz).

5.5.2 UV/vis studies

The fluoride and chloride binding properties of **84·PF$_6$** were further investigated using UV/vis spectroscopic titration experiments in THF. The changes observed in the fluoride titration were very similar to those seen in the corresponding experiment with axle **83·PF$_6$**, but less pronounced (**Figure 5.14**). Between zero and one equivalent the intensity of the absorption band at 323 nm decreased slightly and new features with maxima at approximately 295 nm and 375 nm were formed. The addition of the anion in excess of one equivalent resulted in a general decrease in the absorption of the rotaxane, which is again presumably a consequence of either deprotonation of **84·F** or the formation of a 2:1 (anion:host) complex. As with the axle **83.PF$_6$**, the complexity of the data prevented the determination of an association constant for the binding process.

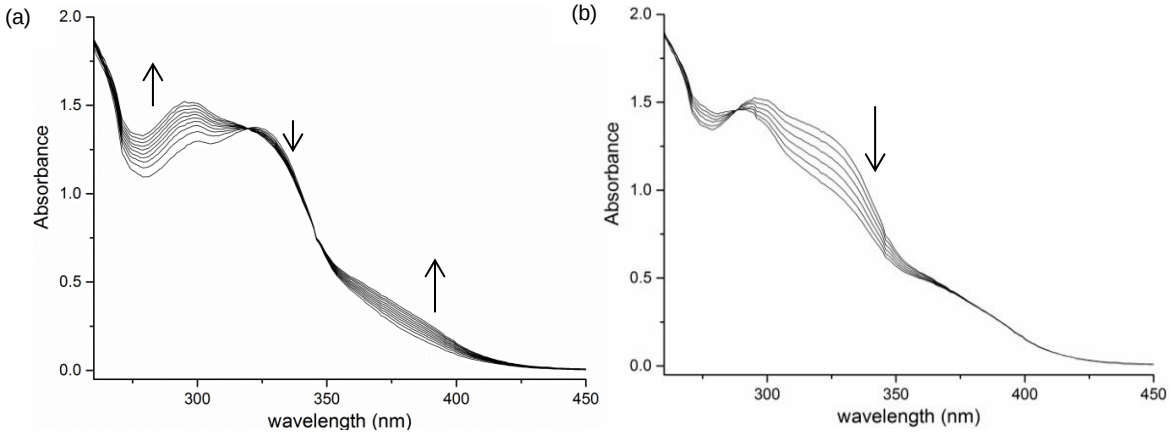

Figure 5.14: UV/visible absorption spectra of **84·PF$_6$** (50 μM concentration) upon addition of (a) up to one equivalent of TBAF·3H$_2$O and (b) up to 2 equivalents of TBAF·3H$_2$O (THF, 298 K)

Addition of up to two equivalents of TBA chloride to **84·PF$_6$** led to no observable changes in the absorption spectra, confirming that the halide anion forms minimal binding interactions with the boron centre.

5.6 Conclusion and future work

The synthesis of the first example of an interlocked host to incorporate a Lewis acidic triarylborane motif has been achieved. ^{1}H NMR titration experiments revealed that the [2]rotaxane **84·PF$_6$** bound fluoride substantially more strongly than chloride, with the observed selectivity related to the alternate binding modes of the two anions. ^{19}F NMR experiments showed that the fluoride adduct of the rotaxane **84·F** adopted two conformations, which were assigned as a cooperative and non-cooperative anion binding mode.

Axle **83·PF$_6$** and rotaxane **84·PF$_6$** were also found to act as colorimetric fluoride sensors, with UV/vis spectroscopy showing this was due to the formation of an intramolecular charge-transfer interaction between the electron-rich fluoroborate group and the electron-deficient pyridinium unit.

Future work will involve further investigations into the nature of the fluoride binding mode of **84·PF$_6$**. A solid-state structure of **84·F** would be required to definitively confirm the presence of the cooperative binding mode proposed. Furthermore, the binding properties of **84·PF$_6$** with other small anions, such as cyanide and azide, which have also been shown to form complexes with triarylboranes,[27,28] would be of interest.

5.7 References

1 J. R. Carton, *Fluoride*, 2007, **39**, 163–172.
2 M. Boiocchi, L. Del Boca, D. E. Gómez, L. Fabbrizzi, M. Licchelli and E. Monzani, *J. Am. Chem. Soc.*, 2004, **126**, 16507–16514.
3 T. W. Hudnall, C.-W. Chiu and F. P. Gabbaï, *Acc. Chem. Res.*, 2009, **42**, 388–397.
4 N. H. Evans and P. D. Beer, *Angew. Chem. Int. Ed.*, 2014, **53**, 11716–11754.
5 C. R. Wade, A. E. J. Broomsgrove, S. Aldridge and F. P. Gabbaï, *Chem. Rev.*, 2010, **110**, 3958–3984.
6 S. Solé and F. P. Gabbaï, *Chem. Commun.*, 2004, 1284–1285.
7 T. W. Hudnall and F. P. Gabbaï, *J. Am. Chem. Soc.*, 2007, **129**, 11978–11986.
8 M. H. Lee, T. Agou, J. Kobayashi, T. Kawashima and F. P. Gabbaï, *Chem. Commun.*, 2007, 1133–1135.
9 T. W. Hudnall, Y.-M. Kim, M. W. P. Bebbington, D. Bourissou and F. P. Gabbaï, *J. Am. Chem. Soc.*, 2008, **130**, 10890–10891.
10 A. Kawachi, A. Tani, J. Shimada and Y. Yamamoto, *J. Am. Chem. Soc.*, 2008, **130**, 4222–4223.
11 Y. Kim and F. P. Gabbaï, *J. Am. Chem. Soc.*, 2009, **131**, 3363–3369.

12 H. Zhao and F. P. Gabbaï, *Nat. Chem.*, 2010, **2**, 984–990.
13 C. R. Wade and F. P. Gabbaï, *Inorg. Chem.*, 2010, **49**, 714–720.
14 A. E. J. Broomsgrove, D. A. Addy, A. Di Paolo, I. R. Morgan, C. Bresner, V. Chislett, I. A. Fallis, A. L. Thompson, D. Vidovic and S. Aldridge, *Inorg. Chem.*, 2010, **49**, 157–173.
15 C. R. Wade and F. P. Gabbaï, *Organometallics*, 2011, **30**, 4479–4481.
16 H. Zhao and F. P. Gabbaï, *Organometallics*, 2012, **31**, 2327–2335.
17 K. C. Song, K. M. Lee, N. V. Nghia, W. Y. Sung, Y. Do and M. H. Lee, *Organometallics*, 2013, **32**, 817–823.
18 S. Yamaguchi, S. Akiyama and K. Tamao, *J. Organomet. Chem.*, 2002, **652**, 3–9.
19 T. W. Hudnall, M. Melaïmi and F. P. Gabbaï, *Org. Lett.*, 2006, **8**, 2747–2749.
20 W. Y. Sung, J. Lee and M. H. Lee, *J. Organomet. Chem.*, 2015, **776**, 143–148.
21 M. R. Sambrook, P. D. Beer, M. D. Lankshear, R. F. Ludlow and J. A. Wisner, *Org. Biomol. Chem.*, 2006, **4**, 1529–1538.
22 Z. M. Hudson, C. Sun, M. G. Helander, Y.-L. Chang, Z.-H. Lu and S. Wang, *J. Am. Chem. Soc.*, 2012, **134**, 13930–13933.
23 L. M. Hancock and P. D. Beer, *Chem. Commun.*, 2011, **47**, 6012–6014.
24 H. W. Gibson, S. H. Lee, P. T. Engen, P. Lecavalier, J. Sze, Y. X. Shen and M. Bheda, *J. Org. Chem.*, 1993, **58**, 3748–3756.
25 C. R. Wade and F. P. Gabbaï, *Dalton Trans.*, 2009, 9169–9175.
26 M. J. Hynes, *J. Chem. Soc. Dalton Trans.*, 1993, 311–312.
27 H. Zhao, L. A. Leamer and F. P. Gabbaï, *Dalton Trans.*, 2013, **42**, 8164–8178.
28 C. R. Wade and F. P. Gabbaï, *Z. Für Naturforschung B*, 2015, **69**, 1199–1205.

Chapter Six

Experimental

6.1 General remarks

6.1.1 Solvents and reagents

All commercial solvents and reagents were used as purchased, unless otherwise stated. Anhydrous solvents were degassed with N_2 and dried by passing them through an MBraun-800 column. Water was distilled and microfiltered using a Milli-Q Millipore machine. Triethylamine was distilled and stored over KOH pellets. Tetrabutylammonium (TBA) salts, Grubbs' second generation catalyst and $[Cu(MeCN)_4][PF_6]$ were stored in a desiccator with P_2O_5. Chromatography was undertaken using silica gel (particle size: 40-63 μm) or preparative TLC plates (20 x 20 cm, 1 cm silica thickness). Size exclusion chromatography was undertaken using Biobeads SX-1. Amberlite® anion exchange columns were prepared/loaded by washing the resin with H_2O, 1M $NaOH_{(aq.)}$, H_2O, 10% wt. $NH_4X_{(aq.)}$ (where X is the required counter-anion), H_2O and finally the solvent system used in the exchange. TBTA was prepared by Dr. Nick White and Dr. Asha Brown.[1] Compound **45·Cl** was made by Sean Robinson,[2] compound **55** was made by Dr. Lydia Gilday[3] and compound **56** was made by Dr. Asha Brown.[4] $FBMes_2$ was prepared by Dr. Remi Tirfoin[5] and stored in a glove box.

6.1.2 Instrumental methods

^1H, ^{13}C, ^{11}B ^{19}F and ^{31}P NMR spectra were recorded using Varian Mercury 300, Bruker AVIII400, Bruker AVII 500 (with cryoprobe), and Bruker AVIII500 spectrometers at 298 K, unless otherwise stated. ^1H-^1H coupling constants are reported over 3-bonds (*J*), unless otherwise stated. Mass spectra were recorded on a Waters LCT Premier instrument (low resolution) or a Bruker μTOF instrument (high resolution). A Biotage Initiator 2.0 microwave was used to perform dielectric microwave heating.

6.2 Synthetic procedures

6.2.1 Experimental details for Chapter 2

Iodotriazole derivative 1

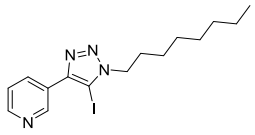

To a solution of 1-azidooctane (113 mg, 0.73 mmol) in THF (2 mL) was added NaI (291 mg, 1.94 mmol) and $Cu(ClO_4)_2.6H_2O$ (359 mg, 0.97 mmol). The mixture was stirred for 5 minutes at room temperature after which TBTA (2.7 mg, 0.005 mmol) and a THF (0.5 mL) solution of DBU (75 mg, 0.49 mmol) were added, followed by 3-ethynyl pyridine (50 mg, 0.49 mmol) and MeCN (2 mL). This was left to stir at room temperature overnight and then diluted with CH_2Cl_2 (20 mL) before being washed with $NH_4OH_{(aq.)}$ (20 mL) and $NaCl_{(sat.\ aq.)}$ (2 x 10 mL). The organics were collected, dried over $MgSO_4$, filtered and the solvent removed under vacuum. The crude material was purified by silica gel column chromatography (99:1 CH_2Cl_2/CH_3OH) to afford the product as a white solid (172 mg, 0.45 mmol, 92%).**^{1}H NMR** (400 MHz, $CDCl_3$) δ = 9.26 (s, 1H, py-*H*), 8.66 (d, *J* = 2.9 Hz, 1H, py-*H*), 8.40 (d, *J* = 8.0 Hz, 1H, py-*H*), 7.46- 7.55 (m, 1H, py-*H*), 4.40 (t, *J* = 7.5 Hz, 2H, -NC*H*$_2$), 1.85-1.95 (m, 2H, -NCH$_2$C*H*$_2$), 1.12-1.40 (m, 10H, C*H*$_2$), 0.82 (t, *J* = 6.7 Hz, 3H, C*H*$_3$). **^{13}C NMR** (100 MHz, $CDCl_3$) δ (ppm): 149.1, 147.9, 147.0, 135.1, 123.5, 51.1, 31.7, 29.9, 29.0, 28.9, 26.4, 22.6, 14.0. **MS** (ESI-MS) *m/z*: 385.0883 $[M + H]^+$ ($C_{15}H_{22}N_4I$ calc. 385.0811).

Prototriazole derivative 2

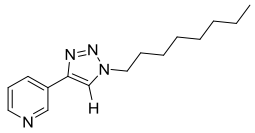

To a solution of 1-azidooctane **1** (151 mg, 0.97 mmol), 3-ethynyl pyridine (100 mg, 0.97 mmol) and TBTA (51 mg, 0.10 mmol) in CH_2Cl_2 (40 mL) was added DIPEA (188 mg, 1.46 mmol) followed by $[Cu(MeCN)_4][PF_6]$ (72 mg, 0.19 mmol). The mixture was stirred at room

temperature overnight and the solvent removed under vacuum. The crude material was purified by silica gel column chromatography (98:2 CH_2Cl_2/CH_3OH) to afford the product as an orange solid (245 mg, 0.95 mmol, 98%). **^{1}H NMR** (300 MHz, $CDCl_3$) δ = 9.00 (1H, s, py-*H*), 8.59 (1H, d, *J* = 4.1 Hz, py-*H*), 8.24 (1H, d, *J* = 5.9 Hz, py-*H*), 7.84 (1H, s, triazole C*H*), 7.38 (1H, t, *J* = 7.9 Hz, py-*H*), 4.43 (2H, t, *J* = 7.8 Hz, -NCH_2), 1.99-1.93 (2H, m, *J* = 6.9 Hz, -NCH_2CH_2), 1.41-1.21 (10H, m, CH_2), 0.88 (3H, t, *J* = 7.2 Hz, -CH_3). **^{13}C NMR** (101MHz, $CDCl_3$) δ = 149.1, 147.0, 144.6, 132.9, 126.9, 123.7, 119.7, 50.5, 31.6, 30.3, 29.0, 28.9, 26.4, 22.5, 14.0. **MS** (ESI-MS) *m/z*: 259.1925 $[M + H]^+$ ($C_{15}H_{23}N_4$ calc. 259.1917)

2-Bromo-*N*-hexylacetamide 3

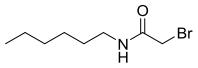

Hexylamine (300 mg, 3.0 mmol) and Et_3N (599 mg, 5.9 mmol) were dissolved in CH_2Cl_2 (100 mL) and cooled to 0^{o}C in an ice bath. A CH_2Cl_2 solution (25 mL) of bromoacetyl bromide (658 mg, 3.3 mmol) was then added drop-wise, after which the solution was allowed to warm to room temperature and left to stir overnight. The mixture was then washed with 10% citric $acid_{(aq.)}$ (100 mL), saturated $NaHCO_{3(aq.)}$ (100mL) and H_2O (2 x 100 mL). The organics were collected, dried over $MgSO_4$, filtered and the solvent removed under vacuum to give the product as an orange oil (622 mg, 2.3 mmol, 76%). **^{1}H NMR** (400 MHz, $CDCl_3$) δ (ppm): 6.48 (br. s, 1H, N*H*), 3.88 (s, 2H, -CH_2-Br), 3.25-3.32 (m, 2H, NHCH_2), 1.49- 1.58 (m, 2H, $NHCH_2CH_2$), 1.23- 1.41 (m, 6H, CH_2), 0.89 (t, *J* = 5.38 Hz, 3H, CH_3).

Iodotriazole acyclic receptor 4

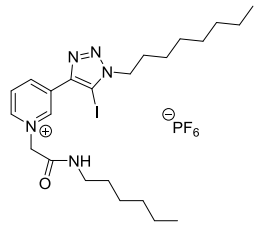

To a suspension of iodotriazole derivative **1** (100 mg, 0.26 mmol) and 2-bromo-*N*-hexylacetamide **3** (87 mg, 0.39 mmol) in dry MeCN (25 mL) was added sodium iodide (6.5 mg, 0.043 mmol). The mixture was heated at reflux for 48 h after which it was cooled to room temperature and the solvent removed under vacuum. The crude material was purified by silica gel column chromatography using 95:5 CH_2Cl_2/MeOH to elute the product. This was subsequently dissolved in CH_2Cl_2 (30 mL) and washed with 0.1 M $NH_4PF_{6(aq.)}$ (8 x 30 mL) and H_2O (2 x 30 mL). The organics were dried over $MgSO_4$, filtered and the solvent removed under vacuum to yield **6.PF$_6$** as a light orange solid (67 mg, 0.10 mmol, 39%). **^{1}H NMR** (400 MHz, $CDCl_3$) δ = 9.36 (s, 1H, py-*H*), 9.12 (d, *J* = 8.2 Hz, 1H, py-*H*), 8.73 (d, *J* = 5.4 Hz, 1H, py-*H*), 8.10 (m, 1H, py-*H*), 6.93 (br s, 1H, N*H*), 5.41 (s, 2H, N^+-C*H*2), 4.47 (t, *J*= 7.21 Hz, 2H, -NCH_2), 3.23- 3.32 (m, 2H, NHCH_2CH_2), 1.89- 1.99 (m, 2H, -NCH_2CH_2), 1.50- 1.58 (m, 2H, $NHCH_2CH_2$), 1.18- 1.35 (m, 16H, CH_2) 0.82- 0.92 (m, 6H, CH_3). **^{13}C NMR** (100 MHz, $CDCl_3$) δ = 163.1, 144.8, 142.8, 131.4, 128.0, 79.2, 62.8, 51.5, 40.6, 31.7, 31.4, 29.7, 29.0, 28.9, 28.8, 26.5, 26.4, 22.6, 22.5, 14.1, 14.0. **^{31}P NMR** (162 MHz, 1:1 $CDCl_3/CD_3OD$) δ = -144.6 (septet, *J* = 714 Hz). **^{19}F NMR** (376 MHz, 1:1 $CDCl_3/CD_3OD$) δ = -71.4 (d, *J* = 714 Hz). **MS** (ESI-MS) *m/z*: 526.2042 $[M - PF_6]^+$ ($C_{23}H_{37}IN_5O^+$ calc. 526.2037).

Prototriazole acyclic receptor 5·PF_6

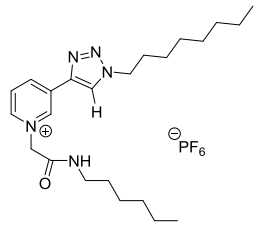

Prototriazole derivative **2** (174 mg, 0.67 mmol) was dissolved in dry MeCN (20 mL) and 2-bromo-*N*-hexylacetamide **3** (179 mg, 0.81 mmol) was added. The mixture was heated at reflux for 72 h after which it was cooled to room temperature and poured into Et_2O (20 mL). The precipitate formed was collected by filtration and dried under vacuum. This was subsequently dissolved in $CHCl_3$ (30 mL) and washed with 0.1M $NH_4PF_{6(aq)}$ (8 x 30 mL) and H_2O (2 x 30 mL). The organics were dried over $MgSO_4$ and the solvent removed under vacuum to give **5·PF_6** as a white solid (234 mg, 0.43 mmol, 64%). **^{1}H NMR** (500 MHz, $CDCl_3$) δ = 9.02 (1H, s, py-*H*), 8.95 (1H, d, *J* = 8.1 Hz, py-*H*), 8.47 (1H, d, *J* = 6.1 Hz, py-*H*), 8.23 (1H, s, triazole C*H*), 7.93 (1H, t, *J* = 7.1 Hz, py-*H*), 6.74 (1H, br s, N*H*), 5.20 (2H, s, -N^+-C*H*2), 4.34 (2H, t, *J* = 7.1 Hz, -NCH_2), 3.27-3.10 (2H, m, NHCH_2), 1.87 (2H, m, -NCH_2CH_2) 1.55-1.37 (2H, m, $NHCH_2CH_2$), 1.30-1.15 (16H, m, CH_2), 0.79 (6H, m, CH_3). **^{13}C NMR** (75 MHz, $CDCl_3$) δ 161.7, 161.6, 142.4, 140.9, 140.2, 138.9, 131.6, 126.8, 122.1, 61.6, 50.0, 39.6, 39.5, 30.7, 30.3, 27.9, 27.85, 27.76, 25.4, 25.36, 21.6, 21.4, 13.0, 12.9. **^{19}F NMR** (282 MHz, $CDCl_3$) δ = -71.1 (d, $^1J_{F,P}$ = 712 Hz). **^{31}P NMR** (122 MHz, $CDCl_3$) δ = -144.2 (septet, $^1J_{P,F}$ = 713 Hz). **MS** (ESI-MS) *m/z*: 400.3071 $[M - PF_6]^+$ ($C_{23}H_{38}N_5O^+$ calc. 400.3071).

Alkyl bromide-appended stopper 16

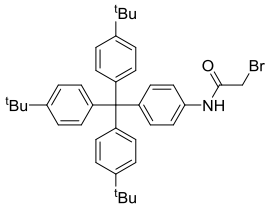

Stopper amine **15** (1.00g, 2.0 mmol) and Et_3N (0.41 g, 4.0 mmol) were dissolved in CH_2Cl_2 (150 mL) and cooled to 0^oC in an ice bath. A CH_2Cl_2 (50 mL) solution of bromoacetyl bromide (0.44 g, 2.2 mmol) was then added drop-wise, after which the solution was allowed to warm to room temperature and left to stir overnight. The mixture was then washed with 10% citric $acid_{(aq.)}$ (200 mL), saturated $NaHCO_{3(aq.)}$ (200mL) and H_2O (200 mL). The organics were collected, dried over $MgSO_4$, filtered and the solvent removed under vacuum to give the product as an off-white solid (1.12 g, 1.79 mmol, 91%). **^{1}H NMR** (300 MHz, $CDCl_3$) δ = 8.09 (1H, br. s, N*H*), 7.40 (2H, d, *J* = 8.4 Hz, NAr-*H*), 7.19-7.26 (8H, m, Ar-*H*), 7.08-7.11 (6H, m, Ar-*H*), 4.02 (2H, s, -C*H*$_2$-Br), 1.31 (27H, s, ^{t}Bu). **^{13}C NMR** (101 MHz, $CDCl_3$) δ = 163.2, 148.5, 144.5, 143.7, 134.4, 131.9, 130.7, 124.2, 118.7, 63.4, 34.3, 31.4, 29.5. **MS** (ESI-MS) *m/z*: 622.2694 $[M - H]^-$ ($C_{39}H_{45}ONBr$ calc. 622.2690).

Iodotriazole derivative 17

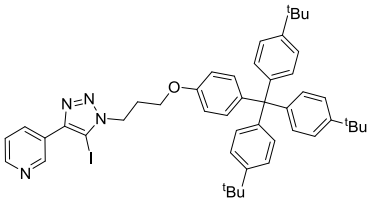

To a solution of propyl-azide stopper **14** (273 mg, 0.47 mmol) in THF (2 mL) was added NaI (186 mg, 1.24 mmol) and $Cu(ClO_4)_2.6H_2O$ (230 mg, 0.62 mmol). The mixture was stirred for 5 minutes at room temperature after which TBTA (1.6 mg, 0.031 mmol) and a THF (0.5 mL) solution of DBU (47 mg, 0.31 mmol) were added, followed by 3-ethynyl pyridine (32 mg, 0.31 mmol) and MeCN (2 mL). This was left to stir at room temperature overnight and then diluted with CH_2Cl_2 (20 mL) before being washed with $NH_4OH_{(aq.)}$ (20 mL) and $NaCl_{(sat.\ aq.)}$

(2 x 10 mL). The organics were collected dried over $MgSO_4$, filtered and the solvent removed under vacuum. The crude material was purified by silica gel column chromatography (99:1 CH_2Cl_2/CH_3OH) to afford the product as a white solid (214 mg, 0.26 mmol, 85%). **^{1}H NMR** (400 MHz, $CDCl_3$) δ = 9.36 (s, 1H, py-*H*), 8.67 (br. s, 1H, py-*H*), 8.37 (d, *J* = 7.8 Hz, 1H, py-*H*), 7.46-7.55 (m, 1H, py-*H*), 7.20-7.25 (m, 6H, Ar-*H*), 7.04-7.12 (m, 8H, Ar-*H*), 6.74-6.79 (m, 2H, OAr-*H*), 4.69 (t, *J* = 7.0 Hz, 2H, CH_2-C*H*$_2$-N), 4.05 (t, *J* = 5.6 Hz, 2H, CH_2-C*H*$_2$-O), 2.46 (m, 2H, CH_2-C*H*$_2$-CH_2), 1.30 (s, 27H, ^{t}Bu). **^{13}C NMR** (101 MHz, $CDCl_3$) δ = 155.1, 147.4, 147.0, 145.7, 143.0, 139.1, 135.1, 131.3, 129.7, 123.1, 112.0, 62.8, 62.0, 47.2, 33.3, 30.4, 28.6. **MS** (ESI-MS) *m/z*: 817.3326 $[M + H]^+$ ($C_{47}H_{54}N_4OI$ calc. 817.3337).

Prototriazole derivative 18

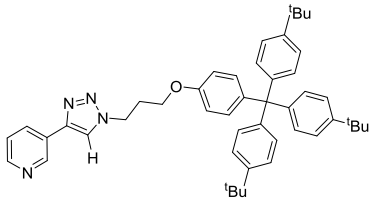

To a solution of propyl-azide stopper **14** (1.00 g, 1.70 mmol), 3-ethynyl pyridine (175 mg, 1.70 mmol) and TBTA (180 mg, 0.34 mmol) in CH_2Cl_2 (150 mL) was added DIPEA (0.44 mL, 2.55 mmol) followed by $[Cu(MeCN)_4][PF_6]$ (127 mg, 0.34 mmol). The mixture was stirred at room temperature overnight and the solvent removed under vacuum to give a yellow residue. This was purified by silica gel column chromatography (98:2 CH_2Cl_2/MeOH) to afford the product as an off white solid (1.093 g, 1.58 mmol, 93%). **^{1}H NMR** (300 MHz, $CDCl_3$) δ = 9.01 (1H, s, py-*H*), 8.59 (1H, d, *J* = 5.1 Hz, py-*H*), 8.22 (1H, d, *J* = 7.6 Hz, py-*H*), 7.89 (1H, s, triazole C*H*), 7.37-7.41 (1H, m, py-*H*), 7.23-7.25 (6H, m, Ar-*H*), 7.07-7.13 (8H, m, Ar-*H*), 6.77 (2H, d, *J* = 8.8 Hz, OAr-*H*), 4.68 (2H, t, *J* = 7.0 Hz, -C*H*$_2$-N), 4.00 (2H, t, *J* = 5.7 Hz, -C*H*$_2$-O), 2.46 (2H, m, CH_2-C*H*$_2$-CH_2), 1.31 (27H, s, ^{t}Bu). **^{13}C NMR** (101 MHz, $CDCl_3$) δ = 156.2, 149.2, 148.4, 147.1, 144.7, 144.0, 140.3, 133.0, 132.4, 130.7, 126.7, 124.1, 123.7, 120.5, 112.9, 63.8, 63.0, 47.4, 34.3, 31.4, 30.0. **MS** (ESI-MS) *m/z*: 691.4359 $[M + H]^+$

($C_{47}H_{55}N_4O$ calc. 691.4370).

Iodotriazole axle 19·Cl

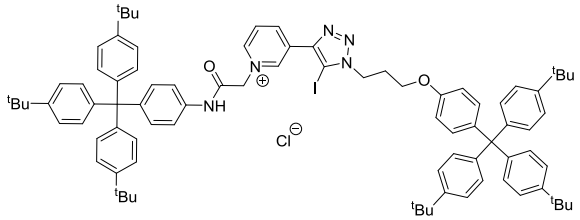

To a suspension of iodotriazole derivative **17** (100 mg, 0.12 mmol) and alkyl bromide stopper **16** (92mg, 0.15 mmol) in MeCN (20 mL) was added NaI (55 mg, 0.37 mmol). The mixture was heated at reflux for 48 h after which it was cooled to room temperature and the solvent removed under vacuum. The crude material was purified by silica gel column chromatography using 98:2 CH_2Cl_2/MeOH to elute the product. This was subsequently dissolved in CH_2Cl_2 (30 mL) and washed with 1M $NH_4Cl_{(aq)}$ (8 x 30 mL) and H_2O (2 x 30 mL). The organics were dried over $MgSO_4$ and the solvent removed under vacuum to give the **19·Cl** as an off-white solid (107 mg, 0.077 mmol, 63%). **^{1}H NMR** (400 MHz, $CDCl_3$) δ = 11.55 (s, 1H, N*H*), 9.76 (s, 1H, py-*H*), 9.27 (d, *J* = 5.0 Hz, 1H, py-*H*), 8.84 (d, *J* = 8.0 Hz, 1H, py-*H*), 7.79 (app. t, *J* = 7.0 Hz, 1H, py-*H*), 7.53 (d, *J* = 8.7 Hz, 2H, NAr-*H*), 7.16-7.25 (m, 28H, Ar-*H*), 6.71 (d, *J* = 8.9 Hz, 2H, OAr-*H*), 6.16 (br. s, 2H, N^+-CH_2), 4.60 (t, *J* = 7.0 Hz, 2H, -CH_2-N), 3.96 (t, *J* = 5.4 Hz, 2H, -CH_2-O), 2.30-2.40 (m, 2H CH_2-CH_2-CH_2), 1.30 (s, 27H, ^{t}Bu), 1.27 (s, 27H, ^{t}Bu). **^{13}C NMR** (101 MHz, $CDCl_3$) δ = 160.2, 155.2, 147.3, 143.4, 143.2, 143.0, 142.8, 141.5, 141.3, 139.2, 133.9, 131.3, 130.8, 130.6, 129.7, 126.6, 123.1, 118.0, 112.0, 81.3, 62.8, 62.2, 62.0, 47.5, 33.3, 30.4, 28.7, 28.5. **MS** (ESI-MS) *m/z*: 1360.6823 $[M - Cl]^+$ ($C_{86}H_{99}N_5O_2I$ calc. 1360.6838).

Prototriazole axle 20·Cl

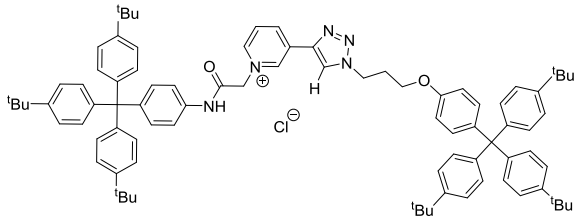

To a suspension of prototriazole derivative **18** (250 mg, 0.36 mmol) and alkyl bromide stopper **16** (269 mg, 0.43 mmol) in MeCN (50 mL) was added NaI (5 mg, 0.04 mmol). The mixture was heated at reflux for 72 h after which it was cooled to room temperature and the solvent removed under vacuum. The crude material was purified by silica gel column chromatography using 95:5 CH_2Cl_2/MeOH to elute the product. This was subsequently dissolved in $CHCl_3$ (30 mL) and washed with 1M $NH_4Cl_{(aq.)}$ (8 x 30 mL) and H_2O (2 x 30 mL). The organics were dried over $MgSO_4$, filtered and the solvent removed under vacuum to yield **20·Cl** as an off white solid (127 mg, 0.10 mmol, 28%). **^{1}H NMR** (300 MHz, $CDCl_3$) δ = 11.58 (1H, s, N*H*), 10.91 (1H, s, py-*H*), 9.03 (1H, d, *J* = 7.7 Hz, py-*H*), 8.84 (1H, s, triazole C*H*), 8.76 (1H, d, *J* = 5.9 Hz, py-*H*), 7.84-7.89 (1H, m, py-*H*), 7.60 (2H, d, *J* = 8.8 Hz, NAr-*H*), 7.19-7.25 (12H, m, Ar-*H*), 7.05-7.13 (16H, m, Ar-*H*), 6.74 (2H, d, *J* = 8.8 Hz, OAr-*H*), 5.87 (2H, br s, N^+-C*H*2), 4.66 (2H, t, *J* = 7.0 Hz, -C*H*$_2$-N), 4.00 (2H, t, *J* = 5.2 Hz, -C*H*$_2$-O), 2.44 (2H, m, CH_2-C*H*$_2$-CH_2), 1.28-1.30 (54H, m, ^{t}Bu). **^{13}C NMR** (126 MHz, 1:1 $CDCl_3$/CD_3OD) δ = 157.2, 149.3, 149.2, 145.2, 145.0, 144.7, 135.8, 133.1, 132.6, 131.5, 131.5, 125.1, 124.9, 124.8, 119.6, 113.8, 64.9, 64.2, 63.9, 34.9, 34.9, 31.7, 29.9. **MS** (ESI-MS) *m/z*: 1234.7865 $[M - Cl]^+$ ($C_{86}H_{100}N_5O_2I$ calc. 1234.7872).

Iodotriazole rotaxane 26·PF6

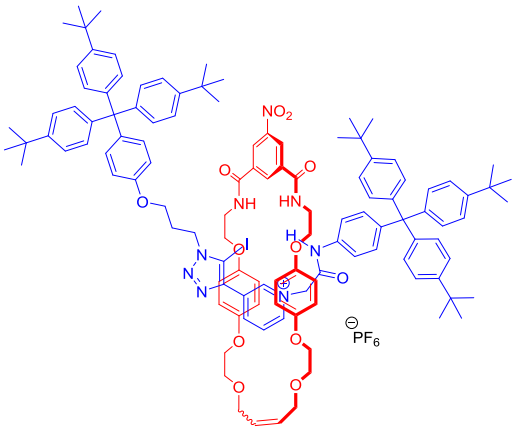

Iodotriazole axle **19·Cl** (45 mg, 0.032 mmol) and bis-vinyl macrocycle precursor **25** (21 mg, 0.032 mmol) were dissolved in CH_2Cl_2 (10 mL) and stirred at room temperature for 1h. Grubbs' second generation catalyst (2.1 mg, 10% by weight) was added and the mixture stirred for 48h, after which another portion of the catalyst was added (2.1 mg) followed by stirring for a further 48h. The solvent was then removed under vacuum and the crude material purified by preparative thin layer chromatography (CH_2Cl_2/MeOH 98:2; followed by EtOAc/ MeOH 98:2). The product was then dissolved in $CHCl_3$ (15 mL) and washed with 0.1M $NH_4PF_{6(aq.)}$ (8 x 20 mL) and H_2O (2 x 20 mL). The organics were dried over $MgSO_4$, filtered and the solvent removed under vacuum to yield **26·PF_6** as a light brown solid (15 mg, 0.007 mmol, 22%). **^{1}H NMR** (500 MHz, 1:1 $CDCl_3$/CD_3OD) δ = 10.27 (s, 1H, axle N*H*), 9.21 (s, 1H, py-*H*), 8.91 (s, 1H, int. macro. Ar-*H*), 8.82 (br s, 2H, ext. macro. Ar-*H*), 8.66 (d, *J* = 8.2 Hz, 1H, py-*H*), 8.58-8.63 (m, 2H, macro. N*H*), 8.53 (d, *J* = 5.2 Hz, 1H, py-*H*), 7.91-7.98 (m, 1H, py-*H*), 7.42 (d, *J* = 8.2 Hz, 2H, axle NAr-*H*), 7.22 (d, *J* = 8.4 Hz, 6H, stopper Ar-*H*), 7.17 (d, *J* = 8.4 Hz, 8H, stopper Ar-*H*), 7.04- 7.09 (m, 8H, stopper Ar-*H*), 7.00- 7.04 (d, *J* = 8.4 Hz, 6H, stopper Ar-*H*), 6.74 (d, *J* = 8.9 Hz, 2H, OAr-*H*), 6.29 (br s, 8H, hydroquinone Ar-*H*), 5.94 (s, 2H, alkene C*H*), 5.47 (s, 2H, N^+-CH_2), 4.30 (t, *J* = 6.6 Hz, 2H,axle -CH_2-N), 3.99-4.07 (m, 4H, macro. CH_2), 3.57- 3.92 (m, 18H, macro. CH_2, axle -CH_2-O), 2.16 (m, 2H, axle CH_2-CH_2-CH_2), 1.25-1.27 (m, 54H, ^{t}Bu). **^{13}C NMR** (126 MHz, 1:1 $CDCl_3$/CD_3OD) δ = 165.5,

156.2, 152.4, 152.4, 148.5, 148.4, 148.2, 144.4, 144.1, 143.7, 143.0, 141.5, 140.2, 136.2, 134.8, 132.2, 131.7, 131.6, 131.0, 124.1, 124.0, 118.8, 114.9, 114.6, 113.0, 82.0, 70.9, 69.2, 67.5, 66.6, 63.6, 63.3, 63.0, 39.8, 34.1, 34.0, 30.9, 29.5, 28.8, 26.6, 26.5, 26.0, 26.0, 25.9. **^{19}F NMR** (470 MHz, 1:1 $CDCl_3/CD_3OD$) δ (ppm): - 71.4 (d, $^1J_{F,P}$ = 714 Hz). **^{31}P NMR** (202 MHz, 1:1 $CDCl_3$/ CD_3OD) δ (ppm): -144.2 (septet, $^1J_{P,F}$ = 714 Hz). **MS** (ESI-MS) *m/z*: 1982.9169 $[M - PF6]^+$ ($C_{118}H_{134}N_8O_{12}I$ calc. 1982.9193).

Prototriazole rotaxane 27·PF6

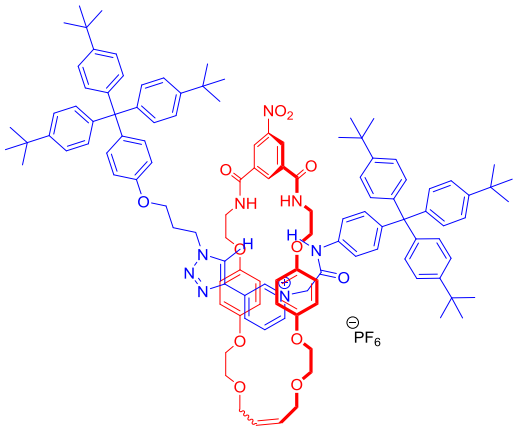

Prototriazole axle **20·Cl** (60 mg, 0.047 mmol) and bis-vinyl macrocycle precursor **25** (31 mg, 0.047 mmol) were dissolved in CH_2Cl_2 (~ 10 mL) and stirred at room temperature for 30 min. Grubbs' 2nd generation catalyst (3.1 mgs, 10% by weight) was added and the mixture stirred for a further 72 h, after which the solvent was removed under vacuum. The crude brown residue was purified using preparative plate thin layer chromatography (98:2 EtOAc/MeOH). The product was then dissolved in $CHCl_3$ (15 mL) and washed with 0.1M $NH_4PF_{6(aq.)}$ (8 x 15 mL) and H_2O (2 x 15 mL). The organics were dried over $MgSO_4$, filtered and the solvent removed under vacuum to yield **27·PF$_6$** as an off-white solid (17 mgs, 0.008 mmol, 18%). **^{1}H NMR** (500 MHz, 1:1 $CDCl_3/CD_3OD$) δ = 8.85 (1H, s, int. macro. Ar-*H*), 8.79 (2H, s, ext. macro. Ar-*H*), 8.77 (1H, s, py-*H*), 8.53 (2H, br. s, macro. N*H*), 8.38 (1H, d, *J* = 8.1 Hz, py-*H*), 8.32 (1H, d, *J* = 5.6 Hz, py-*H*), 8.14 (1H, s, triazole C*H*), 7.83 (1H, m, py-*H*), 7.39 (2H, d, *J* = 8.9 Hz, NAr-*H*), 7.17-7.23 (14H, m, stopper Ar-*H*), 7.02-7.08 (14H, m, stopper Ar-*H*), 6.74

(2H, d, *J* = 8.9 Hz, OAr-*H*), 6.31-6.37 (8H, m, hydroquinone Ar-*H*), 5.94 (2H, br. s, alkene C*H*), 5.24 (2H, s, N^+-CH_2), 4.44 (2H, t, *J* = 7.3 Hz, axle -CH_2-N), 4.00-4.03 (4H, m, macro. CH_2), 3.67-3.88 (18H, m, macro CH_2, axle -CH_2-O), 2.26 (2H, m, axle CH_2-CH_2-CH_2), 1.27 (27H, s, ^{t}Bu), 1.25 (27H, s, ^{t}Bu). **^{13}C NMR** (126 MHz, 1:1 $CDCl_3$/CD_3OD) δ = 166.3, 156.9, 153.2, 153.2, 149.2, 149.0, 144.8, 144.5, 144.0, 141.0, 140.9, 136.9, 135.4, 132.9, 132.5, 131.9, 131.3, 131.3, 130.3, 128.4, 125.9, 124.9, 124.7, 119.4, 115.7, 115.4, 113.7, 71.6, 69.9, 68.3, 67.1, 64.5, 64.1, 63.7, 63.0, 40.7, 34.8, 34.8, 31.8, 30.0. **^{19}F NMR** (470 MHz, 1:1 $CDCl_3$/CD_3OD) δ = -73.0 (d, $^1J_{F,P}$ = 711 Hz). **^{31}P NMR** (202 MHz, 1:1 $CDCl_3$/CD_3OD) δ = -144.4 (septet, $^1J_{P,F}$ = 711 Hz). **MS** (ESI-MS) *m/z*: 1857.0165 $[M - PF_6]^+$ ($C_{118}H_{135}N_8O_{12}$ calc. 1857.0226).

Pyridinium alkyne derivative 28·Br

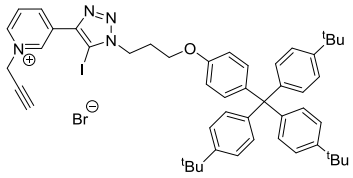

Iodotriazole derivative **17** (100 mg, 0.122 mmol) was dissolved in $CHCl_3$ (5 mL) and propargyl bromide (80 wt. % in toluene, 0.5 mL, excess) was added. The solution was stirred at room temperature for 7 days, after which the formation of a precipitate was observed. This was collected by vacuum filtration, washed with cold $CHCl_3$ and dried under vacuum to yield the product as an off-white solid (55 mg, 0.065 mmol, 53%). **^{1}H NMR** (400MHz, 1:1 $CDCl_3$/CD_3OD) δ = 9.68 (s, 1H, py-*H*), 9.17 (m, 2H, py-*H*), 8.22 (app. t, *J* = 7.3 Hz, 1H, py-*H*), 7.19 (d, *J* = 8.6 Hz, 6H, Ar-*H*), 7.05 (m, 8H, Ar-*H*), 6.72 (d, *J* = 9.0 Hz, 2H, OAr-*H*), 5.74 (d, ^4J = 2.6 Hz, 2H, N^+-CH_2), 4.71 (t, *J* = 7.0 Hz, 2H, -CH_2-N), 4.03 (t, *J* = 5.6 Hz, 2H -CH_2-O), 3.21 (t, ^4J = 2.6 Hz, 1H, -CH_2-C-C*H*), 2.44 (m, 2H, -CH_2-CH_2-CH_2-), 1.26 (s, 27H, ^{t}Bu). **^{13}C NMR** (101 MHz, 1:1 $CDCl_3$/CD_3OD) δ = 156.2, 148.3, 144.1, 143.0, 142.7, 141.0, 140.1,

132.2, 130.6, 128.5, 124.0, 113.0, 81.6, 64.0, 63.0, 51.0, 34.1, 31.0, 29.4. **MS** (ESI-MS) *m/z*: 855.3493 $[M - Br]^+$ ($C_{50}H_{56}N_4OI$ calc. 855.3493).

Bis-iodotriazole axle 29·Br

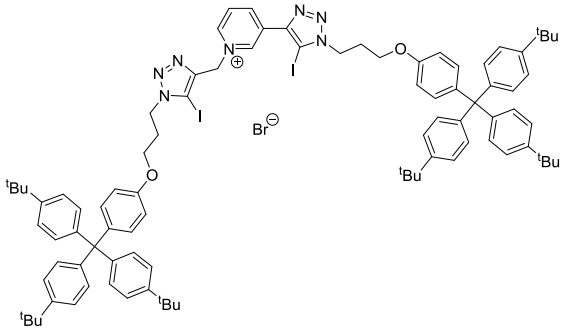

To a solution of propyl-azide stopper **14** (47 mg, 0.08 mmol) in dry THF (2.0 mL) was added NaI (32 mg, 0.21 mmol) and $Cu(ClO_4)_2 \cdot 6H_2O$ (39 mg, 0.11 mmol). The resultant mixture was stirred for 5 minutes before addition of TBTA (2.8 mg, 0.0053 mmol), a THF (0.5 mL) solution of DBU (8.2 mg, 0.053 mmol), alkyne **28·Br** (50 mg, 0.053 mmol) and dry MeCN (2 mL). This was left to stir at room temperature overnight, after which the solvent was removed under vacuum and the crude material purified using preparative thin layer chromatography (EtOAc/MeOH 95:5). The product was then taken up in CH_2Cl_2 (30 mL) and washed with 0.1M $NH_4Br_{(aq.)}$ (8 x 30 mL) and H_2O (2 x 30 mL) to give **33·Br** as a light brown solid (38 mg, 0.024 mmol, 46%). **^{1}H NMR** (400 MHz, $CDCl_3$) δ = 10.10 (br. s, 1H, py-*H*), 9.10 (d, *J*= 8.0 Hz, 1H py-*H*), 8.94 (br. s, 1H py-*H*), 7.94 (m, 1H, py-*H*), 7.22-7.24 (m, 12H, Ar*H*), 7.05-7.10 (m, 16H, Ar*H*), 6.67-6.73 (m, 4H, OAr-*H*), 6.15 (br. s, 2H, N^+-CH_2), 4.54-4.60 (m, 4H, -NC$H_2$$CH_2$), 3.96 (m, 4H, -OC$H_2$$CH_2$), 2.33 (m, 4H, CH_2C$H_2$$CH_2$), 1.30 (br. s, 54H, ^{t}Bu). **^{13}C NMR** (100 MHz, $CDCl_3$) δ = 155.2, 147.3, 143.1, 143.0, 142.2, 141.2, 140.6, 139.3, 139.1, 132.8, 131.2, 129.7, 127.6, 123.1, 112.1, 111.9, 63.1, 63.1, 62.0, 47.6, 47.4, 33.3, 30.4, 28.7, 28.6. **MS** (ESI-MS) *m/z*: 1568.6331 $[M - Br]^+$ ($C_{90}H_{104}N_7O_2I_2$ calc. 1568.6335).

Bis-iodotriazole rotaxane 30·PF_6

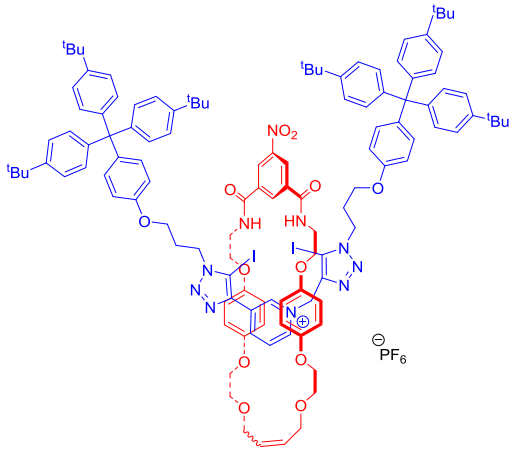

Axle **29·Cl** (47 mg, 0.029 mmol) and bis-vinyl macrocycle precursor **25** (19 mg, 0.029 mmol) were dissolved in dry CH_2Cl_2 (7 mL) and stirred at room temperature for 30 min. Grubbs' second generation catalyst (2 mg, 10 wt. % of macrocycle precursor) was added and the mixture stirred at room temperature for 48 h, after which a second portion of the catalyst (2 mg) was added and the mixture stirred for another 24 h. The solvent was then removed under vacuum and the crude residue was subjected to preparative thin layer chromatography (CH_2Cl_2/CH_3OH 97:3, then EtOAc/CH_3OH 98:2). Further purification was required after this, with the pure product isolated using size exclusion chromatography ($CHCl_3$). The product was subsequently dissolved in CH_2Cl_2 (20 mL) and washed with 0.1M $NH_4PF_{4(aq.)}$ (8 x 20 mL) and H_2O (2 x 20 mL) to give **30·PF_6** as a pale yellow solid (7.4 mg, 0.003 mmol, 11%). **^{1}H NMR** (500 MHz, 1:1 $CDCl_3$/CD_3OD) δ = 9.29 (s, 1H, py-*H*), 8.89 (s, 1H, int. macro. Ar*H*), 8.84 (s, 2H, ext. macro. Ar*H*), 8.74-8.76 (m, 2H, py-*H*), 7.99 (m, 1H, py-*H*), 7.17-7.21 (m, 12H, stopper Ar-*H*), 7.03-7.08 (m, 16H, stopper Ar-*H*), 6.73 (d, *J* = 8.8 Hz, 2H, stopper Ar-*H*), 6.67 (d, *J* = 8.8 Hz, 2H, stopper Ar-*H*), 6.22-6.27 (m, 8H, hydroquinone Ar-*H*), 5.95 (br. s, 2H, alkene C*H*), 5.70 (s, 2H, N^+-CH_2), 4.47 (t, *J* = 6.6 Hz, 2H, -C*H*$_2$-N), 4.39 (t, *J* = 6.2 Hz, 2H, axle -C*H*$_2$-N), 4.03 (m, 4H, macro. C*H*$_2$), 3.69-3.87 (m, 16 H, macro. C*H*$_2$ and axle -C*H*$_2$-O), 2.24 (m, 4H, axle -CH_2-C*H*$_2$-CH_2-), 1.27 (s, 27H, ^{t}Bu), 1.26 (s, 27H, ^{t}Bu). **^{13}C NMR** (125 MHz, 1:1 $CDCl_3$/CD_3OD) δ = 165.5, 156.1, 152.4, 148.3, 144.1, 141.0, 136.3, 132.2,

132.1, 131.8, 130.6, 129.4, 125.0, 124.0, 114.9, 114.5, 113.0, 70.9, 69.2, 67.6, 66.7, 63.7, 63.0, 39.8, 34.1, 31.0, 29.5. **^{19}F NMR** (470 MHz, 1:1 $CDCl_3/CD_3OD$) δ = -74.1 (d, $^1J_{F,P}$ = 702 Hz). **^{31}P NMR** (202 MHz, 1:1 $CDCl_3/CD_3OD$) δ = -146 (septet, $^1J_{P,F}$ = 718 Hz). **MS** (ESI-MS) *m/z*: 2190.8809 $[M - PF_6]^+$ ($C_{90}H_{104}N_7O_2I_2$ calc. 2190.8691).

3-Ethynyl quinolone 31

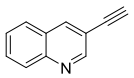

To a suspension of 3-bromoquinoline (1.00 g, 4.81 mmol), $Pd_2(dba)_3$ (92 mg, 0.10 mmol), CuI (46 mg, 0.24 mmol) and PPh_3 (252 mg, 0.96 mmol) in Et_3N (25 mL) was added TMS acetylene (590 mg, 6.01 mmol). The resultant mixture was heated at 75°C for 16 h after which it was cooled to RT, filtered and the solid collected washed with Et_2O (25 mL). The solvent was removed from the filtrate under vacuum to give a yellow oil, which was redissolved in MeOH (25 mL). KOH (445 mg, 7.94 mmol) was added in H_2O (2mL) and the mixture was stirred vigorously for 30 min. More H_2O was added (50 mL) and the solution was extracted with CH_2Cl_2 (3 x 75 mL). The organics were dried over $MgSO_4$, filtered and the solvent removed under vacuum. The crude residue was purified using silica gel column chromatography (hexane/EtOAc 4:1) to afford the product as an off-white solid (579 mg, 3.80 mmol, 79%). **^{1}H NMR** (300 MHz, $CDCl_3$) δ = 8.96 (1H, d, ^4J = 1.8 Hz, quin-H), 8.32 (1H, d, ^4J = 1.8 Hz, quin-H), 8.12 (1H, d, *J* = 8.2 Hz, quin-H), 7.72 - 7.84 (2H, m, quin-H), 7.59 (1H, t, *J* = 7.5 Hz, quin-H), 3.29 (1H, s, alkyne CH). **MS** (ESI-MS) *m/z*: 154.0 $[M + H]^+$ ($C_{11}H_8N$ calc. 154.1).

Prototriazole derivative 32

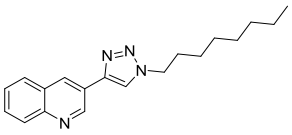

To a solution of 1-azidooctane **1** (100 mg, 0.64 mmol), 3-ethynyl quinoline (99 mg, 0.64 mmol) and TBTA (68 mg, 0.13 mmol) in CH_2Cl_2 (40 mL) was added DIPEA (124 mg, 0.96 mmol) followed by $[Cu(MeCN)_4][PF_6]$ (48 mg, 0.13 mmol). The mixture was stirred at room temperature overnight and the solvent removed under vacuum. The crude material was purified by silica gel column chromatography (98:2 CH_2Cl_2/CH_3OH) to afford the product as an off-white solid (176 mg, 0.57 mmol, 89%). **^{1}H NMR** (300 MHz, $CDCl_3$) δ = 9.32 (1H, br. s., quin-H), 8.70 (1H, d, ^4J = 1.8 Hz, quin-H), 8.13 (1H, d, J = 8.8 Hz, quin-H), 7.97 (1H, s, triazole CH), 7.90 (1H, d, J = 7.6 Hz, quin-H), 7.73 (1H, t, J = 7.5 Hz, quin-H), 7.59 (1H, t, J = 7.5 Hz, quin-H), 4.47 (2H, t, J = 7.3 Hz, -NCH_2), 1.94 - 2.07 (2H, m, -NCH_2CH_2), 1.23 - 1.48 (10H, m, CH_2), 0.88 (3H, t, J = 6.7 Hz, CH_3). **^{13}C NMR** (101MHz, $CDCl_3$) δ = 148.3, 147.7, 144.8, 131.7, 129.5, 129.3, 128.0, 127.9, 127.1, 123.9, 119.9, 50.6, 31.6, 30.3, 29.0, 28.9, 26.5, 22.5, 14.0. **MS** (ESI-MS) *m/z*: 309.20737 $[M + H]^+$ ($C_{19}H_{25}N_4$ calc. 309.20737).

Acyclic quinolinium receptor 33·PF_6

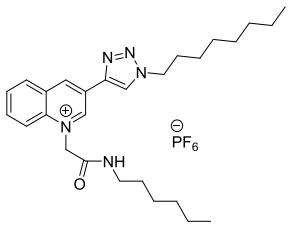

Prototriazole derivative **32** (100 mg, 0.32 mmol) and 2-bromo-*N*-hexylacetamide **3** (108 mg, 0.49 mmol) were dissolved in dry MeCN (25 mL) and NaI (5 mg, 0.03 mmol) was added. The mixture was heated at reflux for 48 h after which it was cooled to room temperature and the solvent removed under vacuum. The crude material was purified by silica gel column chromatography (CH_2Cl_2/CH_3OH 95:5 up to 9:1) to give the product, which was subsequently

dissolved in $CHCl_3$ (30 mL) and washed with 0.1 M $NH_4PF_{6(aq.)}$ (8 x 30 mL) and H_2O (2 x 30 mL). The organics were dried over $MgSO_4$, filtered and the solvent removed under vacuum to yield **33·PF$_6$** as an orange solid (105 mg, 0.17 mmol, 54%). **^{1}H NMR** (300MHz, $CDCl_3$) δ = 9.59 (1H, s, quin-H), 9.53 (1H, s, quin-H), 8.47 (1H, s, triazole CH), 8.23 - 8.34 (2H, m, quin_H), 8.15 (1H, t, *J* = 7.3 Hz, quin-H), 7.95 (1H, t, *J* = 7.5 Hz, quin-H), 7.06 (1H, t, *J* = 5.5 Hz, NH), 5.80 (2H, s, N^+-CH_2), 4.47 (2H, t, *J* = 7.3 Hz, -NCH_2), 3.22 - 3.35 (2H, m, NHC*H*$_2$), 2.01 (2H, s, -NCH_2CH_2), 1.50 - 1.64 (4H, m, CH_2), 1.20 - 1.43 (16H, m, CH_2), 0.78 - 0.94 (6H, m, CH_3). **^{13}C NMR** (101MHz, $CDCl_3$) δ = 162.8, 147.8, 141.9, 140.3, 137.7, 136.0, 130.6, 129.9, 126.2, 122.9, 118.3, 59.3, 51.0, 40.5, 31.7, 31.3, 30.0, 29.0, 28.9, 26.4, 22.6, 22.4, 14.0, 13.9. **^{19}F NMR** (283 MHz, $CDCl_3$) δ = -70.8 (d, $^1J_{F,P}$ = 714 Hz). **^{31}P NMR** (162 MHz, $CDCl_3$) δ = -144.0 (septet, $^1J_{P,F}$ = 711 Hz) **MS** (ESI-MS) *m/z*: 450.3221 $[M - PF_6]^+$ ($C_{27}H_{40}N_5O$ calc. 450.3227).

Prototriazole derivative 34

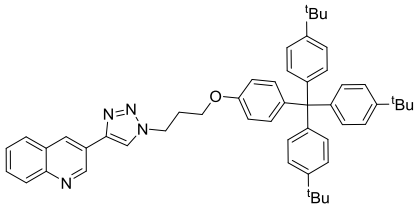

To a solution of propyl-azide stopper **14** (483 mg, 0.65 mmol), 3-ethynyl quinoline (100 mg, 0.65 mmol) and TBTA (69 mg, 0.13 mmol) in CH_2Cl_2 (50 mL) was added DIPEA (127 mg, 0.98 mmol) followed by $[Cu(MeCN)_4][PF_6]$ (48 mg, 0.13 mmol). The mixture was stirred at room temperature overnight and the solvent removed under vacuum. The crude material was purified by silica gel column chromatography (99:1 CH_2Cl_2/CH_3OH) to afford the product as a pale yellow solid (489 mg, 0.43 mmol, 66%). **^{1}H NMR** (300 MHz, d_6-acetone) δ = 9.39 (1H, d, ^4J = 2.3 Hz, quin-H), 8.72 (1H, d, ^4J = 1.8 Hz, quin-H), 8.66 (1H, s, triazole CH), 8.06 (1H, d, *J* = 8.8 Hz, quin-H), 8.00 (1H, d, *J* = 8.2 Hz, quin-H), 7.75 (1H, t, *J* = 7.8 Hz, quin-H), 7.62 (1H, t, *J* = 7.6 Hz, quin-H), 7.27 - 7.36 (6H, m, Ar-H), 7.05 - 7.16 (8H, m, Ar-H), 6.86

(2H, d, *J* = 9.0 Hz, OAr-H), 4.76 (2H, t, *J* = 7.0 Hz, -CH_2-N), 4.11 (2H, t, *J* = 5.9 Hz, -CH_2-O), 2.46 - 2.55 (2H, m, CH_2-C*H*$_2$-CH_2), 1.29 (27H, s, ^{t}Bu). ^{13}C NMR (101MHz, $CDCl_3$) δ = 156.2, 148.4, 144.9, 144.0, 140.3, 132.4, 131.8, 130.7, 129.6, 129.4, 128.1, 127.2, 124.1, 120.7, 112.9, 63.8, 63.0, 47.5, 34.3, 31.4, 30.0. **MS** (ESI-MS) *m/z*: 741.45247 $[M + H]^+$ ($C_{51}H_{57}N_4O$ calc. 741.45269).

Quinolinium axle 35·Cl

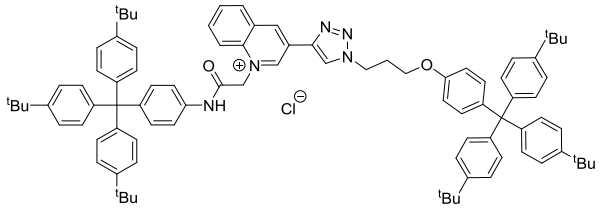

To a suspension of prototriazole derivative **34** (217 mg, 0.0.29 mmol) and alkyl bromide stopper **16** (183 mg, 0.29 mmol) in MeCN (50 mL) was added NaI (132 mg, 0.88 mmol). The mixture was heated at reflux for 7 days after which it was cooled to room temperature and the solvent removed under vacuum. The crude material was purified by silica gel column chromatography using 98:2 EtOAc/MeOH to elute the product. This was subsequently dissolved in $CHCl_3$ (30 mL) and washed with 1M $NH_4Cl_{(aq)}$ (8 x 30 mL) and H_2O (2 x 30 mL). The organics were dried over $MgSO_4$ and the solvent removed under vacuum to give the **35·Cl** as a brown solid (156 mg, 0.12 mmol, 40%). **^{1}H NMR** (500 MHz, $CDCl_3$) δ = 11.78 (1H, s, NH), 11.30 (1H, br. s., quin-H), 9.40 (1H, s, quin-H), 9.20 (1H, s, triazole CH), 8.69 (1H, d, *J* = 9.0 Hz, quin-H), 7.97 - 8.10 (2H, m, quin-H), 7.82 (1H, t, *J* = 7.6 Hz, quin-H), 7.49 (2H, d, *J* = 8.8 Hz, NAr-H), 7.16 - 7.26 (12H, m, Ar-H), 7.00 - 7.12 (16H, m, Ar-H), 6.75 (2H, d, *J* = 9.0 Hz, OAr-H), 6.56 (2H, br. s., N^+-CH_2), 4.72 (2H, t, *J* = 7.2 Hz, -CH_2-N), 4.03 (2H, t, *J* = 5.6 Hz, -CH_2-O), 2.44 - 2.55 (2H, m, CH_2-C*H*$_2$-CH_2), 1.20 - 1.36 (54H, m, tBu). **^{13}C NMR** (126 MHz, $CDCl_3$) δ = 161.3, 156.2, 148.3, 144.1, 144.0, 143.8, 140.8, 140.0, 137.6, 135.9, 135.0, 132.3, 131.5, 130.7, 130.6, 130.5, 129.9, 126.4, 124.3, 124.1, 124.0,

118.8, 113.0, 64.0, 63.3, 63.0, 48.1, 34.3, 34.2, 31.4, 31.3, 30.1, 29.7 **MS** (ESI-MS) *m/z*: 1285.8019 $[M - Cl]^+$ ($C_{90}H_{102}N_5O_2$ calc. 1285.8061).

Quinolinium rotaxane 36·PF$_6$

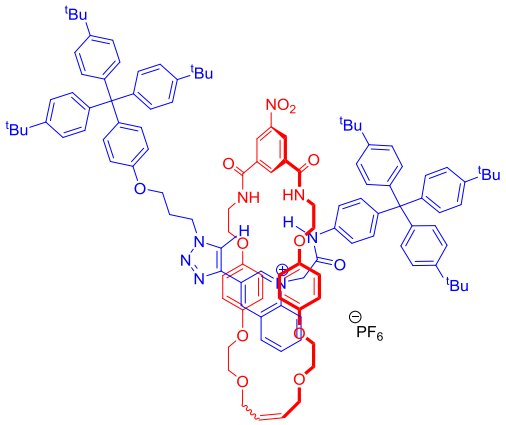

Quinolinium axle **35·Cl** (132 mg, 0.10 mmol) and bis-vinyl macrocycle precursor **25** (65 mg, 0.10 mmol) were dissolved in CH_2Cl_2 (~ 25 mL) and stirred at room temperature for 30 min. Grubbs' 2nd generation catalyst (7 mgs, 10% by weight) was added and the mixture stirred for a further 48 h, after which the solvent was removed under vacuum. The crude brown residue was purified using preparative plate thin layer chromatography (98:2 EtOAc/MeOH). The product was then dissolved in $CHCl_3$ (15 mL) and washed with 0.1M $NH_4PF_{6(aq.)}$ (8 x 15 mL) and H_2O (2 x 15 mL). The organics were dried over $MgSO_4$, filtered and the solvent removed under vacuum to yield **36·PF$_6$** as an off-white solid (15 mgs, 0.007 mmol, 7%). **^{1}H NMR** (500 MHz, 1:1 $CDCl_3/CD_3OD$) δ = 10.21 (1H, br. s., axle NH), 9.40 (1H, s, quin-H), 8.82 (1H, br. s., int. macro. Ar-H), 8.80 (1H, br. s., quin-H), 8.78 (2H, s, ext. macro. Ar-H), 8.52 (2H, br. s., macro. NH), 8.22 (1H, s, triazole CH), 8.14 (1H, d, *J* = 8.2 Hz, quin-H), 8.05 (1H, t, *J* = 7.8 Hz, quin-H), 7.97 (1H, d, *J* = 9.0 Hz, quin-H), 7.84 (1H, t, *J* = 7.5 Hz, quin-H), 7.37 (2H, d, *J* = 7.8 Hz, NAr-H), 6.98 - 7.31 (28H, m, stopper Ar-H), 6.78 (2H, d, *J* = 8.9 Hz, OAr-H), 6.05 - 6.24 (8H, m, hydroquinone Ar-H), 6.02 (2H, br. s., alkene CH), 5.74 (2H, br. s., N+-CH_2), 4.54 (2H, t, *J* = 6.6 Hz, axle -CH_2-N), 3.98 - 4.10 (4H, m, macro. CH_2), 3.92 (2H, t, *J* = 5.0 Hz, axle -CH_2-O), 3.54 - 3.84 (16H, m, macro. CH_2), 2.30 - 2.40 (2H, m, axle

CH_2-C*H*$_2$-CH_2), 1.17 - 1.32 (54H, m, tBu). **^{13}C NMR** (126 MHz, 1:1 $CDCl_3$/CD_3OD) δ = 166.5, 162.3, 157.0, 153.1, 149.3, 149.2, 149.0, 148.1, 145.3, 144.8, 144.5, 142.9, 141.3, 141.1, 138.0, 137.0, 136.7, 135.4, 133.0, 132.5, 132.2, 131.3, 130.3, 129.1, 125.8, 125.1, 124.9, 124.7, 124.4, 119.4, 118.1, 115.5, 115.2, 113.7, 71.7, 69.9, 68.2, 67.3, 64.4, 64.1, 63.7, 48.1, 40.7, 34.8, 34.8, 31.7, 30.3. **^{19}F NMR** (283 MHz, $CDCl_3$) δ = -70.2 (d, $^1J_{F,P}$ = 714 Hz). **^{31}P NMR** (202 MHz, 1:1 $CDCl_3$/CD_3OD) δ = -144.4 (septet, $^1J_{P,F}$ = 711 Hz). **MS** (ESI-MS) *m/z*: 1907.0421 $[M - PF_6]^+$ ($C_{112}H_{137}N_8O_{12}$ calc. 1907.0383).

6.2.2 Experimental details for Chapter 3

1,2-bis(triflyloxy)ethane 37[6]

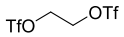

Ethylene glycol (0.31 g, 5 mmol) and pyridine (0.79 g, 10 mmol) were dissolved in CH_2Cl_2 (3 mL) and added dropwise to a solution of trifluoromethanesulfonic anhydride (2.82 g, 10 mmol) in CH_2Cl_2 (7 mL) cooled to 0^{o}C. The mixture was left to stir for a further 10 min after which it was warmed to room temperature and washed with H_2O (2 x 10 mL). The organics were dried over $MgSO_4$, filtered and the solvent removed under vacuum to afford the product as a pale pink oil (1.34 g, 4.1 mmol, 82%). **^{1}H NMR** (400MHz, $CDCl_3$) δ = 4.78 (4H, s, CH_2). **^{19}F NMR** (376MHz, $CDCl_3$) δ = -74.2 (s).

XB acyclic receptor 38·2PF$_6$

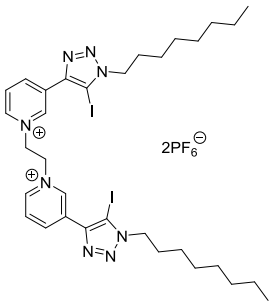

A solution of bis-triflate **37** (19 mg, 0.06 mmol) in CH_2Cl_2 (1mL) was added to a solution of iodotriazole derivative **1** (50 mg, 0.13 mmol) in CH_2Cl_2 (1 mL) in one portion. The mixture was left to stir at room temperature for 24 h after which the precipitate formed was collected

by filtration, washed with Et_2O (20 mL) and dried under vacuum. The product was then dissolved in CH_2Cl_2 (30 mL) and washed with 0.1M $NH_4PF_{6(aq.)}$ (8 x 30 mL) and H_2O (2 x 30 mL). The organics were dried over $MgSO_4$, filtered and the solvent removed under vacuum to yield **38·2PF$_6$** as a white solid (37 mg , 0.034 mmol, 58%). **^{1}H NMR** (400MHz, CD_3CN) δ = 9.32 (2H, s, py-H), 9.20 (2H, d, *J* = 8.2 Hz, py-H), 8.69 (2H, d, *J* = 6.1 Hz, py-H), 8.22 (2H, dd, *J* = 8.2 Hz, *J* = 6.1 Hz, py-H), 5.23 (4H, s, N^+-CH_2), 4.49 (4H, t, *J* = 7.2 Hz, -NCH_2), 1.86 - 1.99 (4H, m, -$NCH_2C\mathit{H}_2$), 1.20 - 1.43 (20H, m, CH_2), 0.82 - 0.94 (6H, m, CH_3) **^{13}C NMR** (101MHz, CD_3CN) δ = 144.9, 144.3, 143.9, 143.7, 133.9, 130.4, 82.5, 61.0, 52.2, 32.5, 30.4, 29.9, 29.7, 27.0, 23.4, 14.4. **^{19}F NMR** (376 MHz, CD_3CN) δ = -72.8 (d, $^1J_{F,P}$ = 707 Hz). **^{31}P NMR** (162 MHz, CD_3CN) δ = -144.6 (septet, $^1J_{P,F}$ = 706 Hz). **MS** (ESI-MS) *m/z*: 398.09579 $[M - 2PF_6]^{2+}$ ($C_{32}H_{46}N_8I_2$ calc. 398.09619).

HB acyclic receptor 39·2PF$_6$

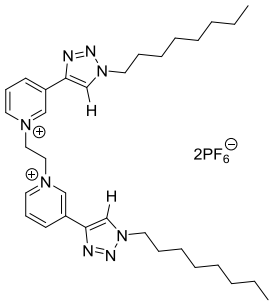

A solution of bis-triflate **37** (57 mg, 0.18 mmol) in CH_2Cl_2 (1mL) was added to a solution of prototriazole derivative **2** (100 mg, 0.39 mmol) in CH_2Cl_2 (1 mL) in one portion. The mixture was left to stir at room temperature for 24 h after which the precipitate formed was collected by filtration, washed with Et_2O (20 mL) and dried under vacuum. The product was then dissolved in CH_2Cl_2 (30 mL) and washed with 0.1M $NH_4PF_{6(aq.)}$ (8 x 30 mL) and H_2O (2 x 30 mL). The organics were dried over $MgSO_4$, filtered and the solvent removed under vacuum to yield **39·2PF$_6$** as a white solid (104 mg , 0.12 mmol, 71%). **^{1}H NMR** (500MHz, CD_3CN) δ = 9.32 (2H, s, py-H), 8.88 (2H, d, *J* = 8.4 Hz, py-H), 8.56 (2H, d, *J* = 6.1 Hz, py-H), 8.40 (2H, s, triazole CH), 8.13 (2H, dd, *J* = 8.1 Hz, *J* = 6.3 Hz, py-H), 5.19 (4H, s, N^+-CH_2), 4.46 (4H, t, *J*

= 7.2 Hz, -NCH_2), 1.88 - 1.98 (4H, m, -NCH_2CH_2), 1.21 - 1.40 (20H, m, CH_2), 0.88 (6H, t, *J* = 6.9 Hz, CH_3). **^{13}C NMR** (126MHz, CD_3CN) δ = 144.4, 143.6, 142.6, 141.2, 134.2, 130.5, 125.0, 60.9, 51.6, 32.6, 30.8, 29.9, 29.7, 27.1, 23.4, 14.4. **^{19}F NMR** (376 MHz, CD_3CN) δ = -72.9 (d, $^1J_{F,P}$ = 707 Hz).

Macrocycle precursor 41

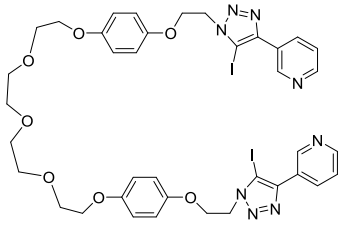

To a solution of bis-azide **40** (100 mg, 0.194 mmol) in THF (2 mL) was added NaI (232 mg, 1.55 mmol) and $Cu(ClO_4)_2.6H_2O$ (287 mg, 0.77 mmol). The mixture was stirred for 5 minutes at room temperature after which TBTA (2.1 mg, 0.004 mmol) and a THF (0.5 mL) solution of DBU (60 mg, 0.39 mmol) were added, followed by 3-ethynyl pyridine (40 mg, 0.39 mmol) and MeCN (2 mL). The mixture was stirred at room temperature for 16 h after which the solvent was removed under vacuum. The crude residue was redissolved in DMSO (20 mL) and addition of an aqueous solution containing EDTA (0.02 M) and NH_4OH (1M) precipitated the pure product which was collected by filtration and dried under vacuum (177 mg, 0.18 mmol, 94%). **^{1}H NMR** (400 MHz, d_6-DMSO) δ = 9.06 (2H, s, py-H), 8.62 (2H, d, *J* = 4.0 Hz, py-H), 8.23 (2H, d, *J* = 7.9 Hz, py-H), 7.55 (2H, dd, *J* = 7.9 Hz, *J* = 4.8 Hz, py-H), 6.84 (8H, s, hydroquinone Ar-H), 4.82 (4H, t, *J* = 5.1 Hz, CH_2), 4.42 (4H, t, *J* = 5.1 Hz, CH_2), 3.95 - 4.01 (4H, m, CH_2), 3.64 - 3.72 (4H, m, CH_2), 3.49 - 3.59 (8H, m, CH_2). **^{13}C NMR** (101MHz, d_6-DMSO) δ = 152.9, 151.8, 149.3, 147.7, 146.3, 134.4, 123.8, 115.5, 115.3, 83.5, 69.9, 69.8, 69.0, 67.5, 66.5, 49.8. **MS** (ESI-MS) *m/z*: 975.11799 $[M + H]^+$ ($C_{38}H_{41}I_2N_8O_7$ calc. 975.11821).

Macrocycle precursor 42

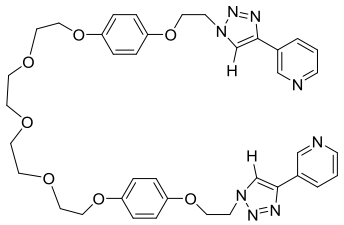

To a solution of bis-azide **40** (100 mg, 0.19 mmol), 3-ethynyl pyridine (40 mg, 0.39 mmol) and TBTA (21 mg, 0.04 mmol) in CH_2Cl_2 (20 mL) was added DIPEA (68 mg, 0.58 mmol) followed by $[Cu(MeCN)_4][PF_6]$ (29 mg, 0.08 mmol). The mixture was stirred at room temperature for 16 h after which the solvent was removed under vacuum. The crude material was purified by silica gel column chromatography (97:3 up to 95:5 CH_2Cl_2/CH_3OH) to afford the product as an orange solid (101 mg, 0.14 mmol, 72%). **^{1}H NMR** (400MHz, $CDCl_3$) δ = 9.04 (2H, br. s., py-H), 8.55 - 8.63 (2H, m, py-H), 8.28 (2H, d, *J* = 7.9 Hz, py-H), 8.10 (2H, s, triazole CH), 7.43 (2H, dd, *J* = 7.9 Hz, *J* = 4.8 Hz, py-H), 6.76 - 6.88 (8H, m, hydroquinone Ar-H), 4.82 (4H, t, *J* = 5.0 Hz, CH_2), 4.35 (4H, t, *J* = 5.0 Hz, CH_2), 4.02 - 4.09 (4H, m, CH_2), 3.79 - 3.85 (4H, m, CH_2), 3.64 - 3.75 (8H, m, CH_2). **MS** (ESI-MS) *m/z*: 723.32471 $[M + H]^+$ ($C_{38}H_{43}N_8O_7$ calc. 723.32492).

XB macrocycle 43·2PF$_6$

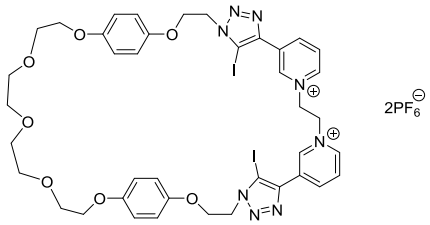

Macrocycle precursor **41** (50 mg, 0.052 mmol) was dissolved in CH_2Cl_2 (18 mL) and a solution of bis-triflate **37** (17 mg, 0.052 mmol) in CH_2Cl_2 (1 mL) was added in one portion. The resultant mixture was stirred at room temperature for 48 h after which the solvent was removed under vacuum and the crude material was purified using silica gel column chromatography (17:2:1 CH_3CN/H_2O/saturated $KNO_{3(aq.)}$). The product was dissolved in

water (6 mL) at 70°C and saturated $NH_4PF_{6(aq.)}$ was added to precipitate **43·2PF$_6$** as a pale yellow solid, which was collected by filtration, washed with H_2O (20 mL) and dried under vacuum (19 mg, 0.15 mmol, 28%). **^{1}H NMR** (400MHz, CD_3CN) δ = 9.17 (2H, d, *J* = 8.4 Hz, py-H), 9.13 (2H, s, py-H), 8.71 (2H, d, *J* = 5.9 Hz, py-H), 8.23 (2H, dd, *J* = 8.1 Hz, *J* = 6.3 Hz, py-H), 6.72 - 6.84 (8H, m, hydroquinone Ar-H), 5.21 (4H, s, N^+-CH_2), 4.81 (4H, t, *J* = 4.9 Hz, CH_2), 4.43 (4H, t, *J* = 4.9 Hz, CH_2), 3.94 - 4.02 (4H, m, CH_2), 3.67 - 3.74 (4H, m, CH_2), 3.51 - 3.62 (8H, m, CH_2). **^{19}F NMR** (377MHz, CD_3CN) δ = -73.0 (d, $^1J_{F,P}$ = 706 Hz). **^{31}P NMR** (162 MHz, d_6-DMSO) δ = -144.2 (septet, $^1J_{P,F}$ = 711 Hz).

HB macrocycle 44·2PF$_6$

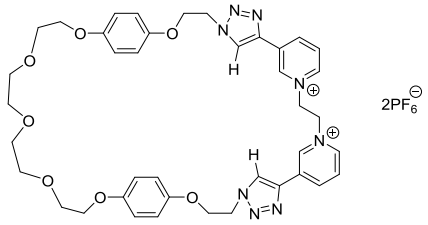

Macrocycle precursor **42** (167 mg, 0.23 mmol) was dissolved in CH_2Cl_2 (80 mL) and a solution of bis-triflate **37** (75 mg, 0.23 mmol) in CH_2Cl_2 (1 mL) was added in one portion. The resultant mixture was stirred at room temperature for 48 h after which the solvent was removed under vacuum and the crude material was purified using silica gel column chromatography (17:2:1 CH_3CN/H_2O/saturated $KNO_{3(aq.)}$). The product was dissolved in water (20 mL) at 70°C and saturated $NH_4PF_{6(aq.)}$ was added to precipitate **44·2PF$_6$** as a yellow solid, which was collected by filtration, washed with H_2O (20 mL) and dried under vacuum (107 mg, 0.10 mmol, 44%). **^{1}H NMR** (400MHz, CD_3CN) δ = 9.13 (2H, s, py-H), 8.92 (2H, d, *J* = 8.2 Hz, py-H), 8.61 (2H, d, *J* = 5.6 Hz, py-H), 8.45 (2H, s, triazole CH), 8.12 - 8.21 (2H, m, py-H), 6.80 (8H, s, hydroquinone Ar-H), 5.17 (4H, s, N^+-CH_2), 4.80 (4H, t, *J* = 4.5 Hz, CH_2), 4.31 - 4.41 (4H, m, CH_2), 3.93 - 4.05 (4H, m, CH_2), 3.67 - 3.78 (4H, m, CH_2), 3.51 - 3.64 (8H, m, CH_2). **^{13}C NMR** (101MHz, CD_3CN) δ = 154.7, 153.2, 144.4, 143.7, 142.5, 141.2, 134.0, 130.6, 125.8, 116.9, 116.6, 71.5, 71.4, 70.4, 69.1, 67.9, 61.1, 51.4. **^{19}F NMR**

(377MHz, CD_3CN) δ = -72.8 (d, $^1J_{F,P}$ = 705 Hz). **^{31}P NMR** (162 MHz, CD_3CN) δ = -144.6 (septet, $^1J_{P,F}$ = 707 Hz).

3,5-bis(iodoethynyl) pyridine 47

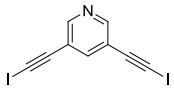

A solution of 3,5-diethynyl pyridine **46** (100 mg, 0.79 mmol) in THF (2.5 mL) was cooled to -78°C and *n*-BuLi (2.5 M in hexanes, 0.69 mL, 1.73 mmol) was added dropwise. The mixture was stirred for 30 min after which a solution of iodine (439 mg, 1.73 mmol) in THF (5 mL) was added dropwise, with the solution left to stir for a further 1h. The mixture was warmed to room temperature and poured into saturated $NaS_2O_{3(aq.)}$. The organics were separated, washed with H_2O (2 x 10 mL) and brine (2 x 10 mL), and then dried over $MgSO_4$, filtered and the solvent removed under vacuum to afford the product as a yellow solid (257 mg, 0.68 mmol, 86%). **^{1}H NMR** (400MHz, $CDCl_3$) δ = 8.59 (2H, d, ^4J = 2.0 Hz, py-H_2, py-H_6), 7.74 (1H, t, ^4J = 2.0 Hz, py-H_4). **MS** (ESI-MS) *m/z*: 379.9 $[M + H]^+$ ($C_9H_4I_2N$ calc. 379.8).

3-azidopropyl 4-methylbenzenesulfonate 48

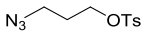

3-Bromopropanol (2.00 g, 14.4 mmol) and sodium azide (1.87 g, 28.8 mmol) were dissolved in H_2O (40 mL) and the mixture was heated at 80°C for 16 h. The solution was cooled to room temperature, extracted with EtOAc (5 x 40 mL) and the organics were dried over $MgSO_4$, filtered and the solvent removed under vacuum. The resulting residue was redissolved in CH_2Cl_2 (100 mL), triethylamine was added (2.57 g, 25.4 mmol) and the solution was cooled to 0°C. *Para*-toluenesulfonyl chloride was then added portionwise over 30 min before the mixture was brought to room temperature and stirred for 16 h. The mixture was then washed with H_2O (75 mL) and the organics were dried over $MgSO_4$, filtered and the solvent removed under vacuum. The crude material was purified by silica gel column chromatography (7:3 up to 1:1 hexane/CH_2Cl_2) to afford the product as a colorless oil (2.54 g,

9.9 mmol, 69%). **^{1}H NMR** (400MHz, $CDCl_3$) δ = 7.81 (2H, d, *J* = 8.2 Hz, Ar-H), 7.37 (2H, d, *J* = 8.2 Hz, Ar-H), 4.12 (2H, t, *J* = 5.9 Hz, -CH_2-O), 3.39 (2H, t, *J* = 6.5 Hz, -CH_2-N), 2.47 (3H, s, CH_3), 1.90 (2H, s, CH_2-C*H*$_2$-CH_2).

Pyridine derivative 49

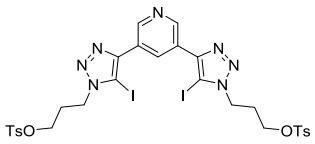

To a solution of 3,5-bis(iodoethynyl) pyridine **47** (100 mg, 0.26 mmol), TBTA (28 mg, 0.05 mmol) and [Cu(MeCN)$_4$][PF_6] (40 mg, 0.11 mmol) in THF (4 mL) was added a solution of azide **48** (135 mg, 0.53 mmol) in THF (1 mL). The mixture was stirred at room temperature for 16 h after which it was diluted with $CHCl_3$ and washed with 0.02 M EDTA/1M NH_4OH(aq.) (20 mL) and brine (2 x 20 mL). The organics were dried over $MgSO_4$, filtered and the solvent removed under vacuum. The crude material was purified by silica gel column chromatography (97:3 CH_2Cl_2/CH_3OH) to afford the product as an off-white solid (201 mg, 0.23 mmol, 86%). ^{1}H NMR (400MHz, $CDCl_3$) δ = 9.22 (2H, d, ^4J = 1.8 Hz, py-H), 8.81 (1H, t, ^4J = 2.0 Hz, py-H), 7.80 (4H, d, *J* = 8.2 Hz, Ar-H), 7.35 (4H, d, *J* = 7.6 Hz, Ar-H), 4.55 (4H, t, *J* = 6.8 Hz, -CH_2-N), 4.16 (4H, t, *J* = 5.8 Hz, -CH_2-O), 2.37 - 2.45 (10H, m, CH_2-C*H*$_2$-CH_2, CH_3). **MS** (ESI-MS) *m/z*: 890.04 $[M + H]^+$ ($C_{29}H_{30}I_2N_7O_6S_2$ calc. 889.98).

Bis-azide 50

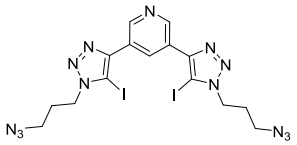

To a solution of pyridine derivative **49** (201 mg, 0.23 mmol) in DMSO (5 mL) was added sodium azide (44 mg, 0.68 mmol). The mixture was stirred at room temperature for 16 h, after which it was diluted with H_2O (20 mL) and extracted with $CHCl_3$ (3 x 25 mL), The organics were washed with H_2O (4 x 25 mL) and then dried over $MgSO_4$, filtered and the solvent

removed under vacuum to yield the product as a cream solid (116 mg, 0.18 mmol, 81%). ^{1}H NMR (500MHz, $CDCl_3$) δ = 9.26 (2H, br. s., py-H), 8.86 (1H, s, py-H), 4.59 (4H, t, *J* = 6.8 Hz, -CH_2-N), 3.48 (4H, t, *J* = 6.2 Hz, CH_2-N_3), 2.27 (4H, quin, *J* = 6.6 Hz, CH_2-C*H*$_2$-CH_2). **MS** (ESI-MS) *m/z*: 632.01 $[M + H]^+$ ($C_{15}H_{16}I_2N_{13}$ calc. 631.97).

Pyridinium axle precursor 51·Cl

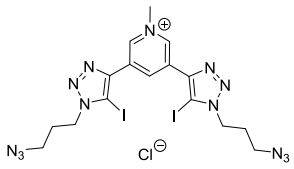

Bis-azide **50** (189 mg, 0.19 mmol) was dissolved in $CHCl_3$ (18 mL) and methyl iodide (2 mL, excess) was added. The mixture was heated at 65^{o}C for 24 h and then cooled to room temperature, with the precipitate formed collected by filtration and washed with $CHCl_3$ (20 mL). The solid was dissolved in CH_2Cl_2 (50 mL) and washed with 1M $NH_4Cl_{(aq.)}$ (8 x 50 mL) and H_2O (2 x 50 mL). The organics were dried over $MgSO_4$, filtered and the solvent removed under vacuum to give **51·Cl** as a yellow solid (14 mg, 0.02 mmol, 11%). ^{1}H NMR (400MHz, 3:1 $CDCl_3$/CD_3OD) δ = 9.93 (1H, s, py-H), 9.42 (2H, s, py-H), 4.62 (4H, t, *J* = 6.9 Hz, -CH_2-N), 4.59 (3H, s, N^+-CH_3), 3.45 (4H, t, *J* = 6.4 Hz, -CH_2-N_3), 2.23 (4H, quin, *J* = 6.6 Hz, CH_2-C*H*$_2$-CH_2). **MS** (ESI-MS) *m/z*: 646.03 $[M - Cl]^+$ ($C_{16}H_{18}I_2N_{13}$ calc. 645.99).

(6^A-*O*-propargyl)-permethylated-β-cyclodextrin 54[7]

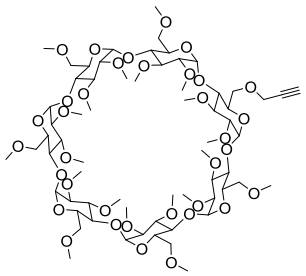

To a solution of propargyl alcohol (446 mg, 7.96 mmol) in dry, degassed DMF (18 mL) was added sodium hydride (60% wt. in mineral oil, 255 mg, 6.37 mmol) in one portion. The suspension was stirred at room temperature for 4 h after which it was cooled to room

temperature and β-cyclodxetrin derivative **53** (250 mg, 0.159 mmol) was added. The mixture was then warmed to room temperature and stirred for a further 16 h before H_2O was added and extractions with EtOAc (4 x 30 mL) were performed. The organics were washed with brine (50 mL) and then dried over $MgSO_4$, filtered and the solvent removed under vacuum. The crude material was purified by silica gel column chromatography (97.5:2.5 EtOAc/MeOH) to afford the product as a glassy solid (183 mg, 0.13 mmol, 79%). **^{1}H NMR** (400MHz, $CDCl_3$) δ = 5.09 - 5.18 (7H, m, CD 1-H), 4.23 (2H, qd, ^2J = 15.9 Hz, ^4J = 2.3 Hz, O-C*H*$_2$CCH), 3.92 (1H, dd, *J* = 10.5 Hz, *J* = 3.7 Hz, CD 6^A-H), 3.16 - 3.89 (101H, m), 2.45 (1H, t, ^4J = 2.3 Hz, O-CH$_2$CC*H*). **MS** (ESI-MS) *m/z*: 1453.88 $[M + H]^+$ ($C_{65}H_{113}O_{35}$ calc. 1453.71).

6.2.3 Experimental details for Chapter 4

Perbenzylated-α-cyclodextrin 58[8]

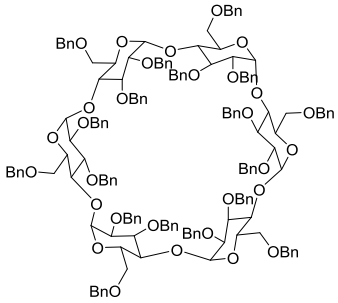

To a solution of dried α-CD (2.00 g, 2.1 mmol) in dry DMSO (42 mL) was added NaH (60% in mineral oil, 2.97 g, 74.2 mmol). Benzyl chloride (9.39 g, 74.2 mmol) was added to the resulting suspension dropwise, over 1 h, and the mixture was left to stir at room temperature for 16h. MeOH (10 mL) was added to quench the remaining NaH, before the mixture was diluted with H_2O (100 mL) and extracted with Et_2O (3 x 100 mL). The organics were washed with brine (100 mL), dried over $MgSO_4$, filtered and the solvent removed under vacuum. The crude material was purified by silica gel column chromatography (1:0 up to 9:1 toluene/EtOAc) to afford the product as a white foam (4.73g, 1.8 mmol, 88%). **^{1}H NMR** (400MHz, $CDCl_3$) δ = 7.09 - 7.26 (90H, m, Ar-H), 5.18 (6H, d, ^2J = 10.9 Hz, CHPh), 5.09

(6H, d, J = 3.3 Hz, 1-H), 4.87 (6H, d, ^2J = 11.0 Hz, CHPh), 4.42 - 4.51 (12H, m, CH_2Ph), 4.40 (6H, d, ^2J = 12.1 Hz, CHPh), 4.31 (6H, d, ^2J = 12.1 Hz, CHPh), 4.14 (6H, t, J = 9.0 Hz, 3-H), 3.95 - 4.08 (12H, m, 4-H, 6-H), 3.90 (6H, d, J = 9.5 Hz, 5-H), 3.42 - 3.55 (12H, m, 2-H, 6-H).

$6^{A,D}$-dihydroxy-perbenzylated-α-cyclodextrin 59[8]

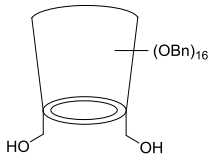

DIBAL-H (25% wt. in toluene, 57 mL, 85.5 mmol) was added dropwise to perbenzylated-α-CD **58** (3.70 g, 1.4 mmol) and the resulting solution was stirred at 50°C for 16 h. The reaction mixture was then cooled to room temperature and poured on to ice (~ 300 g). 1M $HCl_{(aq.)}$ (15 mL) and EtOAc (300 mL) were added and the slurry formed was stirred vigorously for 30 min, after which the mixture was filtered. The organics were separated and the aqueous phase was washed with EtOAc (200 mL). The combined organics were then washed with brine (250 mL), dried over $MgSO_4$, filtered and the solvent removed under vacuum. The crude material was purified by column chromatography (cyclohexane/EtOAc 3:1) to afford the product as a white foam (2.48 g, 1.03 mmol, 72%). **^{1}H NMR** (400MHz, $CDCl_3$) δ = 7.04 - 7.34 (80H, m, Ar-H), 5.71 (2H, d, J = 3.9 Hz, 1-H), 5.44 (2H, d, ^2J = 10.4 Hz, CHPh), 5.18 (2H, d, ^2J = 10.6 Hz, CHPh), 4.83 - 4.93 (4H, m, 2 x CHPh), 4.67 - 4.81 (10H, m, 3 x CHPh, 1-H), 4.28 - 4.58 (18H, m, 9 x CHPh), 4.17 - 4.23 (2H, m, 3-H), 3.61 - 4.12 (28H, m, 3-H, 4-H, 5-H, 6-H), 3.57 (2H, dd, J = 9.7 Hz, J = 3.7 Hz, 2-H), 3.37 - 3.45 (4H, m, 2-H), 3.25 (2H, br. s, OH). **MS** (ESI-MS) *m/z*: 2415.28 $[M + H]^+$ ($C_{148}H_{157}O_{30}$ calc. 2415.08).

$6^{A,D}$-*O*-dimethylsulfonyl-perbenzylated-α-cyclodextrin 60[9]

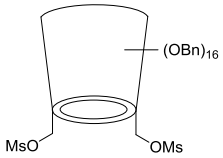

To a solution of diol **59** (105 mg, 0.044 mmol) in CH_2Cl_2 (2 mL) was added triethylamine (18 mg, 0.17 mmol) and methanesulfonyl chloride (20 mg, 0.17 mmol). The mixture was stirred at room temperature for 90 min after which it was washed with saturated $NaHCO_{3(aq.)}$ (10 mL) and H_2O (10 mL). The organics were dried over $MgSO_4$, filtered and the solvent removed under vacuum, with the crude material purified by silica gel column chromatography (3:1 cyclohexane/EtOAc) to afford the product as a white solid (101 mg, 0.039 mmol, 90%). **^{1}H NMR** (400MHz, $CDCl_3$) δ = 7.06 - 7.34 (80H, m, Ar-H), 5.34 (2H, d, ^2J = 10.8 Hz, CH-Ph), 5.17 (2H, d, ^2J = 10.8 Hz, CH-Ph), 5.12 (2H, d, J = 3.7 Hz, 1-H), 5.03 (2H, d, ^2J = 11.4 Hz, CHPh), 4.79 - 4.96 (12H, m, 4 x CHPh, 1-H), 4.31 - 4.60 (20H, m, 9 x CHPh, 6-H), 3.88 - 4.30 (22H, m, 3-H, 4-H, 5-H, 6-H), 3.74 (2H, d, ^2J = 10.4 Hz, 6-H), 3.62 (2H, t, J = 9.0 Hz, 4-H), 3.46 - 3.56 (4H, m, 2-H, 6-H), 3.43 (2H, dd, J = 9.8 Hz, J = 3.2 Hz, 2-H), 3.37 (2H, dd, J = 9.7 Hz, J = 3.2 Hz, 2-H), 2.68 (6H, s, mesyl CH_3) **MS** (ESI-MS) *m/z*: 2571.26 $[M + H]^+$ ($C_{150}H_{161}O_{34}S_2$ calc. 2571.03).

$6^{A,D}$-*O*-dimethylsulfonyl-α-cyclodextrin 61[10]

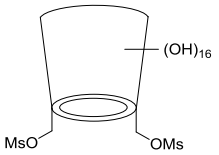

Compound **60** (100 mg, 0.039 mmol) was dissolved in 1:1 EtOAc/MeOH (8 mL) and 10% Pd/C (41 mg, 0.039 mmol) was added. The resulting suspension was placed under a $H_{2(g)}$ atmosphere (~ 5 bar) and stirred at room temperature for 24 h, after which it was filtered through Celite, which was washed with MeOH (20 mL). The solvent was removed under vacuum to afford the product as a white solid (44 mg, > 99%). ^{1}H NMR (400MHz, d_6-

DMSO) δ = 5.52 - 5.81 (12H, m, 2-OH, 3-OH), 4.89 (2H, d, *J* = 3.2 Hz, 1-H), 4.87 (2H, d, *J* = 3.2 Hz, 1-H), 4.80 (2H, d, *J* = 3.2 Hz, 1-H), 4.71 (2H, br. s., 6-OH), 4.54 - 4.61 (2H, m, 6-H), 4.30 (2H, d, ^{2}J = 9.9 Hz, 6-H), 4.08 (2H, br. s, 6-OH), 3.88 - 3.97 (2H, m, 5-H), 3.47 - 3.83 (18H, m, 3-H, 5-H, 6-H), 3.26 – 3.46 (12H, m, 2-H, 4-H), 3.19 (6H, s, mesyl CH_3). **MS** (ESI-MS) *m/z*: 1151.38 $[M + Na]^+$ ($C_{38}H_{64}O_{34}S_2Na$ calc. 1151.26).

$6^{A,D}$-dihydroxy-permethylated-α-cyclodextrin 63[11]

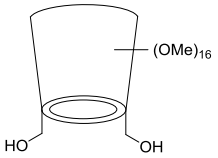

To a solution of diol **59** (1.23 g, 0.51 mmol) in CH_2Cl_2 (7 mL) was added camphorsulfonic acid (2.3 mg, 0.012 mmol) and dihydropyran (129 mg, 1.53 mmol). The mixture was stirred at room temperature for 4 h, after which triethylamine (0.73 mL) and CH_2Cl_2 (40 mL) were added and the mixture was washed with H_2O (3 x 20 mL). The organics were dried over $MgSO_4$, filtered and the solvent removed under vacuum. The residue was redissolved in 7:3 THF/H_2O (50 mL), 10% Pd/C (1.00 g) was added and the mixture was placed under a $H_{2(g)}$ atmosphere (~ 5 bar). It was then stirred at room until ESI-mass spectrometry had confirmed that all of the benzyl groups had been removed (~ 4 days), before it was filtered through Celite, which was washed with 1:1 MeOH/H_2O (100 mL). The solvent was removed under vacuum and the residue was redissolved in dry, degassed DMF (50 mL). The solution was then cooled to 0^{o}C and NaH (60% in mineral oil, 0.98 g, 24.5 mmol) and MeI (3.48 g, 24.5 mmol) were added. The mixture was warmed to room temperature and stirred for 4 h after which, H_2O (50 mL) was added to quench the remaining NaH. The mixture was then extracted with Et_2O (5 x 40 mL) and the combined organics were washed with H_2O (8 x 40 mL). The organics were dried over $MgSO_4$, filtered and the solvent removed under vacuum, with the resulting residue suspended in 80% acetic $acid_{(aq.)}$ and stirred at 40^{o}C for 2 h. The acetic acid was removed under vacuum and co-evaporated with toluene (3 x 20 mL) and the

crude material was purified by silica gel column chromatography (1:0 up to 9:1 EtOAc/MeOH) to afford the product as a white solid (261 mg, 0.22 mmol, 43%). **^{1}H NMR** (400MHz, CD_3OD) δ = 5.11 (2H, d, *J* = 3.3 Hz, 1-H), 5.08 (2H, d, *J* = 3.3 Hz, 1-H), 5.05 (2H, d, *J* = 3.3 Hz, 1-H), 3.99 (2H, dd, *J* = 12.2 Hz, *J* = 3.7 Hz), 3.71 - 3.89 (12H, m,), 3.47 - 3.70 (52H, m,), 3.38 (6H, s, 6-OMe), 3.37 (6H, s, 6-OMe), 3.09 - 3.18 (6H, m, 2-H). **MS** (ESI-MS) *m/z*: 1214.64 $[M + NH_4]^+$ ($C_{52}H_{96}NO_{30}$ calc. 1214.60).

$6^{A,D}$-diazido-permethylated-α-cyclodextrin 65

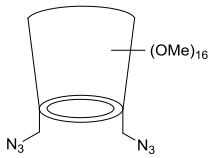

To a solution of diol **63** (200 mg, 0.17 mmol) in CH_2Cl_2 (8 mL) was added triethylamine (68 mg, 0.67 mmol) and methanesulfonyl chloride (77 mg, 0.67 mmol). The mixture was stirred at room temperature for 16 h after which it was washed with saturated $NaHCO_{3(aq.)}$ (10 mL) and H_2O (20 mL). The organics were dried over $MgSO_4$, filtered and the solvent removed under vacuum. The residue was redissolved in dry, degassed DMF (3 mL) and sodium azide (87 mg, 1.34 mmol) was added, with the mixture stirred at 80^{o}C for 16 h. The reaction was then cooled to room temperature, H_2O (10 mL) was added and the mixture was extracted with Et_2O (5 x 20 mL). The organics were washed with brine (50 mL), dried over $MgSO_4$, filtered and the solvent removed under vacuum to afford the product as a glassy solid (200 mg, 0.16 mmol, 96 %). **^{1}H NMR** (400MHz, $CDCl_3$) δ = 5.04 - 5.08 (4H, m, 1-H), 5.02 (2H, d, *J* = 3.4 Hz, 1-H), 3.97 (2H, dd, ^2J = 10.7 Hz, *J* = 3.2 Hz, 6-H), 3.36 - 3.91 (76H, m, OCH_3, 3-H, 4-H, 5-H, 6-H), 3.13 - 3.22 (6H, m, 2-H). **MS** (ESI-MS) *m/z*: 1269.63 $[M + Na]^+$ ($C_{52}H_{90}N_6O_{28}Na$ calc. 1269.57).

Bis-iodotriazole derivative 66

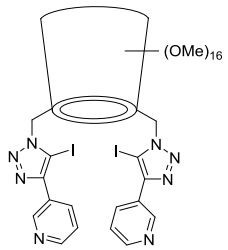

To a solution of bis-azide **65** (40 mg, 0.032 mmol), 3-iodoethynyl pyridine (15 mg, 0.064 mmol) and TBTA (3.4 mg, 0.006 mmol) in THF (2 mL) was added $[Cu(MeCN)_4][PF_6]$ (4.8 mg, 0.013 mmol). The mixture was stirred at room temperature for 16 h after which it was diluted with CH_2Cl_2 (20 mL) and washed with 0.02 M EDTA/1M $NH_4OH_{(aq.)}$ (20 mL) and brine (2 x 20 mL). The organics were dried over $MgSO_4$, filtered and the solvent removed under vacuum. The crude material was purified by preparative thin layer chromatography (93:7 CH_2Cl_2/MeOH) to afford the product as a white solid (55 mg, > 99%). **^{1}H NMR** (400MHz, $CDCl_3$) δ = 9.27 (2H, br. s., py-H), 8.59 (2H, br. s., py-H), 8.31 (2H, d, *J* = 7.9 Hz, py-H), 7.35 (2H, br. s., py-H), 5.26 - 5.30 (2H, m, 6-H), 5.14 (2H, d, *J* = 3.3 Hz, 1-H), 5.03 (2H, d, *J* = 3.2 Hz, 1-H), 4.93 (2H, d, *J* = 3.1 Hz, 1-H), 4.48 - 4.68 (4H, m, 5-H, 6-H), 4.14 (2H, d, *J* = 9.0 Hz), 3.46 - 3.80 (52H, m, 2-OMe, 3-OMe, 3-H, 4-H, 5-H, 6-H), 3.42 (2H, t, *J* = 9.0 Hz, 4-H), 3.20 - 3.28 (4H, m, 2-H), 3.13 (6H, s, 6-OMe), 3.10 (2H, dd, *J* = 10.0 Hz, *J* = 3.2 Hz, 2-H), 3.01 (6H, s, 6-OMe), 2.78 - 2.84 (2H, m, 6-H), 2.71 - 2.77 (2H, m, 6-H). **MS** (ESI-MS) *m/z*: 1727.44807 $[M + Na]^+$ ($C_{66}H_{98}I_2N_8O_{28}Na$ calc. 1727.44721).

Bis-prototriazole derivative 67

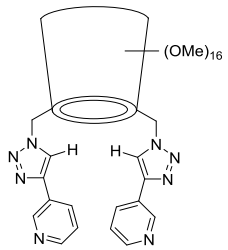

To a solution of bis-azide **65** (40 mg, 0.032 mmol), 3-ethynyl pyridine (6.6 mg, 0.064 mmol) and TBTA (3.4 mg, 0.006 mmol) in CH_2Cl_2 (2 mL) was added DIPEA (12 mg, 0.096 mmol) followed by $[Cu(MeCN)_4][PF_6]$ (4.8 mg, 0.013 mmol). The mixture was stirred at room temperature for 16 h after which it was diluted with CH_2Cl_2 (20 mL) and washed with 0.02 M EDTA/1M $NH_4OH_{(aq.)}$ (20 mL) and brine (2 x 20 mL). The organics were dried over $MgSO_4$, filtered and the solvent removed under vacuum. The crude material was purified by preparative thin layer chromatography (93:7 CH_2Cl_2/MeOH) to afford the product as a white solid (40 mg, 86%). **^{1}H NMR** (400MHz, $CDCl_3$) δ = 8.79 (2H, s, py-H), 8.41 - 8.49 (2H, m, py-H), 8.02 - 8.11 (4H, m, py-H, triazole CH), 7.19 (2H, dd, *J* = 7.8 Hz, *J* = 4.9 Hz, py-H), 5.15 - 5.27 (4H, m, 1H, 6-H), 4.95 - 5.05 (4H, m, 1-H), 4.69 (2H, dd, ^2J = 14.4 Hz, *J* = 8.2 Hz, 6-H), 4.29 - 4.41 (2H, m, 5-H), 4.06 (2H, dd, *J* = 8.8 Hz, *J* = 2.7 Hz, 5-H), 3.42 - 3.72 (52H, m, 2-OMe, 3-OMe, 3-H, 4-H, 5-H, 6-H,), 3.29 (2H, t, *J* = 9.1 Hz, 4-H), 3.22 (2H, dd, *J* = 9.4 Hz, *J* = 3.2 Hz, 2-H), 3.09 - 3.18 (16H, m, 6-OMe, 2-H), 3.02 - 3.08 (2H, m, 6-H), 2.96 (2H, d, ^2J = 10.6 Hz, 6-H). **^{13}C NMR** (101MHz, $CDCl_3$) δ = 149.1, 146.7, 144.4, 132.7, 126.6, 123.6, 121.8, 100.4, 100.2, 99.2, 84.4, 82.4, 82.1, 81.9, 81.8, 81.5, 81.2, 81.1, 81.0, 71.3, 71.2, 71.0, 70.5, 69.9, 61.8, 61.8, 61.6, 59.1, 58.9, 58.1, 58.0, 57.9, 52.0. **MS** (ESI-MS) *m/z*: 1475.65528 $[M + Na]^+$ ($C_{66}H_{100}N_8O_{28}Na$ calc. 1475.65393).

XB receptor 68·2NO$_3$

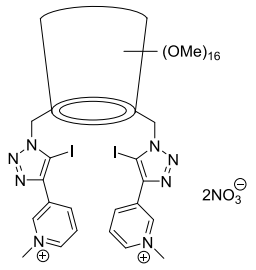

Bis-iodotriazole derivative **66** (55 mg, 0.032 mmol) was dissolved in $CHCl_3$ (2.5 mL) and methyl iodide (0.7 mL) was added. The mixture was stirred at 40^{o}C for 48 h after which, it was cooled to room temperature and the solvent removed under vacuum. The residue was redissolved in 3:1 MeOH/H_2O (20 mL) and passed through a nitrate-loaded Amberlite® column five times. The solvent was removed under vacuum to afford **68·2NO$_3$** as an off-white solid (55 mg, 0.029 mmol, 92%). **^{1}H NMR** (500MHz, $CDCl_3$) δ = 9.42 (2H, br. s., py-H), 9.10 - 9.19 (2H, m, py-H), 9.01 (2H, d, *J* = 8.1 Hz, py-H), 8.14 (2H, t, *J* = 6.6 Hz, py-H), 5.15 - 5.24 (4H, m, 1-H, 6-H), 5.02 (2H, br. s., 1-H), 4.88 (2H, br. s., 1-H), 4.53 - 4.70 (10H, m, N^+-CH_3, 5-H, 6-H), 4.10 (2H, d, *J* = 7.0 Hz, 5-H), 3.82 (2H, d, *J* = 10.1 Hz,), 3.44 - 3.73 (52H, m, 2-OMe, 3-OMe, 3-H, 4-H, 5-H, 6-H), 3.24 (8H, s, 6-OMe, 2-H), 3.16 - 3.21 (2H, m, 2-H), 3.08 - 3.15 (2H, m, 2-H), 2.93 (6H, s, 6-OMe), 2.76 - 2.87 (4H, m, 6-H). **^{13}C NMR** (126MHz, $CDCl_3$) δ = 145.6, 142.5, 142.2, 141.2, 131.3, 128.6, 100.7, 100.4, 98.8, 84.9, 83.3, 82.4, 82.2, 82.1, 81.7, 81.4, 81.1, 81.0, 71.6, 71.4, 71.3, 70.1, 69.7, 61.9, 61.8, 61.7, 59.3, 59.3, 58.4, 57.9, 57.8, 52.6, 49.2. **MS** (ESI-MS) *m/z*: 867.25132 [M - 2NO_3]$^{2+}$ ($C_{68}H_{104}I_2N_8O_{28}$ calc. 867.25192).

HB receptor 69·2NO$_3$

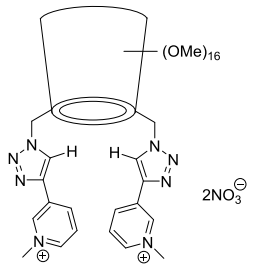

Bis-prototriazole derivative **67** (30 mg, 0.023 mmol) was dissolved in $CHCl_3$ (2 mL) and methyl iodide (0.5 mL) was added. The mixture was stirred at 40^{o}C for 48 h after which, it was cooled to room temperature and the solvent removed under vacuum. The residue was redissolved in 3:1 MeOH/H_2O (20 mL) and passed through a nitrate-loaded Amberlite® column five times. The solvent was removed under vacuum to afford **69·2NO$_3$** as a pale-orange solid (35 mg, 0.022 mmol, 95%). **^{1}H NMR** (500MHz, $CDCl_3$) δ = 9.57 (2H, br. s., py-H), 8.96 (2H, d, *J* = 7.6 Hz, py-H), 8.78 (2H, s, triazole CH), 8.68 (2H, br. s., py-H), 7.97 (2H, br. s., py-H), 5.18 - 5.25 (2H, m, 1-H), 5.01 - 5.11 (4H, m, 1-H, 6-H), 4.86 (2H, br. s., 1-H), 4.71 - 4.79 (2H, m, 5-H), 4.48 - 4.61 (8H, m, N^+-CH_2, 6-H), 4.21 (2H, d, *J* = 8.1 Hz, 5-H), 3.78 - 3.92 (6H, m), 3.43 - 3.76 (46H, m), 3.38 (2H, t, *J* = 9.1 Hz, 4-H), 3.32 (6H, s, 6-OMe), 3.21 - 3.27 (2H, m, 2-H), 3.09 - 3.18 (4H, m, 2-H), 2.91 - 3.00 (8H, m, 6-OMe, 6-H), 2.79 (2H, d, ^2J = 10.7 Hz, 6-H). **^{13}C NMR** (126MHz, $CDCl_3$) δ = 143.8, 141.7, 140.1, 139.6, 132.2, 128.4, 125.7, 100.6, 100.2, 98.3, 83.9, 82.4, 82.2, 82.2, 81.6, 81.3, 81.2, 71.7, 71.4, 71.0, 70.3, 68.9, 61.9, 61.8, 61.6, 59.1, 59.0, 58.8, 57.9, 57.8, 52.4, 48.8. **MS** (ESI-MS) *m/z*: 741.35553 $[M - 2NO_3]^{2+}$ ($C_{68}H_{106}N_8O_{28}$ calc. 741.35528).

Strapped bis-prototriazole derivative 70

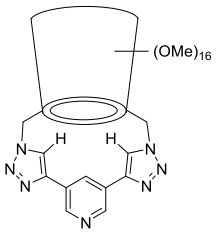

A solution of bis-azide **65** (45 mg, 0.036 mmol) and 3,5-diethynyl pyridine **46** (4.6 mg, 0.036 mmol) in CH_2Cl_2 (3.6 mL) was added to a solution of TBTA (7.7 mg, 0.015 mmol) and $[Cu(MeCN)_4][PF_6]$ (5.4 mg, 0.015 mmol) in CH_2Cl_2 (3.6 mL), in one portion. DIPEA (14 mg, 0.11 mmol) was then added and the mixture was left to stir at room temperature for 4 days. The mixture was then washed with 0.02 M EDTA/1M $NH_4OH_{(aq.)}$ (10 mL) and brine (2 x 10 mL), following which, the organics were dried over $MgSO_4$, filtered and the solvent removed under vacuum. The crude material was purified by preparative thin layer chromatography (95:5 CH_2Cl_2/MeOH) to afford the product as a pale yellow solid (24 mg, 0.017 mmol, 46%). **^{1}H NMR** (400MHz, $CDCl_3$) δ = 9.29 (2H, d, ^4J = 1.7 Hz, py-H), 7.89 (2H, s, triazole CH), 7.66 (1H, s, py-H), 5.20 (2H, d, ^2J = 13.9 Hz, 6-H), 5.09 (2H, d, J = 3.3 Hz, 1-H), 5.02 (2H, d, J = 2.4 Hz, 1-H), 4.96 (2H, d, J = 3.5 Hz, 1-H), 4.64 (2H, dd, ^2J = 14.2 Hz, J = 10.5 Hz, 6-H), 4.22 (2H, t, J = 9.7 Hz, 5-H), 4.02 (2H, dd, J = 9.5 Hz, J = 5.9 Hz), 3.93 (2H, dd, J = 9.7 Hz, J = 3.2 Hz), 3.78 (2H, d, J = 9.8 Hz), 3.41 - 3.71 (48H, m), 3.31 (2H, t, J = 8.6 Hz, 4-H), 3.17 - 3.26 (6H, m, 2-H), 3.01 (2H, d, ^2J = 9.8 Hz, 6-H), 2.91 (6H, s, 6-OMe), 2.77 - 2.85 (8H, m, 6-OMe, 6-H). **^{13}C NMR** (101MHz, $CDCl_3$) δ = 146.2, 145.4, 130.7, 126.4, 120.9, 100.6, 100.5, 100.4, 85.6, 83.6, 82.4, 82.1, 81.9, 81.7, 81.1, 80.9, 80.6, 73.3, 72.5, 71.5, 70.3, 62.1, 61.8, 61.7, 59.2, 58.5, 58.1, 58.0, 57.9, 53.4, 52.7. **MS** (ESI-MS) *m/z*: 1374.62785 $[M + H]^+$ ($C_{61}H_{96}N_7O_{28}$ calc. 1374.62978).

Strapped bis-iodotriazole derivative 71

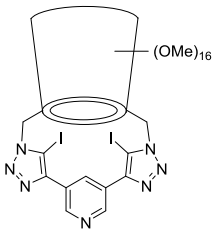

A solution of bis-azide **65** (50 mg, 0.040 mmol) and 3,5-bis(iodoethynyl) pyridine **47** (15 mg, 0.040 mmol) in THF (3.4 mL) was added to a solution of TBTA (7.8 mg, 0.016 mmol) and $[Cu(MeCN)_4][PF_6]$ (5.5 mg, 0.016 mmol) in THF (4 mL), in one portion. The resulting mixture was left to stir at room temperature for 7 days after which, the solvent was removed under vacuum. The residue was redissolved in CH_2Cl_2 (30 mL) and washed with 0.02 M EDTA/1M $NH_4OH_{(aq.)}$ (20 mL) and brine (2 x 20 mL), following which, the organics were dried over $MgSO_4$, filtered and the solvent removed under vacuum. The crude material was purified by preparative thin layer chromatography (93:7 CH_2Cl_2/MeOH) to afford the product as a pale yellow solid (13 mg, 0.008 mmol, 20%). **^{1}H NMR** (500MHz, $CDCl_3$) δ = 9.19 - 9.27 (3H, m, py-H), 5.32 (2H, br. s., 1-H), 5.04 - 5.09 (2H, m, 1-H), 5.00 - 5.04 (2H, m, 1-H), 4.75 - 4.91 (4H, m, 6-H), 4.51 (2H, d, *J* = 8.4 Hz), 4.29 (2H, t, *J* = 8.0 Hz, 5-H), 3.91 (2H, t, *J* = 8.9 Hz), 3.84 (2H, t, *J* = 7.9 Hz), 3.32 - 3.76 (52H, m), 3.13 - 3.26 (16H, m, 6-OMe, 2-H), 3.10 (2H, d, ^2J = 10.2 Hz, 6-H), 3.01 (2H, d, ^2J = 8.7 Hz, 6-H). **^{13}C NMR** (126MHz, $CDCl_3$) δ = 147.3, 146.6, 137.1, 125.5, 99.1, 98.5, 97.2, 83.2, 82.0, 81.8, 81.6, 80.8, 80.6, 79.7, 78.7, 72.3, 72.2, 71.2, 71.0, 69.5, 61.5, 61.4, 60.1, 59.2, 59.1, 58.8, 58.6, 57.2, 54.4. **MS** (ESI-MS) *m/z*: 1626.41915 $[M + H]^+$ ($C_{61}H_{94}I_2N_7O_{28}$ calc. 1626.42307).

Strapped HB receptor 73·NO_3

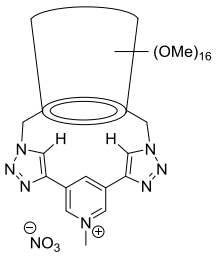

Bis-prototriazole derivative **70** (24 mg, 0.017 mmol) was dissolved in $CHCl_3$ (2.5 mL) and methyl iodide (0.5 mL) was added. The mixture was stirred at 40°C for 24 h after which, it was cooled to room temperature and the solvent removed under vacuum. The residue was redissolved in 3:1 MeOH/H_2O (20 mL) and passed through a nitrate-loaded Amberlite® column five times. The solvent was removed under vacuum to afford **73·NO_3** as a white solid (25 mg, 0.017 mmol, 99%). **^{1}H NMR** (500MHz, D_2O) δ = 9.43 (1H, s, py-H), 9.35 (2H, s, py-H), 9.32 (2H, s, triazole CH), 5.35 (2H, d, *J* = 3.4 Hz, 1-H), 5.27 (2H, d, ^2J = 13.7 Hz, 6-H), 5.17 (2H, d, *J* = 2.4 Hz, 1-H), 5.06 (2H, d, *J* = 3.2 Hz, 1-H), 4.79 - 4.82 (4H, m, 5-H, 6-H), 4.59 (3H, s, N^+-CH_3), 4.30 - 4.36 (2H, m,), 3.99 (2H, dd, *J* = 10.4 Hz, *J* = 8.2 Hz), 3.91 (2H, d, *J* = 9.9 Hz, 5-H), 3.80 (2H, t, *J* = 9.7 Hz), 3.52 - 3.75 (36H, m), 3.49 (6H, s, OMe), 3.45 (6H, s, OMe), 3.40 (2H, dd, *J* = 10.5 Hz, *J* = 2.5 Hz, 2-H), 3.32 (2H, dd, *J* = 10.2 Hz, *J* = 3.5 Hz, 2-H), 3.18 (2H, dd, *J* = 10.1 Hz, *J* = 3.2 Hz, 2-H), 3.01 - 3.09 (4H, m, 6-H), 2.85 (6H, s, 6-OMe), 2.66 (6H, s, 6-OMe). ^{13}C NMR (101MHz, 1:1 $CDCl_3$/CD_3OD) δ = 141.9, 139.6, 139.2, 133.8, 127.7, 101.4, 101.0, 100.7, 86.9, 83.9, 83.4, 83.3, 83.1, 82.9, 82.2, 81.6, 81.1, 72.4, 72.3, 71.5, 71.2, 62.6, 62.4, 62.3, 59.1, 58.6, 58.2, 58.2, 58.2, 54.9. **MS** (ESI-MS) *m/z*: 1388.64108 $[M - NO_3]^+$ ($C_{62}H_{98}N_7O_{28}$ calc. 1388.64543).

Strapped XB receptor 74·NO_3

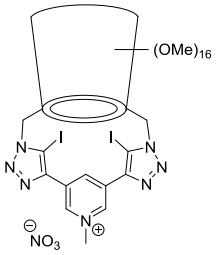

Bis-iodotriazole derivative **71** (8.4 mg, 0.005 mmol) was dissolved in $CHCl_3$ (0.8 mL) and methyl iodide (0.2 mL) was added. The mixture was stirred at 40°C for 24 h after which, it was cooled to room temperature and the solvent removed under vacuum. The residue was redissolved in 3:1 MeOH/H_2O (10 mL) and passed through a nitrate-loaded Amberlite® column five times. The solvent was removed under vacuum to afford **74·NO_3** as an off-white solid (8.5 mg, 0.005 mmol, 96%). **^{1}H NMR** (500MHz, D_2O) δ = 9.91 (1H, s, py-H), 9.49 - 9.57 (2H, m, py-H), 5.36 - 5.44 (2H, m, 1-H), 5.23 (2H, d, *J* = 2.5 Hz, 1-H), 5.15 (2H, d, *J* = 3.2 Hz, 1-H), 4.96 - 5.09 (4H, m, 6-H), 4.68 (3H, s, N^+-CH_3), 4.41 - 4.48 (2H, m, 5-H), 4.26 - 4.35 (2H, m), 3.95 - 4.03 (4H, m), 3.84 (2H, t, *J* = 9.0 Hz), 3.43 - 3.73 (48H, m), 3.31 - 3.40 (4H, m), 3.25 (2H, dd, *J* = 9.5 Hz, *J* = 3.2 Hz, 2-H), 3.11 - 3.23 (16H, m, 6-OMe, 6-H). **^{13}C NMR** (126MHz, D_2O) δ = 144.6, 143.1, 142.9, 130.9, 99.1, 98.3, 97.9, 84.9, 81.5, 81.3, 80.9, 80.8, 80.5, 80.1, 80.0, 78.7, 78.3, 72.3, 72.2, 71.4, 71.1, 70.7, 61.2, 60.3, 59.2, 58.9, 58.9, 58.8, 57.9, 57.7, 55.3, 50.2. **MS** (ESI-MS) *m/z*: 1640.43343 $[M - NO_3]^+$ ($C_{62}H_{96}I_2N_7O_{28}$ calc. 1640.43872).

6.2.4 Experimental details for Chapter 5

***N,N*-dibenzyl-3-bromoaniline 75**[12]

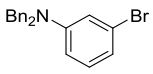

To a suspension of 3-bromoaniline (2.99 g, 17.4 mmol) and K_2CO_3 (7.00 g, 50.6 mmol) in MeCN (100 mL) was added benzyl bromide (10.0 g, 58.5 mmol). The resulting mixture was heated at reflux for 4 h after which it was cooled to room temperature and H_2O (300 mL) was

added. The solution was extracted with EtOAc (300 mL) and the organics were dried over $MgSO_4$, filtered and the solvent removed under vacuum. The crude material was purified by silica gel column chromatography (97:3 hexane/EtOAc) to afford the product as an off-white solid (5.24 g, 15.0 mmol, 86%). **^{1}H NMR** (300 MHz, $CDCl_3$) δ = 7.19 - 7.41 (10H, m, -Ph), 7.01 (1H, t, *J* = 8.2 Hz, Ar-H), 6.90 (1H, t, *J* = 2.3 Hz, Ar-H), 6.79 - 6.86 (1H, m, Ar-H), 6.60 - 6.69 (1H, m, Ar-H), 4.64 (4H, s, CH_2) **MS** (ESI-MS) *m/z*: 352.1 $[M + H]^+$ ($C_{20}H_{19}BrN$ calc. 352.1).

Triarylborane derivative 76[12]

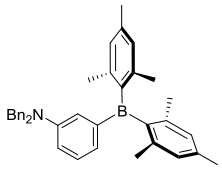

A solution of *N*,*N*-dibenzyl-3-bromoaniline (1.8 g, 5.1 mmol) in THF (60 mL) was cooled to -78^{o}C and *n*-BuLi (1.6 M in hexanes, 3.5 mL, 5.6 mmol) was added dropwise. The mixture was stirred for 1h after which a solution of $FBMes_2$ (1.6 g, 6.1 mmol) in THF (20 mL) was added and the solution was left to stir for a further 1 h. The mixture was then warmed to room temperature and left to stir overnight. H_2O (~5 mL) was added to quench the unreacted *n*-BuLi and the solvent was removed under vacuum, with the resulting residue redissolved in CH_2Cl_2 (100 mL) and washed with saturated $NH_4Cl_{(aq.)}$ (100 mL) and H_2O (100 mL). The organics were dried over $MgSO_4$, filtered and the solvent removed under vacuum. The crude material was purified by silica gel column chromatography (4:1 hexanes/CH_2Cl_2) to afford the product as a pale green solid (1.88 g, 3.5 mmol, 71%). **^{1}H NMR** (400 MHz, $CDCl_3$) δ = 7.22 - 7.30 (8H, m, -Ph, Ar-H), 7.10 - 7.18 (5H, m, -Ph, Ar-H), 6.87 (1H, br. s., Ar-H), 6.72 (4H, s, Mes), 4.55 (4H, s, CH_2), 2.28 (6H, s, Mes), 1.93 (12H, s, Mes) **MS** (ESI-MS) *m/z*: 522.4 $[M + H]^+$ ($C_{38}H_{41}BN$ calc. 522.3).

Aniline derivative 77[12]

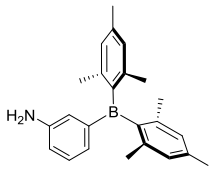

To a solution of **76** (1.00 g, 1.92 mmol) in EtOH (85 mL) was added Pd/C (5% wt., 211 mg) and *para*-toluenesulfonic acid (236 mg, 1.24 mmol). The resulting suspension was stirred at room temperature under a $H_{2(g)}$ atmosphere for 48 h after which it was filtered through Celite and the solvent removed under vacuum. The residue was suspended in 1M $NaOH_{(aq.)}$ (100 mL) and extracted into CH_2Cl_2 (2 x 100 mL). The organics were washed with H_2O (100 mL), dried over $MgSO_4$, filtered and the solvent removed under vacuum. The crude material was purified by silica gel column chromatography (1:1 hexanes/CH_2Cl_2) to afford the product as an off-white solid (492 mg, 1.44 mmol, 75%). **^{1}H NMR** (400 MHz, $CDCl_3$) δ = 7.17 (1H, t, *J* = 7.5 Hz, Ar-H), 6.96 (1H, d, *J* = 7.3 Hz, Ar-H), 6.84 - 6.89 (2H, m, Ar-H), 6.82 (4H, s, Mes), 4.07 (2H, br. s., NH_2), 2.31 (6H, s, Mes), 2.02 (12H, s, Mes) **MS** (ESI-MS) *m/z*: 342.2 $[M + H]^+$ ($C_{24}H_{29}BN$ calc. 342.2).

Pyridine derivative 80[13]

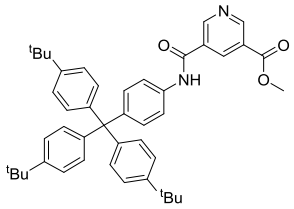

To a suspension of acid **79** (250 mg, 1.38 mmol) in CH_2Cl_2 (30 mL) was added oxalyl chloride (350 mg, 2.76 mmol) and DMF (1 drop, cat.). The mixture was stirred at room temperature, until homogenous, and the solvent was then removed under vacuum. The residue was redissolved in CH_2Cl_2 (30 mL) and added dropwise to a solution of terphenyl amine **15** (696 mg, 1.38 mmol) and triethylamine (282 mg, 2.76 mmol) in CH_2Cl_2 (50 mL) cooled to 0^oC. The mixture was warmed to room temperature and left to stir at room temperature for 2 h

after which it was washed with 10% citric acid$_{(aq.)}$ (2 x 50 mL), saturated $NaHCO_{3(aq.)}$ (2 x 50 mL) and H_2O (2 x 50 mL). The organics were dried over $MgSO_4$, filtered and the solvent was removed under vacuum. The crude material was purified by silica gel column chromatography (99:1 CH_2Cl_2/CH_3OH) to afford the product as an off-white solid (704 mg, 1.06 mmol, 76%). **^{1}H NMR** (400 MHz, $CDCl_3$) δ = 9.36 (1H, d, ^4J = 2.0 Hz, py-H), 9.28 (1H, d, ^4J = 2.2 Hz, py-H), 8.73 (1H, t, ^4J = 2.0 Hz, py-H), 7.86 (1H, s, NH), 7.52 (2H, d, J = 8.7 Hz, NAr-H), 7.20 - 7.30 (8H, m, Ar-H), 7.06 - 7.15 (6H, m, Ar-H), 4.01 (3H, s, O-CH_3), 1.32 (27H, s, tBu) **MS** (ESI-MS) *m/z*: 667.36 $[M + H]^+$ ($C_{45}H_{51}N_2O_3$ calc. 667.39).

Carboxylic acid 81[13]

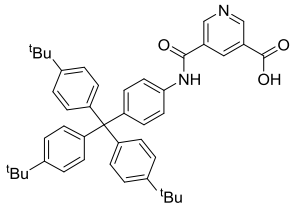

Pyridine derivative **80** (700 mg, 1.05 mmol) was dissolved in 1:1 THF/H_2O (20 mL) and KOH (71 mg, 1.26 mmol) was added. The mixture was stirred at room temperature for 16 h after which it was neutralised using 10% citric acid$_{(aq.)}$ and extracted with CH_2Cl_2 (3 x 20 mL). The organics were dried over $MgSO_4$, filtered and the solvent removed under vacuum to afford the product as a cream solid (570 mg, 0.87 mmol, 83%). **^{1}H NMR** (400 MHz, d_6-DMSO) δ = 13.70 (1H, br. s., -COOH), 10.61 (1H, s, NH), 9.27 (1H, d, ^4J = 2.1 Hz, py-H), 9.21 (1H, d, ^4J = 2.0 Hz, py-H), 8.73 (1H, t, ^4J = 2.0 Hz, py-H), 7.66 (2H, d, J = 8.8 Hz, NAr-H), 7.27 - 7.36 (6H, m, Ar-H), 7.07 - 7.19 (8H, m, Ar-H), 1.26 (27H, s, ^{t}Bu) **MS** (ESI-MS) *m/z*: 653.36 $[M + H]^+$ ($C_{45}H_{51}N_2O_3$ calc. 653.37).

Axle precursor 82

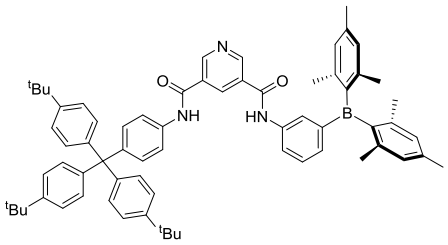

To a suspension of acid **81** (174 mg, 0.27 mmol) in CH_2Cl_2 (20 mL) was added oxalyl chloride (68 mg, 0.53 mmol) and DMF (1 drop, cat.). The mixture was stirred at room temperature, until homogenous, and the solvent was then removed under vacuum. The residue was redissolved in CH_2Cl_2 (15 mL) and added dropwise to a solution of **77** (100 mg, 0.29 mmol) and triethylamine (60 mg, 0.59 mmol) in CH_2Cl_2 (20 mL). The mixture was left to stir at room temperature for 24 h after which it was washed with H_2O (2 x 50 mL). The organics were dried over $MgSO_4$, filtered and the solvent was removed under vacuum. The crude material was purified by preparative plate thin layer chromatography (98:2 CH_2Cl_2/CH_3OH) to afford the product as a white solid (101 mg, 0.10 mmol, 39%). **^{1}H NMR** (500 MHz, $CDCl_3$) δ = 9.21 (1H, s, py-H), 9.19 (1H, s, py-H), 8.59 (1H, s, py-H), 8.20 (1H, d, *J* = 7.8 Hz, -C_6H_4-), 8.09 (1H, s, NH), 8.00 (1H, br. s., NH), 7.51 (2H, d, *J* = 8.5 Hz, NAr-H), 7.40 (1H, t, *J* = 7.6 Hz, -C_6H_4-), 7.35 (1H, d, *J* = 7.3 Hz, -C_6H_4-), 7.31 (1H, s, -C_6H_4-), 7.22 - 7.26 (8H, m, terphenyl Ar-H), 7.08 - 7.14 (6H, m, terphenyl Ar-H), 6.82 (4H, s, Mes), 2.31 (6H, s, Mes), 2.01 (12H, s, Mes), 1.31 (27H, s, ^{t}Bu). **^{13}C NMR** (101 MHz, $CDCl_3$) δ = 163.1, 163.0, 150.6, 150.3, 148.4, 147.0, 144.5, 143.7, 141.3, 140.8, 138.9, 136.9, 135.0, 134.1, 133.2, 131.9, 131.0, 130.7, 130.4, 129.0, 128.2, 127.5, 124.5, 124.2, 119.2, 63.4, 34.3, 31.4, 23.4, 21.2 **MS** (ESI-MS) *m/z*: 976.59344 $[M + H]^+$ ($C_{68}H_{75}BN_3O_2$ calc. 976.59469).

Axle 83·Cl

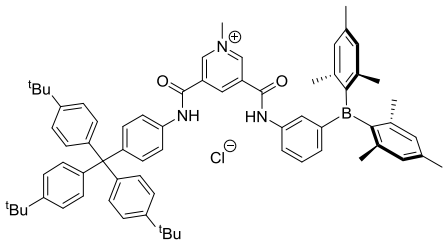

Axle precursor **82** (189 mg, 0.19 mmol) was dissolved in $CHCl_3$ (20 mL) and methyl iodide (2 mL, excess) was added. The mixture was heated at 65°C for 72 h and then cooled to room temperature, with the precipitate formed collected by filtration and washed with cold $CHCl_3$ (20 mL). The solid was dissolved in CH_2Cl_2 (50 mL) and washed with 1M $NH_4Cl_{(aq.)}$ (8 x 50 mL) and H_2O (2 x 50 mL). The organics were dried over $MgSO_4$, filtered and the solvent removed under vacuum to give **83·Cl** as a yellow solid (234 mg, 0.43 mmol, 64%). **^{1}H NMR** (400 MHz, $CDCl_3$) δ = 10.89 (1H, s, NH), 10.81 (1H, s, NH), 10.36 (1H, s, py-H), 9.18 (1H, s, py-H), 8.46 (1H, s, py-H), 8.11 (1H, s, -C_6H_4-), 7.91 (1H, d, *J* = 7.5 Hz, -C_6H_4-), 7.74 (2H, d, *J* = 8.8 Hz, N-Ar-H), 7.16 - 7.33 (16H, m, terphenyl Ar-H), 6.79 (4H, s, Mes), 3.94 (3H, s, N^+-CH_3), 2.27 (6H, s, Mes), 1.99 (12H, s, Mes), 1.30 (27H, s, ^{t}Bu). **^{13}C NMR** (101MHz, $CDCl_3$) δ = 158.4, 158.1, 148.3, 147.0, 146.2, 145.1, 144.0, 141.6, 140.9, 138.6, 137.3, 135.2, 134.7, 134.1, 133.4, 131.5, 130.5, 128.7, 128.3, 128.2, 124.9, 124.4, 119.4, 63.6, 48.9, 34.3, 31.4, 23.5, 21.2. **MS** (ESI-MS) *m/z*: 990.6107 $[M - Cl]^+$ ($C_{69}H_{77}BN_3O_2$ calc. 990.6114).

Rotaxane 84·PF_6

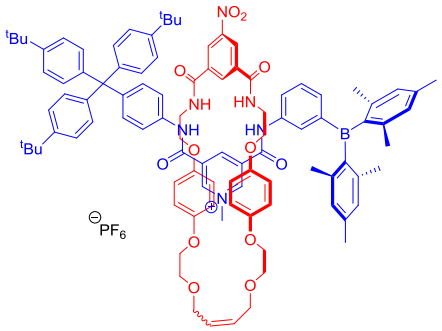

Axle **83·Cl** (50 mg, 0.049 mmol) and bis-vinyl macrocycle precursor **25** (32 mg, 0.049 mmol) were dissolved in CH_2Cl_2 (20 mL) and stirred at room temperature until homogenous. Grubbs' second generation catalyst (4 mg, 10% by weight) was added and the mixture stirred for 72 h. The solvent was then removed under vacuum and the crude material purified by preparative thin layer chromatography (CH_2Cl_2/MeOH 98:2; followed by EtOAc/ MeOH 98:2) and size exclusion chromatography ($CHCl_3$). The product was then dissolved in CH_2Cl_2 (15 mL) and washed with 0.1M $NH_4PF_{6(aq.)}$ (8 x 20 mL) and H_2O (2 x 20 mL). The organics were dried over $MgSO_4$, filtered and the solvent removed under vacuum to yield **84·PF_6** as a yellow solid (44 mg, 0.025 mmol, 51%). **^{1}H NMR** (500 MHz, d_6-DMSO) δ = 10.38 (1H, s, axle NH), 10.32 (1H, s, axle NH), 9.30 (1H, s, py-H), 9.21 (1H, br. s., py-H), 9.20 (1H, br. s., py-H), 9.00 (1H, s, int. macro. Ar-H), 8.83 (2H, t, *J* = 4.8 Hz, macro. NH), 8.75 (2H, s, ext. macro. Ar-H), 8.05 (1H, d, *J* = 8.2 Hz, -C_6H_4-), 7.58 (1H, s, -C_6H_4-), 7.39 - 7.46 (3H, m, NAr-H, -C_6H_4-), 7.30 (6H, d, *J* = 8.4 Hz, terphenyl Ar-H), 7.17 (1H, d, *J* = 7.3 Hz, -C_6H_4-), 7.00 - 7.07 (8H, m, terphenyl Ar-H), 6.29 - 6.38 (8H, m, hydroquinone Ar-H), 5.79 (2H, br. s., alkene CH), 4.33 (3H, s, N^+-CH_2), 3.94 (4H, br. s., macro. CH_2), 3.76 - 3.89 (8H, m, macro. CH_2), 3.59 - 3.70 (4H, m, macro. CH_2), 3.51 - 3.59 (4H, m, macro. CH_2), 2.21 (6H, s, Mes), 1.94 (12H, s, Mes), 1.27 (27H, s, ^{t}Bu). **^{13}C NMR** (126MHz, d_6-DMSO) δ = 164.1, 158.9, 158.5, 152.0, 147.8, 143.6, 141.0, 140.0, 138.5, 137.4, 135.8, 134.7, 133.2, 133.0, 132.2, 130.6, 129.9, 129.1, 128.9, 128.2, 127.5, 124.5, 124.4, 120.2, 114.7, 114.4, 70.0, 68.4, 67.3,

66.1, 62.9, 54.9, 48.7, 34.0, 31.1, 22.9, 20.7. ^{19}F NMR (377MHz, d_6-DMSO) δ = -70.1 (d, $^1J_{F,P}$ = 713 Hz). **^{31}P NMR** (162 MHz, d_6-DMSO) δ = -144.2 (septet, $^1J_{P,F}$ = 712 Hz). **MS** (ESI-MS) *m/z*: 1612.84425 $[M - PF_6]^+$ ($C_{101}H_{112}BN_6O_{12}$ calc. 1612.84594).

6.3 ^{1}H NMR titration protocols

^{1}H NMR titration experiments were performed on a Bruker AVIII500 spectrometer operating at 500 MHz and at a temperature of 298 K. A 0.5 mL initial volume of the host was used at a concentration of 1.5 mM or 2 mM. Solutions of the respective anions, as either their TBA or sodium salts, were added in aliquots, with the chemical shift of the appropriate protons followed over 17 additions. The spectra were referenced to the residual solvent peak or, in the case of the titrations performed in D_2O, to acetone (δ = 2.22 ppm), which was added as an internal standard (< 0.05 % of the total volume of the solution). Association constants were calculated from the data obtained using the WinEQNMR2 software package.[14] An estimate of the association constant and the limiting chemical shifts were added to the programs input file, along with the observed chemical shift of the proton followed and the concentrations of host and guest in each spectrum recorded. Refinement of the data using a non-linear least-squares regression analysis gave an optimised fit between the observed and calculated data for a 1:1 or 2:1 binding stoichiometry, as appropriate. Estimates for the standard error of the association constant calculated were provided by the program, as a standard deviation. However, these errors are only related to the fitting process and do not account for the systematic errors associated with the experimental procedure.

6.4 UV/vis experiments

UV/vis absorption spectra were recorded on a PGT60 U spectrometer at 298 K, using a Hellma Quartz cuvette with a pathlength of 10 mm. The concentrations of the solutions used in the qualitative experiments in Chapters Two and Five are stated in main body of the thesis.

6.5 Fluorescence titration protocol

The fluorescence titration experiments, discussed in Chapter Two, were performed on a Horiba Jobin Yvon Fluorolog spectrometer at 298 K, using a Hellma Quartz cuvette with a pathlength of 10 mm. A 2.5 mL initial volume of acyclic receptor **33·PF$_6$** was used, with a concentration of 10 μM, and solutions of the respective anions (50 mM), as their TBA salts were added up to 400 equivalents in 21 aliquots. The concentration of the host remained constant throughout the titration, with the anion solution made using the stock solution of the host.

The K_a, K_{SV} and ρ values were calculated using the OriginPro 2015 software package, *via* a non-linear least squares regression fit of the experimental data to a 1:1 binding isotherm, monitoring the emission intensity at $\lambda = 432$ nm.

6.6 Isothermal titration calorimetry protocol

The isothermal titration calorimetry experiments, discussed in Chapter Four, were performed on a Microcal PEAQ-ITC automated system and an iTC MicroCalorimeter in unbuffered distilled water at 298 K. An initial concentration of the host of 0.2 mM was used, with a 20 mM solution of $NaReO_4$ added in 35 aliquots. The data from the first addition of 0.5 μL was discarded, with data collected for the subsequent 34 additions of 1 μL. Heats of dilution were measured by a preliminary titration of $NaReO_4$ into water. Values of K_a and ΔH were calculated using the MicroCal PEAQ-ITC Analysis Software, *via* a non-linear least squares

regression fit of the experimental data to the one-set-of-sites model. These values were then used to determine the ΔG and ΔS values.

6.7 References

1 B.-Y. Lee, S. R. Park, H. B. Jeon and K. S. Kim, *Tetrahedron Lett.*, 2006, **47**, 5105–5109.
2 S. W. Robinson, C. L. Mustoe, N. G. White, A. Brown, A. L. Thompson, P. Kennepohl and P. D. Beer, *J. Am. Chem. Soc.*, 2015, **137**, 499–507.
3 V. Aucagne, K. D. Hänni, D. A. Leigh, P. J. Lusby and D. B. Walker, *J. Am. Chem. Soc.*, 2006, **128**, 2186–2187.
4 A. V. Leontiev, C. A. Jemmett and P. D. Beer, *Chem. – Eur. J.*, 2011, **17**, 816–825.
5 É. Dorkó, E. Varga, T. Gáti, T. Holczbauer, I. Pápai, H. Mehdi and T. Soós, *Synlett*, 2014, **25**, 1525–1528.
6 M. F. Salomon and R. G. Salomon, *J. Am. Chem. Soc.*, 1979, **101**, 4290–4299.
7 J. A. Faiz, N. Spencer and Z. Pikramenou, *Org. Biomol. Chem.*, 2005, **3**, 4239–4245.
8 T. Lecourt, A. Herault, A. J. Pearce, M. Sollogoub and P. Sinaÿ, *Chem. – Eur. J.*, 2004, **10**, 2960–2971.
9 E. Deunf, E. Zaborova, S. Guieu, Y. Blériot, J.-N. Verpeaux, O. Buriez, M. Sollogoub and C. Amatore, *Eur. J. Inorg. Chem.*, 2010, **2010**, 4720–4727.
10 B. Bertino-Ghera, F. Perret, B. Fenet and H. Parrot-Lopez, *J. Org. Chem.*, 2008, **73**, 7317–7326.
11 T. Hauch Fenger, J. Bjerre and M. Bols, *ChemBioChem*, 2009, **10**, 2494–2503.
12 Z. M. Hudson, C. Sun, M. G. Helander, Y.-L. Chang, Z.-H. Lu and S. Wang, *J. Am. Chem. Soc.*, 2012, **134**, 13930–13933.
13 L. M. Hancock and P. D. Beer, *Chem. Commun.*, 2011, **47**, 6012–6014.
14 M. J. Hynes, *J. Chem. Soc. Dalton Trans.*, 1993, 311–312.

Chapter Seven

Conclusions

7.1 Conclusions

The work described in this thesis has demonstrated how the anion association strength and anion selectivity properties of a given receptor can be greatly influenced by the nature of the binding interactions it utilises. Particular attention has been paid to further understanding the differences between the ubiquitous hydrogen bonding and the lesser-used halogen bonding interactions. However, the effects of other interactions including electrostatics, dispersion forces, coordinate bond formation and solvophobic effects have also been highlighted.

In Chapter Two, a series of novel [2]rotaxanes containing varying numbers of XB and HB donor groups within their pyridinium axle components were prepared by a chloride templated 'clipping' methodology. This allowed a systematic study to be conducted in which the effect of substituting an HB donor for an XB donor on the receptors' anion binding properties was investigated. Surprisingly, the XB systems **26·PF$_6$** and **30·PF$_6$** were found to bind all of the anions studied, with the exception of iodide, more weakly than the all HB host **27·PF$_6$** in a highly competitive 1:1 $CDCl_3$/CD_3OD solvent mixture. This is the first case in which this has been observed for analogous XB and HB receptors. However, it unlikely that these results are a consequence of a difference in the strength of the two interactions but instead reflect the differing degree to which electrostatics contribute to the binding process within the rotaxanes.

Also of interest was the substantial difference in the anion selectivity trends of the three receptors. The all HB host **27·PF$_6$** was found to bind the tetrahedral oxoanion dihydrogen phosphate more strongly than the halides and acetate. This selectivity is unprecedented for an interlocked anion receptor and suggests that there is a high degree of complementarity between the shape of this anion and the three-dimensional binding pocket of the rotaxane. By contrast, the XB systems **26·PF$_6$** and **30·PF$_6$** were found to bind the larger, more polarisable halides (bromide and iodide) more strongly than chloride and the highly

basic dihydrogen phosphate. Importantly, this selectivity was found to be enhanced as the number of XB donors within the rotaxane's binding pocket was increased from one to two. Such a drastic difference in the selectivity trend of analogous XB and HB receptors has yet to be reported and therefore these results provide one of the strongest pieces of experimental evidence to date of the fundamental differences in the nature of the XB and HB interactions. The anion preferences of rotaxanes **26·PF$_6$** and **30·PF$_6$** suggests that there is a substantial charge-transfer contribution to the XB interaction, whilst that of rotaxane **27·PF$_6$** demonstrates that HB interactions are primarily electrostatic in character.

An acyclic HB receptor **33·PF$_6$** containing a fluorescent quinolinium motif was also prepared. Spectrofluorometric titration experiments revealed it was capable of sensing halides and dihydrogen phosphate *via* a 'turn-off' fluorescence response and that the quenching mechanism had both static and dynamic components. The first example of an interlocked structure to incorporate the quinolinium motif was also described (**36·PF$_6$**), however its sensing capabilities were not investigated due to the low yield in which it was obtained.

In Chapter Three the first investigations into the anion recognition properties of receptors containing the dicationic 1,2-bis(pyridinium)ethane motif were reported. Surprisingly, acyclic receptors **38·2PF$_6$** and **39·2PF$_6$** displayed limited selectivity between a range of singly charged anions in an aqueous-organic solvent mixture. Minimal differences between the association constants of the XB and HB analogues was also observed, which suggested that anion association with these hosts was dominated by electrostatics. Importantly, this demonstrates how interactions of this nature can outweigh the effect of weaker non-covalent forces, such as XB and HB, if a host contains multiple positively charged groups. It was thought that the conformational flexibility of the receptors may also have been a source of the poor selectivity, however the limited solubility of the more

preorganised macrocyclic hosts **43·2PF$_6$** and **44·2PF$_6$** prevented a full comparison of their binding properties.

Chapter Four discussed a series of water-soluble anion receptors containing a permethylated-α-cyclodextrin unit, which exploited the well-known ability of this macrocycle to form inclusion complexes with anionic species. The hosts also contained pendant iodo- or prototriazole motifs, attached to the 1^o rim of the CD unit, which provided additional XB/HB binding interactions. The receptors described constitute the first case in which both these binding interactions have been utilised in concert.

Both the XB and HB dicationic hosts **68·2NO$_3$** and **69·2NO$_3$** displayed impressive selectivity towards the perrhenate anion (ReO_4^-) in pure water, which is significant due the use of this anion as a model for the highly toxic, radioactive pertechnetate anion. Importantly, the association strength of the XB system was significantly larger, demonstrating the superiority of XB interactions for anion recognition in water. Indeed, **68·2NO$_3$** is the most effective receptor reported to date for perrhenate recognition in neutral aqueous media. Interestingly, ITC experiments revealed that the stronger binding by the XB system was the result of a large enthalpic contribution to the association, which is presumably a consequence of the strong XB interactions formed between the host and guest.

The 'strapped' monocationic HB host **73·NO$_3$** exhibited a dramatically different selectivity trend to the dicationic systems, with iodide bound substantially more strongly than other halides, perchlorate and perrhenate. This was attributed to the highly preorganised nature of the prototriazole HB donors within the receptor which presumably generate a binding pocket that is highly complementary to the spherical halide anion.

In Chapter Five, the preparation of the first interlocked host incorporating a Lewis acidic triarylborane motif was reported (**84·PF$_6$**). The [2]rotaxane was found to bind fluoride substantially more strongly than chloride, which was attributed to the ability of the smaller

fluoride anion to form a strong B-F coordinate bond with the sterically protected boron centre. Importantly, the presence of a cooperative HB binding interaction from the macrocycle component was also observed in the fluoride-adduct **84·F**, evidence of which was provided by multinuclear NMR experiments. Although receptors which bind fluoride through a combination of HB and coordinate bond formation have been described previously, this is the first case in which this has been achieved using an interlocked structure and demonstrates the unique binding modes which can only be achieved using hosts of this nature. Furthermore, the rotaxane was demonstrated to function as a colorimetric fluoride sensor due to the formation of an intramolecular charge-transfer interaction upon binding. The presence of this interaction was confirmed using UV/vis titration experiments.

Appendix

X-Ray Crystallographic Data

For all of the structures described in this thesis crystals were grown by the author, and data collection, structure solution and refinement were carried out by Jason Lim and Dr. Asha Brown with help from Dr. Amber Thompson. Diffraction data for compound **76** were collected at 150(2) K[1] using graphite monochromated Mo Kα radiation (λ = 0.71073 Å) on a Nonius Kappa CCD diffractometer. Cell parameter determination and refinement and raw frame data integration were carried out using the DENZO-SMN package.[2] For all other compounds diffraction data were collected at 100(2) K[1] using silicon double crystal monochromated synchrotron radiation (λ = 0.68890 Å) at Diamond Light Source, beamline I19,[3] using a custom-built Rigaku diffractometer. Cell parameter determination and refinement and raw frame data integration were carried out using the CrysAlisPro[4] package. All structures were solved by charge-flipping methods using SUPERFLIP[5] and refined by full matrix least squares on F^2 using the CRYSTALS[6] suite. All non-hydrogen atoms were refined with anisotropic displacement parameters. Where appropriate, disordered regions were modelled using refined partial occupancies, geometric restraints were applied to ensure a physically reasonable model, and thermal and vibrational restraints were applied to maintain sensible ADPs; in addition, when present, diffuse disordered solvent was modelled by treating the discrete Fourier transform of the void region as contributions to the calculated structure factors with PLATON/SQUEEZE.[7,8] Hydrogen atoms were generally visible in the difference map but those attached to carbon atoms were initially positioned geometrically and their positions and displacement parameters refined using soft restraints, after which the positions were used as the basis for a riding model.[9] Occasionally this led to unstable refinements, typically when the hydrogen atoms were attached to atoms with large thermal ellipsoids and the data was of low quality. In these cases the hydrogen atoms were placed at geometric positions and refined using riding constraints. Where amide hydrogen atoms were not visible

in the difference maps they were also inserted at geometric positions and refined using riding constraints. After the construction of a stable, physically reasonable and complete model, the weights were optimised,[10,11] anomalous reflections were omitted, and absent high-angle data were removed using the Wilson plot as a guide to determine the limit of diffraction. This led to convergence of the refinement, giving the final structures.

Rotaxane 30·Cl

Crystals were grown by cooling a 1:1 $CDCl_3$:CD_3OD solution of the [2]rotaxane **30·PF_6** containing a 10-fold excess of TBACl. Some disorder was identified in two of the chloroform solvent molecules and this was modelled using refined partial occupancies over two positions. In addition, enlarged, prolate displacement ellipsoids suggested the presence of disorder in some of the stopper *tert*-butyl functional groups; however, attempts to model this disorder using refined partial occupancies over two sites did not produce a satisfactory model. Poorly-defined electron density was visible in the unit cell, presumably arising from diffuse disordered solvent molecules. Unfortunately no sensible refinement of this electron density could be achieved, and PLATON/SQUEEZE[7,8] was therefore applied in order to account for it during refinement (1557 Å containing 611 electrons).

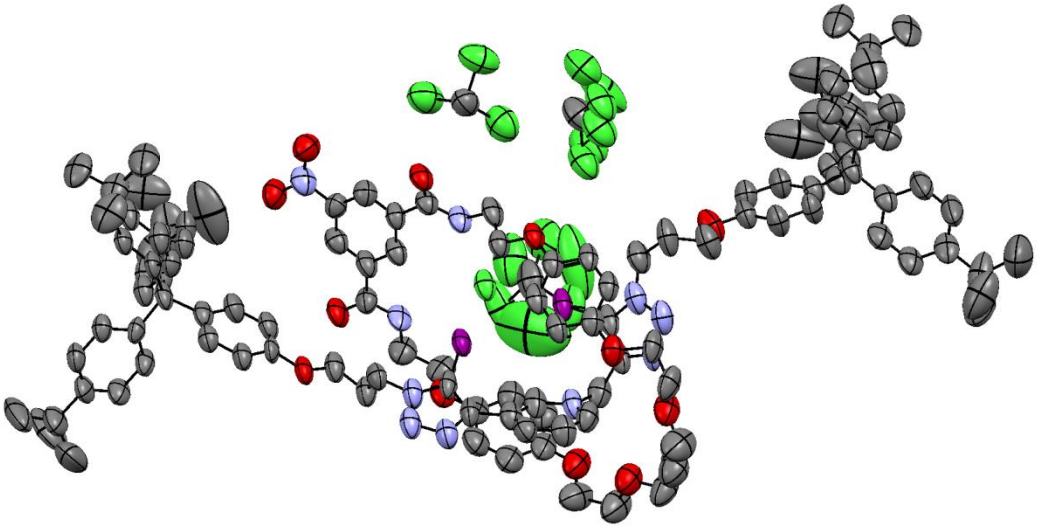

Figure A1. Thermal ellipsoid plot showing the content of the asymmetric unit for the single crystal structure of compound **30·Cl** with displacement ellipsoids drawn at the 50% probability level. Hydrogen atoms have been omitted.

Table A1. Crystal structure data and refinement details for the [2]rotaxane **30·Cl**.

Crystal data	
Chemical formula	$C_{125}H_{141}Cl_{10}I_2N_{10}O_{12}$
M_r	2583.90
Crystal system, space group	Triclinic, *P* -1
Temperature (K)	100
a, *b*, *c* (Å)	16.9177 (7), 17.8060 (6), 27.0854 (9)
α, β, γ (°)	107.104 (3), 108.070 (3), 92.670 (3)
V (Å^3)	7327.9 (5)
Z	2
μ (mm^{-1})	0.67
Crystal size (mm)	0.04 × 0.02 × 0.02
T_{min}, T_{max}	0.84, 0.99
No. of measured, independent and observed [$I > 2.0\sigma(I)$] reflections	21124, 21215, 9084
R_{int}	0.102
$(\sin \theta/\lambda)_{max}$ (Å^{-1})	0.586
$R[F^2 > 2\sigma(F^2)]$, $wR(F^2)$, S	0.087, 0.247, 0.99
No. of reflections used	13420
No. of parameters	1488
No. of restraints	3335
$\Delta\rho_{max}$, $\Delta\rho_{min}$ (e Å^{-3})	1.31, −0.94

Rotaxane 30·Br

Crystals were grown by cooling a 1:1 $CDCl_3$:CD_3OD solution of the [2]rotaxane **30·PF$_6$** containing a 10-fold excess of TBABr. Some positional disorder was identified in one of the stopper *tert*-butyl groups and this was modelled using refined partial occupancies over two positions. Although enlarged, prolate ellipsoids suggested the presence of disorder in many of the other *tert*-butyl groups, attempts to model this using refined partial occupancies did not produce a satisfactory model. A large amount of poorly-defined electron density, presumably arising from diffuse disordered solvent molecules, was also visible in the unit cell. Since a sensible model could not constructed for this electron density, it was modelled with SQUEEZE in PLATON[7,8] (2334 Å containing 874 electrons).

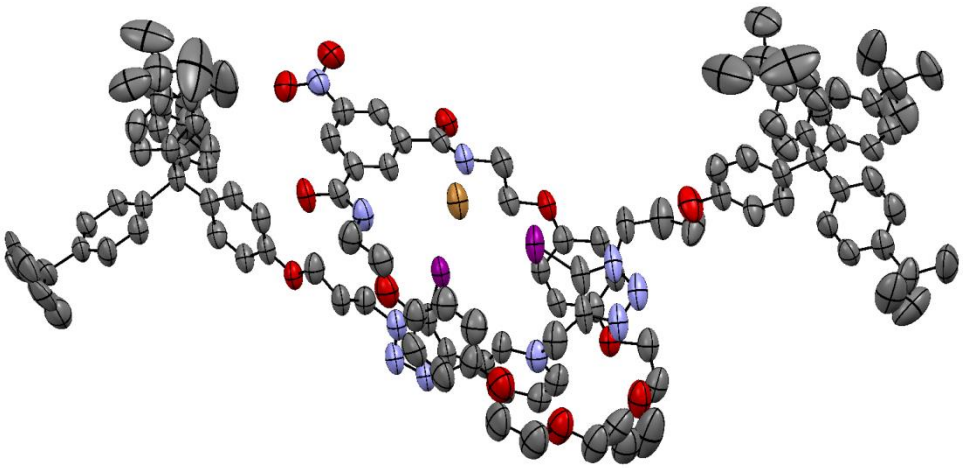

Figure A2. Thermal ellipsoid plot showing the content of the asymmetric unit for the single crystal structure of compound **30·Br** with displacement ellipsoids drawn at the 50% probability level. Hydrogen atoms have been omitted.

Table A2. Crystal structure data and refinement details for compound **30·Br**

Chemical formula	$C_{122}H_{137}BrI_2N_{10}O_{12}$
M_r	2269.22
Crystal system, space group	Triclinic, *P* -1
Temperature (K)	100
a, *b*, *c* (Å)	16.6217 (8), 18.0132 (6), 27.0157 (11)
α, β, γ (°)	107.514 (3), 107.532 (4), 92.735 (3)

V (Å^3)	7269.8 (6)
Z	2
μ (mm^{-1})	0.76
Crystal size (mm)	0.04 × 0.03 × 0.01
T_{min}, T_{max}	0.84, 0.99
No. of measured, independent and observed [$I > 2.0\sigma(I)$] reflections	21242, 21266, 9425
R_{int}	0.081
$(\sin \theta/\lambda)_{max}$ (Å^{-1})	0.587
$R[F^2 > 2\sigma(F^2)]$, $wR(F^2)$, S	0.075, 0.207, 0.97
No. of reflections used	13195
No. of parameters	1352
No. of restraints	1613
$\Delta\rho_{max}$, $\Delta\rho_{min}$ (e Å^{-3})	1.01, −0.95

Acyclic receptor 39·2CF$_3$SO$_3$

Crystals were grown by diffusion of Et_2O into an MeCN solution of **39·2CF$_3$SO$_3$**.

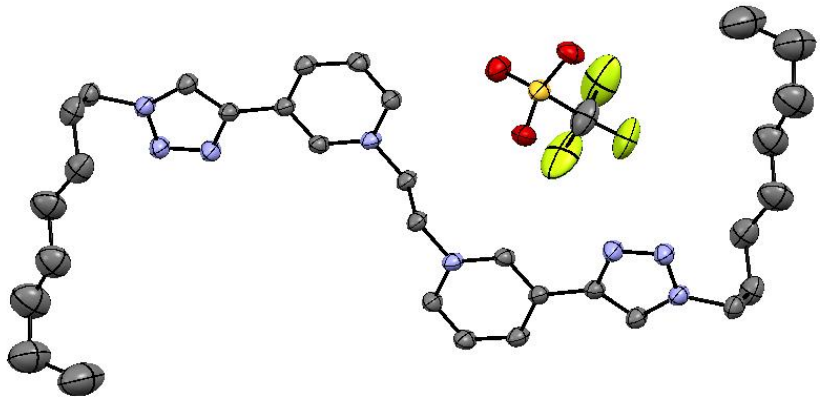

Figure A3. Thermal ellipsoid plot showing the content of the unit cell for the single crystal structure of compound **39·2CF$_3$SO$_3$** with displacement ellipsoids drawn at the 50% probability level. Hydrogen atoms have been omitted.

Table A3. Crystal structure data and refinement details for compound **39·2CF$_3$SO$_3$**.

Chemical formula	$C_{34}H_{48}F_6N_8O_6S_2$
M_r	842.92
Crystal system, space group	Triclinic, P -1
Temperature (K)	100

a, b, c (Å)	7.6025 (3), 9.3752 (4), 15.7776 (9)
α, β, γ (°)	74.6816 (19), 80.3424 (19), 71.444 (3)
V (Å^3)	1023.90 (9)
Z	1
μ (mm^{-1})	0.21
Crystal size (mm)	0.42 × 0.38 × 0.03
T_{min}, T_{max}	0.94, 0.94
No. of measured, independent and observed [$I > 2.0\sigma(I)$] reflections	15069, 4625, 2622
R_{int}	0.073
$(\sin \theta/\lambda)_{max}$ (Å^{-1})	0.650
$R[F^2 > 2\sigma(F^2)]$, $wR(F^2)$, S	0.060, 0.142, 0.93
No. of reflections used	3355
No. of parameters	253
$\Delta\rho_{max}$, $\Delta\rho_{min}$ (e Å^{-3})	0.45, −0.41

Macrocycle 44·2Cl

Crystals were grown by slow evaporation of an MeCN solution of **44·2Cl**.

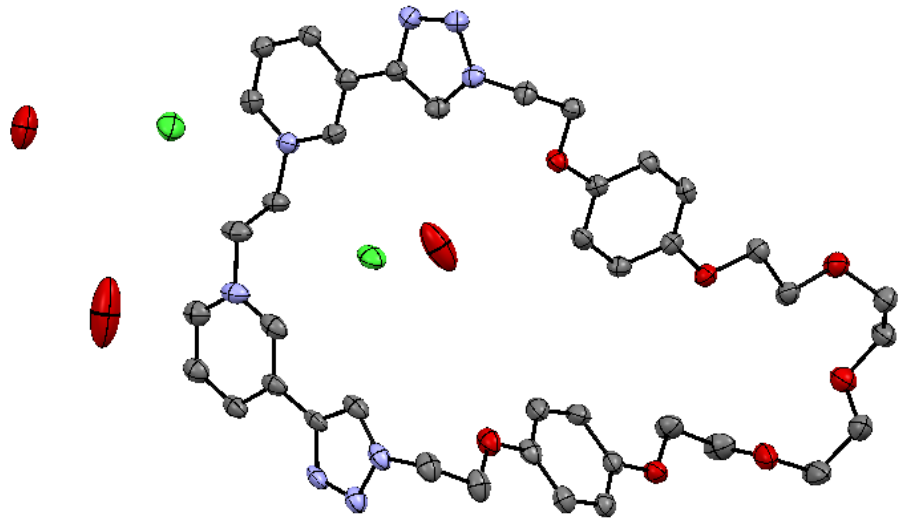

Figure A4. Thermal ellipsoid plot showing the content of the asymmetric unit for the single crystal structure of compound **44·2Cl** with displacement ellipsoids drawn at the 50% probability level. Hydrogen atoms have been omitted.

Table A4. Crystal structure data and refinement details for compound **44·2Cl**.

Chemical formula	$C_{40}H_{52}Cl_2N_8O_{10}$
M_r	875.81
Crystal system, space group	Triclinic, *P* -1
Temperature (K)	100
a, *b*, *c* (Å)	4.9204 (1), 15.9717 (8), 27.4277 (8)
α, β, γ (°)	91.806 (3), 93.491 (2), 90.860 (3)
V (Å^3)	2150.09 (13)
Z	2
μ (mm^{-1})	0.22
Crystal size (mm)	0.05 × 0.03 × 0.03
T_{min}, T_{max}	0.64, 0.99

No. of measured, independent and observed [$I > 2.0\sigma(I)$] reflections	25467, 8078, 4559
R_{int}	0.071
$(\sin \theta/\lambda)_{max}$ ($Å^{-1}$)	0.636
$R[F^2 > 2\sigma(F^2)]$, $wR(F^2)$, S	0.077, 0.201, 0.96
No. of reflections used	6004
No. of parameters	541
$\Delta\rho_{max}$, $\Delta\rho_{min}$ (e $Å^{-3}$)	1.52, −1.47

Triarylborane derivative 76

Crystals were grown by cooling a hexane/CH_2Cl_2 solution of compound **76**.

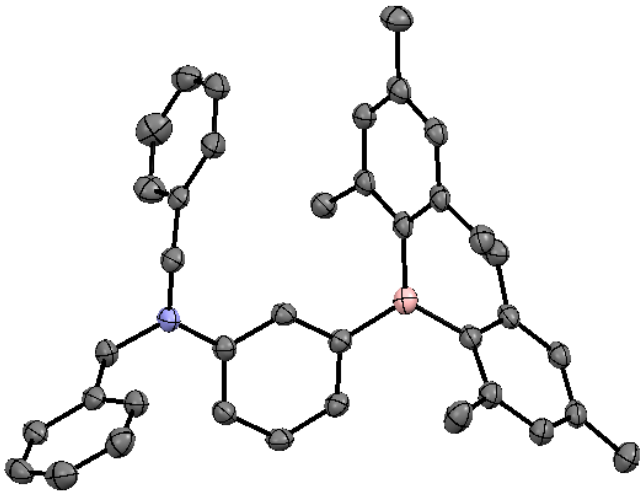

Figure A5. Thermal ellipsoid plot showing the content of the asymmetric unit for the single crystal structure of compound **76** with displacement ellipsoids drawn at the 50% probability level. Hydrogen atoms have been omitted.

Table A5. Crystal structure data and refinement details for compound **76**.

Chemical formula	$C_{38}H_{40}BN$
M_r	521.55
Crystal system, space group	Triclinic, *P* -1
Temperature (K)	150
a, *b*, *c* (Å)	8.7857 (5), 14.2403 (7), 14.4096 (7)
α, β, γ (°)	63.236 (5), 74.613 (5), 73.181 (5)
V ($Å^3$)	1521.45 (15)

Z	2
μ (mm^{-1})	0.06
Crystal size (mm)	0.06 × 0.05 × 0.02
T_{min}, T_{max}	0.53, 1.00
No. of measured, independent and observed [$I > 2.0\sigma(I)$] reflections	15755, 5410, 3399
R_{int}	0.053
$(\sin\theta/\lambda)_{max}$ ($Å^{-1}$)	0.650
$R[F^2 > 2\sigma(F^2)]$, $wR(F^2)$, S	0.052, 0.128, 0.92
No. of reflections used	3989
No. of parameters	361
$\Delta\rho_{max}$, $\Delta\rho_{min}$ (e $Å^{-3}$)	0.24, −0.23

References

1 J. Cosier and A. M. Glazer, *J. Appl. Crystallogr.*, 1986, **19**, 105–107.
2 Z. Otwinowski and W. Minor, in *Methods in Enzymology*, Elsevier, 1997, vol. 276, pp. 307–326.
3 H. Nowell, S. A. Barnett, K. E. Christensen, S. J. Teat and D. R. Allan, *J. Synchrotron Radiat.*, 2012, **19**, 435–441.
4 *CrysAlis Pro*, 2011, Agilent Technologies, Yarnton, Oxfordshire, UK.
5 L. Palatinus and G. Chapuis, *J. Appl. Crystallogr.*, 2007, **40**, 786–790.
6 P. W. Betteridge, J. R. Carruthers, R. I. Cooper, K. Prout and D. J. Watkin, *J. Appl. Crystallogr.*, 2003, **36**, 1487–1487.
7 A. L. Spek, *J. Appl. Crystallogr.*, 2003, **36**, 7–13.
8 P. van der Sluis and A. L. Spek, *Acta Crystallogr. A*, 1990, **46**, 194–201.
9 R. I. Cooper, A. L. Thompson and D. J. Watkin, *J. Appl. Crystallogr.*, 2010, **43**, 1100–1107.
10 J. R. Carruthers and D. J. Watkin, *Acta Crystallogr. Sect. A*, 1979, **35**, 698–699.
11 D. Watkin, *Acta Crystallogr. A*, 1994, **50**, 411–437.